

For New Technology Network

**NTN**®

# TECHNICAL REVIEW

No.  
**84**

**Special Issue: Green Energy Products and  
Machine Tool / Manufacturing Technology**

**November 2016**



NTN GREEN POWER PARK

NTN has established a "Green Power Park", an energy recycling model that supplies wind, water, and solar powered energy to electric vehicles, vegetable factories, etc. within the Advanced Technology R&D Center site located in Kuwana City, Mie Prefecture.

At this Park, we have installed small wind turbine generators, small hydraulic turbine generators (micro hydro turbines), wind / solar powered hybrid streetlamps, etc. developed by NTN, to conduct demonstration tests of natural energy related systems. Through these activities, we are proposing the use of these systems in communities close to the daily lives of everyday citizens.

Small wind turbine power generators have achieved power generation from low wind speed through the adoption of vertical blades, regardless of wind direction and quietness, by reducing noise through NTN's low-torque bearing technology and special blade geometry.

Micro hydro turbines can be used where there are small scale streams, such as irrigation water ways or sewage lines. Specially shaped propeller blades are able to efficiently capture the water stream without disruption, which makes it possible to install a series of micro hydro turbines in a single stream.

The electric power generated by these systems is constantly monitored and optimally controlled by the Monitoring and Control Center for power level of generation, storage, and consumption for efficient circulation of clean natural energy that does not emit CO<sub>2</sub>.

We will strive for continuous improvement of this recycling model by continuing demonstration tests. We will also make the Green Power Park publicly available to local students and customers for environmental learning and awareness of NTN's technologies.

**Overview of Green Power Park**



- |   |   |
|---|---|
| (1) Small wind turbine generator 10 kW                | (5) Micro hydro turbine generator 1 kW      |
| (2) Small wind turbine generator 4 kW                 | (6) Solar photovoltaic power generator 5 kW |
| (3) Small wind turbine generator 2 kW                 | (7) Monitoring and control center           |
| (4) Wind/solar photovoltaic hybrid streetlight 0.3 kW | (8) Vegetable factory                       |



# TECHNICAL REVIEW

**No.84**

**Special Issue;**

**Green Energy Products and Machine Tool  
Manufacturing Technology**

# NTN TECHNICAL REVIEW No.84

## CONTENTS

<b>Preface</b>	For Green Energy Products and Machine Tool / Manufacturing Technology Yoshinori TERASAKA	1
<b>Contribution</b>	Outlook of Wind Energy Business Takao MAEDA Professor, Division of Mechanical Engineering, Mie University	2
<b>Perspective</b>	Green Energy Business and Green Power Park Natsuhiko MORI	14
<b>● Special Issue for Green Energy Products</b>		
	<b>Small Wind Turbine Generator</b> Takaya ADACHI and Ryosuke KARASAWA	22
	<b>Micro Hydro Turbine</b> Tomoya KAWAI, Hiroki MUKAI and Tomomi GOTOU	28
	<b>CFD contribution to development of Small Wind Turbine Generator</b> Takeru ITOU, Ryosuke KARASAWA and Masato YOSHINO	34
<b>● Special Issue for Machine tool and Manufacturing Technology</b>		
	<b>Technical Trend of the Precision Bearings for Machine Tools</b> Naoki MATSUMORI and Keiichi UEDA	40
	<b>ULTAGE Serises Small Size High-Speed Precision Angular Contact Ball Bearings for Machine Tool Spindles</b> Mineo KOYAMA, Keisuke NASU and Takahiro KANAMOTO	46
	<b>Machine Tool Main Spindle Bearings with Air Cooling Spacer</b> Keisuke NASU, Naoya OKAMOTO and Masato YOSHINO	52
	<b>High-performance Sealed Cam Follower</b> Masato TSUJIIHASHI and Seizo AGATA	58
	<b>Introduction of Linear Guides</b> Masaki KAGAMI and Keisuke KAZUNO	63
	<b>Plastic sliding screws</b> Naonari TANIGAWA, Norio ITOU and Tomomi TONOMURA	69
<b>● Technical Papers New Products</b>		
	<b>Strategy of Rolling Contact Fatigue Life Testing and Interpretation of Life Data</b> Takumi FUJITA	74
	<b>Rolling Contact Fatigue Life of Thrust Ball Bearing under Low Lambda Condition</b> Takumi FUJITA, Naoya HASEGAWA, Naoya KAMURA and Toshihiko SASAKI	85
	<b>Speeding up of Parallel Link Angle Control Equipment</b> Kenzou NOSE, Hiroshi ISOBE and Seigo SAKATA	96
	<b>Propeller blade bearings for Aircraft Open Rotor engine</b> Guillaume LEFORT	102
	<b>Products Introduction of Composite Material for Industrial Machinery</b> Shinji KOMATSUBARA, Toshihiko MOURI, Takuji HARANO and Tamaki MIZUTANI	108
<b>● Award Winning Products</b>		
	《The Japan Society for Precision Engineering 2015 Spring Semestrial Meeting "Best Presentation Award", "Young Engineer Award"》 <b>Parallel Link High Speed Angle Control Equipment</b> Naoya KONAGAI	114
	《The Japan Society of Mechanical Engineers 2014 Material ond Processing Division "New Technology Development Award" 》 <b>Materials Development about the Sintered Bearing Prepared by Unification Forming of Different Metals Powder</b> Yosuke SUGAI, Yoshinori ITOU, Toshihiko MOURI and Eiji YUASA	115
	《"Innovative Product Award" 2015 in China》 <b>Machine Tool Main Spindle Bearings with Air Cooling Spacer</b> Wenwei WU and Michihiko KOSAKA	116
	《Equip Auto 2015 Innvation Award》 <b>Press Connected Spline Hub Joint</b> Sebastien GUILLAUME and Claire BIANCHIN	117
<b>Our Line of New Products</b>		118

## *Special Issue for Green Energy Products and Machine Tool/ Manufacturing Technology*



**Yoshinori TERASAKA**  
Managing Director

With global warming being taken on as a major social issue, perspectives on the future of energy are being actively discussed. There is no doubt that further utilization of renewable natural energy sources such as wind, hydro and solar power are being accelerated as alternatives to fossil fuel sources, effective for CO<sub>2</sub> reduction.

In particular, small-scale power generation that can be utilized in the proximity of communities and provide stable and independent power is drawing attention to cope with recent extreme weather or large-scale disasters such as earthquakes.

We have started a mid-term management plan for the three year period starting in 2015 called "NTN100" for the promotion of "business development in new areas". These areas include (1) Energy business, (2) EV business, (3) Robot associated business, and (4) Service solution business using CMS (Condition Monitoring System)." In particular, for the area of Energy business, we have newly established the Natural Energy Product Division to meet the social requirement of CO<sub>2</sub> reduction. We have developed products such as small-scale wind turbine generators with low-torque bearings and specially-shaped blades for wind noise reduction as well as micro hydro turbines. We have also started distribution of hybrid streetlamps. In addition, in the area of EV Business, we have developed in-wheel motors (IWM) and conducted demonstration tests, contributing to the reduction of CO<sub>2</sub>, together with our Natural Energy Business.

On the other hand, NTN contributes to the transformation of manufacturing with one of our base products, precision rolling bearings for machine tools, commonly used in the main spindles of machine tools. These employ NTN fundamental technologies such as materials, heat treatment and tribology. We are glad that we could publish our Special Issue of Technical Review No. 84 for Green Energy Products and Machine Tool/Manufacturing Technology, on this occasion of the 28th Japan International Machine Tool Fair (JIMTOF2016) that takes place from November 17 through November 22 under the theme of "The Future Starts Here".

NTN has been the leading company in precision rolling bearings for machine tools since we launched our ULTAGE Series of precision rolling bearings in the early 2000s, announcing new products and always incorporating state-of-the-art technologies. Again in this issue, we are discussing new technology trends of bearings for machine tools, as well as introducing newly developed products such as small-size, high-speed precision angular contact ball bearings for machine tool spindles and machine tool main spindle bearings with air cooling spacers that address high speed operation.

We will further promote technology/product development in " new business areas" to achieve sales of 1.4 trillion yen in 2025, together with new product development of rolling bearings as part of our base business. We will also contribute to sustainable social development through these corporate activities, always responding to the requirements of the industry.

# For New Technology Network

## Outlook of Wind Energy Business



**Takao MAEDA**

Professor, Doctor (Engineering) Department of Mechanical Engineering,  
Mie University

The size of large wind turbines are increasing year by year, and some wind turbines have diameter of 160 m and more. An installation sites of large wind turbines were mainly onshore in the past, but are changed to mountainous regions and offshore. The technology corresponds to the installation sites are also developed. On the other hand, small wind turbines is useful for distributed power system, which is introduced in advanced countries as well as developing countries of power shortage and weak electric grid. In particular, introduction of small wind turbines is much increasing by the certification system for promotion of small wind turbine in Japan. From the view which focuses on the difference between the large wind turbines and the small wind turbines, this paper introduces a market trend, state of the art and the prospective of wind turbines.

### 1. Introduction

The first time wind turbines for power generation were developed was in the 1970s when aircraft manufactures developed large wind turbines and small factories developed small wind turbines. However, the high-tech wind turbines developed by the aircraft manufacturers were not cost effective and withdrawn from the market. On the other hand, small factories gathered different technologies from different areas of industry to create small wind turbines of about 10m in diameter through trial and error. Since the 1980s, development has been focused on technologies for large wind turbines due to the policy of targeting large size turbines, and through technical evolution the current mainstream has become diameters of 80m and output of 2MW.

Recently, the distributed wind turbine concept has been reconsidered and small wind turbines of several kW to several tens of kW have been developed for low power-grid areas and remote islands. In the domestic market, activities involving small wind turbines have been more widespread while some municipalities have introduced subsidies to small wind turbines of several kW for residential use.

Wind turbines are equipment that extract energy from the wind and convert it to electric power.

However, the wind that wind turbines capture can vary in space or time. Therefore, creativity is required for extracting electric power from unstable and low-density wind energy. This article discusses the market trend and differences of technologies between large and small wind turbines, as well as from a future technical perspective.

### 2. Trends of the wind turbine market

#### 2.1 Large wind turbine market

As shown in [Fig. 1](#)<sup>1)</sup>, global installation of large wind turbines is 432GW as of the end of 2015. Even in 2015 alone, 63GW of wind turbines are newly installed with annual growth of approx. 20%. Since the capacity of a nuclear power plant is 1GW, there are wind turbines with the capacity equivalent of over 400 nuclear power plants in the world. As shown in [Fig. 2](#)<sup>1)</sup>, China and the U.S. account for over half of the global installed base, with China having the most. As shown in [Fig. 3](#)<sup>1)</sup>, 31GW of wind turbines were installed in 2015 in China alone, which account for half of the new global installations. There are several reasons why wind turbine installations are active in China. First, as opposed to large power plants such as thermal power plants which require a long time from assessment to start of operation, wind turbines can be installed in a

few months as long as the wind conditions are favorable. Another reason for the fast growth is that China is promoting the wind turbine industry as a national policy for increasing employment. In Europe, installation of "offshore wind turbines" has recently become active; however, as shown in Fig. 1, the

installed base of offshore wind turbines is still 12GW among the global installed base of 432GW. Therefore, it is apparent that on-shore wind turbines are still the mainstream.

On the other hand, in Japan, renewable energy feed-in tariff programs started in July 2012 and expansion of installation of wind turbines was expected together with other renewable energy. However, the requirement of an environmental assessment equivalent for construction of large buildings was also implemented for wind turbines from October 2012, which prevented the introduction of wind turbines. It takes over three years to complete environmental assessment procedures, which slowed down the introduction. Because of this policy, as if applying acceleration and braking at the same time, the domestic introduction of wind turbines, as shown in Fig. 4<sup>2, 3)</sup>, is still very low with 3GW (2143 units) of installed base and 0.2GW of new installation in 2015; this only accounts for 0.5% of the total power supply in Japan. This is significantly low compared to the EU which covers 11.4% of the demand with wind power, which indicates a large potential for domestic wind power introduction. Japan Wind Power Association conducts wind potential and feasibility studies for installation sites of wind turbines and created the roadmap shown in Fig. 5<sup>4)</sup>. This roadmap aims for installation of 75GW of wind turbines to cover 20% of the domestic power demand. As of February 2016, the capacity of new wind turbines approved by the Ministry of Economy, Trade and Industry is 2.65GW, double the current installed base of 3GW when installed. The objective of the present wind power industry is to achieve "grid parity," which is to offer prices and reliability equivalent to that of the conventional power generation such as thermal power plants.

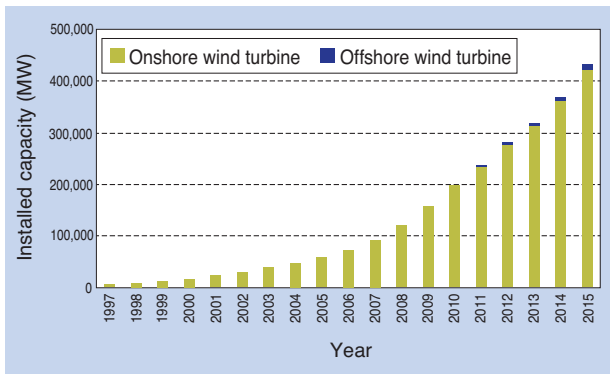


Fig. 1 Worldwide trend of total installed capacity of large wind turbines<sup>1)</sup>

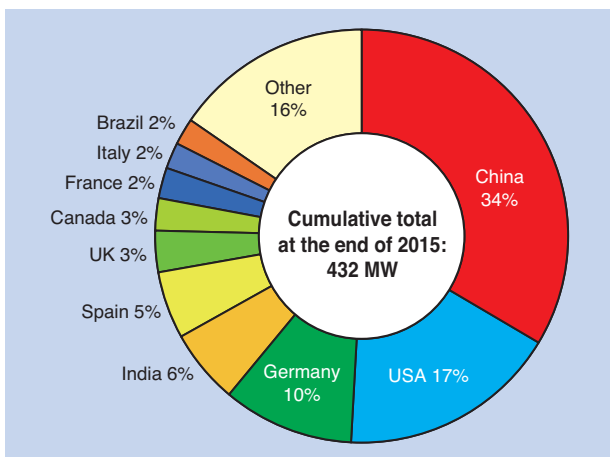


Fig. 2 Worldwide total installed capacity of large wind turbines<sup>1)</sup>

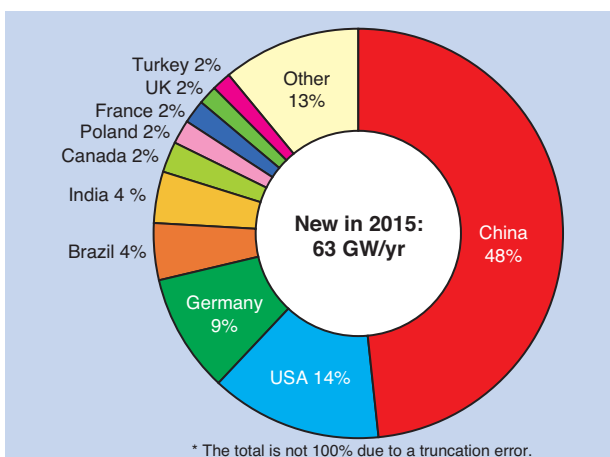


Fig. 3 Worldwide annual installed capacity of large wind turbines<sup>1)</sup>

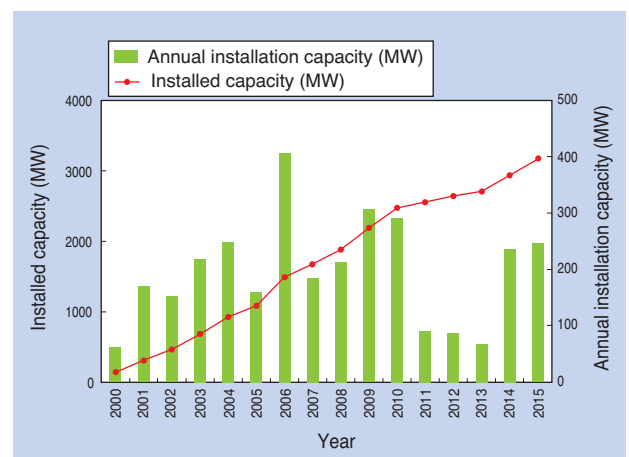


Fig. 4 Domestic trend of installed capacity of large wind turbines<sup>2, 3)</sup>

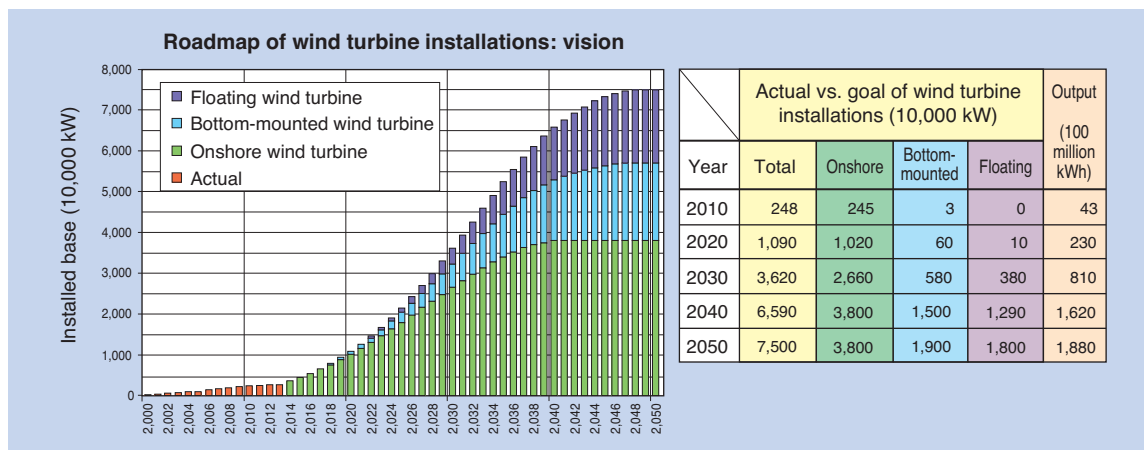


Fig. 5 Roadmap of domestic installed capacity of large wind turbines by Japan Wind Power Association <sup>4)</sup>

## 2.2 Small wind turbine market

Small wind turbines are defined to have "a rotor swept area of less than 200m<sup>2</sup>" according to the international standard IEC 61400-2.

Therefore, for propeller-type horizontal-shaft wind turbines, those with a diameter of less than 16m and up to an output power of 50kW are classified as small wind turbines.

As shown in Fig. 6 <sup>5)</sup>, the global installed base of small wind turbines as of the end of 2014 is 945,000 units, with annual growth of 8%. As shown in Fig. 7 <sup>5)</sup>, the installed capacity is 830MW, with annual growth of 11%. The fact that the capacity growth is larger than the unit growth reveals that the average size is increasing, even with the small wind turbine category. The average size increased year on year, from 0.66kW in 2010, 0.84kW in 2012 to 0.87kW in 2014. However, this trend varies from country to country; for example, the average size is 0.5kW in China, 1.4kW in the U.S., and 4.7kW in the UK. In addition, the definition of small wind turbines in the UK is less than 100kW, determined by an association for wind power, and in the U.S. the definition varies from less than 100kW to less than 200 kW, depending on the state.

A significantly large installed base is found in China, U.S., and UK. That is because, those countries, which traditionally have large small-sized wind turbine markets, have achieved cost reduction due to mass production that resulted in accelerated introduction; as opposed to countries with smaller markets having difficulty in achieving similar cost reduction.

World Wind Energy Association created a roadmap of small wind turbines <sup>5)</sup>. The annual new installation has been increasing by 19 to 35% until 2012, and then the growth rate slowed to 11% by 2013 to 2014. However, since associations and industries associated with small wind turbines in different countries are taking steps to expand adoption, the

growth rate has started to recover from 2015, and the annual growth rate is conservatively estimated at 20%, reaching around 1.75GW of installed capacity by 2020 and annual installation capacity is estimated to reach 240 MW.

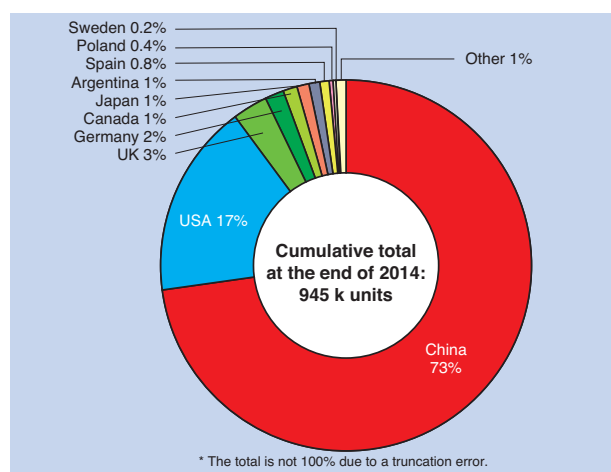


Fig. 6 Worldwide total installed units of small wind turbines <sup>5)</sup>

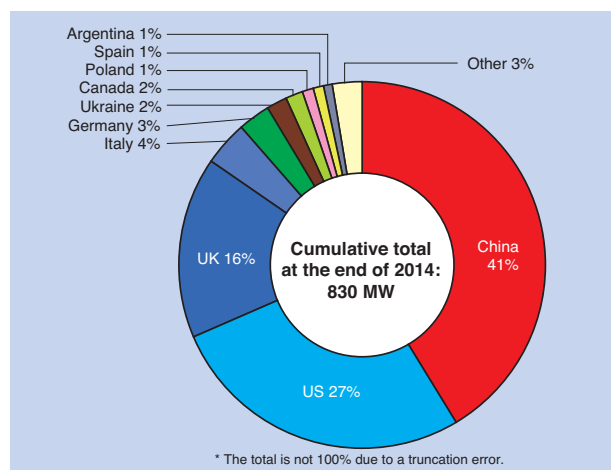


Fig. 7 Worldwide total installed capacity of small wind turbines <sup>5)</sup>

As shown in Fig. 8<sup>6)</sup>, among 327 small wind turbine manufactures in the world, 74%, which represents 242 companies, manufacture horizontal axis type turbines, 18% or 60 companies manufacture vertical axis type turbines, and 6% or 19 companies manufacture both horizontal and vertical axis type wind turbines. There are no vertical axis type wind turbines for large-scale production. Mechanically, it is more difficult to produce vertical axis type wind turbines compared to horizontal axis type as mentioned later. Therefore, it is noteworthy that the vertical axis type wind turbines are produced in a certain quantity for small-scale wind turbines.

The scope of applications for small wind turbines are as follows:

- Power source for residential use
- Commercial/factory power source
- Power source for fishing boats and leisure boats
- Hybrid power generation with solar batteries, etc.
- Power source for cattle farm, farmland, and remote islands, etc.
- Mobile power source for excursions
- Power for water pumps
- Power source for water desalination and purification
- Power source for remote monitoring
- Material for education/research purposes
- Power source for communication equipment

Promoting small wind turbines requires "cost reduction," "policy," "standard and certification", and "careful examination of wind conditions." The installation cost of small wind turbines is \$6,230/kW in the U.S. and \$1,900/kW in China. In the UK, the cost is \$6,181/kW for 1.5kW to 15kW and \$4,876 for 15 kW to 100 kW<sup>5)</sup>. In spite of efforts for cost reduction by small wind turbine manufacturers, expansion of the market is required for cost reduction; therefore the role of policy

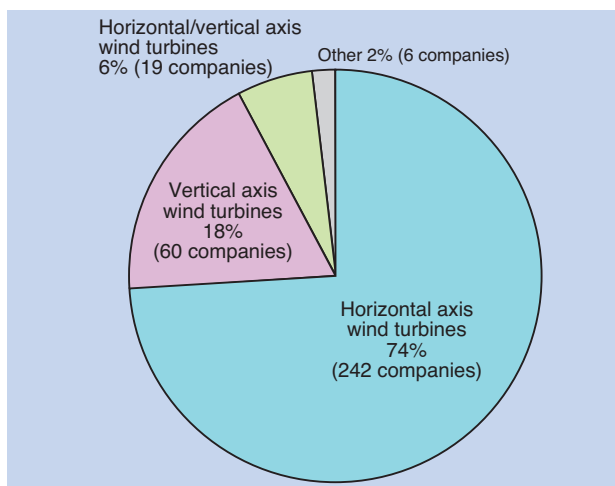


Fig. 8 Orientation by worldwide small wind turbine manufacturers<sup>6)</sup>

and support is significant.

In many countries, there are policies supporting promotion of small wind turbines. Since feed-in tariffs and purchasing of surplus electricity programs, which are also being introduced in Japan, are enabling revenue based on the generated power, good profit can be achieved if reliable small wind turbines are installed at the sites with favorable wind conditions. On the other hand, support such as favorable tax systems and subsidies of installation costs only provide help for the hardware of small wind turbines when installed, regardless of whether they produce power or not. Therefore, their contribution for sound development of the small wind turbine industry is small.

For sound development of the small wind turbine market, it is required to increase adoption of reliable small wind turbines. The roles that standardization and certification can play are significant for that. The process of standardization is in good progress as IEC 61400-2 for design requirements for small wind turbines, IEC 61400-12-1 for power performance measurement, and IEC 61400-11 for acoustic noise measurement are already established and test and certification organizations in different countries have adopted them. Since various technologies associated with small wind turbines are making progress every day, the International Energy Agency (IEA) Wind Task 27 is engaged in international joint research with information exchange for pre-standard research and development in different countries.

The wind condition maps addressed regarding large wind turbines have already been created in many countries. They have examined wind conditions at the height of 50m or more from the ground. However, as the small wind turbines are installed at the height of 30m from the ground, the wind condition maps for large wind turbines are not sufficient. The forecast of wind conditions is particularly difficult since there are many obstacles that disrupt wind flow in areas closer to the ground, such as buildings and trees. Therefore, research for understanding the characteristics of local wind behavior and prediction is indispensable in order to increase power output and adoption rate of small wind turbines.

### 2. 3 Trend of the domestic wind turbine industry

The wind turbine industry has large supporting industries similar to the automobile industry. A large wind turbine consists of around 10,000 components and its technological and economical ripple effects are as significant as the automobile industry. However, since the related areas are so widespread into the mechanical, electrical, chemical, civil engineering fields, etc., no clear industry picture has been captured in

Japan. On the other hand, promotion of wind turbine power generation related industries is being considered from the viewpoint of improving global environment problems and promoting environmental industries by green innovation, etc. The Japan Society of Industrial Machinery Manufacturers is conducting research on the wind turbine related machinery industry in order to understand the actual industrial status, such as the current activities in manufacturing of wind turbine related machinery industries, and contribute to the promotion of building infrastructure of a new industry<sup>7)</sup>. This research group consists of the members of wind power generation related businesses, related industrial associations, and academic experts and analyzes correlation of various businesses, studies research statistical methods on production, etc., analyzes industry for production, export, etc. and studies industrial promotion policy. Until now, Japanese wind power related businesses have been developing business on their own; however, this initiative is research to precede efforts by the nation for entry into an ever growing global market, and the neighboring Chinese market which has become the largest in the world. In the past few years, new introduction and revenue of the wind turbine industry in the Japanese domestic market have shown decreasing trend; however, revenue started to increase from 2014 and wind turbine and component manufacturers are expecting the global market to increase 1.5 times and the domestic market to increase 1.6 times in 2020 compared to the market size in 2015.

### 3. Wind power generation technologies

#### 3.1 Mechanism and classification of wind turbines

Wind turbines are categorized into horizontal axis and vertical axis types. As shown in Fig. 9, the centrifugal force from rotation acts on the blades as tensile force with horizontal axis wind turbines, in contrast, the centrifugal force acts as bending moment on the blades in case of the vertical axis type wind turbines as shown in Fig. 10. Since a long object such as a blade is more susceptible to bending than tensile force, vertical axis type wind turbines are more affected by centrifugal force on the blades. In addition, the rotation speed of the blades tends to be slower as they become larger, for example, a few to tens of rotations per minute; therefore, their own weight gives more impact to the overall load than centrifugal force. In contrast, small wind turbines tend to experience hundreds to thousands of rotations per minute; therefore, centrifugal force affects more on the load of the blades.

Furthermore, as shown in Fig. 11, considering incoming wind to horizontal axis wind turbines, the wind

load acting on a blade is the same during rotation regardless of the azimuth angle (rotating direction position); therefore, the torque acting on the blades is constant.

On the other hand, as shown in Fig. 12, blades of a vertical axis type wind turbine receive both strong and

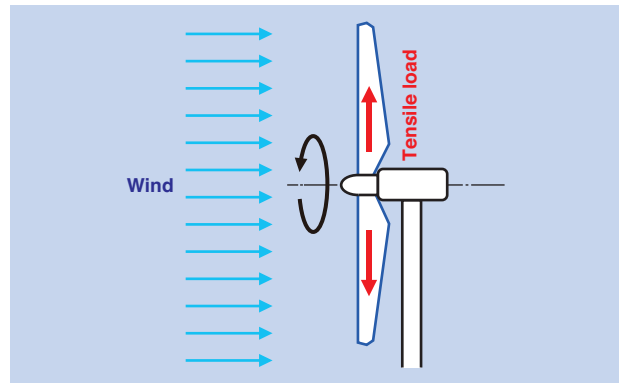


Fig. 9 Load acting on blade of horizontal axis wind turbine by rotor rotation

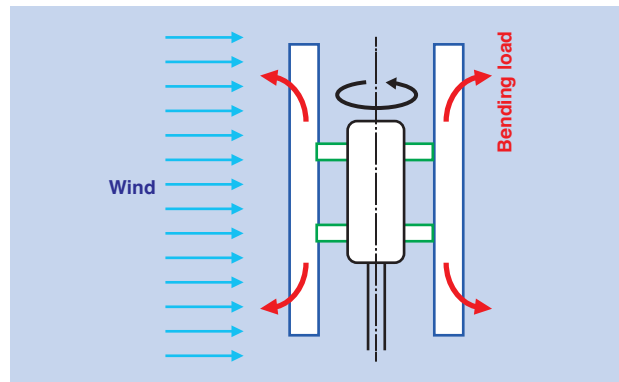


Fig. 10 Load acting on blade of vertical axis wind turbine by rotor rotation

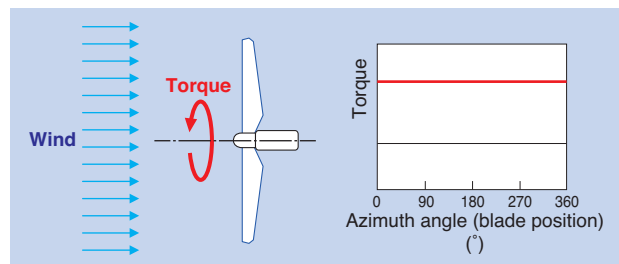


Fig. 11 Torque acting on blade of horizontal axis wind turbine

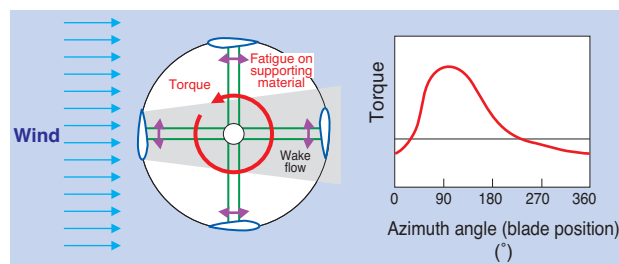


Fig. 12 Torque acting on blade of vertical axis wind turbine

weak winds during rotation, as the downwind blade goes through the wind that is slowed by the upwind blade (wake flow). This means that the main shaft and supporting material experience greater fatigue as the torque changes during rotation in the case of vertical axis type wind turbines. Since the natural wind is not constant, blades of horizontal axis wind turbines experience fatigue; however, the fatigue of vertical axis wind turbines is greater than that of horizontal axis wind turbines due to the impact of wake flow.

### 3. 2 Design standards of wind turbines

Design standards for wind turbines are established by the International Electrical Commission (IEC). As shown in **Table 1**, IEC61400-1<sup>8)</sup> for on-shore large wind turbines, IEC61400-2<sup>9)</sup> for small wind turbines, IEC61400-3<sup>10)</sup> for offshore wind turbines are established, in addition to other standards for components of wind turbines.

The best known standard, IEC61400-1 for on-shore large wind turbines, is classified into class I, II and III depending on the wind speed (from fast to slow) considering the different wind characteristics of the installation sites, and category A, B and C, for each of the wind speed class, depending on the turbulence (from large to small), as shown in **Table 2**. Therefore, there are 9 wind design specifications, i.e. 3 wind speed classes x 3 turbulence categories. In addition, a special class S is defined for sites where the conditions exceed class I and category A, requiring

**Table 1** Wind turbine standards by International Electrical Commission

International Electrical Commission (IEC)	Corresponding domestic standards (JIS)
IEC 61400-1: (Onshore) wind turbine design requirements	JIS C1400-1
IEC 61400-2: Small wind turbine design requirements	JIS C1400-2
IEC 61400-3: Offshore wind turbine design requirements	JIS C1400-3
Additionally, several standards are specified on noise measurement methods, performance test methods, power quality, certification, protection from lightning, blade load test methods, etc.	

**Table 2** Large wind turbine class by IEC 61400-1 (Note: Class T and category A+ are expected to be added to edition 4.0)

Wind turbine class	I	II	III	T*	S
Reference wind speed $V_{ref}$ (m/s) (10 minute average reference wind speed)	50	42.5	37.5	57	Value specified by designer
Average wind velocity $V_{ave}$ (m/s) (annual average wind speed)	10	8.5	7.5	10, 8.5, 7.5	
Turbulence category $I_{ref}$ (expected turbulence strength at wind speed of 15m/s)	A+*	0.18			
	A	0.16			
	B	0.14			
	C	0.12			

(\*specifies wind characteristics to be added in edition 4)

the designer to establish specific wind conditions. These standards are subject to review every few years to cope with the progress of wind turbine technologies incorporating new data and insights as they are revised.

On the other hand, the standard for small wind turbines, IEC61400-2, is also classified into similar classes as shown in **Table 3**; however, since the small wind turbines are often installed in the areas with low wind speed, class IV is added for lower wind speed. Considering the fact that the small wind turbines are low and usually installed in the areas with larger turbulence because of the buildings and trees, the turbulence category is set to 0.18, which is larger than those for large wind turbines.

**Table 3** Small wind turbine class by IEC 61400-2

Wind turbine class	I	II	III	IV	S
Reference wind speed $V_{ref}$ (m/s) (10 minute average reference wind speed)	50	42.5	37.5	30	Value specified by designer
Average wind velocity $V_{ave}$ (m/s) (annual average wind speed)	10	8.5	7.5	6	
Turbulence category $I_{ref}$ (nondimensional characteristic value of turbulence strength at wind speed of 15m/s)	0.18				

## 4. Technology for large wind turbines

**Fig. 13** shows the components of large wind turbines. The wind energy is converted into rotational energy by the blades and into electricity by the step-up gears and generator inside the nacelle (machine room).

### 4. 1 Wind turbines that address severe wind characteristics

In Europe, favorable sites for large wind turbines, that is, flat with good wind conditions, are already saturated with wind turbines and therefore, they are installed in more difficult sites such as mountainous

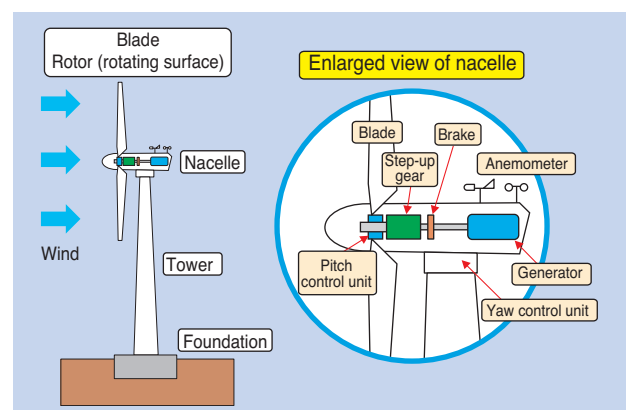


**Fig. 13** Components of large horizontal axis wind turbine

areas and offshore locations.

The challenges of installing wind turbines in complex topography such as mountainous areas include how to withstand fatigue produced in the wind turbines due to strong wind and turbulence and how to increase generated power in the midst of turbulent wind. Particularly in Japan, it is important to determine how to prevent damage due to the extreme load on wind turbines caused by typhoons. In the past, it was understood that considering the impact of turbulence due to complex topology and typhoons on wind turbines was unique to Japan. However, this is becoming a common challenge throughout the world as there are areas of strong turbulence such as the Pacific-rim and Mediterranean coasts, as well as apparent extreme wind cases caused by tornadoes and cyclones. Conventional wind turbine design requirements did not specify special wind conditions and strong turbulence such as typhoons. IEC 61400-1 ed. 4, which is soon to be published, is expected to include tropical storm wind class T which withstands strong wind from typhoons, and high turbulence category A+ which withstands strong turbulence from complex topography in mountainous areas, based on the proposal from Japan.

#### 4.2 Offshore wind turbines

The advantage of offshore wind turbines is to be able to use faster and less turbulent wind than on land; however, because of the high cost of foundations, transmission lines and maintenance, large wind turbines are used to increase unit output. Additionally, "wind farms" are being created by installing many wind turbines in one location to pursue economies of scale from large-scale projects.

Offshore wind turbines are affected by wind load as well as wave load. Therefore, traditional strength design considers the total load by simply adding wind and wave loads together. However, this method may create excessive safety factors; therefore, current design methods explore optimum load evaluation by coupled analysis of wind and wave loads. Japan also has some offshore wind turbine installations such as a 2MW turbine along the coast of Kamisu-shi, Ibaraki Prefecture, owned by a private company, and full-scale offshore wind turbines off Choshi-shi, Chiba Prefecture and Hibikinada, Kitakyushu-shi from demonstration tests by New Energy and Industrial Technology Development Organization (NEDO).

Since evolution of the technology of offshore wind turbines is significant, IEC 61400-3 for design requirements of offshore wind turbines published in 2009 is already under review. The current offshore wind turbine design standard is specified based on

wave data of the North Sea. However, the wave characteristics in the Pacific-rim, including Japan, are different. In addition, Japan has a rich database of wave data accumulated over the years, so Japan is proposing adoption of such data during the review of the IEC standard. Inclusion of proposals from Japan in the international standards is important for Japanese wind turbines to be adopted in the global market.

In addition, "floating wind turbines," which are offshore wind turbines floating in the sea, are recently drawing broad attention. "Floating wind turbines" have been considered as technology of the distant future; however, the start of a demonstration test of 2MW class floating wind turbines by Norway in 2009 instantly captured world attention. Japan is also conducting world-leading demonstration tests of floating wind turbines, namely, 2MW floating wind turbines in the Goto Islands, and 3 types of floating wind turbines such as 2MW, 5MW, and 7MW off Fukushima. The bottom mounted offshore wind turbines were the result of cooperation between the rotational machine and civil engineering of marine structure construction. The floating wind turbines are the result of cooperation between the wind turbines and shipbuilding technology. Therefore, realization of floating wind turbines is a new technological stage in the history of wind turbines.

With this trend in the background, wind turbines are becoming larger and larger. The largest wind turbine in the world is installed offshore from Fukushima Prefecture, as shown in [Fig. 14](#), with 167m of diameter and 7MW of rated output and the height of the upper tip of the blade at 189 m. Future wind turbines are expected to become even larger and various countries are conducting research of the reference wind turbine concept of over 10MW (diameter of 200m). In Japan, NEDO also presented 10MW reference wind turbines in the research of wind turbines of over 10MW <sup>11)</sup>.

The concept that supports ultra large wind turbines includes reduction of the number of blades from 3 to 2, adoption of downwind rotor position from upwind, compact and lightweight drive trains (a set of drive equipment including step-up gears and a generator), etc.

The current mainstream 3-blade wind turbines have advantages of relatively small load variance and a visually acceptable design. On the other hand, 2-blade wind turbines make it possible to reduce torque and attain more compact drive train by increasing rotation speed, thus, achieving cost reduction.

Most of the current wind turbines are designed with the upwind method in which the rotor is positioned upstream of the tower as shown in [Fig. 15](#); only a few

models adopt the downwind method. It seems the downwind method is more logical when considering the weathercock effect; however, the downwind method creates fatigue loading as the tower blocks the wind and the blades go through the lower speed wake flow. Therefore, most of the large wind turbines adopt the upwind method where the nacelle is forced to face upwind by the yaw control system. However, when it comes to ultra large wind turbines, the blades may be deflected by the wind load and hit the tower; therefore, the downwind method is considered to be more favorable.

For cost reduction, it is essential to reduce the weight of the wind turbine; therefore, a lightweight

drive train, which accounts for a large portion of the turbine weight, is required. The current mainstream large wind turbines of a few MW adopt high speed drive trains, where rotor rotation of several tens of rpm is increased by approximately 100 times through step-up gears and transmitted to the generator. However, step-up gears of a high speed-up ratio often give trouble; therefore, direct drive trains, where a multi-polar generator is adopted instead of step-up gears, may also be used. Since the direct drive train has its own shortfalls, such as difficulty of manufacturing and cost for rare earth permanent magnets, future wind turbines over 10MW will probably adopt mid-speed drive trains combining step-up gears with an appropriate speed up ratio and multi-polar generators with an appropriate number of poles.

### 4.3 Peripheral equipment of wind turbines

In addition to the technologies of large wind turbines themselves, various technologies are being studied for increasing adoption rates and preventing failures. When wind turbines become large, each component becomes large as well, making it difficult to repair. Especially for offshore wind turbines, it is important to prevent failure because of the limited access due to the weather conditions and difficult repair work in the sea. The vibration and temperature of the main components have been traditionally monitored by the Supervisory Control and Data Acquisition (SCADA) system; however these are mainly used for stopping operation in emergencies or abnormal conditions. Therefore, research of the Condition Monitoring System (CSM), for more sophisticated supervisory control than SCADA, is underway to prevent trouble from occurring. In addition, wind turbines use feedback control as they adopt pitch control by monitoring wind speed and generated power. However, the generated power may increase if feed-forward control is achieved by forecasting the incoming wind to wind turbines. Therefore, research for controlling operation by measuring upstream wind with riders (wind measurement equipment using laser) installed on the nacelle is also underway. Although various riders dedicated for wind turbines have already been developed, technology to use the upstream wind data for controlling operation of wind turbines is still under development.



**Fig. 14** Largest-diameter wind turbine in world (diameter: 167 m, rated power: 7 MW, height of blade top: 189 m Courtesy : Toru Nagao)

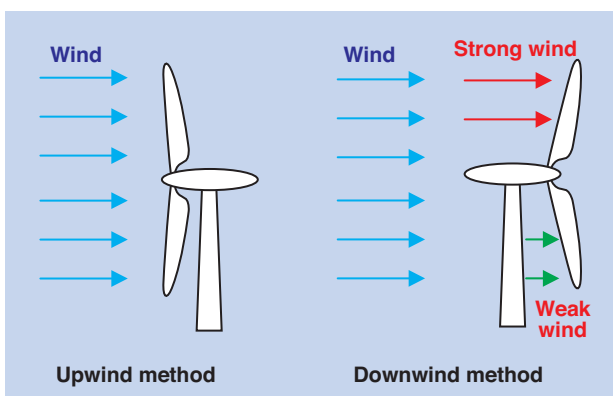


**Fig. 15** Upwind turbine and downwind turbine

## 5. Technology for small wind turbines

In general, small wind turbines are not equipped with pitch control units or step-up gears since space for storing components is limited. Also, no yaw control units are equipped for wind direction control, only adopting free-yaw control which passively uses wind load.

### 5.1 Value of small wind turbines

Large wind turbines require sufficiently large sites for installation. Therefore, they are often installed in remote areas far from populated urban areas. However, since large demand comes from urban areas, electric power generated by wind turbines in remote areas is required to be transmitted to the consumption areas by transmission lines. Therefore, from the standpoint of producing energy on-site at the consumption areas, it is more desirable to install wind turbines in urban areas. In addition, since the power grid is weak in isolated islands and settlements, it is desirable to generate power in those regions from an energy security standpoint, even if installation of large wind turbines is difficult. Due to these circumstances, it is expected that small to mid-size wind turbines will be introduced in urban areas, and isolated islands and settlements, as a "distributed power source" with adequate capacity for the particular demand of the region. Especially in the U.S., where large areas adequate for installation of large wind turbines with good wind conditions are mostly located in the central regions of the North American continent, and the large demand is concentrated in the coastal areas, the cost of long transmission lines is an issue. Therefore, the American Wind Energy Association has been focused on the introduction of small wind turbines for on-site power generation. Also in Japan, the purchase price of feed-in tariffs for electricity generated by small wind turbines is set at the highest among all renewable energies in order to promote them.

The cost of small wind turbines per output is high compared with large wind turbines; therefore, cost reduction is the next challenge. In addition, labeling programs which indicate power capacity, noise level, tolerance (wind turbine class), etc., are being adopted globally, so that users can select their most desired model from a diverse line-up of small wind turbines. Also in Japan, Nippon Kaiji Kyokai is offering a certification program for small wind turbines to ensure their safety and reliability, as feed-in tariff programs started in 2012.

### 5.2 Technology challenges for small wind turbines

Since small wind turbines are not just the miniaturization of large wind turbines, they have their own technology challenges.

Large wind turbines are equipped with pitch control units for changing blade angles according to the wind speed. When large wind turbines stop operation, the pitch angle of the blades becomes almost 90 degrees to completely bypass the wind to stop the rotor rotation. When the wind starts, the blades gradually start opening with the pitch angle changing from 90 degrees toward 0 degrees, and the rotor starts rotating with the wind. When the wind speed is relatively low, the pitch angle is set to almost 0 degrees, enlarging the wind reception area of the blades to increase the generated power. When the wind speed exceeds the rated power of the generator, the pitch angle is adjusted to gradually bypass the wind in order to maintain the rated output. When the wind speed exceeds the design limit, the pitch angle is set to almost 90 degrees to completely bypass the wind and the turbine stops operating.

On the other hand, small wind turbines are usually not equipped with pitch control because of the high cost and lack of space for incorporating the pitch control unit. Therefore, the pitch angle is fixed to 0 degrees. With a pitch angle of 0 degrees, activation of wind turbines is difficult even when the wind starts blowing, as the blades lose momentum. Therefore, lighter blades and generators with small rotational resistance are desirable. In terms of lighter blades, the mainstream materials for large wind turbine blades are composite materials such as fiber glass reinforced plastics for extending fatigue life. However, various materials such as metal, composites, wood, etc., are used for small wind turbines, not standardized materials. With respect to generators, those with the smallest possible starting torque are desirable to improve the starting characteristics; however, permanent magnet type synchronous generators are often used, which present a cogging problem. Small wind turbine manufacturers are manufacturing those generators internally, and there are no general purpose generators for small wind turbines addressed to market expansion. Comparing the dimensional ratio of small wind turbines and large wind turbines, the weight of blades and starting torque of generators for current small wind turbines are significantly large. Therefore, it can be assumed that cost reduction of small wind turbines will be achieved when lightweight and high performance components become available through volume efficiency along with the expansion of the market. In addition, it is difficult to stop operation of small wind turbines with the fixed pitch angle of 0 degrees when strong wind is present. Therefore, small wind turbines often use braking with load resistance in addition to short braking of the generators. In addition to these brakes, horizontal axis wind turbines may use furling control, which is to direct a wind turbine sideways, and vertical axis wind turbines

may use mechanical brakes, as well.

Natural wind contains turbulence of variable duration. Because of large rotor inertia, large wind turbines absorb variance of wind load against high frequency turbulence, such as instant wind speed change, only to respond with rotation against wind turbulence of a long time scale. On the other hand, small wind turbines have small rotor inertia; therefore, the rotation changes even with instant wind speed change. The rotation rapidly becomes high with sudden high wind speed, and conversely, the rotation rapidly becomes low or stops with sudden low wind speed. As a result, in an environment where wind speed is low with significant variation, small wind turbines are unstable, repeating power generation and no power generation. Lighter blades are desirable from the standpoint of starting characteristics; however, relatively heavier blades are desirable from the standpoint of stable output. This is a trade-off relation. In contrast, even if vertical axis wind turbines have a lower output coefficient, since they have higher rotor inertia and their operation does not depend on the wind direction, the output is more stable.

The use of small wind turbines is categorized into an independent power source method, separated from the grid and grid connection methods, connected to the power system. In the rural regions where only a small amount of power is required, the independent power source method is used with small wind turbines and solar power generation.

For example, they are used for streetlights in rural areas and as the power source for radio wave relay stations, where the cost of installing transmission lines is excessive. In these cases, the power generated by small wind turbines is stored in batteries before use. On the other hand, if connected to the grid, power generated by small wind turbines can be sold to power companies by feed-in tariff programs. However, there are no certified power conditioners for small wind turbines, which are indispensable in the connection of small wind turbines and the grid, making the procedure of grid connection complicated. For increased adoption of small wind turbines, certified power conditioners are required, such as the case for solar-light power generation. The grid connection requirements for small wind turbines are currently being discussed at NEDO.

### 5.3 Standardization of small wind turbines

Large wind turbines are subject to the design requirements of IEC 61400-1 under the aeroelastic model considering the aerodynamics of wind load and elasticity of the structure. On the other hand, small wind turbines are allowed to use simplified load models, by IEC 61400-2, which uses simplified design procedures, in addition to the aeroelastic model.

The simplified load model allows easy calculation assuming the running rotation speed, etc. for small wind turbines; however, IEC 61400-2 only specifies the simplified load model for small horizontal axis wind turbines, not for small vertical axis wind turbines. Globally, horizontal axis wind turbines are the mainstream; however, in Japan, there are many vertical axis wind turbines installed; therefore, creation of design guidelines for small vertical wind turbines is urgently required. With these situations in the background, a research for building the world first simplified load model for vertical axis wind turbines was conducted in Japan<sup>12, 13)</sup>, and it was specified as the standard by the Japan Small Wind Turbines Association<sup>14)</sup>.

However, while the ultimate load safety factor in the aeroelastic model is set to 1.35 since the precise design is assumed in the model, the safety factor for the simplified load model is set at 3.0, as the model allows for a simple design. Many small wind turbines are designed using the simplified model with a high safety factor, which leads to higher cost.

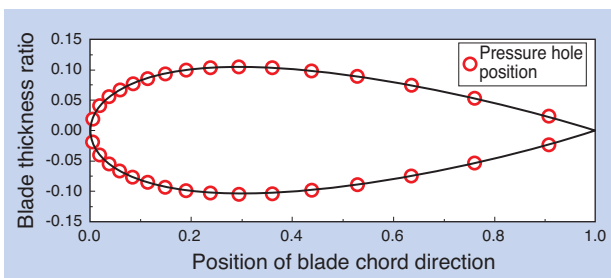
For horizontal axis wind turbines, the general-purpose aeroelastic model is built, which can be used for large and small wind turbines. However, there are no aeroelastic models for vertical axis wind turbines. Therefore, an aeroelastic model for vertical axis wind turbines is under development, aiming for cost reduction in vertical axis wind turbines<sup>15)</sup>. In order to build an aeroelastic model, it is necessary to compare and evaluate load acting on the actual vertical axis wind turbine and load calculated by the model. Therefore, load acting on the vertical axis wind turbine is measured in detail, by wind tunnel experiments, as shown in Fig. 16. Since the rotation of vertical axis wind turbines is produced by the blades, a pressure measurement hole is created on the rotating blade surface, as shown in



Fig. 16 Wind tunnel experiment of vertical axis wind turbine (Mie University Large Wind Tunnel)

**Fig. 17**, and the static pressure on the blade surface is measured by the pressure sensor installed on the rotating system. An example of the measured pressure distribution is shown in **Fig. 18**. It can be seen that the pressure distribution varies depending on the azimuth angle of the blades. By integrating the area enclosed by this pressure distribution and calculating the rotational direction component, the rotational force that acts on the blades can be calculated as shown in **Fig. 19**. This figure reveals that the rotational force of running vertical axis wind turbines can be changed by the azimuth angle of the blades, as well as by the circumferential speed ratio  $\lambda$  (ratio of rotor

circumferential speed to wind speed). In addition, as shown in **Fig. 20**, behavior such as stalling can be learned by measuring flow around the blades of the vertical axis wind turbines during operation, improving accuracy of the aeroelastic model. After analyzing the performance of vertical axis wind turbines and the details of load from these wind tunnel experiments, final evaluation of the aeroelastic model will be performed to consider the impact of unsteady wind on performance and load of the vertical axis wind turbines. We believe that, through these studies, the aeroelastic model for vertical axis wind turbines will be developed and low-cost and highly reliable vertical axis wind turbines can be designed.



**Fig. 17** Pressure taps on blade of vertical axis wind turbine

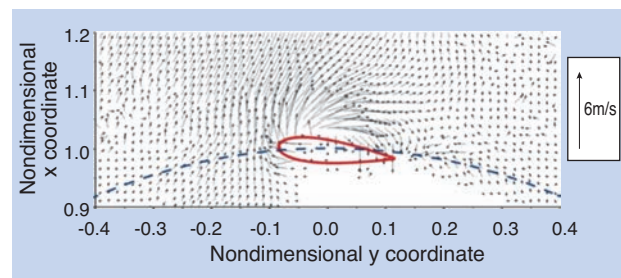


**Fig. 20** Flow around rotating blade of vertical axis wind turbine

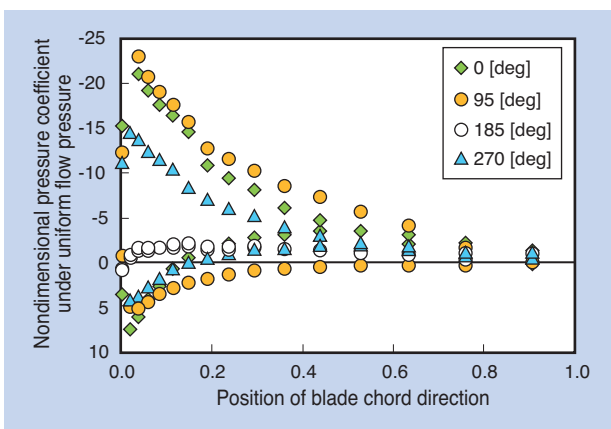


**Fig. 18** Pressure distribution on blade of vertical axis wind turbine in operation

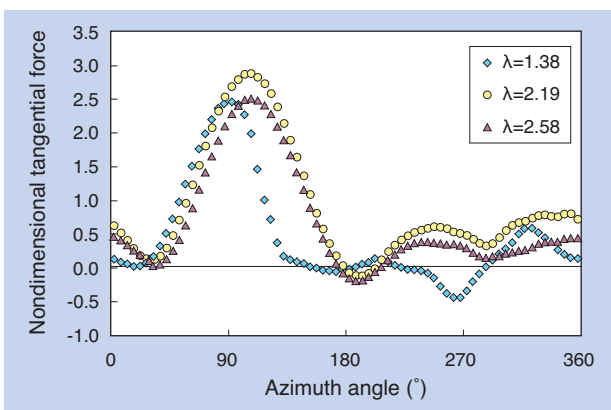


**Fig. 19** Tangential force on blade of vertical axis wind turbine

## 6. Summary

Large wind turbines are becoming ultra large as installation sites move from onshore to offshore, reaching a diameter of 200m and output of over 10MW.

The generated power is proportional to the square of the rotor diameter and the cost of the wind turbine increases proportional to the cube of the rotor diameter; therefore, the cost per generated power becomes higher as the size increases. Therefore, progress in NTN's practical research related to the Condition Monitoring System (CMS) aimed for improved availability and prevention of failure is highly expected. In addition, some innovative technology development is also expected, for example, an experimental study of airborne wind turbines is underway, where only a propeller is floating in the air, suspended by wires, eliminating the tower which accounts for a large proportion of the wind turbine cost.

On the other hand, small wind turbines, which are deployed in different sites and applications from large wind turbines, also face the challenge of cost reduction for increased introduction. Therefore, the industry is addressing adoption of common components for small wind turbines and a certification program of equipment for grid connection. In addition,

it is expected that a global standard for aeroelastic analysis codes will be established for small wind turbines also, like their large counterparts, which enables design of low-cost small wind turbines by reducing excessive safety factors while ensuring reliability. This should contribute to the wide adoption of small wind turbines.

## References

- 1) Global Wind Energy Council, Global Wind Report Annual Market Update 2015, (2015) pp.8-19.
- 2) Situation of wind power generation in Japan, New Energy and Industrial Technology Development Organization (NEDO) home page <http://www.nedo.go.jp/library/fuuryoku/state/1-01.html> (accessed on 6/25/2016)
- 3) Cumulative installed base of wind turbines as of the end of 2015, Japan Wind Power Association (JWPA) home page <http://log.jwpa.jp/content/0000289449.html> (accessed on 6/25/2016)
- 4) Japan Wind Power Association, JWPA Wind Vision Report - Aiming for truly reliable power supply - , Japan Wind Power Association (2016) p.3.
- 5) Pitteloud, J.D. and Gsanger, S., Small Wind World Report 2016, Summary, World Wind Energy Association (2016).
- 6) Gsanger, S. and Pitteloud, J., Small Wind World Report 2014, Summary, World Wind Energy Association, (2014).
- 7) Research report on wind power generation related machinery industry, March, 2016, Research Committee on Wind Power Generation Related Machinery Industry, The Japan Society of Industrial Machinery Manufacturers (2016) pp.3-47.
- 8) International Electrical Commission, Wind Turbines – Part 1: Design requirements, Edition 3.0 Amendment 1, (2010).
- 9) International Electrical Commission, Wind Turbines – Part 2: Design requirements for small wind turbines, Edition 3.0, (2013).
- 10) International Electrical Commission, Wind Turbines – Part 3: Design requirements for offshore wind turbines, Edition 1.0, (2009).
- 11) New Energy and Industrial Technology Development Organization, Achievement Report on Natural Energy (including Wind Energy) Technology Research and Development/Wind Power Generation Advanced Practical Research and Development/Research of Wind Turbine over 10 MW (component technology) FY2013 to FY2014, New Energy and Industrial Technology Development Organization (NEDO), (2015) pp.3\_1-3\_29.
- 12) Takao Maeda, and five others, Wind tunnel experiment on flow and fluid force of straight-bladed vertical axis wind turbine, turbo machine, 42 (2), (2014) pp.100-106.
- 13) Maeda, T., Kamada, Y., Murata, J., et al., Measurements of flow field and pressure distribution of straight-bladed vertical axis wind turbine, Proceedings of European Wind Energy Association Conference 2013, Web site, (2013) 8p.
- 14) Japan Small Wind Turbines Association, JSWTA 0001 Standard on performance and safety of small wind turbines, ed. 2, (2013) pp.9-17.
- 15) Junsuke Murata, Takao Maeda, Yasunari Kamada, Tatsuhiko Ogasawara, Kento Shimizu, Development and Validation of Analysis Method for Straight-Bladed VAWT, Proceedings of the 37th Wind Energy Application Symposium, (2015) pp.361-364.

### <Author biography>

#### Takao Maeda

**Professor, Doctor (Engineering) Department of Mechanical Engineering, Mie University**

1991	Doctoral course, Graduate School of Engineering, Nagoya University, Mechanical Engineering and Mechanical Engineering Second Specialization, Completed
1991	Supporting staff, School of Engineering, Nagoya University
1992	Instructor, Faculty of Engineering, Mie University
1995-1996	Fellowship Researcher, TU Delft Wind Energy Institute
1997	Assistant Professor, Faculty of Engineering, Mie University
2005	Professor, Faculty of Engineering, Mie University
2006	Professor, Graduate School of Engineering, Mie University
2006-2007	Head of Mie University Satellite Venture Business Laboratory
2009	to present Head of Energy and Environmental Engineering Research Center, Mie University

#### [Specialty]

Fluid engineering, fluid machinery, wind turbine engineering

#### [Academic society and committee affiliations]

Japan Wind Energy Association: Director (2005-), Program Committee Chairperson (2006-), Vice President (2014-)

Turbomachinery Society of Japan: Director (2011-2012)

The Japan Society of Industrial Machinery Manufacturers: Research Committee on Wind Power Generation Related Machinery Industry, Chairperson (2010-)

The Japan Electrical Manufacturers' Association: Wind Power Generation System Standardization Committee, Vice Chair (2013-)

New Energy Foundation: New Energy Industrial Conference, Wind Power Committee, Vice Chair (2014-)

# Green Energy Business and Green Power Park

Natsuhiko MORI\*



From the point of view of energy supplying and environmental protection, the renewable energy is the ultimate one to realize a sustainable society.

"NTN100", NTN's medium-term management plan which started in April 2015, has been promoting the business development of a new area, "Energy Business" using the natural energy of wind and water.

This article introduces the environment surrounding Small Wind Turbines and Micro Hydro Turbines which NTN is developing, and "Green Power Park" established in April, 2016, proposing the energy recycling society with low carbon emission using the familiar power generation technology.

## 1. Introduction

Since the Industrial Revolution which started in the 18th century in England, humans have been using underground resources such as carbon, oil, and nuclear fuel, converting them into energy for driving civilization and increasing consumption of underground resources.

As a result of the massive consumption of these underground resources, concerns have been raised about the ongoing stable supply of energy and environmental destruction in recent years.

Energy such as solar light, solar heat, hydraulic power, wind power, biomass and geothermal power is called "natural energy" and can be renewed in a relatively short time, even when used. Therefore, it is effective for supplementing fossil fuels such as oil and carbon, which are currently the main energy sources in Japan.

In addition, natural energy is an excellent energy source because it emits little CO<sub>2</sub>, which can cause global warming when it is used for power generation and producing heat.

Wind power is the largest natural energy source used for electric power generation, which accounts for 2.7% of total global power generation and almost 1/2 of all natural energy (48%) (Fig. 1).

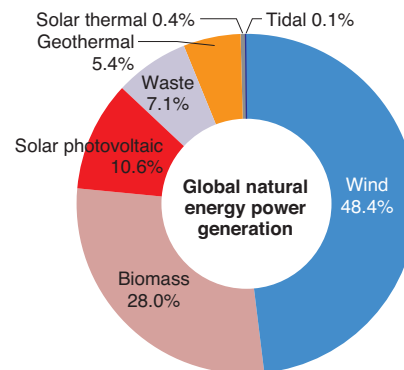


Fig. 1 Recyclable energy power generation in the world <sup>1)</sup>

## 2. Working on energy business

NTN is moving forward with business development in the following new areas in the mid-term business plan, "NTN100", which started in April, 2015 for the period until March, 2018.

- (1) Energy business (use of natural energy)
- (2) EV business (vehicle automation, safety revolution)
- (3) Robot associated business (working and living with people)
- (4) Service solution business (use of big data)

\*Senior Executive Officer and Corporate General Manager, New Product and Business Strategic Planning Headquarters

This article will discuss the environment around small wind turbines and micro hydro turbines that NTN is working on.

NTN signed an agreement for exclusive implementation of patents and designs on innovative and highly efficient blades for wind and hydro turbines in late 2014, obtaining the rights for exclusive use of those patents and designs. NTN combined knowledge accumulated in low-torque/lubrication technologies and this efficient blade technology together to advance development of products in a special project until March 2016, and established the Natural Energy Product Division on April 1, 2016 for development, launch, and broad distribution of commercial products.

This business corresponds to the above mentioned (1) Energy business, including small wind turbines and micro turbines aiming for 30 billion yen of sales by 2025.

### 3. Environment around small wind turbines and micro hydro turbines

#### 3.1 Installed base and forecast of small wind turbines

Total introduction of new wind turbines in 2015 was 433GW (Fig. 2) with only 0.1% of them being small wind turbines, generally defined as less than 100kW of output, equivalent to around 300MW per year.

Breakdown by country indicates that China accounts for the largest share, followed by the USA and UK, the top three countries accounting for the major portion of the total share. In Japan, small wind turbines are defined as less than 20kW by the Electric Utility Industry Law and Nippon Kaiji Kyokai Certification program with only 4,200kW of installed base by 2014.

The small wind turbine market includes over 100 models in many countries, which indicates that the global market for small wind turbines is still in the early development stage with an expectation for annual growth of around 20% moving forward (Fig. 3).

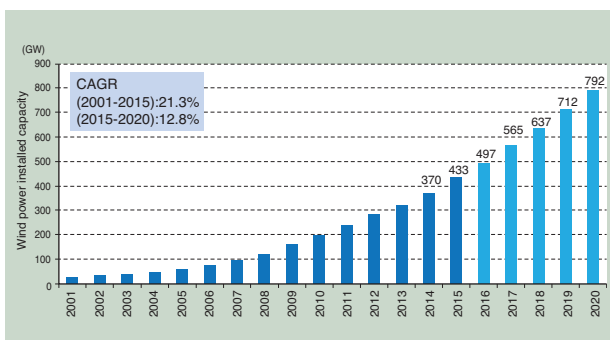


Fig. 2 Wind power installed capacity in the world <sup>1)</sup>

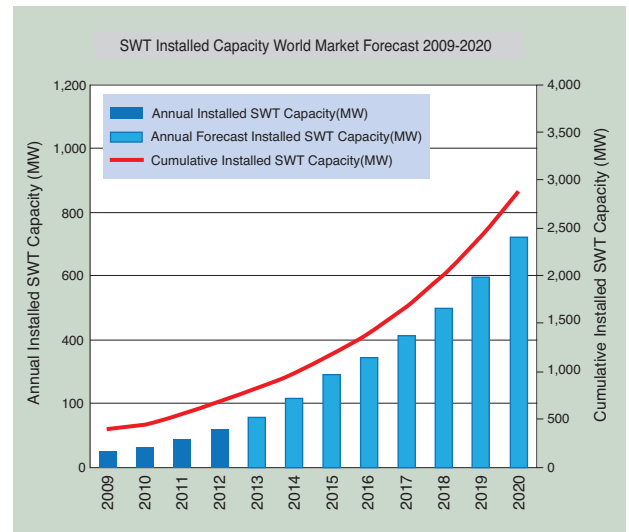


Fig. 3 SWT installed capacity world market <sup>2)</sup>

#### 3.2 Purchase price of electric power from small wind turbines in key countries

The purchase price of electric power in the U.S. is, although slightly different dependent on the regions, in the range of 16.2 to 17.2 yen/kWh and in the UK, 27.3 yen/kWh (conversion rate: 132 yen/EUR). In Japan, the purchase price from sizes less than 20kW is very high, at 55 yen/kWh, based on the feed-in tariff program (Table 1).

Table 1 Small wind feed-in tariff picking worldwide <sup>3)</sup>

Country/Region	Size Limit	EUR/kWh	Country/Region	Size Limit	EUR/kWh
Chinese Taipei	1-10kW	0.185	Japan	<20kW	0.418
Canada				≥20kW	0.167
Ontario	<10kW	0.074	Lithuania	<10kW	0.095
Nova Scotia	<50kW	0.332		10-350kW	0.092
Cyprus	<30kW	0.220	Portugal	<3.68kW	0.432
	Off-grid	0.190	Slovenia	<50kW	0.095
Greece	<50kW	0.250	Switzerland	<10kW	0.247
	>50kW	0.090	UK	<100kW	0.207
	Off-grid	0.100	USA		
Italy	1-20kW	0.285	Indiana	5-100kW	0.130
	20-200kW	0.262	Hawaii	<20kW	0.123
	0.2-1.0MW	0.146		20-100kW	0.105
Israel	<15kW	0.250	Vermont	<15kW	0.180

### 3.3 Small wind turbine market in Japan

The small wind turbine market in Japan is estimated to be around 2.2 billion yen in 2020, accounting for around 17% of the global market in monetary base (14% in unit base). The market is expected to grow 4 to 5% per year (Table 2).

**Table 2** Japan & worldwide market of small wind turbine <sup>4)</sup>  
unit: million yen, units

		Actual		Estimate	Forecast				
		2011	2012	2013	2014	2015	2016	2017	2020
Japanese market	Amount	1,300	1,500	1,700	1,800	1,800	1,800	1,900	2,200
	Units	1,700	2,000	2,300	2,500	2,600	2,600	2,740	3,200
Overseas markets	Amount	10,400	10,900	11,300	11,500	11,700	11,800	12,000	12,800
	Units	18,400	19,400	20,100	20,700	21,200	21,500	46,600	23,300

### 3.4 Application of small wind turbines for the disaster prevention field

Reflecting on the damage from recent disasters, municipalities are looking to multiple measures of protection from both structure and non-structure standpoints, drastically changing the assumption of magnitude of potential disasters.

In Kochi Prefecture, near the anticipated seismic center of the Great Nankai Trough Earthquake, evacuation towers are being built as the risk of an ultra quick tsunami is high after an earthquake hits the region, with tower construction plans at 117 sites within the prefecture (Fig. 4).

Also, a plan to install CCTV (closed circuit television) cameras for collecting information on disasters is well underway. In these disaster prevention areas, it is critical to ensure the availability of a stable and independent power supply with little



**Shimoda-Mito evacuation tower against tsunami in Shimanto City, Kochi Prefecture <sup>5)</sup>**

Second tower w/9m in height (18.6m above sea level) next to the existing tower w/6m in height  
Max. capacity: 320, Equipped with life jackets at the highest platform;  
Cost: 19.53 million yen

**Fig. 4** Evacuation tower in Kochi

effects during blackout caused by an earthquake or tsunami for activating CCTV cameras, supplying power for light at evacuation centers and cell phones, etc. Solar panels and small wind turbines are effective; however, the power output period may not be stable.

A hybrid method combining solar panels, small wind turbines and batteries is advantageous; however, due to cost, a combination of solar panels and small wind turbines may be more desirable.

### 3.5 Small hydraulic turbine market in Japan and micro hydro turbines

The installed base of small hydraulic turbines in Japan up to 2012 and the market size between 2013 and 2020 are shown in Table 3. Small hydraulic power is defined for capacity less than 1,000kW (1MW) which is subject to the RPS law <sup>(note)</sup>.

(Note) "Act on Special Measures Concerning New Energy Use by Operators of Electric Utilities" published in June 2002, which is to promote use of new energy by mandating use of electric power generated by new energy over a certain volume to utility companies.

**Table 3** Market of micro hydro turbine in Japan <sup>4)</sup>

Unit: million yen, capacity: kW

		Actual		Estimate	Forecast				
		2011	2012	2013	2014	2015	2016	2017	2020
Japanese market	Amount	1,370	1,170	2,370	2,290	1,900	1,700	1,700	1,600
	Capacity (kW)	5,220	4,450	9,050	9,140	7,740	6,850	6,800	6,600

Due to the feed-in tariff program, in particular the market of 200 to 1,000kW with a purchase price of 29 yen/kWh extended until 2014, and the proportion of the share of less than 200kW for industrial facilities with a purchase price of 34 yen/kWh is expected to increase after 2015.

There are over 10,000 sites which are adequate for small hydraulic power generation in Japan, and demand in Niigata and Gifu is high for power generation using river water. For use of agricultural water ways, Fukushima, Aichi, and Tochigi are promising. The reconstruction demand continues in the Tohoku region. Support from the Ministry of Agriculture, Forestry and Fisheries, and local governments can also be expected.

Asaka Canal in Fukushima Prefecture, originating from Lake Inawashiro, consists of many waterways that run into Abukuma River with a total length of around 50km and are used for drinking water and farmland irrigation. There are many spots adequate for small hydraulic power generation in this canal with stable flow rate; therefore, NTN is conducting demonstration projects of small hydraulic power

generation. By promoting small hydraulic power generation business, ripple effect for new business using the canal can be expected.

Small hydraulic power generation provides highly efficient energy conversion and stable power generation for 24 hours due to a stable water flow (Table 4). Conventional hydraulic power generation involves water entitlement and complex legal procedures, in addition to the high installation cost of head type hydraulic power plants. Smaller hydraulic power plants, in particular, have not been actively promoted. However, micro hydro turbines, which can be easily installed using stream water, are attracting attention from this successful demonstration project (Fig. 5, 6). For details, see [Product Introduction] "Micro Hydro Turbine."

**Table 4** Advantages & disadvantages of micro hydro turbine

<b>Advantage</b>	Much higher energy conversion efficiency compared with other power generation methods
	Higher energy density and stable power generation
	Small footprint compared with solar photovoltaic power generation
	Abundant endowments not yet developed
<b>Disadvantage</b>	Complex legal procedures such as River Act
	Limited installation sites
	Entitlements of stake holders with water use
	Low awareness



**Fig. 5** Micro hydro turbine

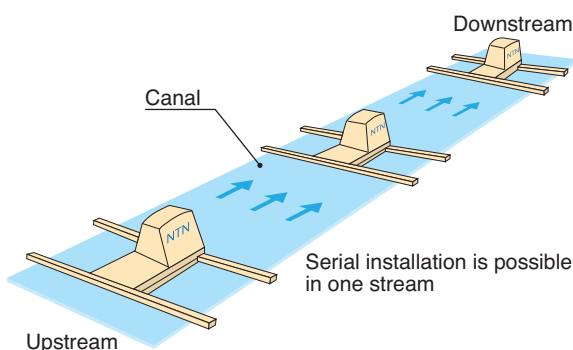


**Fig. 6** Installation of micro hydro turbine

**Overview of three major canals and potential capacity of small hydraulic power generation**

Agricultural water ways in Japan extend 400,000 km.

The length of three major canals, Asaka Canal (Fukushima prefecture), Nasu Canal (Tochigi prefecture) and Lake Biwa (Shiga and Kyoto prefectures) are 500 km, 357 km and 45 km, respectively. An overview of these three major canals and calculated potential power generation capacity from micro hydro turbines are shown in Table 5.

Assuming installation of 100kW/km (100 units of 1kW installed every 10m) in 20% of the main watercourse, the respective capacity from Asaka Canal is 1,040kW, 330kW in Nasu Canal, and 220kW in Lake Biwa Canal.

**Table 5** 3 major canals and endowments of micro hydro turbine

	Asaka Canal	Nasu Canal	Lake Biwa Canal
Region	Fukushima Prefecture	Tochigi Prefecture	Shiga and Kyoto Prefectures
Total extension	Approx. 500km	357km	45km
Main watercourse	52km	16.3km	11.1km
Branch aqueduct	96km	96km	8.4km
Endowments applicable to NTN micro hydro turbines (estimate)	1,040kW	330kW	220kW

**3. 6 Feed-in tariff program for renewable energy in Japan**

The feed-in tariff program (FIT) started on July 1, 2012 mandating utility companies to purchase electric power generated from natural energy sources (solar, wind, water, geothermal and biomass) at a price determined by the government for a certain duration (Fig. 7).

The actual certification of small wind turbines amounted to 4,500kW by the end of 2015; however, the actual approved grid connection was limited to 364kW, or 8% of certification. The progress of the actual grid connection is slow, partly due to unstable output of wind power influenced by weather conditions, which in turn affects the stable supply of the grid (Fig. 8, 9).

The ultimate energy for achieving sustainable society is natural energy. Therefore, widespread use of natural energy is desired, by technological pursuit of stable supply and resolution of cost challenges.

Wind power	20kW or more	Less than 20kW	Offshore wind power <sup>(※)</sup>
Purchase price	22 yen + tax	55 yen + tax	36 yen + tax
Purchase duration	20 years	20 years	20 years

※Access by boat, etc. is required both for installation and operation/maintenance.

Hydropower	1,000kW or more, less than 30,000kW	200kW or more, less than 1,000kW	Less than 200kW
Purchase price	24 yen + tax	29 yen + tax	34 yen + tax
Purchase duration	20 years	20 years	20 years

Small to mid-hydro turbines using existing aqueduct <sup>(※)</sup>	1,000kW or more, less than 30,000kW	2,000kW or more, less than 1,000kW	Less than 200kW
Purchase price	14 yen + tax	21 yen + tax	25 yen + tax
Purchase duration	20 years	20 years	20 years

※Upgrade of electric facility and penstock using existing installed aqueducts.

Solar photovoltaic	Less than 10kW			
	Purchase of excessive power	Dual generation/purchase of excessive power	Support of output control not required	Support of output control required
Purchase price	31yen	33 yen	25 yen	27 yen
Purchase duration	10 years		10 years	

※Device to support output control is required in the area for demand/supply control of Hokkaido, Tohoku, Hokuriku, Chugoku, Shikoku, Kyushu and Okinawa Power Companies.

Solar photovoltaic	10kW or more
Purchase price	24 yen + tax
Purchase duration	20 years

Fig. 7 IFIT purchase price in FY2016 (per 1kWh) <sup>6)</sup>

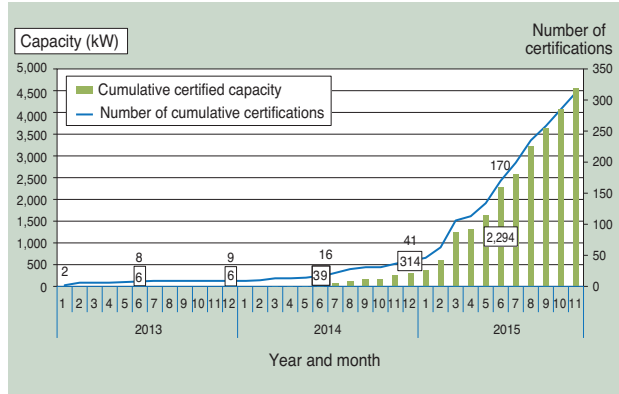


Fig. 8 Approved small wind turbine by FIT 7)

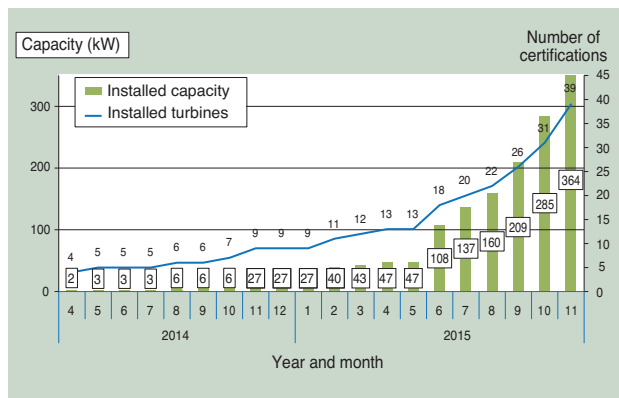


Fig. 9 SMT System interconnection result with Electric Power Co. 7)

#### 4. Introduction of Green Power Park

We have established Green Power Park, equipped with wind, water, and solar power generation devices within the Advanced Technology R&D Center site located in Kuwana City, Mie Prefecture, in an area of

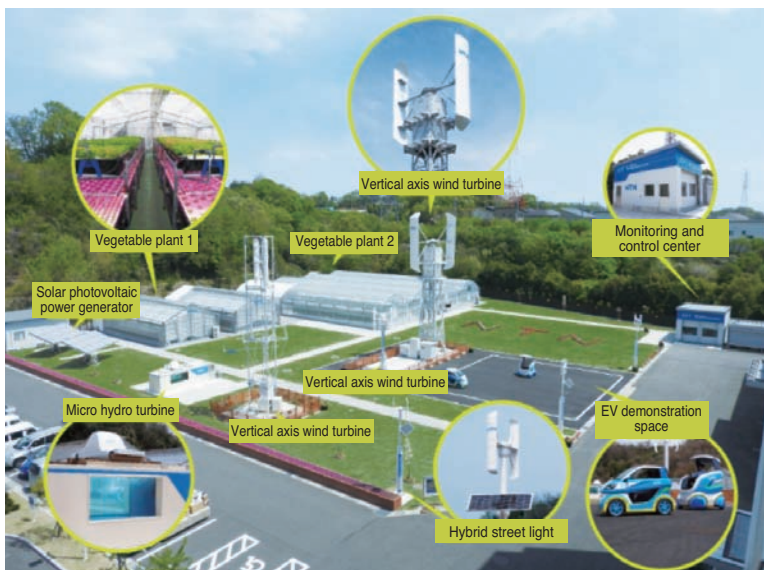


Fig. 10 Green Power Park

6,300m<sup>2</sup> (Fig. 10). There are vegetable plants and charging stations for electric vehicles, powered by electricity generated from natural energy, for demonstration of recirculation of natural energy.

Also installed are 6 small wind turbines (vertical axis wind turbines), consisting of 2kW, 4kW, and 10kW each, and 3 hybrid street lights. In addition, NTN's two in-wheel motor vehicles, Q'mo, are charged with power generated by natural energy.

Furthermore, an IoT room is provided for overseeing the power generation condition and battery charging condition of the entire park.

The park was selected as one of the sites for "2016 Junior Summit in Mie" from April 22 to 28, 2016 in Kuwana City, Mie Prefecture, and introduced as a model for low carbon and energy recirculating society without disrupting nature.

#### 4.1 Small wind power generation unit

Small wind power generation units are defined as having output of less than 20kW, which do not require major construction work and installable in narrow spaces in public parks and car parking areas. Their roles are diverse, as they can be used to supply power on isolated islands where no grid power is available, as an emergency power supply during disaster, or as clean energy for regular residential homes.

##### (1) Characteristics of vertical axis wind turbines

NTN's vertical axis wind turbines produce little wind noise due to their proprietary thick blade geometry. In addition, they can efficiently generate power with natural wind from any direction with significantly varied wind conditions (Fig. 11).



Fig. 11 10kW Wind Turbine

##### (2) Hybrid street lights

Hybrid street lights are a 0.3kW clean energy power generation system using two types of natural energy : wind and solar light (Fig. 12).

They generate power with both wind turbines and solar panels during the daytime and charge the built-in battery. They also generate power with wind turbines to light the LED lamps. The capability of generating power with both wind and solar light makes it an effective power supply for emergencies.

This can also benefit risk management devices such as cell phone charging capability and surveillance cameras.



Fig. 12 Hybrid street light

#### 4.2 Micro-hydro power turbine

Head-type hydraulic power plants, in general, require major construction for retaining water.

In contrast, micro hydro turbines are small hydraulic power generation systems capable of generating power using small water flows, such as water channels and streams, and are easy to install (Fig. 13).

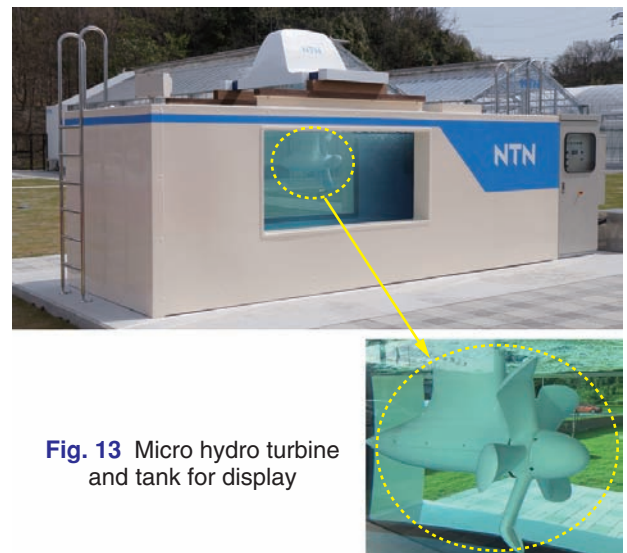


Fig. 13 Micro hydro turbine and tank for display

### 4.3 Tracking-type solar power generation

Based on the "tracking-type solar power generation" made by another manufacturer, the NTN-developed cylinder type motor driven linear module is installed (Fig.14). Adoption of ball screws for a feed screw mechanism achieved high repeat positioning accuracy and durability for use over a long period of time. In addition, application of grooves on the internal raceway of the housing, used as a linear motion guide, and adoption of rolling bearings as the guide roller made it possible to realize smooth linear motion and high rigidity.



Fig. 14 Tracking-type solar power generation

### 4.5 Q'mo

Q'mo is an electric vehicle that allows "pivot turning" and "lateral movement." This is a new-generation ultra-small electric mobility vehicle, which allows movement, such as the pivot turn not found in conventional vehicles with built-in in-wheel motors on all four wheels (Fig. 16).

"Q'mo II" with an improved operability "multi-driving system", obtained a light vehicle license plate and became the world's first electric mobility vehicle permitted to drive on public roads.



Fig. 16 Q'mo

### 4.4 Vegetable plant

Vegetable plants use natural energy within Green Power Park, supplying power for hydroponic cultivation of vegetables such as lettuces and tomatoes (Fig. 15).

We are aiming to increase yield and establish a model for sustainable recirculating of vegetable plants by efficient and systematic cultivation with no impact from natural environmental change and reduced use of power.

First vegetable plant: 300m<sup>2</sup>

Second vegetable plant: 1,000m<sup>2</sup>



Fig. 15 Vegetable plant

### 4.6 Monitoring and control center

The monitoring and control center allows efficient distribution of power from various operational conditions by monitoring and controlling power generation, storage and consumption conditions in real time on all the equipment in the Green Power Park (Fig. 17).

In addition, a display that shows real time indication of power generation and storage conditions of the entire Green Power Park are installed in the lobby of the Advanced Technology R&D Center (Fig. 18).



Fig. 17 Monitoring and control center



Fig. 18 Green Power Park monitoring display

## 5. Conclusion

Renewable natural energy, such as wind, water, and solar power, is critical for achieving a sustainable society, and more advanced utilization is required.

NTN is making contributions for achieving a low-carbon and energy recirculating society in the world through small wind turbine and micro hydro turbine.

## References

- 1) Sustainable Japan [Energy] Global installed base of wind turbines and business environment-2015 Overview-  
<http://sustainablejapan.jp/2016/05/06/wind-power-market/11154>
- 2) Small Wind World Report 2014  
<[http://uwea.com.ua/uploads/docs/SWWR\\_2014.pdf](http://uwea.com.ua/uploads/docs/SWWR_2014.pdf)> p.12.
- 3) Small Wind World Report 2014  
<[http://uwea.com.ua/uploads/docs/SWWR\\_2014.pdf](http://uwea.com.ua/uploads/docs/SWWR_2014.pdf)> p.10.
- 4) Fuji Keizai "2013 New market of electric energy system."
- 5) Referred from Shimanto City Website, Publication Shimanto April, 2013 issue,  
<http://www.city.shimanto.lg.jp/gyosei/pdf/h25/kouhou04.pdf> p.1.
- 6) Agency for Natural Resources and Energy Website  
[http://www.enecho.meti.go.jp/category/saving\\_and\\_new/saiene/kaitori/kakaku.html](http://www.enecho.meti.go.jp/category/saving_and_new/saiene/kaitori/kakaku.html)
- 7) Source for actual small wind turbine FIT certifications, and actual grid connection installed base:  
[http://www.fit.go.jp/statistics/public\\_sp.htm](http://www.fit.go.jp/statistics/public_sp.htm)

Photo of author



**Natsuhiko MORI**  
Senior Executive Officer and  
Corporate General Manager,  
New Product and Business Strategic  
Planning Headquarters

## Small Wind Turbine Generator



**Takaya ADACHI\***  
**Ryosuke KARASAWA\***

Small wind turbine as one of renewable energies has received remarkable attention and rapidly become popular due to low-initial-cost and space-saving for construction compared to large wind turbine. NTN is taking on development of the small wind turbine using our technology.

This paper describes the technology and features regarding NTN's small wind turbine products.

### 1. Introduction

Utilization of natural energy has been an urgent matter in the world from the standpoint of global warming and depletion of fossil fuels. Japan, with few natural resources, depends on other countries for the majority of energy resources, including oil. Therefore, it is imperative to improve the energy supply structure.

In addition, utilization of diverse energy sources, including natural energy, is being sought out more than ever since the experience of the Great East Japan Earthquake<sup>1)</sup>.

Hence, a feed-in tariff program was started in July, 2012 as a policy for promoting natural energy in Japan, with particular emphasis on small wind turbines with the highest purchase price of 55 yen/kWh (in the case of small wind turbines of less than 20kW).

NTN is developing highly efficient and very quiet small wind turbines for commercialization by leveraging their proprietary blades. This article introduces their characteristics and progress of their development.

### 2. About small wind turbine generators

Wind turbine generation is a power generating method which produces electric power by transmitting the rotating motion produced by the wind power to the generator. Wind that exists everywhere in nature is a typical clean energy that does not emit any CO<sub>2</sub> or waste.

The small wind turbine is defined by JIS C 1400 as a wind turbine with a swept area (area of turbine blades receiving wind) of 200m<sup>2</sup> or less and output of less than 20kW, as defined by the Electricity Business Law<sup>1, 2)</sup>.

Large wind turbines face challenges such as high initial costs per station and restriction of installation sites due to high noise and environmental issues.

In contrast, small wind turbines are less restricted by installation costs and construction duration, and can be easily installed in public places such as parks and schools due to their small size. In addition, they can be easily deployed as an emergency power supply during natural disasters.

### 3. Types of small wind turbine generators

There are many different types of small wind turbines; however, in general, they can be broadly classified into horizontal axis wind turbines (HAWT) and vertical axis wind turbines (VAWT), from the position of the rotational axis against the wind direction. They can also be classified into lift type or drag type, depending on the principle of operation. Fig. 1 shows the typical wind turbine types.

Each type has its own characteristics, which are briefly described in the following paragraphs<sup>1-3)</sup>.

Horizontal axis wind turbines have a rotational axis parallel to the wind direction and include propeller type, sail-wing type, Netherlands type and multi-wing type. Horizontal axis wind turbines need to make the turbine rotational blades face the wind direction.

\*Engineering Dept. Natural Energy Products Division

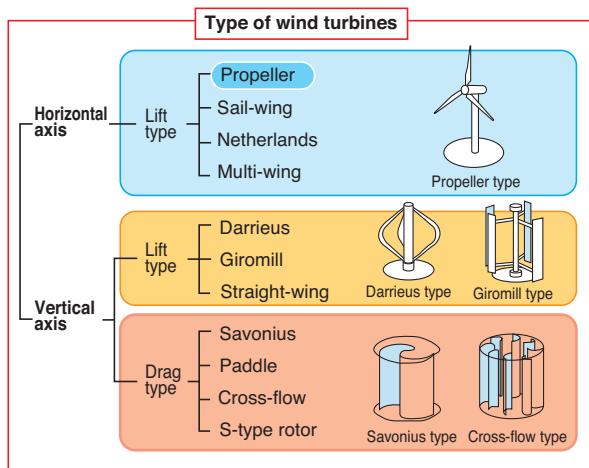


Fig. 1 Wind turbine category 4)

The control method for tracking the wind direction so that turbine rotational blades face the wind is called "yaw control", and includes forced yaw control, which uses a control device to force the yaw control and free-yaw control, which uses air flow for autonomous control. Wind turbines with rotational blades located on the upstream side of the tower are called upwind type, and those with rotational blades located on the downstream side of the tower are called downwind type (Fig. 2).

Vertical axis wind turbines have their rotational axis perpendicular to the wind direction (often perpendicular to the ground), and include Darrieus type, straight-wing type, Savonius type and cross-flow type. Vertical axis wind turbines can rotate by receiving wind from any direction; therefore they do not require yaw control.

Lift type and drag type are categorized by the principle of operation. Lift type mainly uses lift force and includes propeller type, Darrieus type and straight-wing type. Lift type wind turbines can produce high circumferential speed ratio of a few times to 10 times that of the wind speed, which make them suitable for power generation.

On the other hand, drag type wind turbines mainly use drag force and include Savonius type and cross-flow type. Drag type wind turbines cannot produce higher rotational speed than the wind speed; however,

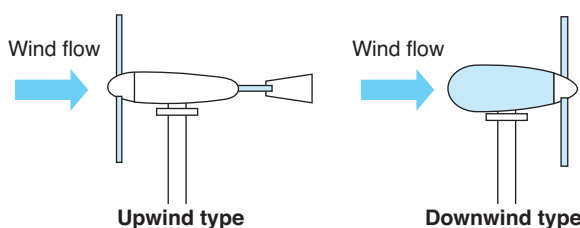


Fig. 2 Type of horizontal axis wind turbine

with their larger torque, they are frequently used for power operation such as pumping water and milling.

#### 4. NTN's proprietary wing design

NTN's proprietary wing design can be used in both vertical axis and horizontal axis wind turbines. Fig. 3 shows their respective designs.

Characteristics common to both horizontal and vertical axis wind turbines are as follows:

- 1) Little wind noise even under strong wind condition
- 2) High wing efficiency

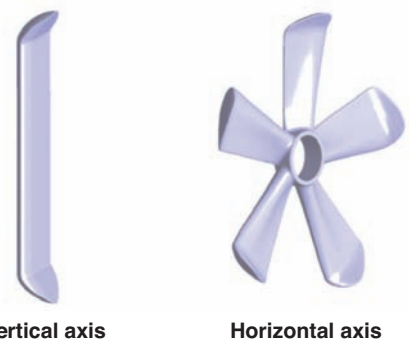


Fig. 3 Design of NTN blade

Common horizontal axis three-blade propeller type wind turbines are characterized by having the best rotational speed for efficient power generation on the high side, as well as thinner wings which produce high wind noise. This does not cause any problems if installed in remote areas with no residential areas nearby; however, this high noise creates problems if installed in populated areas such as towns and parks. NTN wind turbines with proprietary wings have the best rotational speed for efficient power generation on the lower side, compared to those of other manufacturers, and the unique thick wing design reduces wind noise even under strong wind conditions. In addition, the unique tip design of the winglet reduces the wingtip vortex and resulting loss, eliminating most of the wind noise (Fig. 4).

The high efficiency of the wing is attributed to two characteristics of the wing: the first is the winglet on the tip of the wing and the second is the unique wing cross-sectional design. The winglet is a small wing generally seen on the main wing of aircrafts, also called a wingtip. The wingtip prevents vortex, which may be produced at the tip from the lower surface of the wing to the upper face, resulting in improved fuel efficiency (Fig. 5). NTN's winglet adopts a unique angle and tip shape design on top of the winglet

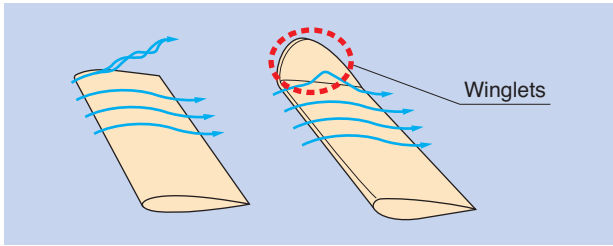


Fig. 4 Change of the flow by winglets

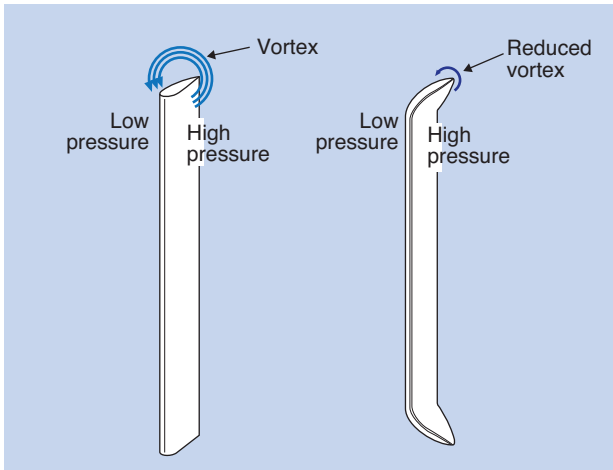


Fig. 5 Effect of Winglet

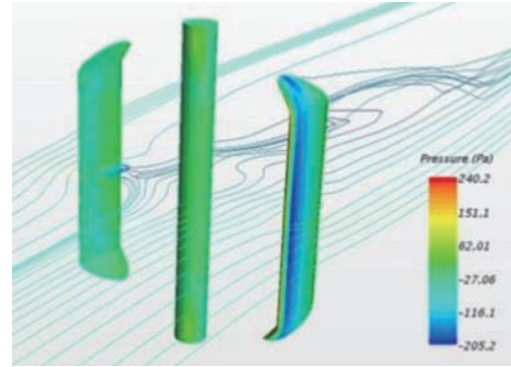


Fig. 6 Result of fluid analysis



Fig. 7 Picture of Wind Tunnel

design adopted by aircrafts, to reduce wingtip vortex and energy loss due to vortex leaving the wing, which has improved the wing efficiency. The result of fluid analysis is depicted in Fig. 6.

In addition, the cross sectional shape of the wing with a unique thickness produces rotational force from a complete stop even with no pitch angle, and creates great lift force at the optimum rotational speed. Furthermore, no pitch angle means reduced resistance for rotation, maintaining rotational speed even with weaker wind. When the wind starts blowing again, the wings can capture the wind with the optimum rotation speed - increasing efficiency in varied wind conditions.

NTN conducted wind tunnel experiments in order to obtain basic data of wind turbine wings. The wind tunnel experiments were conducted at Mie University, which possesses one of the largest wind tunnel facilities in Japan. The wind tunnel facility is a circulation flow type (Fig. 7) where the turbine was placed in the open measurement area. The experimental wind turbine is shown in Fig. 8.

Collection of accurate data from the wind tunnel experiment enabled significant improvement in simulation accuracy. The results were used for design, which helped reduce the development time. We will continue developing highly efficient and safe wind turbines.

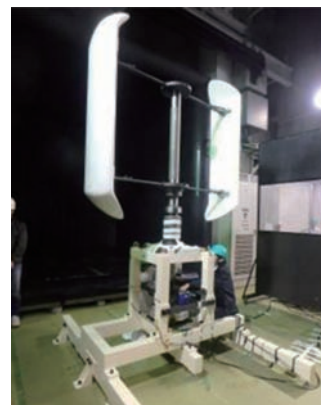


Fig. 8 Wind Turbine for laboratory test

## 5. Hybrid street lights

This is a hybrid power generation system combining wind power generators and solar power generators. Their appearance is shown in Fig. 9, specifications are shown in Table 1, and the structure is shown in Fig. 10.

NTN hybrid street lights are an independent power supply system and can be used as street lights where no power cables are available, or as an emergency power supply in the case of disasters, such as



Fig. 9 Hybrid street light

Table 1 Specification of hybrid street light

Wind power generator	Rated output	0.2kW
	Rotor diameter	0.8m
	Wing length	1.2m
	Wind turbine type	Vertical axis
	Brake	Electric
	Survival wind speed	60 m/s (max. instantaneous wind speed)
Solar electric generation	Rated output	90W
LED illumination	Power consumption (nominal)	10W
	Illuminance	900lm

※Product appearance and specification are subject to change without notice.

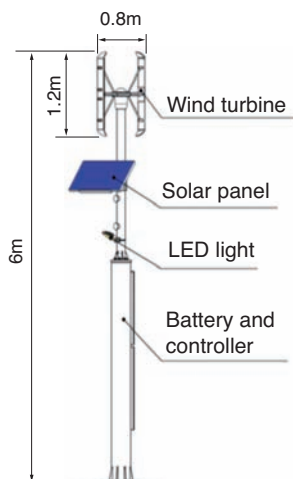


Fig. 10 Structure of Hybrid street light

charging stations for mobile telephones and a power source for telecommunication equipment.

The battery of this product can turn on the LED lamp for approximately 5 days, when fully charged, assuming use of 12 hours/day.

They can operate electric brakes under strong wind conditions for slower rotation, bypassing wind power, as a safety measure. Being highly safe and very quiet,

NTN hybrid street lights can be installed in many places such as parks, schools, city halls, hospitals, disaster evacuation centers, bus stops and parking areas-serving as a symbol of the town. They can also be used as advertising towers by installing electronic signs, or as surveillance towers by installing surveillance cameras. The appearance can be customized by user request. Fig 11. shows several examples of customization including the installation of a bench.

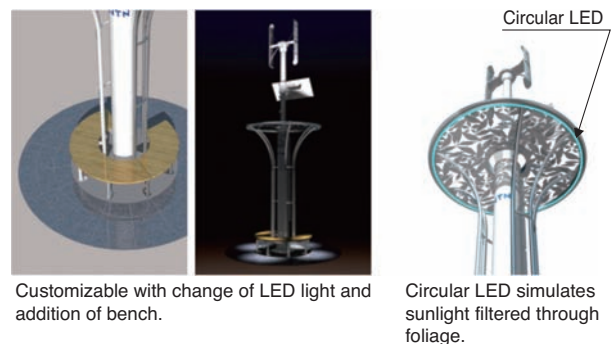


Fig. 11 Customization example

## 6. 10kW vertical axis wind turbine

The rate for purchasing power from small wind turbines of less than 20kW in Japan in FY2016 is 55 yen/kWh, which is the highest in the FIT program, for the duration of 20 years.

Stable and efficient power generation is required for selling electric power at the rate of 55 yen/kWh during this period.

In order to deploy small wind turbines, certification must be obtained from the Minister of Economy, Trade and Industry. Nippon Kaiji Kyokai, which was authorized as the certification body for wind power generation products in 2013, issues type approval "ClassNK", which is required for application of FIT.

NTN's 10kW vertical axis wind turbines are currently in development with specifications to meet the ClassNK type approval.

The structure of 10kW vertical axis wind turbines is shown in Fig. 12, and the specifications are shown in Table 2.

This 10kW vertical wind turbine also produces little wind noise, like the hybrid street lights, even under strong wind conditions, and generates power efficiently even in the area of frequently changing wind direction due to the vertical axis structure.

In addition, it adopts NTN's expertise in bearings and rotary machines acquired over many years for the optimum design of low-torque and long-life drive line.

Highly efficient and quiet small vertical axis wind turbines can be installed in places where conventional wind turbines could not be installed.

In March, 2016, we built an experimental wind turbine in NTN's Advanced Technology R&D Center (Fig. 13). We are collecting data from this experimental turbine for further improvement.

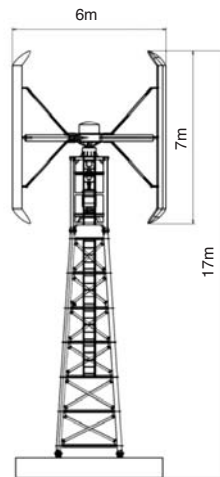


Fig. 12 Structure of 10kW vertical axis wind turbine

Table 2 Specification of 10kW vertical axis wind turbine

Rated output	10kW
Rated wind speed	12m/s
Rotor diameter	6m
Wing length	7m
Turbine type	Vertical axis
Brake	Mechanical, electric (dual brake)
Survival wind speed	60m/s (max. instantaneous wind speed)



Fig. 13 10kW vertical axis wind turbine

## 7. Safety of 10kW vertical axis wind turbines

The specifications for small wind turbines for ClassNK were developed based on IEC international standards, specifying safety, reliability, performance and noise property of wind turbines.

Particularly, strict requirements are in place for safety issues, as failure due to over-rotation during storms may result in a severe accident5).

NTN adopts dual brakes, namely, mechanical and electrical brakes, to be used under strong wind conditions.

In addition, the safety of wind turbines is assured by adopting a design of applying mechanical brakes even when power is lost due to submergence of the control panel in assumed natural disasters such as lightning, earthquakes and tsunami.

Wings are also required to be highly safe and reliable.

The safety of the wing strength is ensured by strength tests using the actual wings, in addition to analytical strength verification (Fig. 14).

ClassNK process verifies these safety requirements on the strength and system safety, as well as design documents including quality of manufacturing. In addition, it is required to conduct a type approval test to ensure stable operation for the specified period\*1 by building the wind turbine for approval at the test site. NTN plans to conduct this type approval test in 2017 for ClassNK type approval.

\*1: Requirements of type approval test

- (1) Secure operation during the test period
- (2) Operation for more than 6 months
- (3) Power generation for over 2,500 hours regardless of wind speed
- (4) Power generation of over 250 hours at the wind speed of 10.2m/s or more
- (5) Continuous test for over 25 hours under the wind condition of 15m/s or more

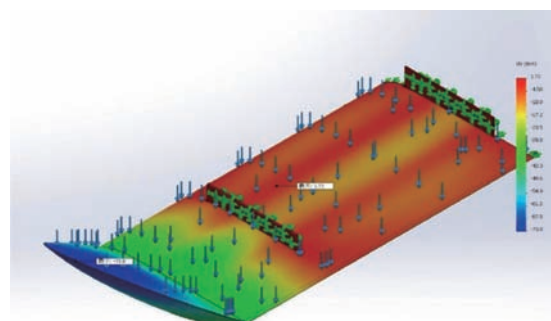


Fig. 14 Result of FEM analysis

## 8 . Wing performance

We have conducted performance test of NTN's wing at the large wind tunnel test facility at Mie University. The test was conducted by using two types of specimens with the same swept area, namely, NTN's vertical axis blades with proprietary wing geometry and winglets as shown in Fig. 15, and conventional wings without winglets as shown in Fig. 16 measuring the torque of each rotational speed under certain wind speeds for performance verification.

Fig. 17 shows the results under a wind speed of 6m/s. Compared with the conventional specimen, NTN's wing was proven to be approximately 1.5 times higher in performance.

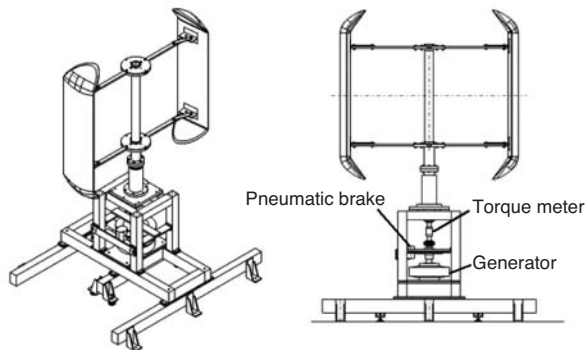


Fig. 15 NTN's vertical axis wind turbine

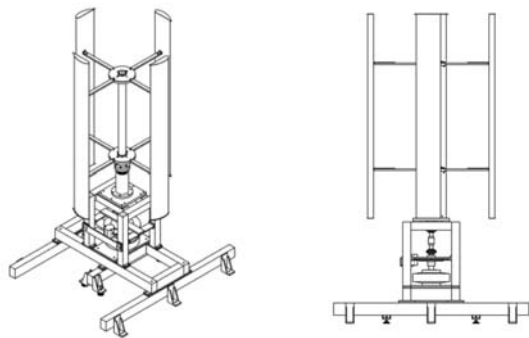


Fig. 16 General vertical axis wind turbine (non winglet)

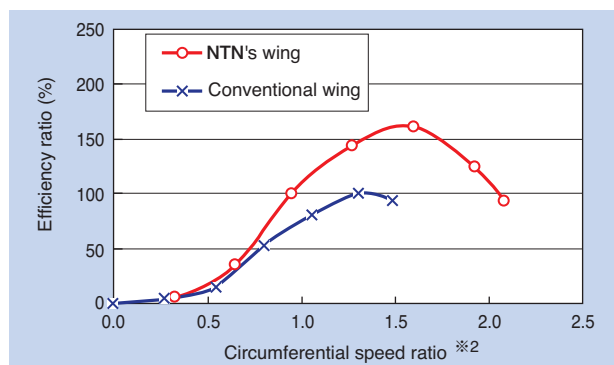


Fig. 17 Result of performance

※2 Circumferential speed ratio is the ratio of rotational speed (circumferential speed of wing) and wind speed.

## 9. Conclusion

In this article, we have discussed the characteristics of recent natural energy, small wind power generation systems, and NTN's proprietary technology and development.

It is expected that the products will be used in various places under different environments due to their low cost, small footprint, and ease of deployment.

In the market, addressing the needs for a low carbon society, development of small wind power generators is well underway. NTN will also contribute to this trend by incorporating its own unique technologies to improve its products every day, with clear differentiation from the competition. With this approach, we will continue proposing new products that contribute to the revenue of the Natural Energy Division and address market demand.

## References

- 1) New Energy and Industrial Technology Development Organization (NEDO): NEDO Renewable Energy Technology White Paper, 2nd Edition (2013). Chapter 1, 4-11, Chapter 3, 4-9
- 2) Japan Small Wind Turbines Association: Small Wind Turbine Guide Introductions 2nd Edition (2012), 6-29.
- 3) Izumi Ushiyama: Wind Energy, Ohmsha, (2005), 49-53.
- 4) Referred from New Energy and Industrial Technology Development Organization (NEDO) website: <http://www.nedo.go.jp/content/100544818.pdf>
- 5) Japan Small Wind Turbines Association, JSWTA 0001 Standard on performance and safety of small wind turbines, ed. 2, (2013) 1-6.

## Photo of authors



Takaya ADACHI  
Engineering Dept.  
Natural Energy Products Division



Ryosuke KARASAWA  
Engineering Dept.  
Natural Energy Products Division

# Micro Hydro Turbine

**Tomoya KAWAI\***  
**Hiroki MUKAI\***  
**Tomomi GOTOU\***



Demand of renewable energy such as hydroelectric power generation is increasing rapidly from rise of global warming and the interest to the energy mix. The one for which hydroelectric power generation uses the gap of the water is general. NTN has developed micro hydro turbine for small water flow (NTN micro hydro turbine) which is used in agricultural canal and industrial canal of existence. This paper introduces the features and the structure of the products of NTN.

## 1. Introduction

Energy issues are a global challenge that must be dealt with in order to achieve a sustainable society.

Some of the key initiatives include reducing greenhouse gas emissions, increasing renewal energy usage to phase out fossil fuel dependency, and diversifying sources of natural energy.

The estimated energy mix for FY2030 includes more than double the amount of natural energy compared to the mix before the Great Earthquake of East Japan, indicating an expectation of future growth <sup>1)</sup>. **Fig. 1** shows the estimated energy mix for FY2030.

In Japan, a feed-in tariff (FIT) program was started in July, 2012 as a policy to expand the introduction of natural energy. FIT is a program that mandates utility companies to purchase electric power generated by

natural energy at a predetermined price in order to promote the use of natural energy and make it easier for businesses to recover investments from natural energy development <sup>2)</sup>.

**Fig. 2** shows the purchase price of hydraulic power in the FIT program.

The rate of 34 yen/kWh for hydraulic power less than 200kW is more favorable than the other hydraulic power generation classes. Hydraulic power generation is more limited by location than solar power or wind power; however, it provides stable power generation with small variation. Therefore, the market is expected to grow moving forward.

This article discusses the flow-through small hydraulic power generator (micro hydro turbine) that NTN is developing with highly efficient blades that possess unique geometry.

Energy mix/amount (100 million kWh)

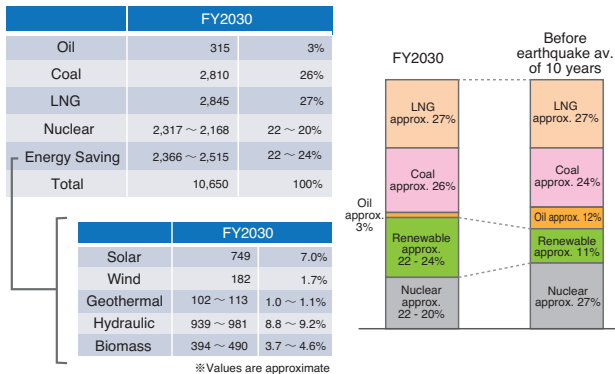


**Fig. 1** The power supply construction in 2030 <sup>1)</sup>

	≥1,000kW, <30,000kW	≥200kW, <1,000kW	<200kW
<b>Hydraulic</b>			
Purchase price	24 yen + tax	29 yen + tax	34 yen + tax
Purchase duration	20 years	20 years	20 years
<b>Small/medium hydraulic using existing waterway <sup>(*)</sup></b>			
Purchase price	14 yen + tax	21 yen + tax	25 yen + tax
Purchase duration	20 years	20 years	20 years

※Using existing waterways and upgrading electric facilities and high pressure steel pipes.

**Fig. 2** Price of the hydroelectric power generation <sup>2)</sup>

\*Engineering Dept. Natural Energy Products Division

## 2. About micro hydro power generation

Hydraulic power is produced by turning hydraulic turbines with water and transmitting the motion energy to a generator. Hydraulic power is a type of natural energy, like solar or wind power, that is free of greenhouse gas emissions.

The "Guidebook for Implementation of Micro Hydropower Generation (NEDO 2003)" categorizes those with an output of 100kW or less as micro hydropower generators. In addition, relatively small power generators that produce 1000kW or less may be collectively called small hydraulic power generators<sup>3)</sup>.

In this article, micro hydropower generators will be called micro hydro turbines. **Table 1** shows the categorization of hydraulic power generators.

**Table 1** Division of hydroelectric generator<sup>4)</sup>

Division	Power output kW
Large hydraulic	≥100,000
Medium hydraulic	10,000~100,000
Small hydraulic	1,000~10,000
Mini hydraulic	100~1,000
Micro hydraulic	≤100

Medium hydraulic power generation faces challenges such as high installation costs and restricted installation sites.

In contrast, micro hydro turbines can be easily installed in existing water channels, such as agricultural water ways, which can reduce the overall cost. In addition, they can be used for charging batteries and as an independent power supply in the case of emergencies, such as natural disasters.

## 3. Flow-through hydropower generation

Existing mainstream hydraulic power generators are head type. Generated power is determined by the flow rate and effective head, as shown in equations (1) and (2).

$$\text{Generated power} = \text{Theoretical hydropower} \times \eta \quad (1)$$

$$\text{Theoretical hydropower: } P = g \times Q \times H \quad (2)$$

Where  $\eta$  is efficiency,  $g$  is gravity,  $Q$  is water use,  $H$  is effective head.

On the other hand, the generated power of micro hydro turbines developed by NTN is determined by the swept area of the micro hydro turbine and flow rate, as shown in equation (3).

$$\text{Generated power: } P = 1/2 \times \rho \times A \times v^3 \times \eta \quad (3)$$

Where,  $\rho$  is water density,  $A$  is swept area,  $v$  is flow rate and  $\eta$  is efficiency.

## 4. Types of hydro turbines

The hydro turbines used for hydraulic power generators are classified by their shape and structure and are broadly categorized into impulse water turbines and reaction water turbines<sup>5)</sup>. **Fig. 3** shows the types of hydro turbines.

Impulse water turbines use water injected from the nozzle which is flushed onto the bucket of the impeller to rotate the turbine. For example, the Pelton turbine shown in **Fig. 4** corresponds to this category.

Reaction turbines use the speed energy and pressure energy of the water to rotate the impeller. For example, the Francis turbine shown in **Fig. 5** corresponds to this category.

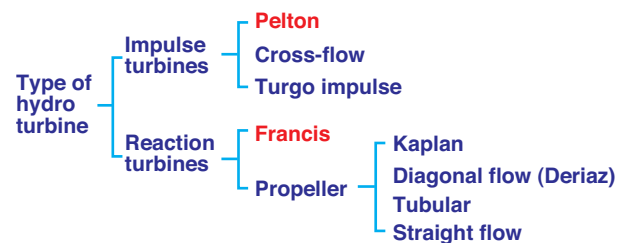


**Fig. 3** Form of hydroelectric generator<sup>5)</sup>

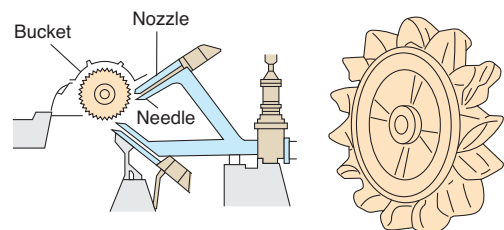


**Fig. 4** Pelton wheel<sup>5)</sup>

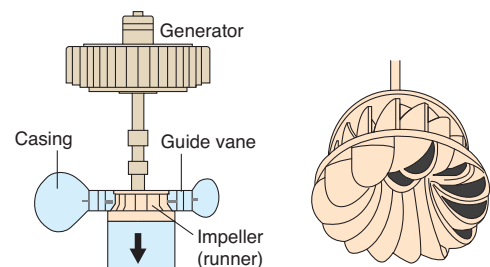


**Fig. 5** Francis turbine<sup>5)</sup>

## 5. Structure and characteristics of micro hydro power turbines

NTN is developing flow-through small hydraulic turbines (micro hydro turbines) with proprietary wing shapes which can be installed in existing agricultural and industrial waterways. Installation costs can be significantly reduced since there is no need to change or add waterways. The key configuration is shown in Fig. 6 and Table 2.

**Table 2** Example of structure

Component	Specifications
Turbine wing	φ 900mm
Gear box	Gear ratio 2.5
Generator	Permanent magnet synchronous generator Rating 1.5kW
Beam	Adjusted based on waterway

### 5. 1 Hydro turbine wings

Hydro turbine wings are shown in Fig. 7 . Wings with NTN's proprietary geometry improve upon the efficiency of conventional generator wings through the following distinctions:.

- Thick cross sectional structure
- Winglet structure
- Wide wing tip



**Fig. 7** Blade of hydro turbine

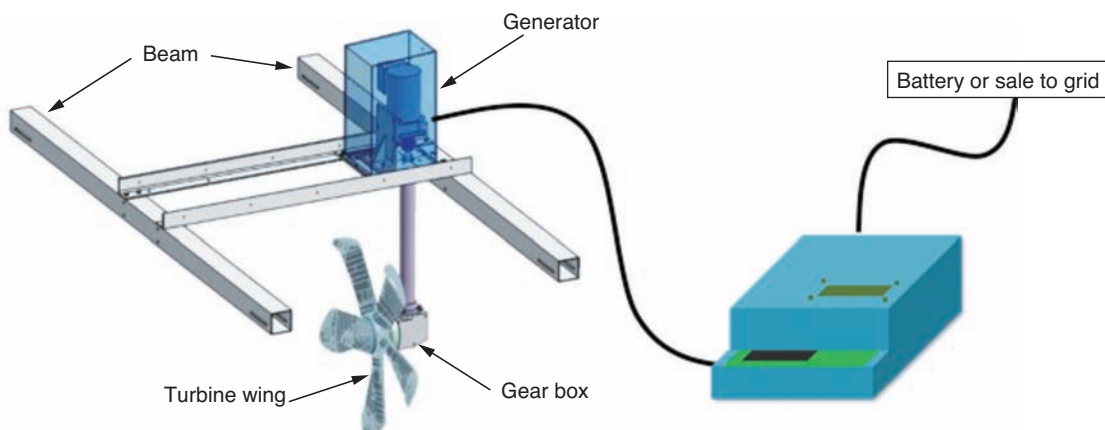


**Fig. 6** System configuration

#### 5. 1. 1 Thick cross sectional structure

The cross sectional structure is thickened to increase lift force in the rotational direction. This allows for a reduction in the pitch angle. By reducing the pitch angle, the resistance on the rotational direction is reduced to increase lift force and power generation efficiency.

#### 5. 1. 2 Winglet structure

As shown in Fig. 8, a wingtip vortex is observed when the tip of the wing is flat. The wingtip vortex disrupts the flow behind the wing and reduces lift force. For example, with aircrafts, the design called winglet, which bends the tip of the wing as shown in the right side of the Fig. 8, prevents reduced fuel efficiency by the wingtip vortex. NTN turbine wings have winglets with a proprietary shape and tip angle that reduce energy loss by reducing the wingtip vortex.

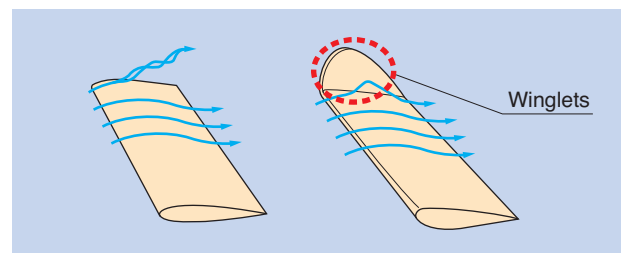


**Fig. 8** Change of the flow by Winglets

#### 5. 1. 3 Wide wing tip

The wing is gradually widened toward the tip to increase the force applied to the wingtip. This efficiently produces running torque.

**5.2 Low torque/low environmental load bearings**

Low torque bearings that NTN has been developing for many years are used for rotational components to achieve low friction loss. In addition, NTN grease for food processing machines is used as a lubricant for bearings and gears in order to minimize the impact on the surrounding environment, even when accidentally leaked into waterways.

**5.3 Ease of installation**

As shown in Fig. 9, micro hydro turbines can be installed on waterways only by placing beams which span the width of the waterways. As shown in Fig. 10, a turbine can be installed with one mobile crane and three workers within one hour. In addition, there is no need for upstream flow to be stopped or other major installation work.

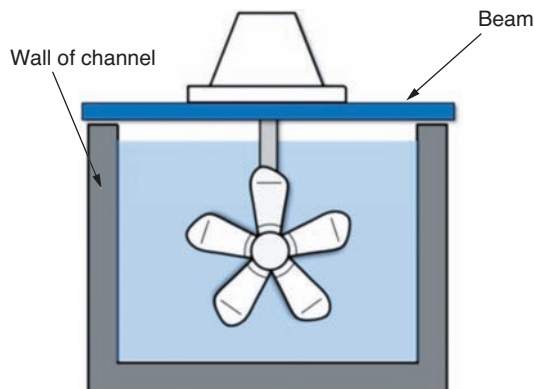


Fig. 9 Installation image to a canal



Fig. 10 Installation operation

**5.4 Use of existing waterways**

Since micro hydro turbines generate power by using the flow of running water, no head is needed; therefore, no major construction, such as dams or headraces, is required. This results in lower initial costs and easier installation.

**5.5 Serial installation of multiple units**

Micro hydro turbines can efficiently convert energy of running water into electric power with NTN's proprietary wing geometry. There is no interference when multiple units are installed in a single waterway for increasing power output. Fig. 11 shows a diagram of serial installation.

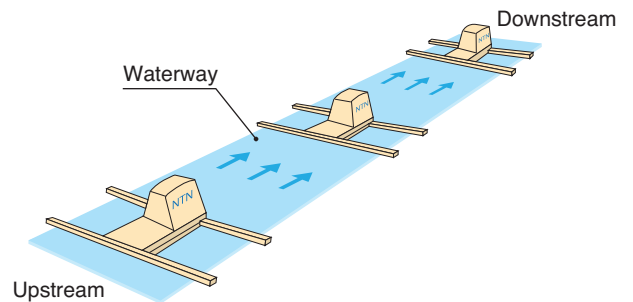


Fig. 11 Instillation of micro hydro turbine

**6. Measures against incoming foreign objects**

**6.1 Debris screen**

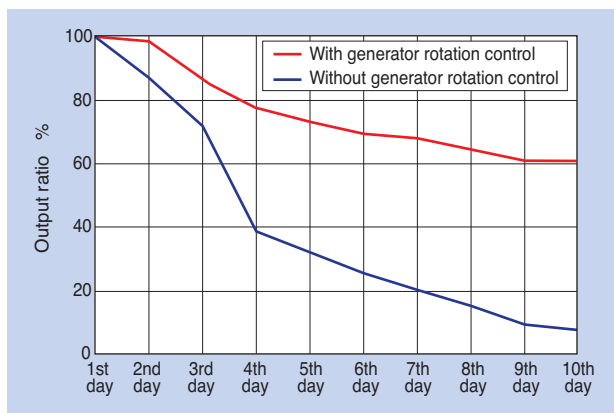
Since micro hydro turbines are installed in the open waterways, countermeasures against incoming debris are required. The type and amount of debris vary depending on the environment of the waterways; however, debris screens such as the one shown in Fig. 12 are typically used. Debris screens prevent foreign objects larger than the designed size; however, foreign objects need to be removed from the screen. Even if automatic removal systems are available, they are expensive and not appropriate for small hydraulic power generation systems. Therefore, regular maintenance is required. We are working on a solution to simplify debris screen maintenance work.



Fig. 12 Dust removal screen

### 6. 2 Debris removal by controlling generator rotation

Foreign objects caught in the rotating wings are pressed into the wings with water pressure and are not likely to come out. Therefore, rotation can be slowed down to reduce the water pressure so that the water flow washes the foreign objects away. **Fig. 13** shows the results of a test to wash away foreign objects by controlling generator rotation. The time period it took for the generator to reduce its power output to 60% was increased by more than three times (3 days to 10 days). We are continuing verification testing for implementation in commercial products.



**Fig. 13** The reduction preventive effect of the amount of electric power generation by the generator control

### 6. 3 Turbine axis cover

Foreign objects entangled around the axis are hard to remove, resulting in reduced efficiency. An axis cover is used as a countermeasure against entanglement of foreign objects on the axis which may affect rotation of the turbine wings, as shown in **Fig. 14**.



**Fig. 14** Cover of blade axis

## 7. Demonstration test conducted at Asaka Channel

A demonstration test was conducted at New Asaka Channel in Sukagawa-shi, Fukushima Prefecture from June to August, 2016. The test overview and cross section of the Channel under the demonstration test are shown in **Fig. 15** and **Fig. 16**, respectively.

Asaka Channel is one of the three largest channels in Japan and runs from Lake Inawashiro through the Ou Mountains. We obtained significant cooperation from the Land Improvement District, relevant authorities and organizations for this demonstration test.

Generation performance, impact on the waterway, maintainability, etc. were verified during this demonstration test. The test conditions are shown in **Table 3**. The measured data of flow rate and generated power, as well as the calculated result,



**Fig. 15** Verification test at Asaka canal

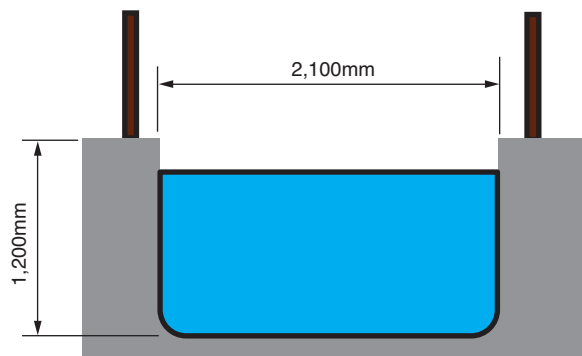


**Fig. 16** Cross section of Asaka canal

**Table 3** Electric power generation test condition

Item	Condition
Turbine wing	φ900mm
Generator	Rating 1.5kW
Generator control	Electronic load
Measured flow rate	1.6 m/s

which assumes the generated power is proportional to the cube of the flow rate, is shown in Fig. 17. The test result is the output of the generator and does not reflect controller efficiency. We will use the obtained data in development for commercialization. In addition, we will continue our test in order to verify durability.

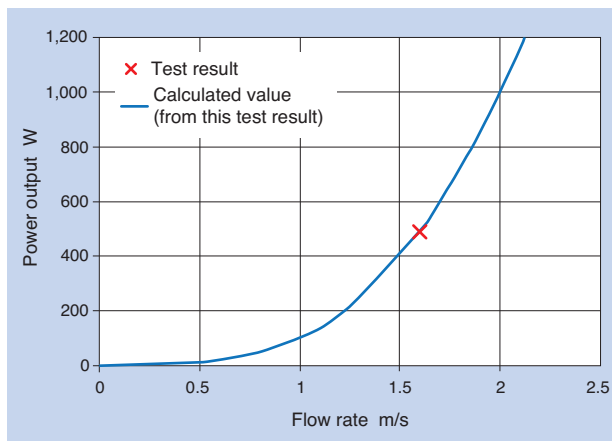


Fig. 17 Relations of flow velocity and electric power generation

## References

- 1) Ministry of Economy, Trade and Industry: Long-term Energy Supply and Demand Outlook and related materials
- 2) Ministry of Economy, Trade and Industry home page: "Nattoku!" Renewable energy  
[http://www.enecho.meti.go.jp/category/saving\\_and\\_new/saiene/kaitori/kakaku.html](http://www.enecho.meti.go.jp/category/saving_and_new/saiene/kaitori/kakaku.html)
- 3) Ministry of Economy, Trade and Industry, Agency for Natural Resources and Energy, Pacific Consultants Co., Ltd.: Overview of Guideline for Introduction of Small/Medium Hydraulic Power Generation Plan, February, 2014
- 4) Agency for Natural Resources and Energy home page: Small Hydraulic Power Generation Information Site  
<https://www.env.go.jp/earth/ondanka/shg/page01.html>
- 5) Ministry of Economy, Trade and Industry, Agency for Natural Resources and Energy home page: Small hydraulic power generation information site  
[http://www.enecho.meti.go.jp/category/electricityand\\_gas/electric/hydroelectric/mechanism/waterwheel/](http://www.enecho.meti.go.jp/category/electricityand_gas/electric/hydroelectric/mechanism/waterwheel/)

## 8. Conclusion

In this article, we have discussed types and characteristics of hydraulic power generation, the structure of NTN's proprietary high-efficient wing technology and debris removal methods of micro hydro turbines. Safe and highly reliable micro hydro turbines are necessary as they use agricultural and industrial waterways, which are very much involved in the lives of the local communities. We will continue our bench tests and demonstration tests to develop highly efficient and reliable micro hydro turbines and introduce them into the market.

### Photo of authors



Tomoya KAWAI  
Engineering Dept.  
Natural Energy Products  
Division

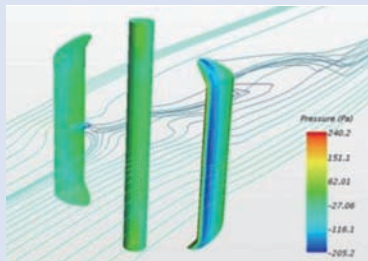


Hiroki MUKAI  
Engineering Dept.  
Natural Energy Products  
Division



Tomomi GOTOU  
Engineering Dept.  
Natural Energy Products  
Division

# CFD Contribution to Development of Small Wind Turbine Generator



Takeru ITOU\*  
Ryosuke KARASAWA\*  
Masato YOSHINO\*\*

Currently, renewable energy products are attracting in the world. NTN is developing small wind turbine products which are able to easily construct by low-initial-cost. This paper describes a Computational Fluid Dynamics (CFD) of blade which is one of evaluation methods for small wind turbine.

## 1. Introduction

With the advancement of computers, calculation using Computational Fluid Dynamics (CFD) has become more accessible. Traditional evaluation with wind tunnels and field tests requires a number of specimens for tests to be created according to evaluation conditions which may significantly increase cost. In addition, large specimens require large wind tunnels, meaning that availability and usable equipment may be limited. Furthermore, when wind tunnels are not used outdoor tests pose various challenges. For example the topology in Japan does not offer abundant wind or wind with a stable direction. Development of CFD has potential for solving these challenges.

CFD is a numerical analysis method for calculating fluid behavior using computers, which has been developed along with the improvement of computer performance. In general, it involves dividing the space where fluid exists into grids and then apply Navier-Stokes equations, which are the dominant equations for fluid motion. The equations are applied to discretized grid space, solving differential equations numerically as a boundary value problem or initial value problem. CFD started in the 1960's and thanks to very active research for applications to real problems, significant progress was achieved in the 1980's<sup>1)</sup>. However, up until the 1980's only laboratories of national research institutions and large enterprises could use this method because research

and application of CFD required high performance computers, such as super-computers. Recently, with the evolution of computers, regular computers have acquired the same performance as super-computers of the past by combining image processing software<sup>2)</sup>. This makes the CFD analysis readily available to anyone who owns a computer and has the skill to run such analysis. .

CFD analysis can be conducted relatively easily by using commercial CFD analysis software.

The use of CFD analysis brings not only a reduction of development costs, but also acquisition of detailed information about the flow field (e.g. air flow), which is one of the greatest benefit.

Revealing the details of the flow field is extremely helpful for developing new products in terms of design/development of products that use flow, and for improvement in efficiency, etc. However, the solution acquired from the CFD analysis is not an exact solution but an approximate solution, and may lead to an unrealistic solution if the wrong conditions are given. In order to ensure reliability of the solution from the CFD analysis, it is necessary to verify the alignment of solutions between test data from wind tunnel tests, etc and the CFD analysis.

In this article, we will report the results of the CFD analysis for the blades of the wind turbine generator developed by NTN and the results of the tests conducted with the wind tunnel at Mie University. Then we will compare the two outcomes.

\*Engineering Dept. Natural Energy Products Division

\*\*Advanced Technology R&D Center

## 2. CFD analysis

### 2.1 Analysis model

We applied CFD analysis to the blades of the horizontal axis wind turbine (HAWT) and the vertical axis wind turbine (VAWT). We call the forward direction of the blade rotation “the leading edge” and the backward direction “the trailing edge”.

NTN's blade is a lift type blade with quiet operation even in high-speed rotation thanks to the proprietary thick blade cross sectional geometry. The thick geometry allows smooth air flow along the blade surface producing lift force toward the forward direction of rotation, creating torque even with small pitch angle (angle of blade relative to the rotational axis). In other words, air resistance during windless conditions is small. In addition, the unique tip design of the blade reduces the blade tip vortex and the resulting loss, achieving high quietness. The blade under analysis is shown in Fig. 1, the cross section of the horizontal axis blade is shown in Fig. 2, and the cross section of the vertical axis blade is shown in Fig. 3, respectively.

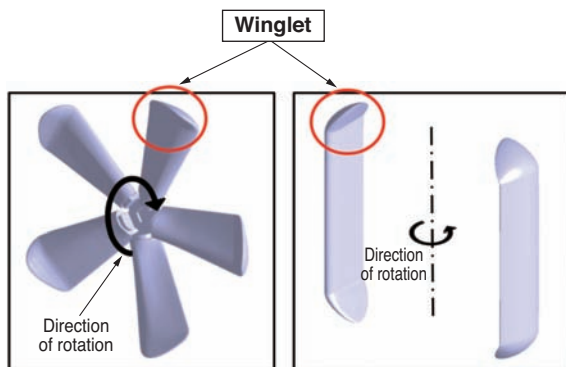


Fig. 1 Analysis model (left:HAWT, right:VAWT)

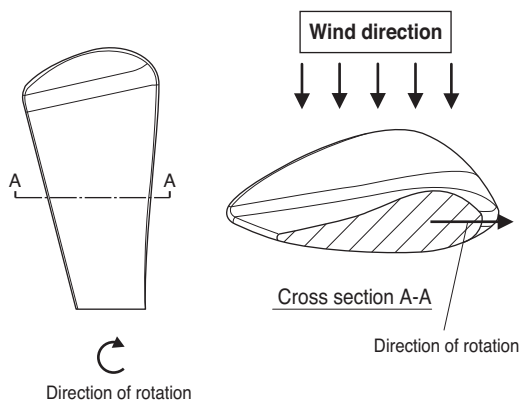


Fig. 2 Wing and cross-section of HAWT

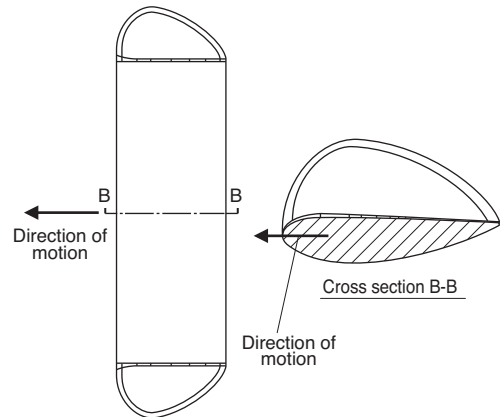


Fig. 3 Wing and cross-section of VAWT

### 2.2 Analysis conditions

The analysis conditions of the horizontal axis and vertical axis turbines are shown in Table 1.

In general, the appropriate wind speed for wind power generation is said to be 6m/s or more. Therefore, the CFD analysis was conducted at a wind speed of 6m/s. We used the commercially available fluid analysis software STAR-COM+ for this analysis. The method used was the finite volume method/implicit unsteady analysis. Raynolds-average model (RANS) was used for the turbulent flow model. The boundary layer grids around the blade were set to 20 layers, and the growth rate between grids was set to 1.5 to observe air flow turbulence. In addition, in order to increase computation speed, the horizontal axis wind turbine was divided into five increments along the rotational direction, and the vertical axis wind turbine was divided into two in the vertical direction.

Table 1 Analysis condition

Type	Wind speed m/s	Rotational speed min <sup>-1</sup>
Horizontal axis blade	6	10
		20
		30
		40
		50
		60
		70
		80
		90
		100
		110
		120
		130
		140
		150
Vertical axis blade	6	50
		100
		150

### 3. Wind tunnel test

#### 3. 1 Wind tunnel facility

The wind tunnel facility at Mie University was used. The appearance and overview of the facility is shown in Fig. 4.

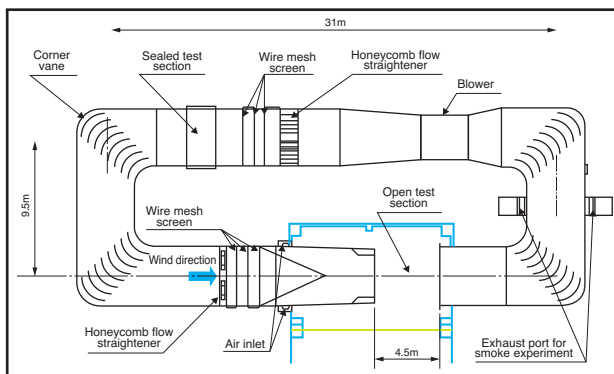


Fig. 4 Wind tunnel

#### 3. 2 Wind tunnel test conditions

Conditions of the wind tunnel are shown in Table 2.

Table 2 Wind tunnel test condition

Type	Wind speed m/s	Rotational speed min <sup>-1</sup>
Horizontal axis blade	6	20
		40
		60
		80
		100
		120
		140
		160
		180
		200
		220
		240
260		
280		
298		
Vertical axis blade	6	18
		36
		54
		72
		90
		108
		116

#### 3. 3 Wind tunnel test specimen

The outline drawings of the horizontal axis and vertical axis wind turbines used in this test are shown in Fig. 5 and Fig. 6, respectively. Torque meters were set to each specimen to calculate the power of the blades from the running torque and from the rotational speed. The specimens were equipped with pneumatic brakes for safety reasons.

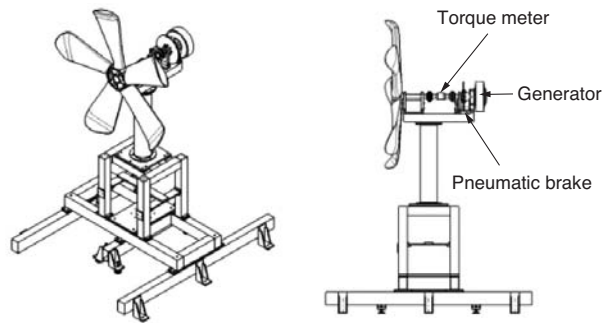


Fig. 5 HAWT test model

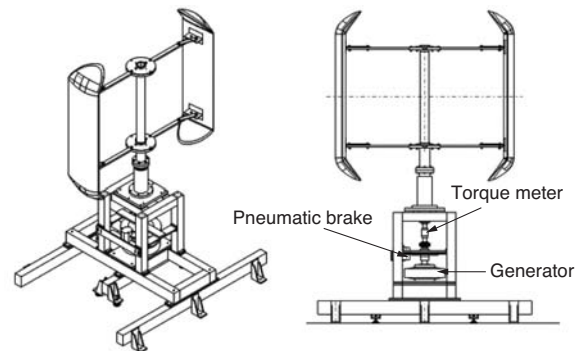


Fig. 6 VAWT test model

### 4. Results

#### 4. 1 Horizontal axis wind turbine

Results of the CFD analysis and the wind tunnel test for the horizontal axis wind turbine are shown in Fig. 7. From Fig. 7, it was verified that the results of the CFD analysis and the wind tunnel test were mostly aligned and that the analysis was adequate.

The kinetic energy of the wind that goes through the swept area (area where the blades of the turbine receive wind) is hereby called blade power.

The increase of the blade power to 50 - 100 min<sup>-1</sup> range of rotational speed was then examined with the CFD analysis. The pressure fields around the blade at the rotational speed of 50 min<sup>-1</sup> (Point A) and 70 min<sup>-1</sup> (Point B) are shown in Fig. 8, and the flow field is shown in Fig. 9, respectively. Fig. 9 is a diagram showing the speed vector around the cross section of the blade at the point where negative pressure is

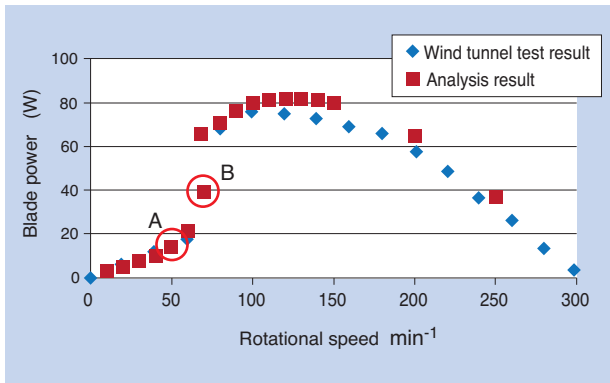


Fig. 7 Result of HAWT wind tunnel test and CFD

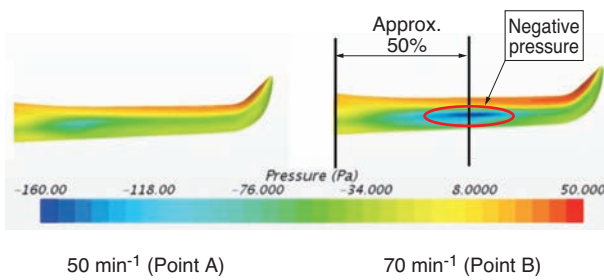


Fig. 8 Blade pressure field

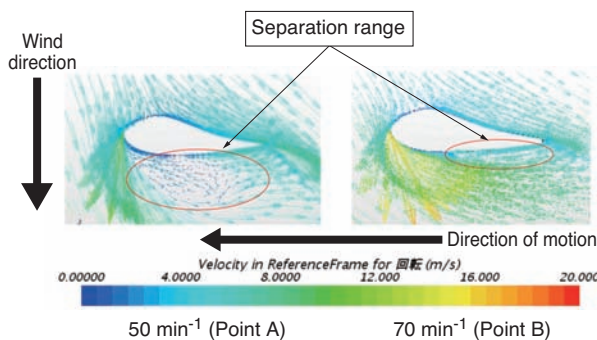


Fig. 9 Blade flow field

generated (approximately along 50% of the blade length) with a rotational speed of 50 min<sup>-1</sup> and 70 min<sup>-1</sup>.

From Fig. 8, it is revealed that the negative pressure is generated at the middle point of the blade with a rotational speed of 70 min<sup>-1</sup>. On the other hand, no negative pressure is observed at the middle of the blade with 50 min<sup>-1</sup>. This indicates that at 70 min<sup>-1</sup>, the blade power was increased by the presence of strong negative pressure. In addition, from Fig. 9, it was observed that air flow does not exist along the lower side of the blade with 50 min<sup>-1</sup>, but exists with 70 min<sup>-1</sup>. This suggests that the air flow changed as the incoming wind angle changed due to increased blade circumferential speed and the air flow was accelerated on the blade's surface. As the air flow on the blade surface accelerated without being separated from the

blade, a strong negative pressure was generated on the leading edge, resulting in increased torque. From the above, in the case of horizontal axis turbines where the blade rotational speed and circumferential speed ratio change at every point from the center of rotation to the tip of the blade, it is critical to make the shape of the blade match both the wind speed and circumferential speed throughout the wind turbine in order to generate strong negative pressure. The analysis model used for this CFD analysis of horizontal axis blades captured separation and adhesion of air flow, indicating that this analysis model was adequate.

#### 4.2 Vertical axis wind turbine

The results of the CFD analysis and wind tunnel test for the vertical axis wind turbine are shown in Fig. 10.

From Fig. 10, it was verified that the results of the CFD analysis and wind tunnel test were mostly aligned around 50 min<sup>-1</sup>. However, the results of the CFD analysis and the wind tunnel tests differ around 100 min<sup>-1</sup> and over. This error is believed to be a consequence of the fact that the resistance of the arm which connects the main spindle and blade was not considered.

In general, air resistance is expressed as follows:

$$\text{Air resistance} = C_t \times 1/2 \times \rho \times A \times V^2$$

$$C_t = \text{drag coefficient} \quad \rho = \text{air density}$$

$$A = \text{project area} \quad V = \text{velocity}$$

and proportional to the square of the velocity.

Therefore, resistance at the arm becomes greater as the circumferential speed increases. For confirmation, we conducted the CFD analysis of the blades with arm and main spindle at 100 min<sup>-1</sup>. The model with arm is shown in Fig. 11, and the CFD analysis result is shown in Fig. 12, respectively.

As shown in Fig. 12 errors from the test data decreased from around 30% to 7% by considering

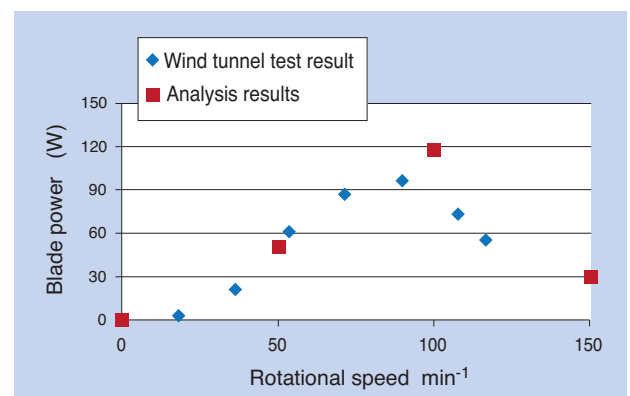
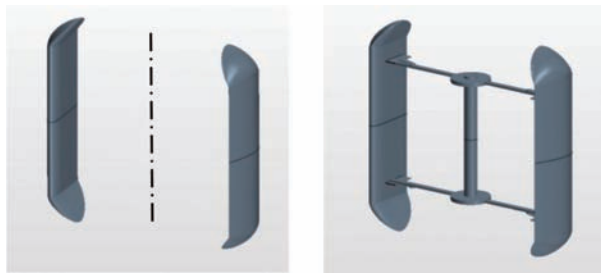


Fig. 10 Result 1 of VAWT wind tunnel test and CFD

arm resistance. This means that arm resistance cannot be ignored when conducting the analysis. It is generally understood that it is hard to conduct accurate calculations with the CFD analysis for vertical axis wind turbines because the air flow on the blade surface changes in complex patterns. However, for this CFD analysis, the results matched well with the wind tunnel test results at low speed, even though only the blade was considered. Also, errors could be sufficiently reduced at higher speed, when the arm was also considered.

Next, the pressure field around the blades was verified by the CFD analysis. Since the vertical axis wind turbine we consider in this article is a 2-blade system, one rotation produces a 2-cycle fluctuation in the process. In the case of the rotational speed of the blade being  $100 \text{ min}^{-1}$ , the fluctuation will be as shown in Fig. 13.



(a) Without arm (b) With arm  
**Fig. 11** Analysis model with arm and shaft

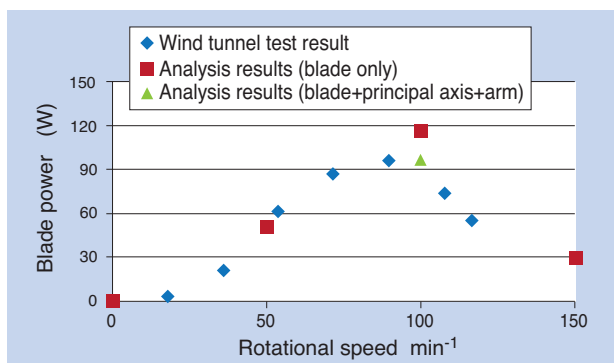


**Fig. 12** Result 2 of VAWT wind tunnel test and CFD

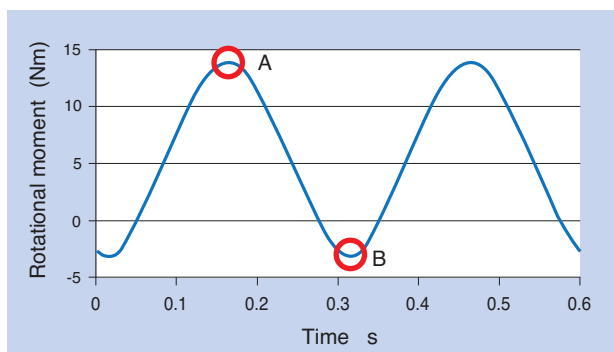


**Fig. 13** Blade rotational moment

At point A, where the rotational moment of the blades reaches the maximum, the pressure field around the blades creates a positive moment that contributes to power generation (Fig. 14).

Wind flowing in from the outside diameter of the blade (1) is accelerated by the forward blade shape producing strong negative pressure on the forward blade (1). This means that the force rotating the turbine is created at the blade (1).

At point B, where the rotational moment of the blades is minimum, the pressure field around the blade will create a negative moment to reduce the rotation (Fig. 15).

Strong positive pressure can be confirmed at the forward portion of the blade (1). The positive pressure is generated because the wind collides with the blade and stays in the area, which pushes the turbine in the opposite direction. In addition, the blade (2) is not working on either side since the variation of pressure distribution around the blade is small. In other words, with this wind direction and blade position, there is a force pushing the turbine rotation backward.

In practice, the turbine does not stop due to the inertia of rotation.

As summarized above, we could verify the performance of the blade with NTN's proprietary shape by using the CFD analysis.

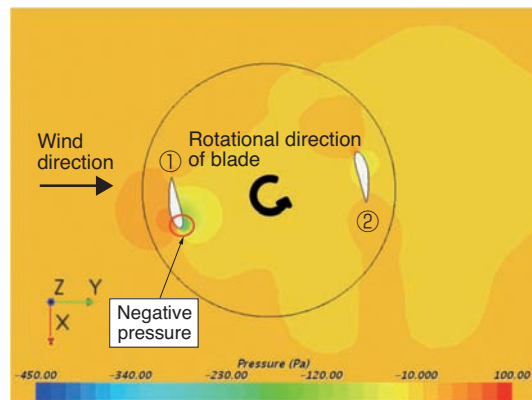
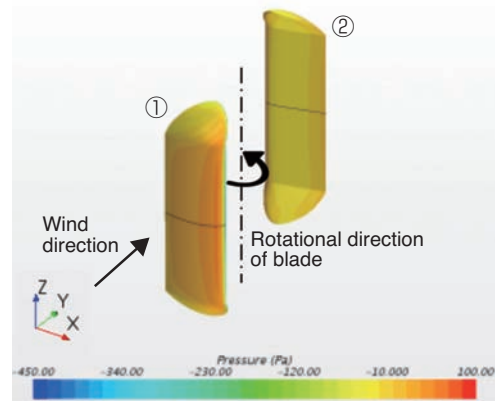


**Fig. 14** Blade pressure field (above:surface, below cross-section)

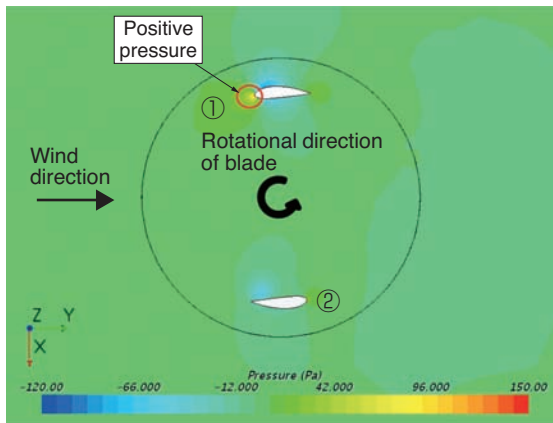
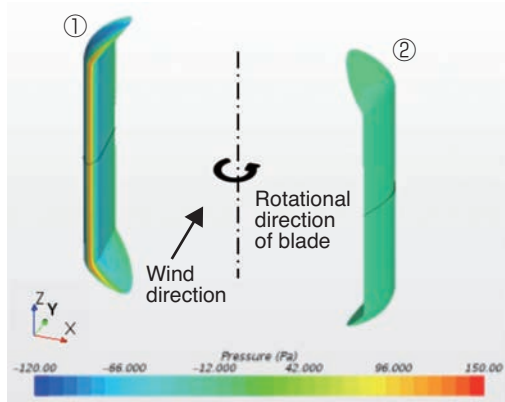


**Fig. 15** Blade pressure field  
(above:surface, below:cross-section)

## 5. Conclusion

We have evaluated NTN's small wind power turbines with wind tunnel tests as well as the CFD analysis. We obtained the following results from the test data and analysis results:

- The results from the wind tunnel tests and the CFD analysis matched. By using the method adopted in this article, performance of wind turbines can be estimated by using the CFD analysis.
- The output mechanism could be reviewed by pressure distribution/flow field obtained from the CFD analysis.
- By revealing the output mechanism, improvement points of the blade shape such as the cross-sectional shape and size were clarified.

Use of the CFD analysis greatly contributes to the reduction of development cost and new product development. We will continue working on the refinement of blade analysis technology using the CFD analysis to develop natural energy products with higher efficiency for business growth.

## References

- 1) Yoshiaki Nakamura, "Historical Review and Prospect on CFD", Proceedings of the 28th Symposium on Computational Fluid Dynamics, Presentation No. S01-1, JSFM, (2014) P1.
- 2) Hisaaki Daiguji, "History of the Japan Society of Computational Fluid Dynamics", the Japan Society of Computational Fluid Dynamics Journal, Vol. 10, No. 3, (2002) P233.

## Photo of authors



**Takeru ITOU**  
Engineering Dept.  
Natural Energy Products Division



**Ryosuke KARASAWA**  
Engineering Dept.  
Natural Energy Products Division



**Masato YOSHINO**  
Advanced Technology  
R&D Center

## Technical Trend of the Precision Bearings for Machine Tools


 ULTAGE

Naoki MATSUMORI\*

Keiichi UEDA\*

NTN has been developing, manufacturing and selling the precision bearings for many years to support the progress of the machine tools which are called "Mother Machine" and "Mother of Industry", too. And the bearings have been also globally supporting the manufacturing of the automobile industry and non-automobile industries like medical, energy, transportation and aerospace. In this article, technical trend of the precision bearings for machine tools are introduced below with trend histories and NTN activities.

### 1. Introduction

Recently, machine tools have further improved their performance in order to address diverse requirements from various industries, including automobiles, aircrafts and I.T. In addition to being equipped with the basic performance of the "Mother Machine" such as "high speed, high rigidity and high precision," new models are also being developed one after another with new capabilities and concepts. Such capabilities and concepts include (1) integrated capabilities to cope with consolidated manufacturing processes, (2) 5-axis manipulation to achieve complex and highly precise processes such as curved surfaces, (3) small form factors for energy saving and leaving a small footprint, (4) multi-functionality for improved operability and (5) condition monitoring mechanisms for high reliability <sup>1)</sup>.

To support the above efforts, precision bearings for machine tools are also making progress with new technologies and new products. For example, new technology has been developed to achieve both high speed and high rigidity, which at a high level, are usually in a trade-off relationship, as well as technology to further improve lubricant reliability for grease lubricated high speed main shafts.

In this article, we will discuss technology trends in precision bearings for machine tools, including past transitions and our previous work.

### 2. Transition of technology trends in bearings for machine tools

Recently, machine tools have been bipolarized into a high speed/high precision machine group, including mainly 5-axis machine tools and micro precision machine tools, and a low-priced machine group for customers in emerging countries.

In this way, technology trends in machine tools (next page) are diversified; as such, precision bearings used for machine tools also require new characteristics in addition to high speed, high rigidity and high precision.

**Fig. 1** shows the requirements for precision bearings for machine tools. They can be broadly divided into three phases.

First, until around 2000, bearing technology for improving the basic performance of machine tools, i.e., high speed, high rigidity and high precision and the resulting products were required. With this background, the following products were developed: ceramic bearings which are lighter than steel bearings and therefore more appropriate for high-speed and high contact pressure; small size rolling elements with reduced centrifugal force at high-speed operation; and air-oil lubrication with increased lubrication reliability enabling ultra-high speed operation.

Subsequently, during 2001 to 2014, the requirement for high speed, high rigidity and high precision continued, but long-life and environmental considerations were added as important criteria. Here,

\*Industrial Machinery Engineering Dept., Industrial Business HQ.

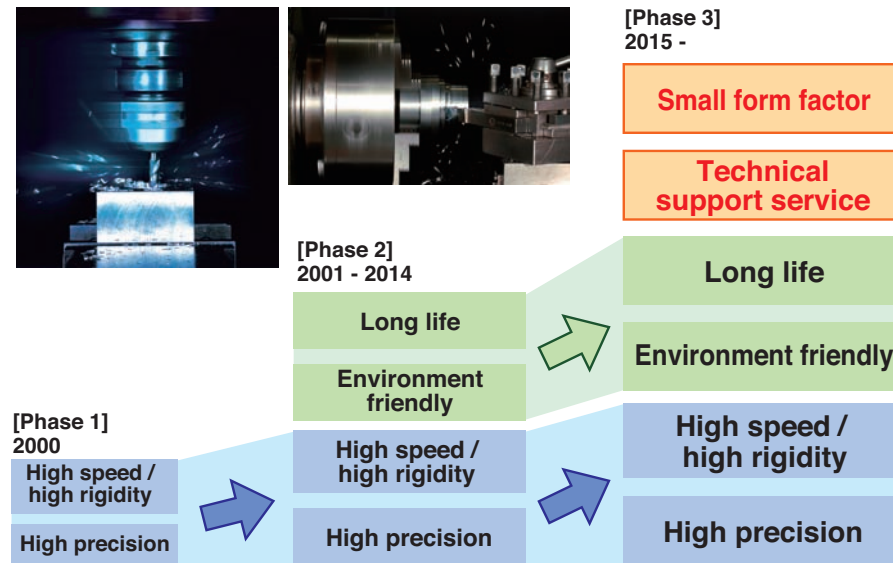


Fig. 1 Needs for the precision bearings for machine tools

**[Machine Tools; Recent Technical Trends]**

- Increase of processing difficult-to-cut materials such as titanium and ultra-hard materials, resulting in further high rigidity requirements for main spindles
- Demand for high efficiency/high precision processing by multi-spindle/multi-function machines
- Small machine tools for processing small objects (Objective: smaller footprint for machine installation, more installed machines per square meter, energy saving, cost reduction, etc.)
- Pursuit of automation, high intelligence, improved operability by high functionality of NC interface and software
- Support of IoT (Internet of Things)
- Prevention of coolant and chips/powder from entering into main spindles
- Prevention of burnout of bearings and other machine components from poor lubricant
- Energy saving, reduction of environmental burden
- Cost reduction by consolidating main spindles
- Insight of the status of the actual machine operation (CMS\* Technology)

\* CMS: Abbreviation of Condition Monitoring System

long-life means the improvement of durability for grease lubricated bearings, with reduced costs and reduced load on the environment compared with air-oil lubrication. For example, high speed/high precision bearings dedicated to grease lubrication were developed with technologies such as grease for high speed and long-life operation, double sealed bearings to increase retention of grease, and grease pockets to

retain as much grease as possible near the raceway<sup>2)</sup>.

In addition, environmental consideration means energy saving and eco-friendliness. Specifically, this means increased capability of grease lubrication bearings with a low environmental burden in high speed areas, low consumption of lubricant oil and compressed air for air-oil lubrication, suppressed oil mist, and low noise generation to reduce the physical burden on the machine tool workers. To address these requirements, eco-friendly air oil lubricated bearings using proprietary nozzles to supply air oil to the outer diameter surface of inner rings, which is subsequently supplied in the bearings with centrifugal force were developed. Angular contact ball bearings with re-lubricating holes on the outer rings were also developed<sup>2)</sup>.

At the present (2015 and after), small machine tools are being actively developed resulting in the technical requirements for small size bearings becoming more rigorous. For example, some small machine tools use compressed air supplied to the main spindle for air cooling and air seals for the small space requirement of the main spindle, instead of ordinary housing cooling (outer cylinder cooling).

With grease lubricated bearings, grease may leak outside the bearings due to compressed air; therefore, measures must be taken.

In addition, as the products, machining methods and users of the machine tools have become diversified, the considerations and proposals for designing main spindles have increased; the respective requirements are increasing, together with design frequency of the main spindles. To support design efforts for the main spindles and reduce the development lead time of machine tools, a "technical

calculation system for bearings of machine tool main spindle" is being developed. The new tool will allow customers to automatically calculate the characteristic values of bearings and main spindle in a short amount of time<sup>3)</sup>.

To address the above requirements, NTN has been long engaged in research and development, manufacturing and distribution of precision bearings for machine tools, resulting in the market introduction of the "ULTAGE Series" High Speed Angular Contact Ball Bearing "HSE Type", which was developed in 2000.

ULTAGE is a name created from the combination of "ultimate," and "stage," to represent NTN's pursuit for the highest level of precision in machine tool bearings. Our concept is to achieve ultra-high speed, high precision and high reliability while coordinating harmony with our environment.

The history of precision bearings for machine tools, ULTAGE Series, is shown in Fig. 2. Since the development of High Speed Angular Contact Ball Bearing "HSE Type" and Angular Contact Ball Bearing with High Speed Seal "BNSxxxLLB Type," many new products have been introduced in the market. In Fig. 2, the concept of each product is broken down by color. Similarly to Fig. 1, blue in Fig. 2 represents "high speed, high rigidity and high precision," green

represents "long life and environmental friendly", and yellow represents "small form factor and technical support service", indicating that the ULTAGE Series addresses various needs for precision bearings for machine tools.

In the next section, we will discuss the technical trends in "high speed, high rigidity and high precision," "long life and environmental friendly", and "small form factor and technical support service", included in the ULTAGE Series.

### 3. Technical trends of "high speed, high rigidity and high precision"

In order to increase the rigidity of bearings, increasing the pre-load during assembly and increasing the load carrying capacity of bearings are effective. However, these adjustments lead to a rise in temperature during operation resulting in deterioration of machining accuracy due to thermal expansion. Therefore, it is critical to suppress heating during operation in order to increase the rigidity of bearings for faster operation<sup>4)</sup>. Specific methods to reduce heating during operation include adoption of the aforementioned ceramic rolling elements and small size rolling elements, as well as optimization of the bearing contact angle and improved raceway

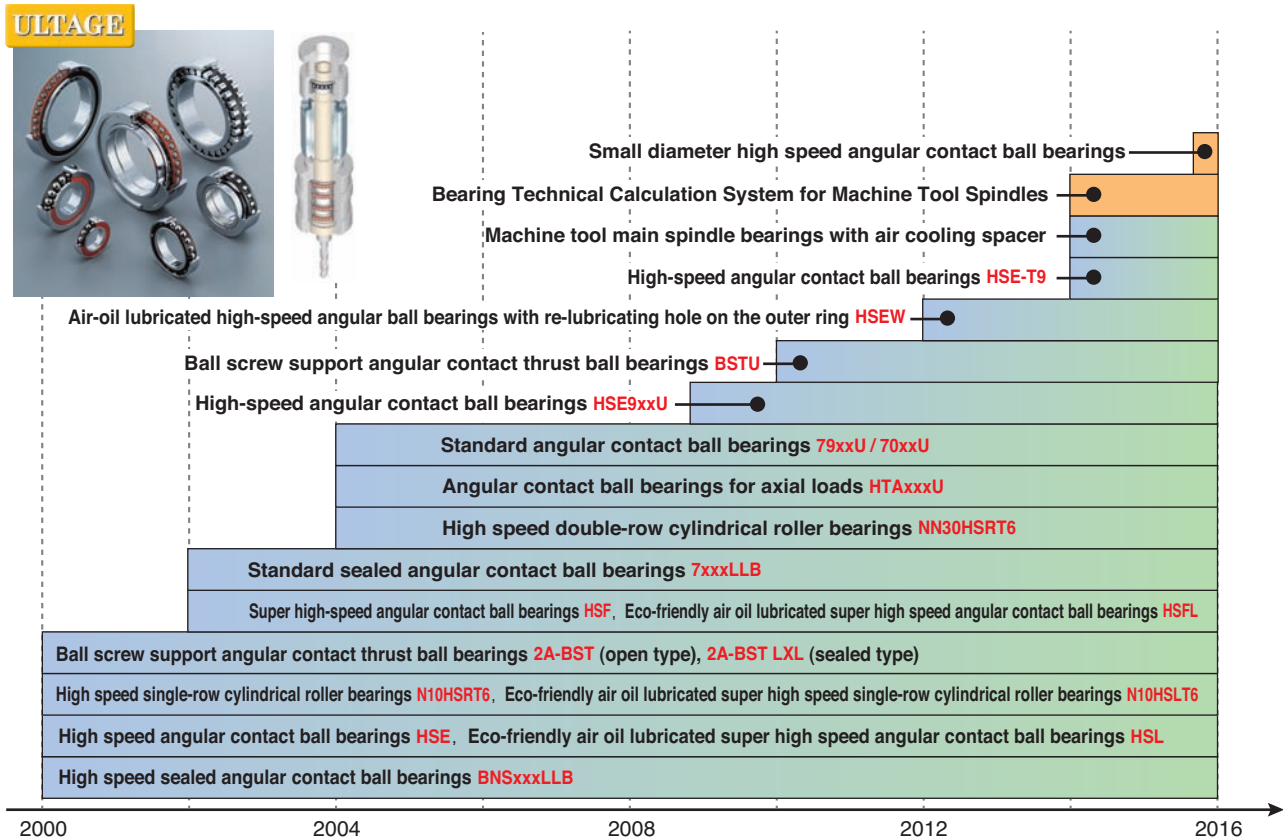


Fig. 2 Development history of NTN precision bearings for machine tools ULTAGE series

geometry of the inner/outer rings.

Special bearing steel with superior wear resistance and anti-galling properties is also used for raceways to increase durability against contact pressure during high-speed/high load operation and under high pre-load conditions<sup>5)</sup>.

Various improvements are also made for cages, such as changing the material from conventional high tension brass to PEEK (polyetheretherketone) resin in order to reduce the weight to 1/4 or less<sup>6)</sup>; adoption of the most appropriate shape for the supply/drain of oil in air oil lubrication; and retention of grease in grease lubrication<sup>7)</sup>. Precision bearings for machine tools incorporating the above measures are shown in Fig. 3.

The most recent trend is the increased demand for 5-axis machine tools with multiple machining capabilities and complex machine tools, which require bearings for the main spindles to offer both high speed and high rigidity at a high level. To that end, it is important to keep the temperature of the bearings low during operation. Therefore, we are proposing "machine tool main spindle bearings with air cooling spacers" and applying air-cooling technology to the bearings (Fig. 4)<sup>4, 8)</sup>.

Machine tool main spindle bearings with air cooling spacers are equipped with air cooling nozzles in addition to oil supply nozzles for air-oil lubrication, on the outer ring spacers. These are incorporated between angular contact ball bearings in back-to-back arrangements (DB arrangement). Air cooling nozzles are at offset positions from the axial center,; the compressed air at room temperature injected from these nozzles (hereinafter cooled air) goes through the space between the inner and outer spacers, as well as inside the bearings, swirling in the rotational direction of the axis. The cooling air removes heat from the surface of the inner ring spacer to cool it down.

The air nozzles of the cooling air are offset so that the cooling air stays around the surface of the inner ring spacer longer. This extends the heat exchange time between the cooling air and the inner ring spacer surface, and increases the cooling effect of the inner ring spacer.

When the inner ring spacer is cooled down, the adjacent bearing inner ring is also cooled. As a result, the difference in temperature between the bearing inner ring and outer ring, and the contact stress on the raceway surface can be reduced to achieve both high speed and high rigidity at a high level.

To meet the precision requirements for bearings used in machine tools, ultra-high precision bearings were developed which reduce Non-Repetitive Run-Out (NRRO) of the bearings. This is done by controlling the size variation of rolling elements per bearing and

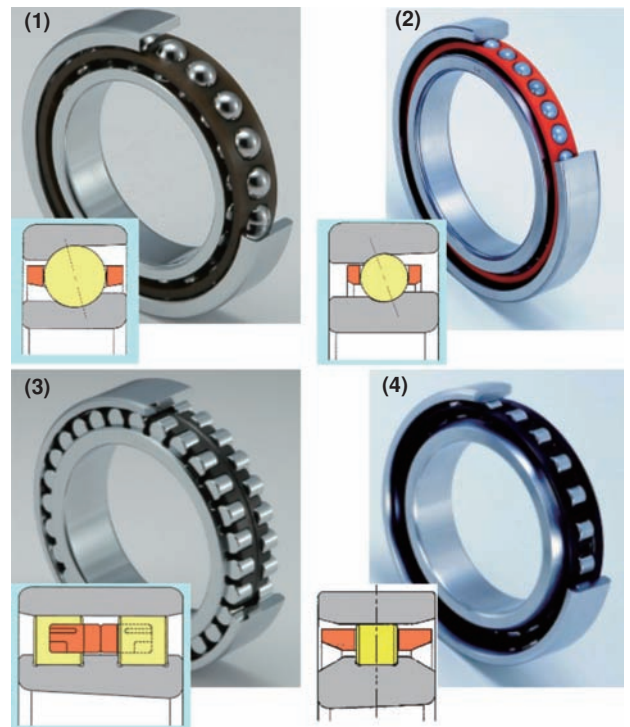


Fig. 3 NTN precision bearings for machine tools ULTAGE series

- (1) Standard angular contact ball bearings 79xxU/70xxU
- (2) High speed angular contact ball bearings HSE
- (3) Super high speed double-row cylindrical roller bearings NN30HSRT6
- (4) Super high speed single-row cylindrical roller bearings N10HSRT6

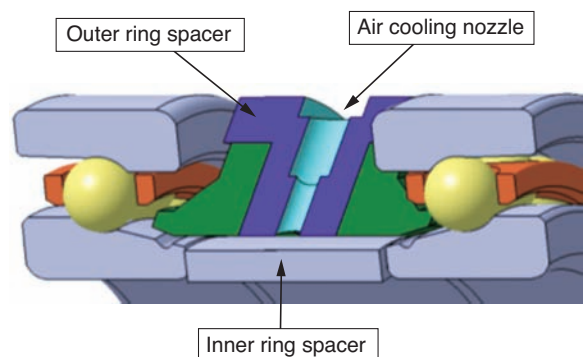


Fig. 4 Machine tool main spindle bearings with air cooling spacer

controlling the angle components of raceway roundness. NTN supports bearings with NRRO of  $0.3 \mu\text{m}$  or less, which are adopted in the ultra-high precision machining center and the main spindles of lathes<sup>5)</sup>.

#### 4. Technical trends in long-life and environment support

As described in Section 2, long-life means improved durability for grease lubricated bearings, with reduced costs and reduced environmental impact compared with air-oil lubrication. "High-speed sealed angular contact ball bearings BNSxxxLLB" (Fig. 5) are based

on the high-speed/high rigidity bearings described in the previous section, but with the additional of double seals for higher retention of grease and grease pockets for retaining grease closer to the rolling elements in order to achieve durability of over 20000 hours in ultra-high speed operation of  $d_{mN}$  value <sup>1)</sup> 1,400,000.

For environmental requirements, eco-friendly air oil lubricated bearings (Fig. 5) were developed enabling the reduction of lubricant oil and compressed air consumption, as well as the reduction of oil mist and low noise.

Furthermore, in recent years, angular contact ball bearings with outer ring supply holes are being seen in the market, which are equipped with re-lubricating holes on the outer ring instead of the conventional method of supplying air oil from the outer ring spacer (Fig. 6)<sup>9)</sup>. This reduces the spacer width because a nozzle hole is not necessary, and contributes to the compact design and increased rigidity of the main spindles by placing bearings on the tip side of the machine tool. "Bearings with re-lubricating holes on the outer ring (HSEW)" can reduce the consumption of lubrication oil and compressed air by using air oil lubrication method from the outer ring. In addition, wind noise and oil mist can be reduced by an optimized oil supply hole size.

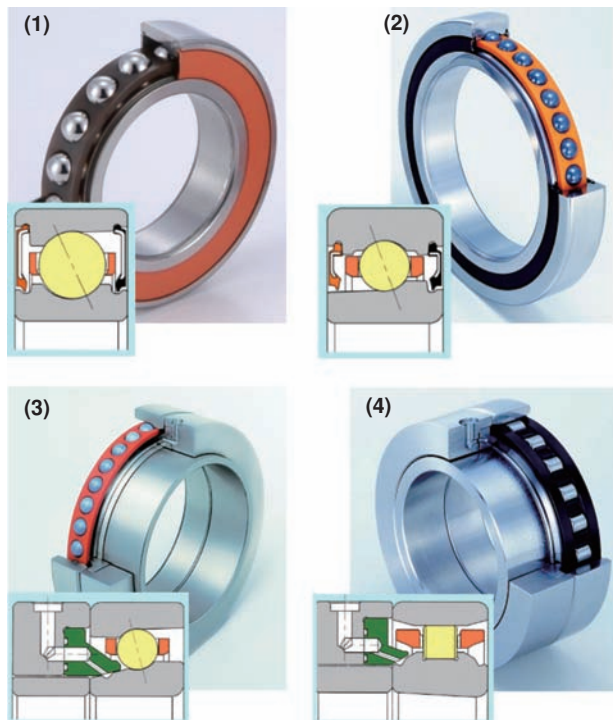


Fig. 5 NTN precision bearings for machine tools ULTAGE series

- (1) Standard sealed angular contact ball bearings 7xxxLLB
- (2) High speed sealed angular contact ball bearings BNSxxxLLB
- (3) Eco-friendly air oil lubricated high speed angular contact ball bearings HSL
- (4) Eco-friendly air oil lubricated super high speed single-row cylindrical roller bearings N10HSLT6

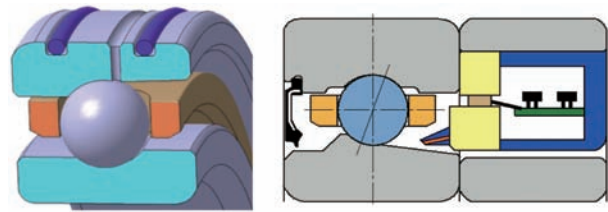


Fig. 6 New bearings for long-life and environmental friendly  
 Left : High speed angular contact ball bearings with re-lubricating hole on the outer ring HSEW  
 Right : "Grease Lubricating Unit with Self-generating Power Supply" for main spindles

A "grease lubricating unit with self-power generator" is also under development for main spindles to further expand the allowable range of operation at high speeds, and reduce the environmental burden (Fig. 6)<sup>10)</sup>. This unit will be incorporated in the outer ring spacer adjacent to the bearings and be equipped with a power generator, pump and lubricating oil. It will have a self-powered generator which leverages the temperature difference that arises between the bearing inner ring and outer ring during bearing operation to enable automatic re-lubrication without an external supply of electric power or lubricating oil. Currently, efforts for commercialization are underway.

### 5. Technical trends in small form factors and technical support services

Demand for small spindles is growing due to the increase of the machining needs for small products such as smart phones and precision/micro processing for medical device components, as well as the highly active development of low-cost/small footprint machine tools for emerging countries.

Some small spindles use compressed air supplied into the spindles for air cooling and air seals, for small space requirement of spindles, instead of ordinary housing cooling (outer cylinder cooling). With grease lubricated bearings, grease may leak outside the bearings due to the compressed air; therefore, measures must be taken. Sealed bearings are effective for preventing grease leakage; however, it will be harder for compressed air to flow within the spindles, reducing the cooling effect and blocking the capability to prevent foreign objects from entering. Therefore, NTN developed the "ULTAGE Series Small Size High-speed Angular Contact Ball Bearings" (Fig. 7)<sup>11)</sup>.

These bearings adopt newly designed seals to prevent grease leakage and increase lubrication life, while ensuring the easy flow of compressed air. They also achieve reduced vibration by optimizing the internal design of the bearings.

Recently, machine tool manufacturers, and

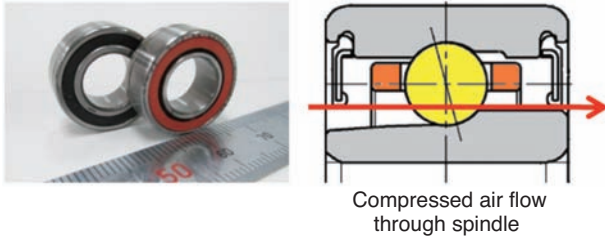


**Fig. 7** ULTAGE small size high-speed precision angular contact ball bearings

customers specializing in spindles, are developing a wide array of products addressing user needs. To support these development efforts, we have developed the "Bearing Technical Calculation System for Machine Tool Spindles". This tool allows customers to automatically calculate the properties of precision rolling bearings used for main spindles of machine tools such as the main spindle rigidity and bearing life, very quickly (Fig. 8)<sup>3)</sup>.

This system can calculate the properties of 10 types of main spindle layouts with varied bearing types, arrays and pre-load methods. First, customers will send the data required for the calculation, such as bearing type and usage conditions, in the dedicated Excel® file to the dedicated server by email<sup>2)</sup>. Upon receiving the data, the server automatically conducts calculations based on the input data, and automatically sends the calculation results such as the spindle rigidity and bearing life to the customer, instantaneously. Conventionally, it takes at least one day to respond to customers with the report of the calculation results from the time we received the requests<sup>3)</sup>. However, this system produces the calculation results in approximately 10 minutes from the time the customer sends the email.

In addition, since the customers can conduct calculations as many times as required, they can shorten the time needed to choose between spindle design options.

Furthermore, since the server is available at all times, customers can use the system without any time restrictions.

The final specifications of bearings require review

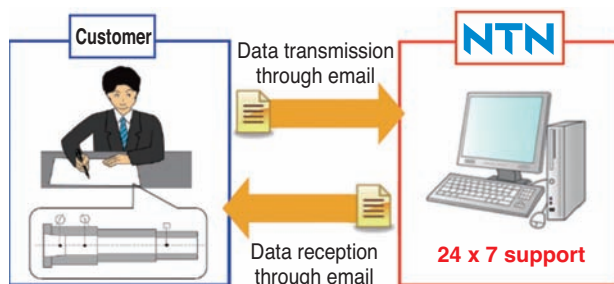


**Fig. 8** Bearing technical calculation system for machine tool spindles

meetings by the customers and NTN; however, this system can shorten the design process before then, contributing to a reduced lead time for development of the main spindles and machine tools.

## 6. Summary

As the materials, shapes, processing methods and processing conditions of the products are diversified, the requirements for performance of machine tools and precision bearings used by those tools are expected to be even more rigorous.

NTN will continue to work to further improve the performance and quality of its products, as well as enhance the technical support and proposals, including enhanced speed and capabilities of technical calculation, in order to respond to customer needs sincerely and precisely.

## References

- 1) Shouhei Hashizume: New Technologies on Precision Bearings for Machine Tools, Machine Design, Vol. 60, No. 1 (Jan issue, 2016) 28.
- 2) NTN Catalog: Precision Rolling Bearings, CAT. No. 2260-IV/J, 14.10.02 82.
- 3) Keiichi Ueda, Yushi Onda and Shouhei Hashizume: Bearing Technical Calculation System for Machine Tool Spindles, NTN TECHNICAL REVIEW, No. 82, (2014) 49.
- 4) Yushi Onda, Kikuo Fukada, Yohei Yamamoto and Masato Yoshino: Machine Tool Main Spindle Bearings with Air Cooling Spacer, NTN TECHNICAL REVIEW, No. 82, (2014) 38.
- 5) Hiroshi Tako and Yasutsugu Tanaka: Technical Trend of Machine Tool Bearings, NTN TECHNICAL REVIEW, No. 78, (2010) 8.
- 6) Naota Yamamoto and Mamoru Mizutani: High Speed and Long Life Double-Row Cylindrical Roller Bearings, NTN TECHNICAL REVIEW, No. 72, (2004) 42.
- 7) Keiichi Ueda: ULTAGE Standard Angular Contact Ball Bearings, 79U/70U type, NTN TECHNICAL REVIEW, No. 72 (2004) 30.
- 8) Keisuke Nasu, Naoya Okamoto and Masato Yoshino: Machine Tool Main Spindle Bearings with Air Cooling Spacer, NTN TECHNICAL REVIEW, No. 84, (2016) 52.
- 9) Futoshi Kosugi and Kouji Nishino: Air Oil Lubrication Bearings with Re-lubricating Hole on the Outer Ring for Machine Tools, NTN TECHNICAL REVIEW, No. 78 (2010) 41.
- 10) Kaoru Omoto and Hiroyoshi Ito: Development of the Lubricating Oil Supply Unit with Self-generating Power Supply, NTN TECHNICAL REVIEW, No. 80, (2012) 48.
- 11) Mineo Koyama, Keisuke Nasu and Takahiro Kanamoto: ULTAGE Series Small Size High-Speed Precision Angular Contact Bearings for Machine Tool Spindles, NTN TECHNICAL REVIEW, No. 84, (2016) 46.

## Photo of authors



Naoki MATSUMORI  
Industrial Machinery  
Engineering Dept.,  
Industrial Business HQ.



Keiichi UEDA  
Industrial Machinery  
Engineering Dept.,  
Industrial Business HQ.

# ULTAGE Serises Small Size High-Speed Precision Angular Contact Ball Bearings for Machine Tool Spindles




Mineo KOYAMA\*  
Keisuke NASU\*  
Takahiro KANAMOTO\*\*

For high-speed, long-life and low vibration demand of small size machine tools and small size spindle, NTN developed small size high-speed angular contact ball bearings for machine tool spindles and added it to the ULTAGE family. The bearings can hold more grease than current bearings through the new designed seal and modified grease filling, even if compressed air goes through the bearing. Moreover the bearings perform lower vibration through the process modification of raceways. In this document, we introduce the design points, test datas and analysis results .

## 1. Introduction

Recently, machining needs for small products such as smart phones and precision/micro processing needs for medical device components are increasing. Also, the development of low-cost machine tools with a small footprint for emerging countries is highly active. Therefore, the demand for small spindles is increasing. Many small spindles adopt a structure to use compressed air for internal cooling and to prevent foreign objects from entering. However, when grease lubrication is used, compressed air can cause the grease to leak from the bearings, resulting in a shorter lubrication life.

Sealed bearings are effective for preventing grease purge, however, it is harder for the compressed air to flow within the bearings, reducing the cooling effect on the spindle and limiting the capability to prevent foreign objects from entering.

The newly developed "small size high speed angular contact ball bearing" adopts a new seal design to reduce grease purge while securing easy flow of compressed air inside bearings. There are measures in place to better retain the grease by adjusting the seal position and pressure. In addition, the processing of the bearing raceway was optimized, increasing product

machining accuracy of the spindle, improving the quality of the machined surfaces, and reducing vibration.

## 2. Small spindle structure

Fig. 1 shows a general schematic of a small size spindle with a built-in motor. Medium to large high speed spindles with built-in motors usually adopt the outer cylinder cooling method, where heat is removed from the motor and bearings by circulating coolant to stabilize the spindle temperature. This cooling method requires ancillary facilities and running costs, as well as a larger spindle outer diameter. Also for medium to large high speed spindles, a Labyrinth, or air seal structure, is often used to protect the tip of the tool by blocking cutting fluid and chips from the machining location.

In contrast, in the case of small size spindles with limited space and low cost requirements, compressed air is supplied from the rear side of the spindle to cool down the motor and bearings. The compressed air, which is exhausted from the tip of the tool, also works as an air seal. For this cooling method to work, the bearings used in small size spindles require easy flow of compressed air through the spindle and grease retention for high lubrication reliability.

\* Industrial Machinery Engineering Dept., Industrial Machinery Division

\*\* Product Design Department, Industrial Machinery Division

※1 To the left of the photo is one side of the developed bearing (front side/black seal) and to the right of the photo shows the other side of the product (back side/orange seal).

※2 ULTAGE is a name created from the combination of "ultimate," and "stage," signifying performance in any application expressing NTN's idea of exploring the ultimate performance of precision bearings.

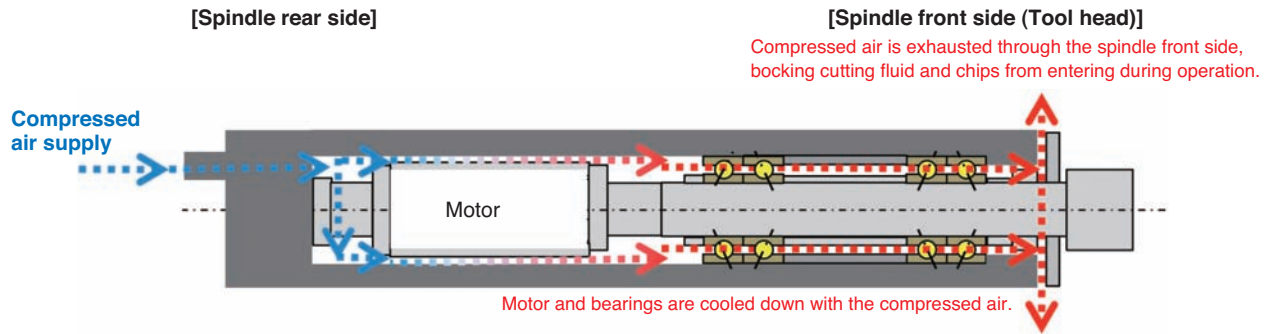


Fig. 1 Example of small size spindle

### 3. Benefits of the developed product

#### 3. 1 Achieving both compressed air flow and grease retention

As described in the previous section, compressed air is supplied inside the spindle and runs through the inside of the bearings. The developed product ensures this compressed air can flow while increasing grease retention. Fig. 2 shows the challenges faced by the conventional product and the benefits of the developed product.

The open type conventional product <sup>1)</sup> has a wide opening for easy compressed air flow, but the grease is likely to escape. The sealed type conventional product reduces grease purge risk, but the compressed air does not flow easily through the small gap in the seal lip.

On the other hand, the developed product adopts a new seal design to reduce grease leakage while allowing easy flow of compressed air. The increased

bearing width allows grease lubrication from both sides of the bearing, for an increased total fill amount.

Also, a grease pocket is created close to the outer ring raceway to increase grease retention. In addition, the processing method of the bearing raceway was optimized, increasing product machining accuracy of the spindle, improving quality of the machined surfaces, and reducing vibration.

In the next section, we will discuss the results of the analysis conducted before adopting this specification and an example of the test results.

#### 3. 2 Flow of compressed air through the developed seal

Fig. 3 shows a fluid analysis simulation of the compressed air flow through the developed product when actually incorporated into the spindle. The flow is shown when compressed air is supplied from one end of the double-row back-to-back arrangement, and exhausted out the other end.

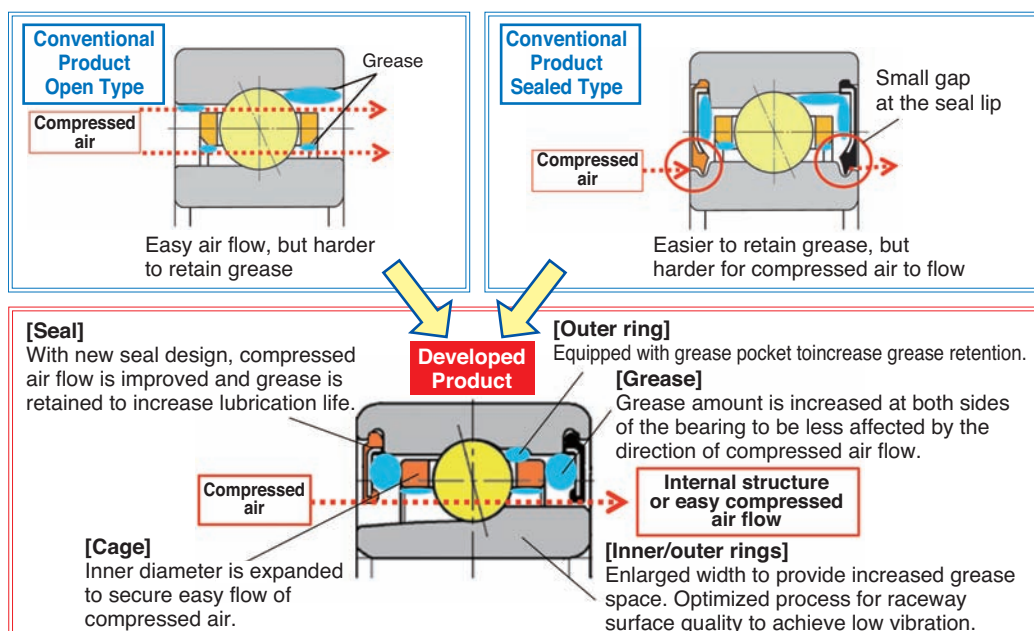


Fig. 2 Small size high-speed angular contact ball bearings (Comparison of conventional design and development design)

The developed product allows an almost straight stream-line from the front side of the first bearing where the compressed air is supplied to the back side, then to the front side of the second bearing where the compressed air is exhausted. The adoption of a newly designed seal with an increased gap between the seal inner diameter on the back side and inner ring allows this stream-line flow.

The flow rate of the compressed air is high in the space between the seal inner diameter and the inner ring, while it is low in the space between the seal inner diameter and the outer ring.

From this, it is expected that this design will prolong lubrication life by retaining abundant grease in the space between the seal inner diameter and the outer ring, which is less affected by the compressed air.

### 3.3 Bearing grease behavior due to compressed air

In the previous section, we described the expectation of improved grease retention in the space between the seal inner diameter and outer ring with adoption of the new seal design. In order to confirm, the behavior of the grease was analyzed using fluid analysis. The result is shown in Fig. 4. Condition 1 shows the status of the grease after operation, when a grease amount of approximately 30% of the bearing space is injected mainly on the back side of each of the bearings. Abundant grease is retained in the space between the seal inner diameter and outer ring, which is less affected by the compressed air. However, the grease amount retained in the bearings on the exhaust side of the compressed air is lower

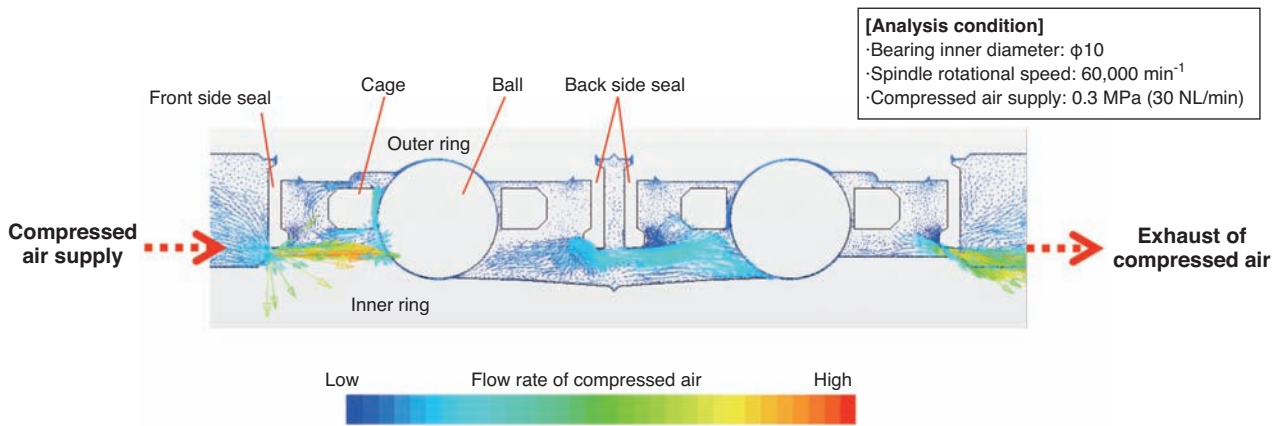
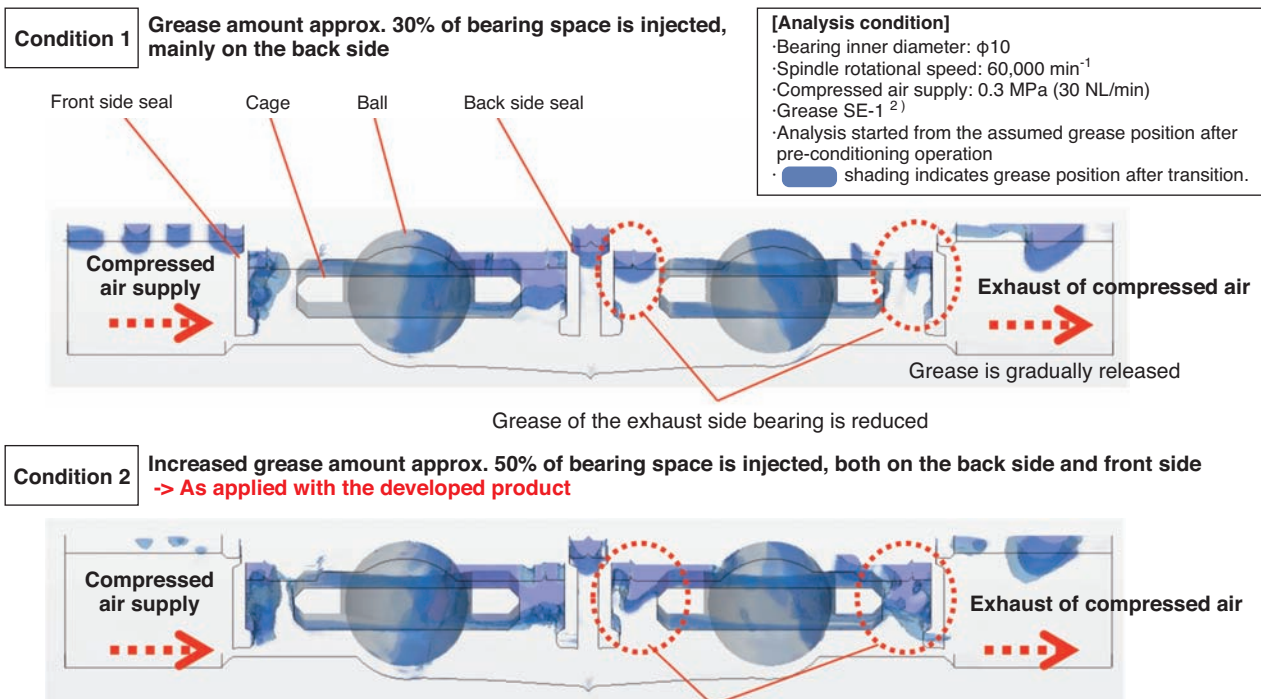


Fig. 3 Fluid analysis result of compressed air flow through the bearings



Transition of grease due to compressed air flow is suppressed by filling the space on the exhaust side with grease

Fig. 4 Fluid analysis result of grease movement figure by compressed air through the bearings

compared with the bearings on the supply side.

Condition 2 uses a grease amount of approximately 50% of the bearing space, injected both on the back side and front side of each bearing. In this case, the grease is sufficiently retained in the bearings on the exhaust side also, which means that a longer lubrication life can be expected.

In the case of a back-to-back arrangement, compressed air flows from the front side of a bearing to the back side of another set of bearing. Therefore, it is necessary to increase grease retention regardless of the direction of compressed air flow, which makes condition 2 more favorable, as an increased amount of grease is retained, both on the back side and front side of each bearing.

### 3.4 Evaluation test results

In order to verify the actual effect of the fluid analysis results described in the previous section, a test was conducted by operating a spindle with the developed product built in. The spindle was operated at a speed of 60,000min<sup>-1</sup> for 500 hours, continuously, and the grease amount and grease condition inside the bearings was confirmed after the test. Results are shown in Fig. 5.

In this test, compressed air of 0.3MPa (30NL/min) was used, which is the highest level recommended for this size of bearings.

The developed product uses a grease amount of approximately 50% of the bearing space, injected both on the back side and front side of each bearing. The

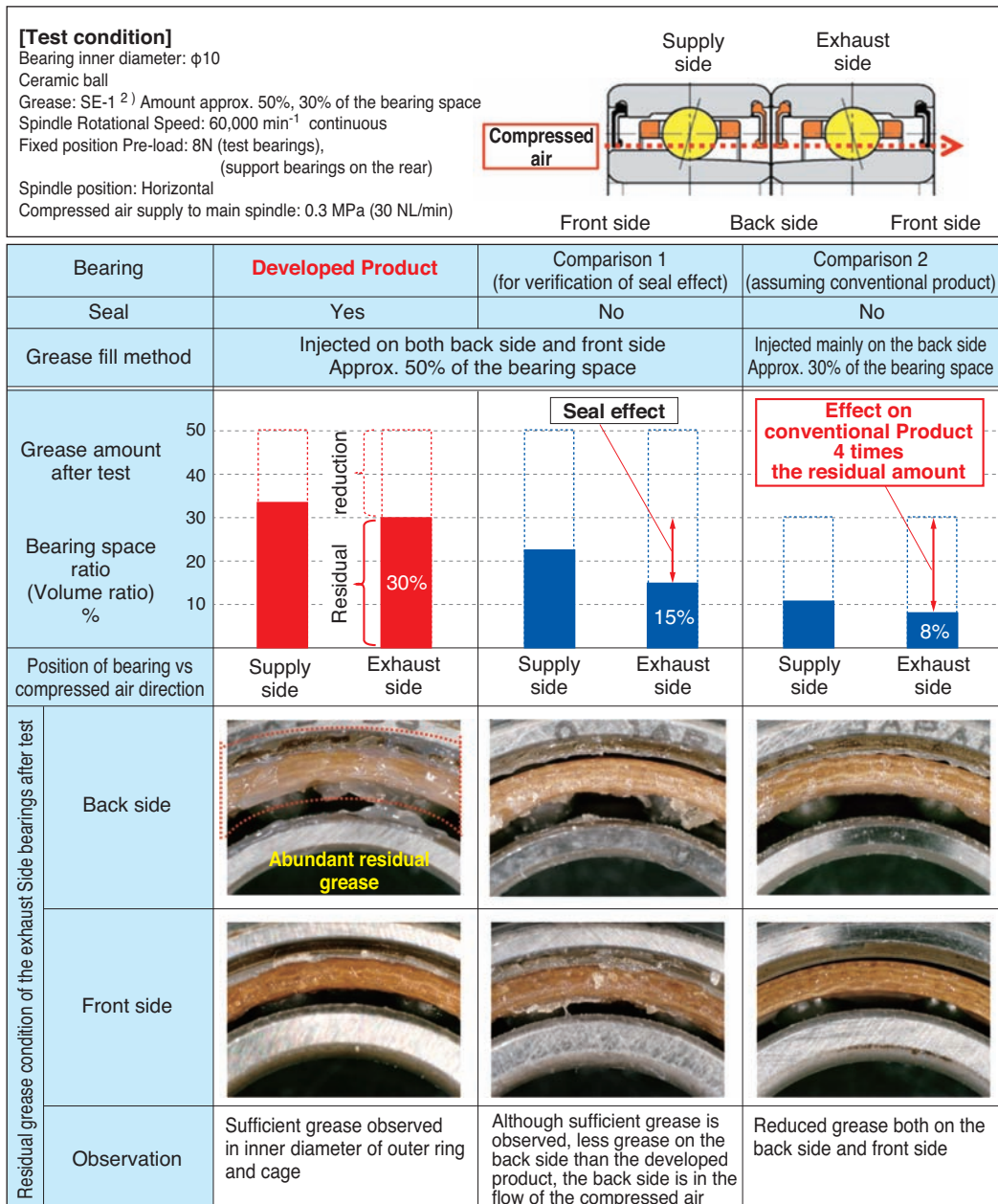


Fig. 5 Grease amount and situation after 500 hour driving under compressed air supply through the spindle

grease amount after 500 hours was decreased to 30% of the bearing space; however, that amount is still sufficient for continued operation and grease retention around the rolling elements, outer ring inner diameter surface, and cage surface was verified to be sufficient.

Next, a test without a seal was conducted to verify the effect of the seal (Fig. 5 Comparison 1). In the case of Comparison 1, the grease in the bearings on the exhaust side had decreased to 15% of the bearing space. This amount is also sufficient for continued operation; however, the grease amount at the back of the exhaust side bearing is lower than in the developed product.

Subsequently, another test was conducted with a grease amount of approx. 30% of the bearing space, for comparison with the conventional product. Results are shown in Fig. 5 Comparison 2.

Grease in the bearing on the exhaust side had

decreased to 8% of the bearing space. No abnormalities were found in the test bearings, which suggests continued operation is still possible; however, in order to retain stable lubrication for a long time under the condition of compressed air flow, it is considered important to supply an increased amount of grease on both sides, as shown in the developed product.

#### 4. Durability under compressed air flow

Currently, NTN is conducting a test on a spindle built with the developed product, supplying 0.3MPa (30NL/min) of compressed air, for over 6,000 hours of continuous operation at the speed of 60,000 min<sup>-1</sup> (Fig. 6). Additional test samples to gather data on durability are to be added.

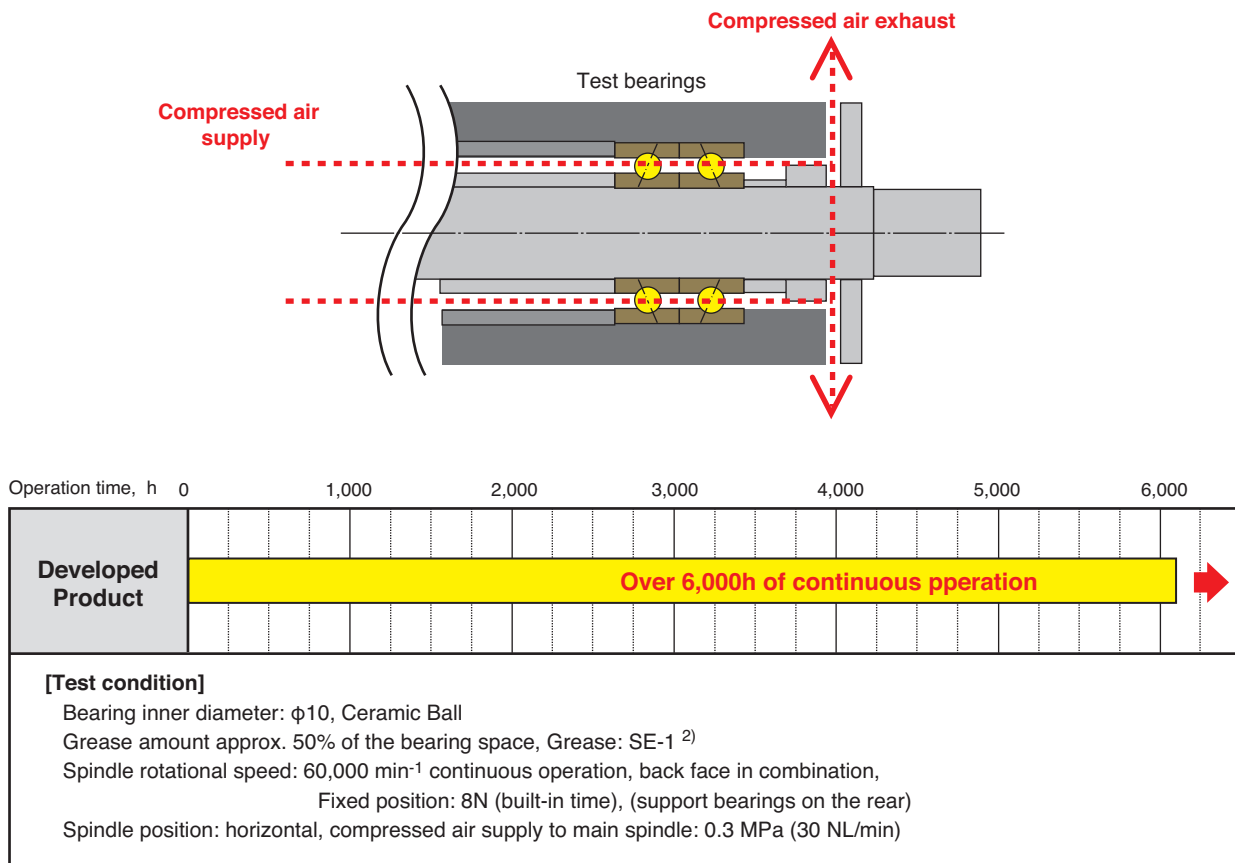


Fig. 6 Durability test in high-speed operation under compressed air supply through the spindle

## 5. Reduction of bearing vibration

The application range of small size spindles is expanding from conventional drilling and other auxiliary uses such as deburring to sub-spindles of machine tools and machining of small products.

Among others, applications for precision micro-processing are promising, which require low vibration in order to increase the quality of the machined surface.

The developed product has achieved approximately 50% of vibration reduction by optimizing the bearing internal design<sup>3)</sup> and the processing quality of the raceway surface on the inner and outer rings (Fig. 7). By reducing the vibration in bearings, the vibration property of the spindle is improved, which should contribute to the expansion of applications for small size spindles.

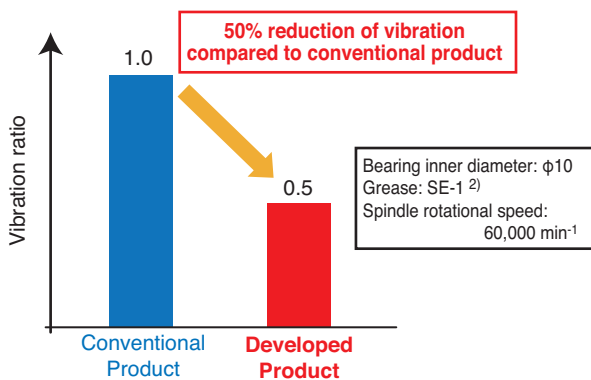


Fig. 7 Effect of vibration reduction

## 6. Summary

The developed ULTAGE Series Small Size High-Speed Angular Contact Ball Bearings achieve both improved compressed air flow and increased retention of the required grease amount. These improvements are made without degrading the spindle cooling and air seal effects, allowing the continued use of compressed air flow inside the bearings to cool the spindle, while contributing to a long lubrication life under high speed operation.

NTN will continue to work on performance improvements of bearings for the main spindles, in order to further improve reliability of machine tools.

### References

- 1) Hiroshi Takiuchi and Futoshi Kosugi: "ULTAGE" Series Precision Bearings for Machine Tools, NTN TECHNICAL REVIEW, No. 72, (2004) 26.
- 2) Takayuki Kawamura: Research on the Lubrication Mechanism of Grease for High Speed Bearings, NTN TECHNICAL REVIEW, No. 76, (2008) 39.
- 3) Tomoya Sakaguchi and Yoshinobu Akamatsu: Simulation for Ball Bearing Vibration, NTN TECHNICAL REVIEW, No. 69, (2001) 69.

### Photo of authors



Mineo KOYAMA  
Industrial Machinery  
Engineering Dept.,  
Industrial Business HQ

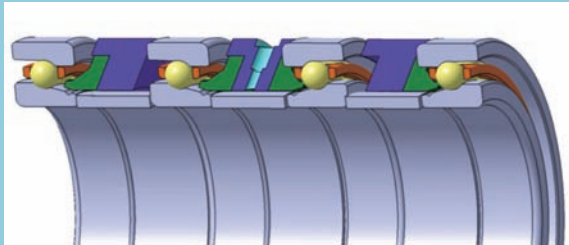


Keisuke NASU  
Industrial Machinery  
Engineering Dept.,  
Industrial Business HQ



Takahiro KANAMOTO  
Product Design Department,  
Industrial Business HQ

## Machine Tool Main Spindle Bearings with Air Cooling Spacer



Keisuke NASU\*  
Naoya OKAMOTO\*\*  
Masato YOSHINO\*\*\*

NTN developed "Machine Tool Main Spindle Bearing with Air Cooling Spacer" which can perform high-speed and high-rigidity at the same time with higher level than ever, through the original air cooling technology. We carried out the performance tests of the cooling technology in various practical applications of machine tool spindles. In this paper, the results of the above mentioned tests and fluid analysis regarding the cooling technology are introduced as follows.

### 1. Introduction

The main spindles of machine tools are required to have both high rigidity and high precision when machining difficult-to-machine materials or components with complex shapes. Additionally, high speeds and highly precise rotation are required to machine molds for machine components and medical field components. Although the requirements for the main spindles of machine tools vary depending on the machining method and the products to be machined, there has recently been increased demand for 5-axis machine tools with multiple machining capabilities, as well as complex machine tools which require spindles and bearings that offer both high speed and high rigidity at a high level<sup>1)</sup>. To that end, it is important to keep the temperature of the bearings low during operation, and NTN has developed "machine tool main spindle bearings with air cooling spacers", and applied its proprietary air-cooling technology to the bearings<sup>2)</sup>.

In this development, we demonstrated the cooling of the bearings as well as noise reductions by improving the shape of the outer ring spacer. This time, in order to demonstrate its practicality, we implemented this technology with bearings and operating conditions which are commonly found in machine tool main spindles and verified the cooling effects.

### 2. Structure and cooling mechanism

The structure of bearings with air cooling spacers is shown in Fig. 1 and the fluid analysis results are shown in Fig. 2. NTN's proprietary eco-friendly air-oil lubrication nozzle<sup>3, 4)</sup> is applied to outer ring spacers between the angular contact ball bearings in a back-to-back arrangement (DB arrangement) for reductions in air-oil and noise. Additionally, a separate air cooling nozzle is included.

The air cooling nozzles are at offset positions about the center axis. The compressed room temperature air injected from these nozzles (hereinafter cooling air) goes through the space between the inner and outer spacers as well as the inside of the bearings, revolving in the rotational direction of the inner ring. The cooling air removes heat from the surface of the inner ring spacer to cool it down.

The air nozzles of the cooling air are offset so that the cooling air remains near the surface of the inner ring spacer longer, allowing more time for the cooling air to remove the heat from the inner ring spacer surface, thereby increasing the cooling effects of the inner ring spacer.

When the inner ring spacer is cooled down, the adjacent bearing inner ring is also cooled. As a result, the difference in temperature between the bearing inner ring and outer ring (hereinafter, inner/outer ring

\* Industrial Machinery Engineering Dept., Industrial Business HQ

\*\* Product Design Dept. Industrial Business HQ

\*\*\* Advanced Technology R&D Center

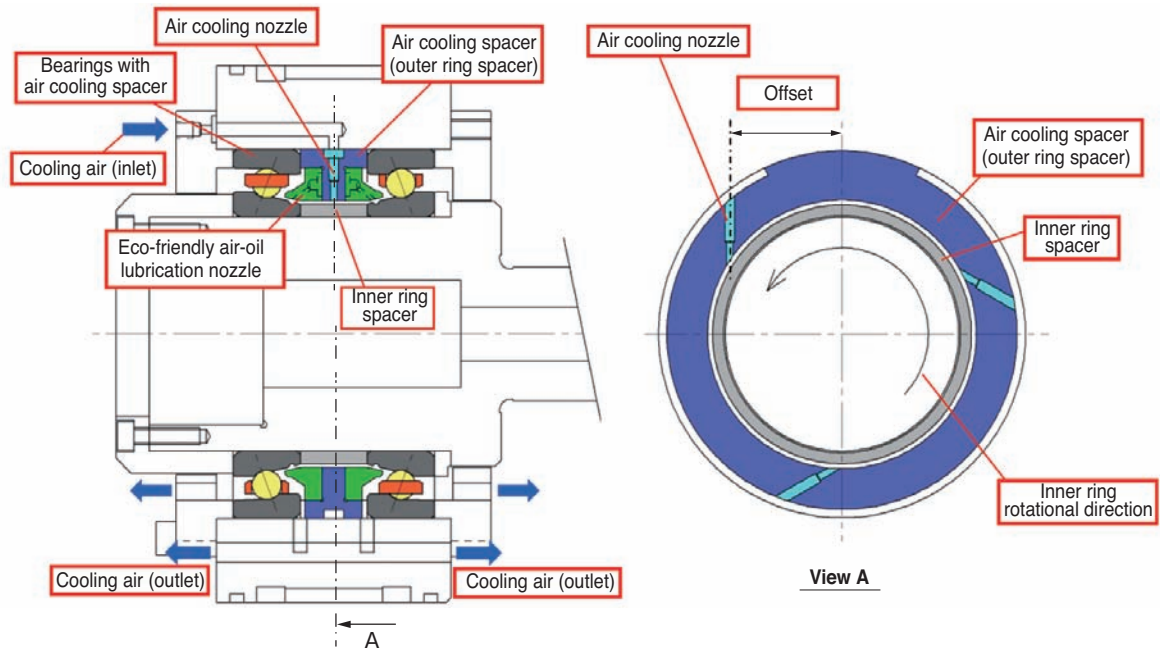


Fig. 1 Structure of the bearing with air cooling spacer

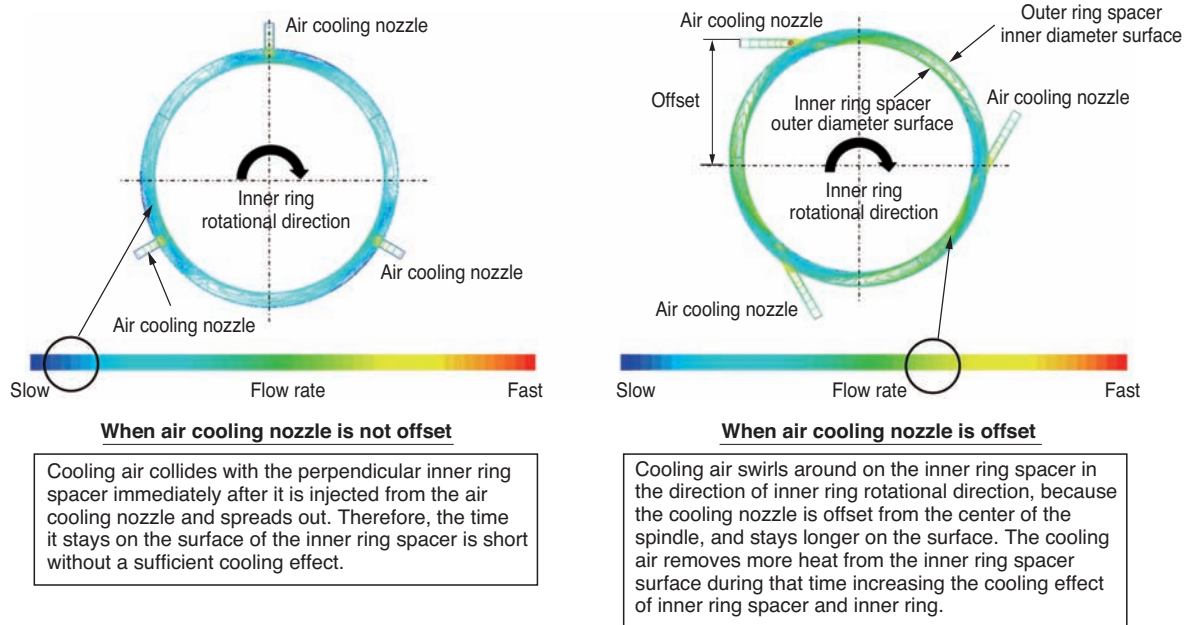


Fig. 2 Cooling air flow between inner and outer spacers (Fluid analysis results)

temperature difference) is reduced, and the contact stress on the raceway surface decreases to allow for both high speed and high rigidity at a high level.

### 3. Cooling effects

In order to verify the cooling effects with bearings and operating conditions which are commonly found in machine tool main spindles, high speed operation testing was conducted under the four conditions shown in Table 1.

The nozzle offset was set to 80% of the radius of the inner ring spacer outer diameter<sup>2)</sup>.

Table 1 Test conditions

Bearing arrangement	Main spindle drive method	
DB  (Back-to-back)	[Test 1] Motor direct	[Test 2] Built-in motor
DTBT  (Tandem back-to-back)	[Test 3] Motor direct	[Test 4] Built-in motor

### 3. 1 Cooling effects of back-to-back arrangement (DB arrangement)

Cooling effects of the bearings with air cooling spacers under DB arrangement was confirmed with the high speed operation testing. The test conditions are shown in Table 2, the structure of the tester is shown in Fig. 3, and the test results are shown in Fig. 4. This test was conducted with a DB spacer width of 22mm, almost the same width as the bearing, a

**Table 2** Test conditions for DB arrangement

Test bearings	φ70 x φ110 x 20 5S-2LA-HSL014 equivalent (Eco-friendly air-oil lubricated angular contact ball bearings with ceramic balls)
Pre-load method	Fixed position pre-loading (Pre-loading ON after built-in)
Rotational speed	0~23,000min <sup>-1</sup>
Lubrication method	Air-oil lubrication
Amount of lubricant	0.03mL/10min
Lubricant	ISO VG32
Lubrication air flow rate	30NL/min
Cylinder cooling	Yes, Sync w/room temperature
Spindle position	Horizontal spindle

condition where heat is not easily released because the bearings (which are heat sources) are close to each other.

In the case of a direct motor drive, inner/outer ring temperature difference at 17,000 min<sup>-1</sup> ( $d_{mN}$  value 1,530,000) was confirmed to decrease by approx. 2°C with cooling air of 100NL/min, approx. 5.5°C with 200NL/min, and approx. 7.5°C with 300 NL/min compared with no cooling air conditions. Due to these decreases in inner/outer ring temperature difference, the maximum contact stress on the bearing raceway surface at 17,000 min<sup>-1</sup> is reduced by approx. 10% at 100NL/min, approx. 15% at 200NL/min, and approx. 20% at 300NL/min.

As a result, the stress at 17,000 min<sup>-1</sup> with no cooling air supply and the stress at 21,000 min<sup>-1</sup> with a supply of 300NL/min cooling air are equivalent, which allows for a 25% increase in speed.

In the case of the built-in motor drive, the inner/outer ring temperature difference at 17,000 min<sup>-1</sup> ( $d_{mN}$  value 1,530,000) was confirmed to decrease by approx. 5°C with cooling air of 100NL/min, approx. 8°C with 200NL/min, and approx. 11°C with 300 NL/min

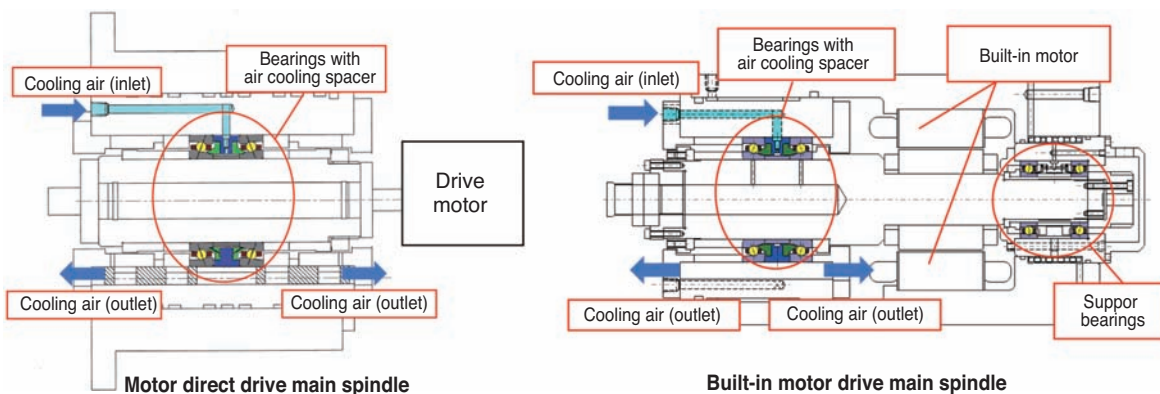
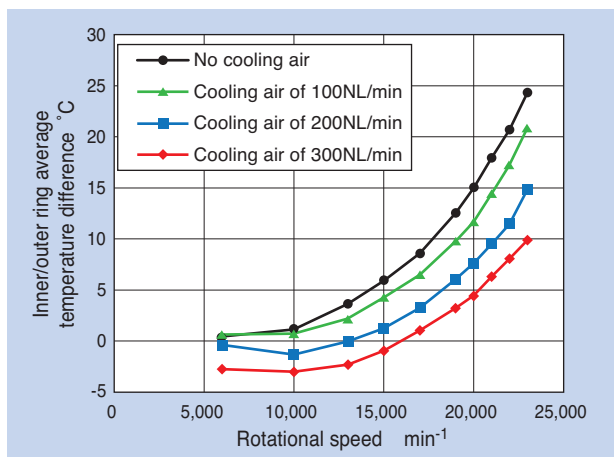
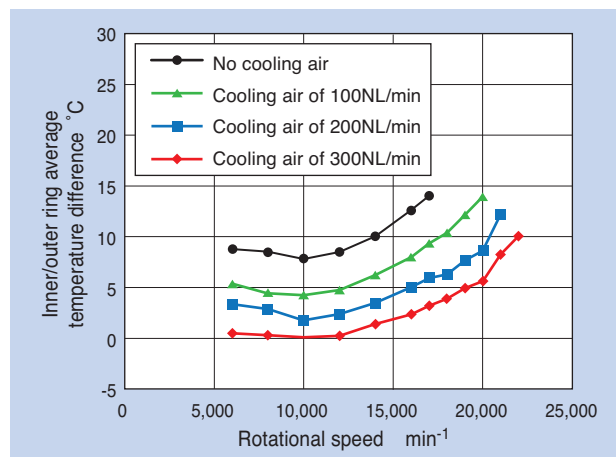


**Fig. 3** Test spindles for DB arrangement



**Results with motor direct drive main spindle**



**Results with built-in motor drive main spindle**

**Fig. 4** Relation between cooling air amount and temperature difference between inner ring and outer ring (In case of DB arrangement)

compared with no cooling air conditions. Due to these decreases in inner/outer ring temperature difference, the maximum contact stress on the bearing raceway surface at 17,000 min<sup>-1</sup> is reduced by approx. 15% at 100NL/min, approx. 20% at 200NL/min, and approx. 25% at 300NL/min. As a result, the contact pressure at 17,000 min<sup>-1</sup> with no cooling air supply and the contact pressure at 22,000min<sup>-1</sup> with a supply of 300NL/min cooling air are equivalent, which allows for a 30% increase in speed.

In either main spindle drive method, the cooling effects of bearings with air cooling spacers were verified.

In addition to the test with a spacer width of 22mm as described earlier, a test with a spacer width of 66mm was also conducted, verifying the cooling effects<sup>2)</sup>.

### 3.2 Cooling effects of tandem back-to-back arrangement (DTBT arrangement)

Following the evaluation test with DB arrangement in the previous chapter, cooling effects of the bearings with air cooling spacers under DTBT arrangement was

confirmed with a high speed operation test. The configuration of the tester is shown in Fig. 5 and test conditions are shown in Table 3. This test was also conducted with a DB spacer width of 22mm, similar to the test with DB arrangement in the previous chapter.

The results for the direct motor drive are shown in Fig. 6. The inner/outer ring temperature difference at 17,000 min<sup>-1</sup> ( $d_{min}$  value 1,530,000) was confirmed to decrease by approx. 6°C with 300NL/min compared with no cooling air conditions. Due to this decrease of inner/outer ring temperature difference, the maximum contact stress on the raceway surface at 17,000 min<sup>-1</sup> is reduced by approx. 15%, allowing for a 17% increase in speed.

Subsequently, a test with a built-in motor drive was conducted. With this drive method, the bearing temperature is bound to be affected by the heat from the motor as the built-in motor is close to the bearings.

To verify this effect, a high-speed test was first conducted without cooling air. The inner/outer ring temperature difference at 17,000 min<sup>-1</sup> ( $d_{min}$  value 1,530,000) is shown in Fig. 7. In this test, larger inner/outer ring temperature differences were

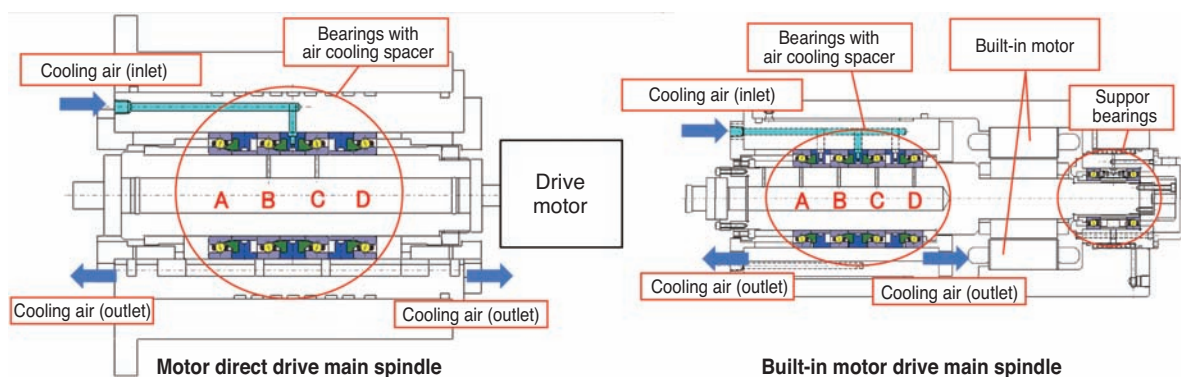


Fig. 5 Test machines for DTBT arrangement

Table 3 Test conditions for DTBT arrangement

Test bearings	φ70 x φ110 x 20 5S-2LA-HSL014 equivalent (Eco-friendly air-oil lubricated angular contact ball bearings with ceramic balls)
Pre-load method	Fixed position pre-loading (Pre-loading ON after built-in)
Rotational speed	0~23,000min <sup>-1</sup>
Lubrication method	Air-oil lubrication
Amount of lubricant	0.03mL/10min
Lubricant	ISO VG32
Lubrication air flow rate	30NL/min
Cylinder cooling	Yes, Sync w/room temperature (21 ± 1°C)
Spindle position	Horizontal spindle

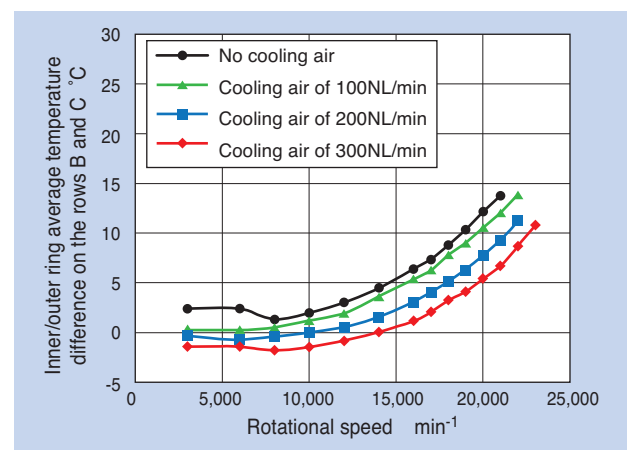


Fig. 6 Relation between cooling air amount and temperature difference between inner ring and outer ring (Coupling direct motor system, in case of DTBT arrangement)

observed on bearings closer to the motor. Therefore, methods to cool down row C and row D, which showed larger inner/outer ring temperature differences and higher maximum contact stress on the raceway surface, were considered.

The relationships between the supply point of cooling air, supply amount, and inner/outer ring temperature difference are shown in Fig. 8. When cooling air was supplied at 300NL/min between DB (Fig. 8 (1)), the inner/outer ring temperature difference at 17,000min<sup>-1</sup> ( $d_{mN}$  value 1,530,000) decreased by approx. 7°C at row C and approx. 3°C at row D as compared to the case where no cooling air was supplied. When cooling air of 300NL/min was supplied between DT (Fig. 8 (2)), the inner/outer ring temperature difference at 17,000min<sup>-1</sup> ( $d_{mN}$  value

1,530,000) decreased by approx. 7°C at rows C and D. When cooling air of 150NL/min was supplied between both DB and DT for a total of 300NL/min (Fig. 8 (3)), the inner/outer ring temperature difference at 17,000 min<sup>-1</sup> ( $d_{mN}$  value 1,530,000) was verified to decrease by approx. 5.5°C at row C and approx. 5°C at row D.

From the above, this test has verified that rows C and D, which are mostly affected by the heat produced by the built-in motor, can be intensively cooled down by concentrating the supply of cooling air between DT, closer to the built-in motor.

#### 4. Fluid analysis result

In the DTBT arrangement of the built-in motor drive main spindles described in the previous chapter, when cooling air is supplied between DT closer to the built-in motor, the cooling air is supplied to the space on the front side of row C and to the space on the back side of row D. We simulated how the air oil and cooling air would flow through those spaces with fluid analysis. Results are shown in Fig. 9.

The cooling air injected from the air cooling nozzle revolves along the surface of the inner ring spacer in the direction of spindle rotation, then flows to row D, which has a larger exhaust space, and finally exhausts in the spindle's direction.

Additionally, Fig. 9 also shows the streamline of air oil injected from the air-oil lubrication nozzle with a red line. We have verified that the streamline of air oil reached the bearing raceway surface on all four rows, including rows C and D, which are closer to the air flow nozzle.

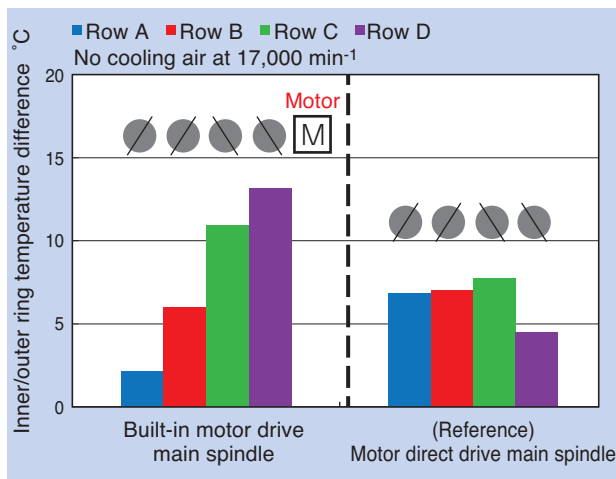


Fig. 7 Temperature difference between inner ring and outer ring without cooling air (Coupling direct motor system and built-in motor drive system, in case of DTBT arrangement)

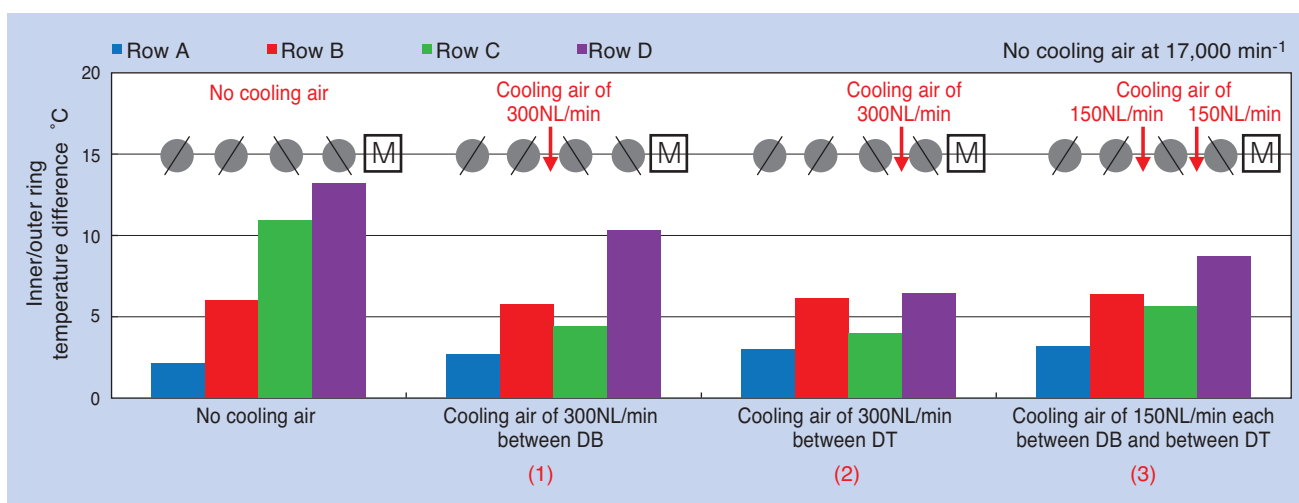
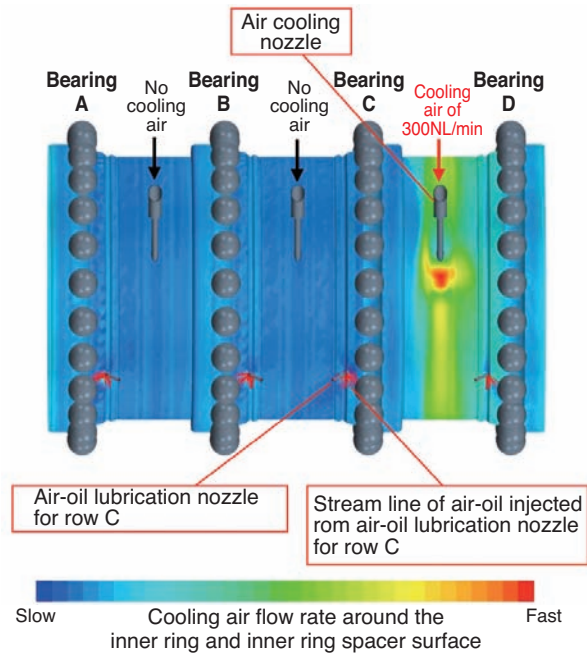


Fig. 8 Relation between cooling air point and each bearing's temperature difference between inner ring and outer ring (In case of DTBT arrangement)



**Fig. 9** Cooling air flow on inner ring and inner spacer surface (Fluid analysis results)

## 5. Summary

NTN has developed "machine tool main spindle bearings with air cooling spacers" with air cooling technology. In order to demonstrate its practicality, we verified the cooling effects by applying this technology on bearings and operating conditions which are commonly found in machine tool main spindles, and confirmed achievement of high speed and high rigidity at a high level.

This development can contribute to the advancement of machine tools in any application with regard to higher speed, higher rigidity, and higher reliability. We will continue working on enhancements and contributing to performance improvements of machine tools.

## References

- 1) Shouhei Hashizume: New Technologies on Precision Bearings for Machine Tools, *Machine Design*, Vol. 60, No. 1 (Jan issue, 2016) 28.
- 2) Yushi Onda, Kikuo Fukada, Yohei Yamamoto and Masato Yoshino: Machine Tool Main Spindle Bearings with Air Cooling Spacers, *NTN TECHNICAL REVIEW*, No. 82, (2014) 38.
- 3) Kenji Fujii, Masatsugu Mori and Yoshimi Ota: Noise Reduction for Machine Tool Main Spindle Air Oil Lubrication Bearings, *The Japan Society for Precision Engineering, Autumn Meeting 2000 Proceedings* (2000) 449.
- 4) Yoshinobu Akamatsu and Masatsugu Mori: Minimizing Lubrication Supply in an Air-Oil Lubrication System, *NTN TECHNICAL REVIEW*, No. 72, (2004) 12.

## Photo of authors



Keisuke NASU  
Industrial Machinery  
Engineering Dept.,  
Industrial Business HQ



Naoya OKAMOTO  
Product Design Dept.  
Industrial Business HQ



Masato YOSHINO  
Advanced Technology  
R&D Center

## High-performance Sealed Cam Follower

Masato TSUJHASHI\*

Seizo AGATA\*



Cam follower is used for guide rail, index machine and so on. In these mechanisms, cam follower is often mounted outside exposing position. Therefore cam follower might be exposed to fluid such as cutting oil, and improvement of seal performance to prevent grease leakage is needed.

This article introduces the feature and the performance of reinforced seal type cam follower.

### 1. Introduction

Cam followers are stud type track roller assemblies comprised of rollers and thick-walled outer rings. The outer ring is designed to roll directly on a track surface. Cam followers are mainly used as eccentric rollers and guide rollers.

Cam followers can be categorized into two groups: cage type and full-complement roller type. The caged type is best suited for high-speed operation because the rollers are guided by the cage. In contrast, the full-complement roller type has a larger load rating than the caged type and is more suited for high load (typically low-speed) applications.

Depending on where they are used, the grease inside the bearings may leak, causing an early failure due to insufficient lubrication. NTN's cam followers include a sealed type as the standard offering. However, the seals do not completely work to prevent grease leakage as they are provided mainly for blocking dust from entering the bearing.

In this article, we will describe the high performance sealed cam follower developed to cope with the grease leakage issue.

### 2. Structure of typical cam followers

The structure of typical cam followers is shown in Fig. 1.

These cam followers consist of a stud, an outer ring, two side plates and several rollers. Since the outer ring rolls directly on the track of the customer's application, the outer ring is designed with a thick cross-section so that it can withstand impact loading. In addition, full-complement cam followers comprised of a cage and full-complement rollers are available in the same envelope dimensions. Furthermore, rubber seals are available as an option for these cam follower bearings. However, keep in mind that the rubber seal of the standard series is for sealing out dust from the bearing and not for excluding liquids from entering the bearing.

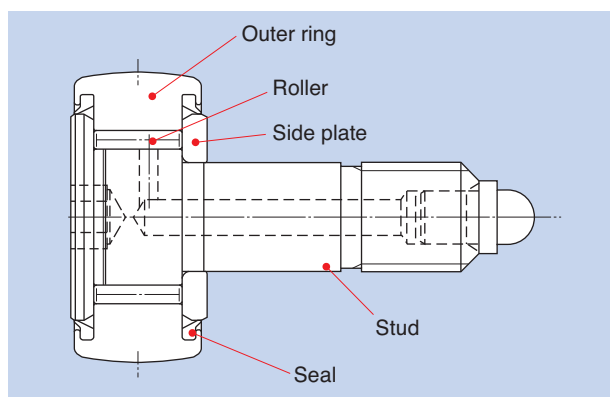


Fig. 1 Structure of cam follower

\* Industrial Machinery Engineering Dept., Industrial Business HQ

### 3. Usage in machine tool applications under ambient conditions

Cam followers are frequently used in carry guide and cam drive areas of the indexing cam mechanism in machine tool applications <sup>1)</sup>.

**Fig. 2** shows a common machine tool application where cam follower bearings are used (a turret mechanism) <sup>2)</sup>.

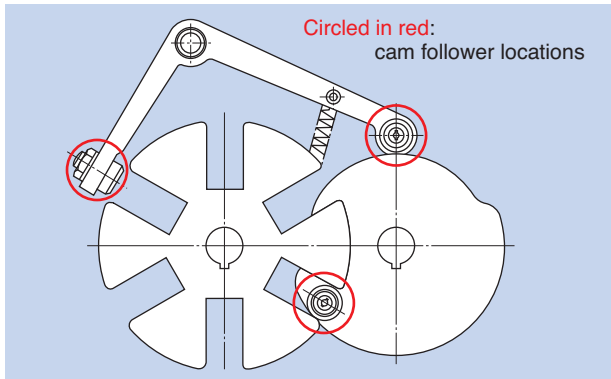
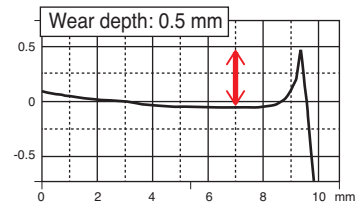
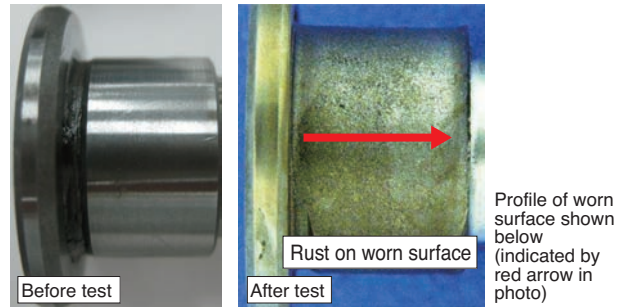


**Fig. 2** Example of cam follower for machine tool

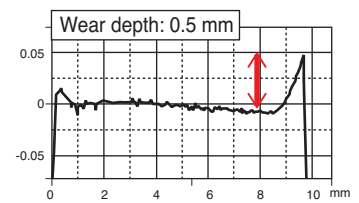
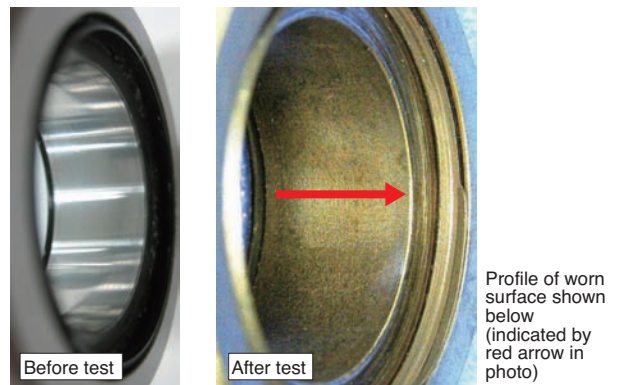
Since the cam drive assembly is located in the machine interior, it is directly exposed to cutting oil. When cam followers are used in this environment, grease leakage prevention is very important. Furthermore, for environmental reasons, recently cutting oil is more commonly using a water base <sup>3)</sup>. Water-based cutting oil is more likely to mix with grease if it enters the cam follower compared to conventional cutting oils. Therefore, now it is even more important to stop cutting oil from penetrating cam followers to prevent lubrication failure which leads to premature bearing failure.

### 4. Wear condition from cutting oil penetration

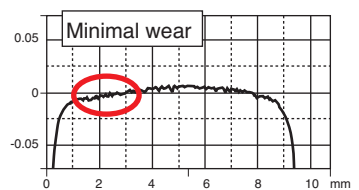
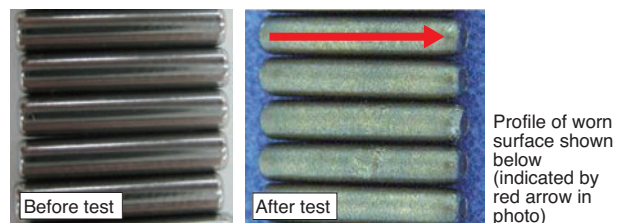
An example of wear when cutting oil penetrated a machine tool cam follower bearing is shown in **Fig. 3**. The worn bearings were equipped with standard rubber seals and its design was equivalent to the bearing shown in **Fig. 1**. When the failed bearings were inspected, it was revealed that the grease was completely gone. It was determined that the internal grease leaked when cutting oil entered the cam follower. Once the grease was used up, the oil film inside the cam follower was no longer maintained, allowing the components to have metal-to-metal contact with each other and resulting in severe wear on both the stud and the outer ring race. Rust was also observed on the bearing components. NTN has



**(a)** Stud



**(b)** Raceway of outer ring



**(c)** Roller

**Fig. 3** Example of worn cam follower with grease leakage

developed a high-performance sealed cam follower to address such reduced life issues caused by grease leakage.

## 5. High performance sealed cam follower

### 5.1 Features

#### (1) Superior sealing performance

Anti-fluid penetration performance: 80% reduction in fluid penetration into bearing seal compared to conventional seal

#### (2) Dimensionally compatible

The outer diameter of the new design is dimensionally compatible with the standard series since only the seal and internal bearing geometry was changed. Also, common grease is compatible with the new seal design.

### 5.2 Bearing specifications

Structure changes were minimized to ensure compatibility with the standard series. Specifically, the modifications focused on seal geometry and the seal contact with the outer ring, stud and side plate. A comparison of the sealing structure of the current and new cam follower designs parts is shown in Fig. 4.

The geometry of the bearing areas not shown in these diagrams is the same as Fig. 1. A picture of a cam follower with the new seal design is shown in Fig. 5.

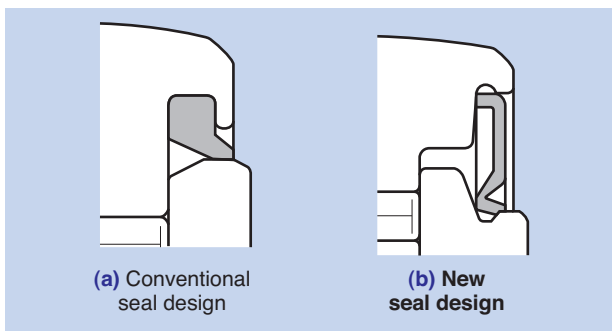


Fig. 4 The shape of the seal



Fig. 5 Cam follower with development seal

The seals used in the standard cam follower series (hereinafter, conventional seals) are molded exclusively with rubber, which is not very resistant to external pressure and is insufficient to prevent fluid penetration. Conventional seals are primarily designed for excluding dust and are sufficient for that purpose. On the other hand, the seals NTN just developed (hereinafter, developed seals) are designed with a core metal insertion together within the rubber molding to ensure rigidity of the seal to prevent deformation from external pressure. In addition, double lips were incorporated into the seal structure and the contact surface was optimized to improve both its anti-penetration performance and minimize its operating torque.

### 5.3 Roller follower applications

Roller followers are bearings used in similar applications as cam followers. The structure of ordinary roller followers is shown in Fig. 6. Roller followers are cam followers with the stud substituted with an inner ring and are used when the spindle is provided by the customer. Since the internal structure is the same as the cam followers, the developed product described in this article can also be applied to roller follower bearings.

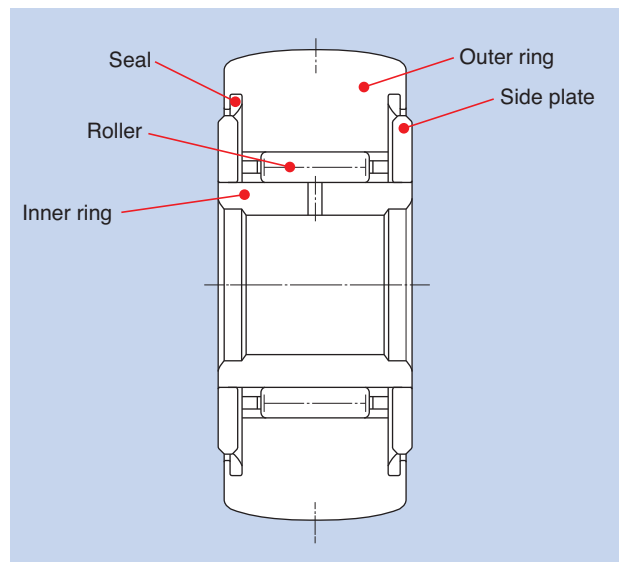


Fig. 6 Structure of roller follower

## 6. Performance

### 6.1 Comparison of anti-fluid penetration performance

Fig. 7 and Table 1 show the test rig and test conditions of the anti-fluid penetration performance comparison test.

The evaluation method for test performance is to compare the water content of the internal residual grease after testing is completed. The results of this test are shown in Fig. 8 and post-test pictures of bearings are shown in Fig. 9.

Fig. 8 displays a significant improvement in the anti-fluid penetration performance. The water content inside the bearings with newly developed seals was reduced by 80% compared to bearings with conventional seals.

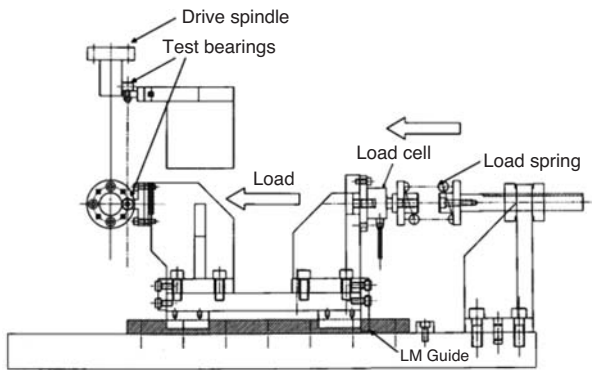


Fig. 7 Test rig

Table 1 Test condition

		Conventional sealed product	New sealed product
Bearing size	Stud diameter	$\phi 12$	←
	Outer diameter	$\phi 32$	←
	Total width	45	48.5
Grease		Shell Alvania grease S3 Color: light brown	
Rotational speed		500 min <sup>-1</sup> (inner ring rotation)	
Load		392N	
Temperature		Room temperature	
Test run time		30 minutes	
Water injection procedure		Spray 20ml of water with a syringe every 15 seconds, aiming at the contact area between the seal lip and side plate	

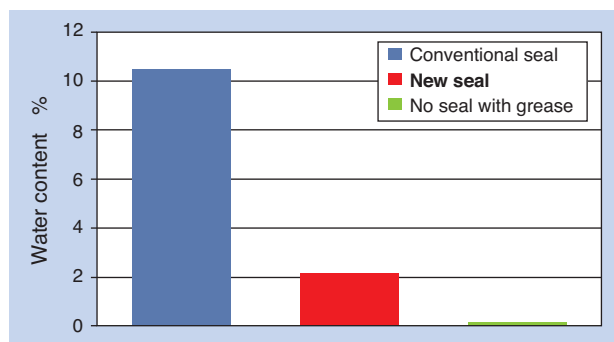


Fig. 8 Water content after the test



(a) Conventional product



(b) Developed product

Fig. 9 Inside of bearing after the test

### 6.2 Starting torque

Because of the structural change to improve anti-fluid penetration performance (increased seal interference), the new cam follower design has an increased starting torque. To determine the relative impact of this higher torque, a starting torque verification test was conducted. The test conditions are shown in Table 2 and the corresponding test results are shown in Fig. 10. The developed cam follower product showed an increase of 30% in starting torque compared to the conventional design.

Table 2 Test condition

		Conventional sealed product	New sealed product
Bearing size	Stud diameter	$\phi 12$	←
	Outer diameter	$\phi 32$	←
	Total width	45	48.5
Grease		Shell Alvania grease S3	
Temperature		Room temperature	
Load		No load	



Fig. 10 Test result of starting torque

### 6.3 Verification of outer ring slippage

With the verification test mentioned in section 6.2, an increase in starting torque was confirmed in the newly developed product. This increased starting torque can hinder outer ring rotation and cause slippage with the track surface. Therefore, to verify if slippage occurs between the outer ring and track surface during operation, a test was conducted with the actual load. When the bearing load is 4% or less of  $C_{or}$ , the rolling elements inside the bearing may be impeded from performing a smooth rolling motion. Therefore,  $0.04C_{or}$  was determined to be the practical minimum load for this bearing and was used as the test load. The rig used for this test is the same as shown in Fig. 7. No slippage was observed during testing under the conditions shown in Table 3. This test result confirmed smooth bearing rotation during operation under the practical load which determined there is no outer ring slippage problem with the new bearing design.

Table 3 Test condition

		Conventional sealed product	New sealed product
Bearing size	Stud diameter	$\phi 12$	←
	Outer diameter	$\phi 32$	←
	Total width	45	48.5
Grease		Shell Alvania grease S3	
Load		810 N ( $0.04C_{or}$ )	
Rotational speed		200, 500, 1000min <sup>-1</sup>	
Test run time		30 seconds at each rotational speed	
Temperature		Room temperature	
Verification method		Visual inspection	

## 7. Summary

By enhancing the seals of cam followers from the current design to the new design, we could significantly improve anti-fluid penetration performance.

The new improved seals are able to replace existing seals without increasing the size of the bearing outer diameter to easily improve bearing anti-fluid penetration performance. Therefore, we will actively promote the use of these bearings in customer applications.

## References

- 1) Yuichi Danjo, Applications of Cam Followers and Roller Followers, NTN TECHNICAL REVIEW No. 55 (1989), 61-72
- 2) Satoshi Nakamura, Miniature Cam Followers for Index Table, NTN TECHNICAL REVIEW No.60 (1992), 67-74
- 3) Shigehiro Iwata, Eco-Friendly Water Soluble Cutting Oil - Development Trends - Journal of the Japan Society for Precision Engineering, No.68, 7, 2002, 919-922

### Photo of authors



Masato TSUJHASHI  
Industrial Machinery  
Engineering Dept.,  
Industrial Business HQ



Seizo AGATA  
Industrial Machinery  
Engineering Dept.,  
Industrial Business HQ

# Introduction of Linear Guides

Masaki KAGAMI\*  
Keisuke KAZUNO\*



Man has moved heavy loads since ancient times using rotation and linear movement or a combination of both. Linear guides based on these movements have realized the linear motion with high capacity, compact, long stroke and high accuracy.

Linear guides have been used for various applications, for example; machine tools, assembling machines, automation machines, and have many past results. This article introduces basic structure and features and applications of linear guides.

## 1. Introduction

Automation in manufacturing is expanding in order to increase efficiency and save manpower at production sites. The guidance mechanisms of automated equipment are required to be lightweight and have a high load carrying capacity, high rigidity, small footprint, high precision, low friction and environmental resistance.

Currently, NTN has significant business for linear guides led by the European market. Recently, we started production and sales of second generation linear guides, an improvement on conventional (first generation) linear guides. Second generation linear guides have achieved an increased load carrying capacity, increased life, and lower noise compared with conventional products by optimizing the geometry and surface finish of various components.

In this article, we will describe the basic configuration, features and applications of our linear guides <sup>1, 2)</sup>.

## 2. Linear guide basics

### 2.1 Basic configuration

As shown in **Fig. 1**, the linear guide assembly mainly consists of a rail, runner block, rolling elements (balls), end plate, and end seal. The balls roll between the rail and runner block track surface and are picked up by the end plate at the end of the runner block. Then, they travel through the circular path of the

runner block and are sent back to the track surface. In this way, the balls continue rolling in an unlimited circular motion, enabling guidance with low friction <sup>3)</sup>.

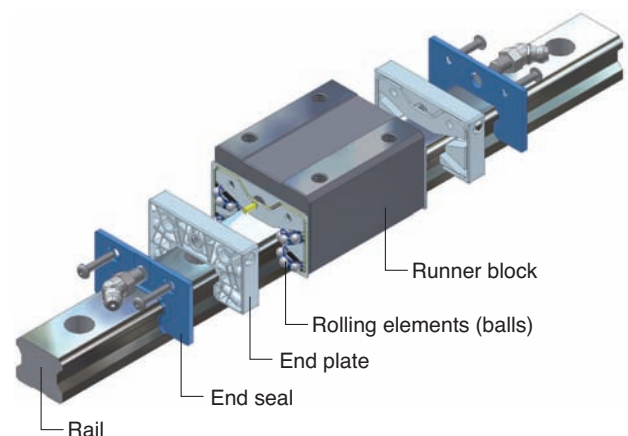


**Fig. 1** Basic structure of linear guides

### 2.2 Error compensation capability

Components and support structures which are used to install linear guides have deviations in flatness and parallelism. In addition, errors can occur in the installation of linear guides, as well. These errors can be compensated for/averaged by using multiple rails/runner blocks (**Fig. 2**). In the case of the commonly used two-rail/two-runner block configuration, the running accuracy of the movable stage increases 80% compared to the mounting surface flatness (**Table 1**).

\* Robot Engineering Department, Industrial Business HQ

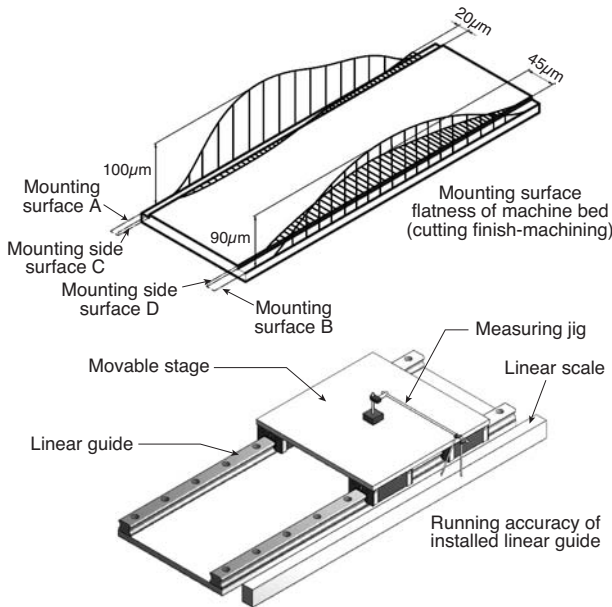


Fig. 2 Error compensation

Table 1 Mounting surface flatness and running accuracy

Mounting surface	Straightness $\mu\text{m}$		Running accuracy
	Mounting surface flatness	Running accuracy	
Base	A	100	17
	B	90	
Side	C	20	4
	D	45	

### 3. Features of linear guides

A wide series of NTN linear guide products for various industries and uses are available for users to select the best specifications for their particular needs.

#### 3.1 Standard linear guide and miniature linear guide

The linear guide series can be categorized into standard linear guides and miniature linear guides (Fig. 3). Standard linear guides provide a lineup with rail widths of 15 - 55 mm, and miniature linear guides provide a lineup with rail widths of 7 - 15 mm. In the future, we will expand the range of the lineup to smaller and larger rail widths.

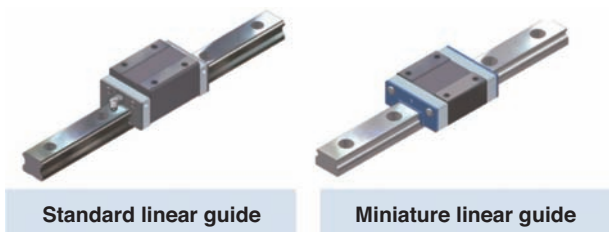


Fig. 3 Lineup of Linear guides

#### 3.2 Linear guides with retainer

In general, linear guides use a type with balls almost completely filling the circulation path (full-ball type). In addition, we offer linear guides with a retainer to hold and separate the rolling elements (Fig. 4).

##### [Features of linear guide with retainer]

- Superior high speed operation
- Low heat generation
- Low noise
- Smooth motion
- Improved lubrication performance
- Uniform distribution of load
- Long life

The retainer prevents metal contact between adjacent the balls (Fig. 5). Compared with the full-ball type with no retainer, the relative slip speed at the ball contact surface is 1/2 and the contact pressure is also lower, resulting in reduced heat generation and wear. In addition, the retainer has a pocket structure for retaining lubricant, through which lubricant is delivered

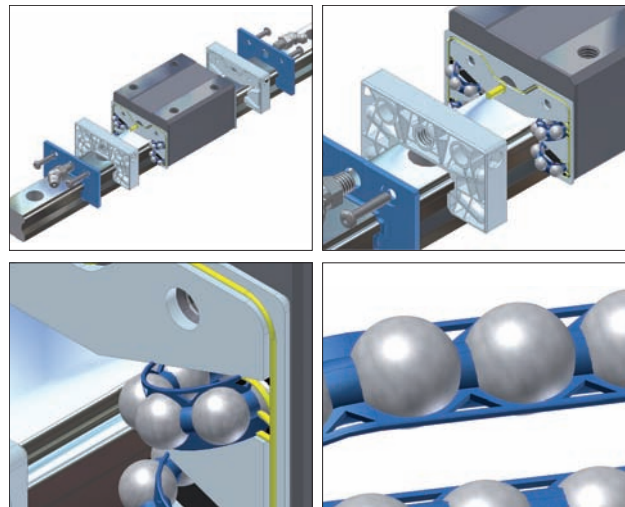
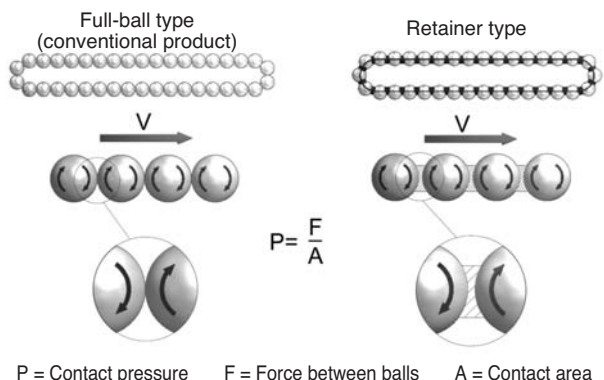


Fig. 4 Linear guides with retainer



P = Contact pressure    F = Force between balls    A = Contact area

Fig. 5 Schematic view of the contact surfaces





Fig. 9 Tools for lubrication

### 4.3 Lubrication from the top of runner blocks

Lubrication is also possible from the lubrication adapter on top of the end plate by attaching a dedicated adapter to the runner block (Fig. 10).

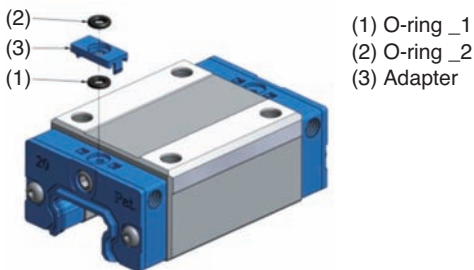


Fig. 10 Lubrication adapter

### 4.4 Lubrication system LU1

The lubrication system LU1 is capable of lubricating the track surface of the rail when installed on the end plate of the runner block (Fig. 11). Since it provides continuous lubrication, maintenance free operation can be achieved for an extended period.

For regular use, no oil supply is required for LU1. However, if oil shortage is a concern, such as for use in severe environments, it is also possible to re-supply oil from the top of the cover. In addition, even when LU1 is installed, grease zerks and lubrication fittings can also be directly installed <sup>1, 2)</sup>.

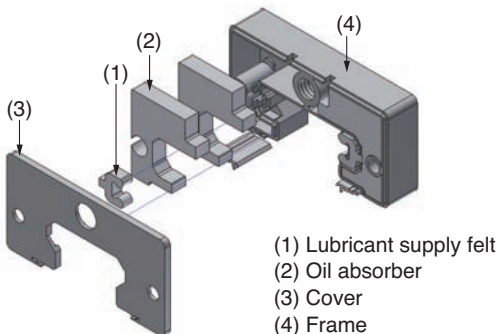


Fig. 11 Structure of LU1

## 5. Seal options

A combination of multiple seals can be chosen to achieve the most appropriate sealing depending on operating conditions. An example of seal options is shown in Fig. 12.

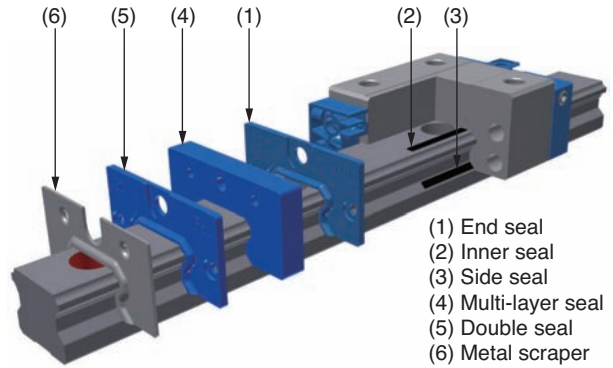


Fig. 12 Sealing options

## 6. Application to linear modules

Linear modules incorporate linear guides for high load capacity and long stroke applications (Fig. 13, Fig. 14) <sup>4)</sup>.

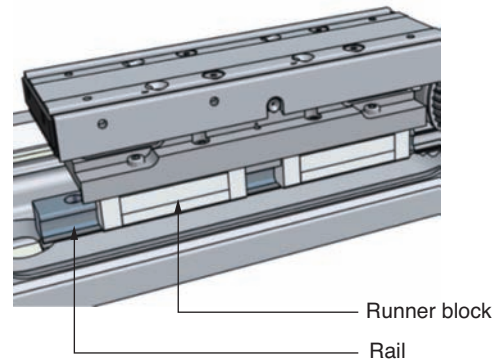


Fig. 13 Linear module with linear guides



Fig. 14 High load capacity linear module for lifting axis

For long stroke applications exceeding 10 meters in length, shipping to the installation site may become problematic. In such cases, the linear module can be divided into pieces of several meters for transportation and then connected at the installation site. By using linear guides which are pre-cut at a predetermined length, the linear module can be easily divided/connected, making it possible to shorten the time for installation work at the site.

In addition, all linear guides used in linear modules come with retainers. Adoption of linear guides with retainers allows quiet, long-life and long maintenance-free operation.

Linear guides are currently used in various automation facilities in automobile and industrial plants by leveraging these features.

## 7. Wireless linear scale system

Linear scales are often used for devices that require precise positioning, such as semiconductor test equipment and machine tools. Currently, we are developing a "wireless linear scale system" which combines linear guides and sensor units (Fig. 15)<sup>5)</sup>.



Fig. 15 Wireless measuring linear system

### 7.1 System configuration

Key components of the wireless linear scale are shown in Table 3 and the system model is shown in Fig. 16.

### 7.2 System features

The wireless linear scale system consists of a rail with a magnetic scale installed on the side and a sensor unit connected to the runner block. As opposed to the conventional linear scale system which requires a significant space for installation, this system has achieved compact size by integrating the scale and sensor within the linear guide.

Since the gap between the detection sensor head and magnetic scale is adequately controlled by the

Table 3 Main components

Appearance	Feature
	<ul style="list-style-type: none"> <li>· Integrated magnetic scale (with protective cover)</li> <li>· Rail length: up to 2,500mm</li> <li>· Wireless power supply capability (transmitter)</li> </ul>
	<ul style="list-style-type: none"> <li>· Built-in detection sensor head</li> <li>· Positioning signal output (wireless)</li> <li>· Wireless power supply capability (receiver)</li> </ul>
	<ul style="list-style-type: none"> <li>· Positioning signal reception (wireless)</li> <li>· Signal output to controller</li> <li>· Power supply to rail</li> </ul>

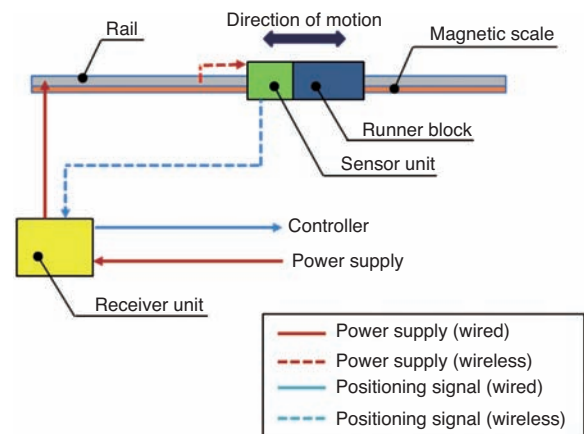


Fig. 16 System model

runner block, adjustment work is not required. Labor can be significantly reduced compared with ordinary linear scale installation work.

As the sensor unit is capable of wireless signal output and wireless power supply –signal/power cables are not required (Fig. 17).

### [Features]

- Compact
- Easy assembly
- No cables are required for the sensor unit
- Cover to prevent foreign objects from entering

Contamination of the magnetic scale is prevented by the protective cover. In addition, sensor units and runner blocks can be equipped with the seal option shown in Fig. 12. With these measures, even if foreign objects are attached to the rail, they can be prevented from entering the sensor unit.

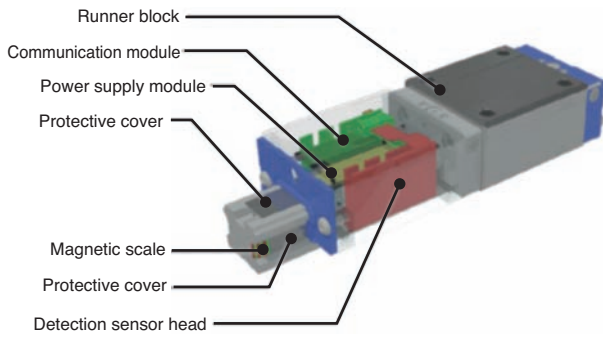


**Fig. 17** Inside structure of wireless sensing unit

## 8. Summary

In this article, we discussed the basic structure, features and applications of linear guides. We will strive for their introduction into global markets for automation and labor saving at production sites.

### References

- 1) NTN Linear Guide Catalogue, CAT No. 6018/J
- 2) NTN-SNR, Linear Guide Catalogue, (2015)
- 3) Mitsumasa Wada, Linear Guide for High Load, THE TRIBOLOGY No.342, (2016) 16-18
- 4) NTN, Linear Module Catalogue, CAT. No. 6107-II/J

### Photo of authors



**Masaki KAGAMI**  
Robot Engineering  
Department,  
Industrial Business HQ



**Keisuke KAZUNO**  
Robot Engineering  
Department,  
Industrial Business HQ

# Plastic Sliding Screws

Naonari TANIGAWA\*  
 Norio ITOU\*\*  
 Tomomi TONOMURA\*



Plastic parts have high design freedom and high corrosion resistance, can carry out weight saving and compactification and are low in cost. Therefore, plastic parts substitute metal parts in many industrial fields. Plastic sliding screws (plastic nut and metallic screw shaft) are one of them, and these are widely used for food machinery and medical machinery parts. This article introduces features and performance of plastic sliding screws.

## 1. Introduction

Feed screws, which convert the rotating motion of motors to linear motion, are used in the load carrying mechanism of industrial machines, food machines, medical devices, etc. Feed screws are categorized into ball screws and sliding screws. Sliding screws with copper-based nuts are used with grease. On the other hand, screws with plastic-based nuts can be used without lubrication.

**Table 1** shows the comparison of the performance of NTN's plastic sliding screws with other manufacturers' sliding screws and ball screws. Ball screws are characterized by large permissible load and screw efficiency; however, they are expensive. Since they are lubricated with grease, these screws are not suitable for use in environments where grease performance deteriorates, such as under water or in high temperatures. In contrast, plastic sliding screws

have a lower permissible load capacity but are well suited for broad ambient conditions, such as in vacuums and high temperatures. In addition, they are quieter and inexpensive. Furthermore, they can reduce weight and size. However, corrosion resistance and heat resistance vary depending on the materials for screw shafts and nuts; therefore, appropriate selection based on their application is required. In this article, we will discuss NTN's plastic sliding screws (hereinafter, sliding screws) and NTN's high-load plastic sliding screws (hereinafter, high-load sliding screws) with increased permissible load capacity<sup>1, 2)</sup>.

## 2. Sliding screws

Sliding screws consist of plastic nuts and stainless steel screw shafts, as shown in **Fig. 1**. **Table 2** shows the materials and the specifications.

**Table 1** Comparison of features various sliding screws

Item	NTN plastic sliding screw	Sliding screw oil-impregnated POM by another manufacturer	Ball screw
Lubrication	Not required Operable with lubricant	Not required Operable with lubricant	Required Grease
Corrosion resistance	◎	△	×
Screw accuracy	○	△~○	◎
Screw efficiency	○	△~○	◎
Noise	◎	○	△
Heat resistance	◎	△	△

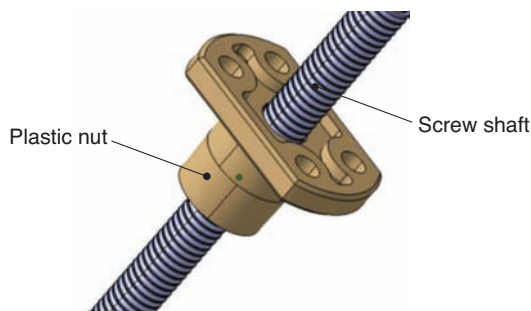


**Fig. 1** Plastic sliding screw

\* Engineering Dept. NTN Engineering Plastics Corporation  
 \*\* Planning Dept. NTN Engineering Plastics Corporation

The plastic nut (BEAREE AS5000) is based on polyphenylenesulfide (PPS) and blended with special fluorocarbon resin and solid lubricants to improve friction/wear resistance properties. As the impact resistance is also improved, they are more durable than regular plastic sliding screws.

Fig. 2 shows the comparison of properties of BEAREE AS5000, which is the material for our plastic nuts, and commercially available PPS-based sliding material with fluorocarbon resin. BEAREE AS5000 is particularly superior in wear resistance and friction coefficient, in addition, improvement is made to impact strength, which is a weak point of PPS. Fig. 3 shows the cross section SEM image. The improved property of BEAREE AS5000 against commercially available

**Table 2** Specification of our plastic sliding screws

Part	Material
Plastic nut	BEAREE AS5000
Screw shaft	SUS304 (thread rolling)
Accuracy class	Ct10 (JIS B 1192)
Cumulative lead error	±0.21/300mm

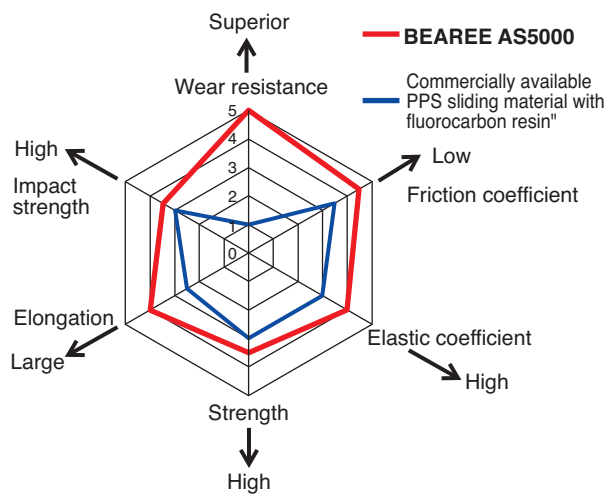


**Fig. 2** Features of BEAREE AS5000

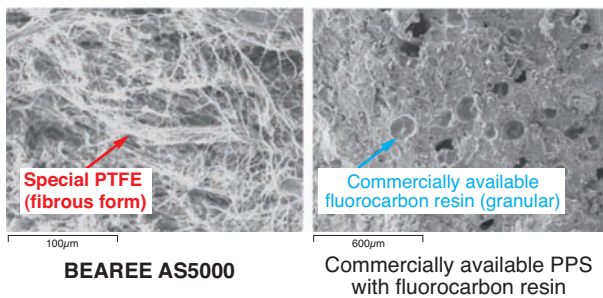


**Fig. 3** Cross section SEM images

PPS with fluorocarbon resin was made possible by the three dimensional presence of the special fluorocarbon resin in the molding.

A comparison test of our sliding screws against other manufacturers' sliding screws was conducted under the conditions listed in Table 3 up to a travel distance of 200 km. In general, an increase of axial clearance of up to 0.3 mm due to operation is considered to be permissible. As shown in Fig. 4, the increase of the axial clearance of the sliding screw of another manufacturer exceeded 0.3 mm with a travel distance of around 70 km. In contrast, the increase of the axial clearance of our sliding screw was 0.2 mm or less, even after a travel distance of 200 km, which indicated it was still usable for continuing operation.

**Table 3** Test condition of wearing test

Screw nominal diameter	8mm
Nominal lead	24mm
Number of threads	6
Axial load	100N
Rotational speed	500min <sup>-1</sup>
Lubrication	None (dry friction)

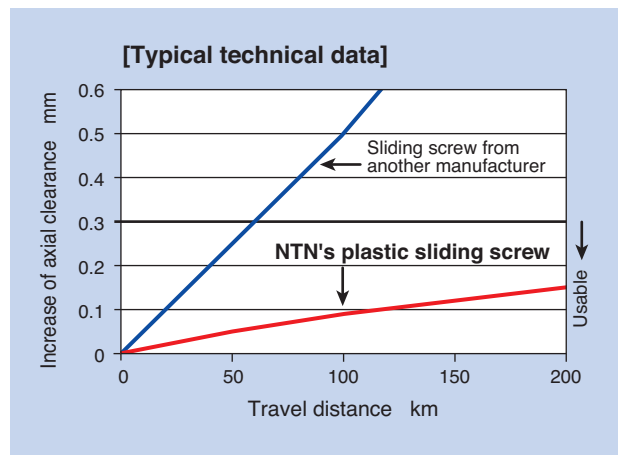


**Fig. 4** Relationship between axial clearance increase and nut motion distance

### 3. Examples of applications

The sliding screws are adopted by medical devices and food machines since they can be used with no oil or grease lubricant. **Table 4** shows a record of actual use. Among others, **Fig. 5** shows an example of application in food fryers and noodle boilers.

**Table 4** Applications

Field	Name of device	Adopted part
Medical	Vision tester	Focusing XY axis
	Analysis equipment	Specimen carrying drive shaft
	Dialyzer	Pump actuator shaft
	Anesthesia apparatus	Elevator drive shaft
Food processing machine	Vending machine	Cup carrying drive shaft
	Processing machine	Fryer/noodle boiler elevator
	Wrapping machine	Packing elevator
Other	Semiconductor manufacturing equipment	Substrate positioning driver
	Electronic microscope	Specimen positioning XY axis

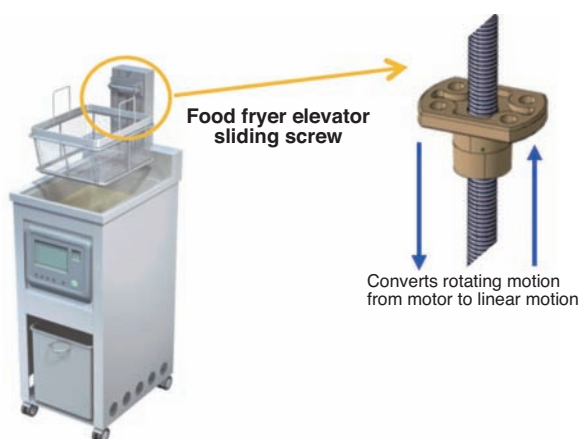


**Fig. 5** Application for food fryer

### 4. High-load sliding screws

Since the sliding screws use plastic nuts, there was a risk of flange failure or thread wear when the load significantly exceeded the permissible load capacity. However, lubrication-free and low-noise operation is also required for high-load applications, which have been addressed by sliding screws for low-load applications. In order to address this requirement, NTN has developed high-load sliding screws with metal composite material as shown in **Fig. 6**.

BEAREE AS5000, which was discussed in Section 2, is used for injection molded threads on top of the aluminum-based nut, as a composite nut, to improve permissible load capacity and heat dissipation.

The aluminum is processed with special etching to improve adhesiveness with BEAREE AS5000.

**Table 5** shows comparison of load carrying capacity and **Fig. 7** shows variation of shaft surface temperature during operation. The plastic nut material used in both nuts is BEAREE AS5000 with improved friction/wear resistance. However the high-load sliding screw uses thin-walled composite molding which provides better heat dissipation; therefore, the temperature rise at the screw surface is approx. 1/4 of the sliding screw.

In addition, the permissible axial load capacity of the high-load sliding screw is double and the static fracture load is nine times higher than the sliding screw, due to the composite molding effect.

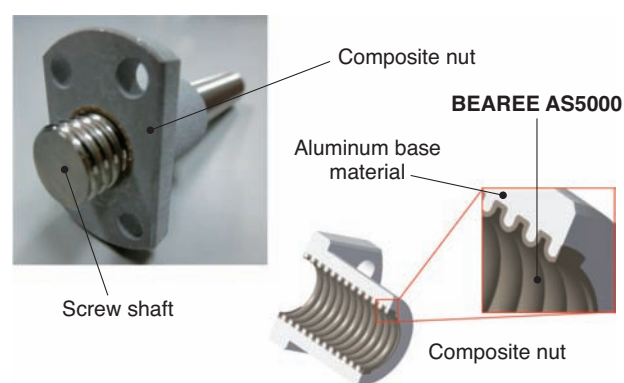
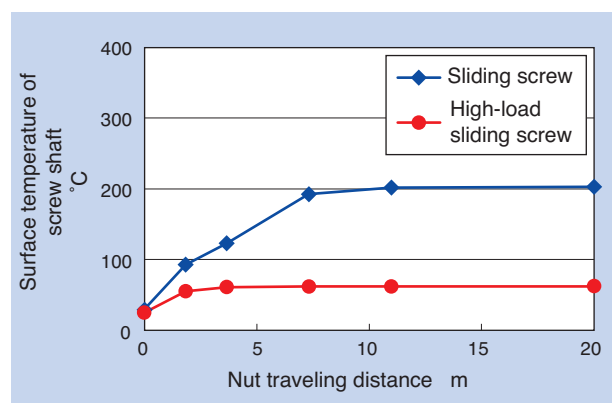


**Fig. 6** Plastic sliding screw for heavy condition

**Table 5** Comparison of load limit

Item	Sliding screw	High-load sliding screw
Permissible axial load	600N	1,500N
Static fracture load of nut	2.7kN	24kN



[Screw test condition]  
Screw specification: shaft diameter: 12mm, lead: 2mm, thread: 1  
Load: 600N, Rotational speed: 200 min<sup>-1</sup>, room temperature, no lubrication"

**Fig. 7** Surface temperature of screw shaft

Next, Fig. 8 shows the increase of axial clearance after operation.

The high-load sliding screw has less wear, approx. 1/3 of the sliding screw. Since the rise in surface temperature is small, the elastic coefficient of the BEAREE material is maintained and reduction of frictional shear is small. Therefore, there is little change in screw efficiency with good friction properties.

Adhesiveness was evaluated during the environmental resistance test under the exposure conditions in Table 6. Adhesiveness was tested by measuring the maximum load when only BEAREE AS5000 was shorn (Fig. 9). In addition to measurement of adhesiveness, the appearance of

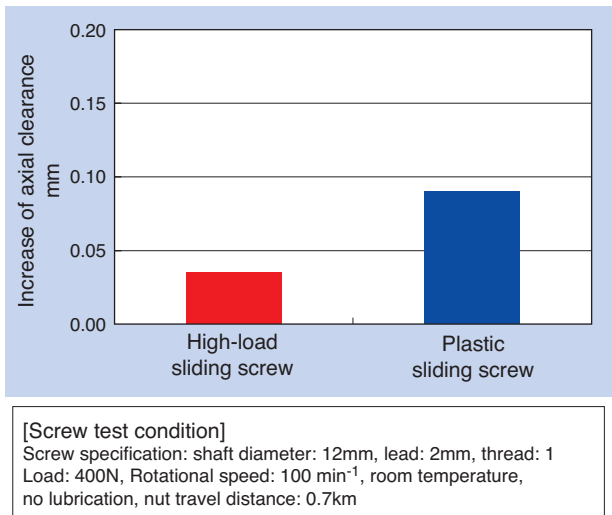


Fig. 8 Axial clearance increase

Table 6 Test condition of environment resistance

Item	Condition
Exposure to high temperature	150°Cx500hrs
Exposure to constant temperature/humidity	80°C, 95%RHx500hrs
Immersion in hot water	90°Cx500hrs

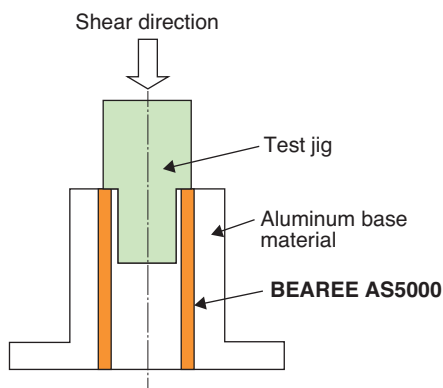


Fig. 9 Schematic of adhesion strength test

nuts was also observed. The result is shown in Fig. 10 - 12. In all of these exposure tests, reduction of adhesiveness was 5% or less. In addition, no abnormality was found, such as rust, in the appearance of the nuts after exposure tests.

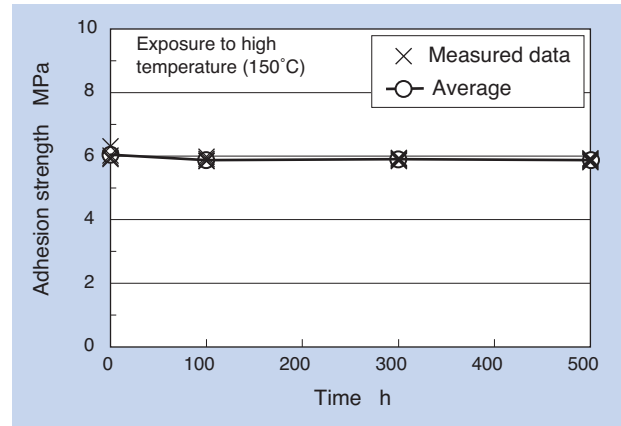


Fig. 10 Adhesion strength variation in high temperature exposure test

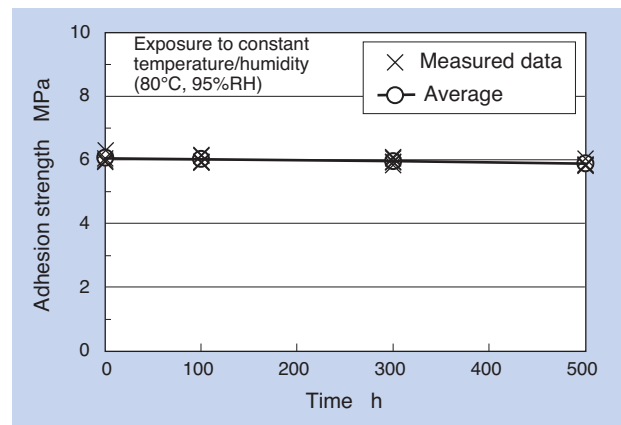


Fig. 11 Adhesion strength variation in temperature and humidity controlled test

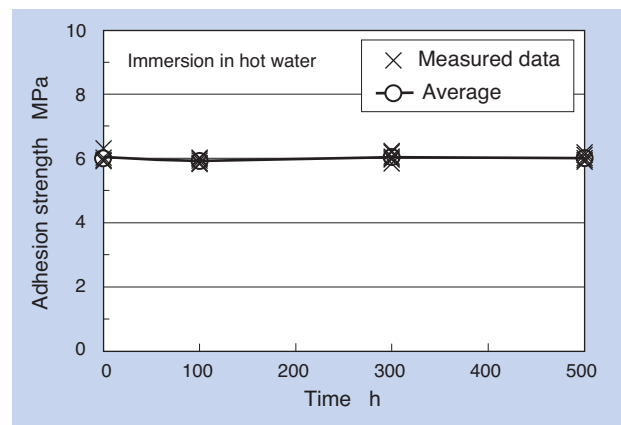
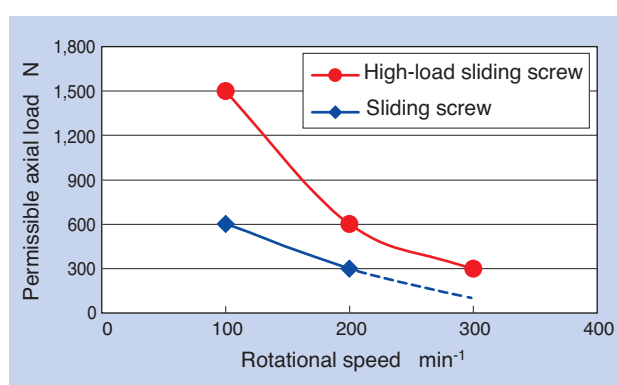


Fig. 12 Adhesion strength variation in hot water test

**Fig. 13** shows the relation between the permissible axial load and rotation speed of sliding screws and high-load sliding screws. A test of 20 sets was conducted, defining 200 times of back and forth motion under a predetermined rotational speed and load as one set (the screws were cooled down to room temperature by stopping the motion between each set with a total of 2,000 times of back and forth motion). The permissible axial load was determined as the maximum load before the increase of axial clearance reached 0.1 mm without nut fracture. The high-load sliding screw had a permissible axial load twice as high as the sliding screw.



**[Screw specification]**

screw shaft: 12mm, lead: 2mm, 1 thread

**[Test condition]**

Room temperature, no lubrication (dry), stroke  $\pm 1,180$ mm, A test of 20 sets was conducted defining 200 times of back and forth motion under the predetermined rotational speed and load as one set (screws were cooled down to room temperature by stopping the motion between each set with a total of 2,000 times of back and forth motion)  
The permissible axial load was determined as the maximum load before the increase of axial clearance reached 0.1mm without nut fracture.

**Fig. 13** Speed and axial load limit

## 5. Conclusion

In this article, we have discussed NTN's plastic sliding screws which convert the rotating motion of motors into linear motion in lubricant (oil or grease) free operation, and NTN's high-load plastic sliding screws with high permissible load capacity.

Market needs for lightweight and small sliding screws will grow further in many fields, including medical devices and food processing machines. NTN will continue addressing those requirements by offering products to contribute to customer product development.

## References

- 1) Takuya Ishii and Yoshihide Himeno, Functional Improvement of Resin Sliding Bearing Through e Combination with Metal, Journal of the Japan Society of Polymer Processing, 25 (2013), 2, 73
- 2) Yoshio Oki, Product Introduction and Complex Technology of Resin, Sintered Metal and Magnet for Growth Markets, NTN TECHNICAL REVIEW No. 82 (2014), 12

## Photo of authors



Naonari TANIGAWA  
Engineering Dept.  
NTN Engineering Plastics  
Corporation



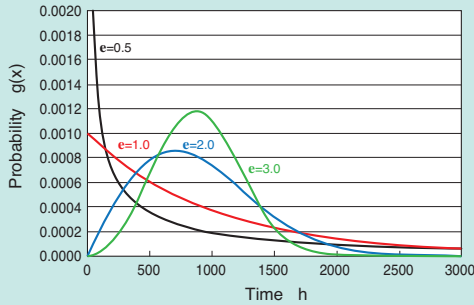
Norio ITOU  
Planning Dept.  
NTN Engineering Plastics  
Corporation



Tomomi TONOMURA  
Engineering Dept.  
NTN Engineering Plastics  
Corporation

# Strategy of Rolling Contact Fatigue Life Testing and Interpretation of Life Data

Takumi FUJITA\*



Rolling contact fatigue (RCF) life testing is essential to evaluate rolling bearing performance. Generally, the probability density distribution of RCF lives follow a Weibull distribution, and its wide variation in life data is common. Thus, the test design and result interpretation without statistics are highly likely to lead to

incorrect conclusions for rolling bearing performance. This report introduces statistical procedures of the test design and result interpretation in two types of RCF testings which are called "fixed time test" and "accelerated test". In addition, several calculations applied in the procedures are explained.

## 1. Introduction

The life data of rolling bearings (hereinafter, "bearings") is known to follow the Weibull distribution<sup>1, 2)</sup>. **Fig. 1** shows the results of calculation of the ratio of 90% life over 10% life from the cumulative distribution function of the Weibull distribution for each shape parameter value (hereinafter, "Weibull slope"). Since the Weibull slope indicating variation of bearing life data is usually around 1.1 ( $(10/9, 9/8)^{1-3}$ ), it is not exceptional if the life test of bearings contains data with a difference of around 16.5 times within 10 life data. As it is clear from this fact that the life data of the rolling contact fatigue life test (hereinafter, "life test") has significant variation, the planning and interpretation of the life test needs to be based on statistical evidence to avoid the risk of deriving a wrong conclusion.

Therefore, the planning and data interpretation of life tests are of high interest for engineers and researchers who are engaged in the actual life tests. This paper discusses how to proceed with truncated tests and accelerated tests in the form of case studies. Here, truncated tests are defined as tests to decide

that there are no performance issues if no failures are experienced for a predetermined time or loading cycles, and accelerated tests are defined as tests to compare performance from the life estimated by the Weibull plots. The details of calculations are shown in the appendices.

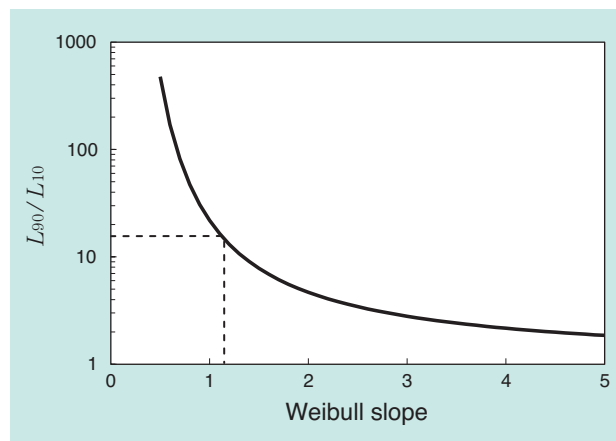


**Fig. 1** Relationship between  $L_{90}/L_{10}$  and Weibull slope

\* Advanced Technology R&D Center

## 2. Truncated test

### 2.1 Truncated test procedure

Fig. 2 shows the truncated test procedure. In the truncated test, test condition and target life (10% life or 50% life) are determined first. Then, the number of test samples to be provided and the truncated life to be set for guaranteeing the target life are examined. The relationship between the number of test samples to meet the target life and the truncated life can be obtained by using the equation shown in Appendix 1. There are other factors to be considered, such as the restriction of test period and number of testers, for determining the actual number of test samples and truncated life.

After the test starts, if the test samples survive until the end of the predetermined truncated life, the test bearings are considered to have passed, but if failures are encountered, it is necessary to consider whether the test should continue. From the viewpoint of efficiently reducing the test time, it is recommended to set the number of test samples to 6 or more, or desirably, 9 or more<sup>4)</sup>. For deciding if the test should continue, probability of meeting the target life by continuing the test with the remaining undamaged test bearings, as well as if there is enough room for extending the test period are examined. The probability can be obtained by using the equation in

Appendix 2. If it is probable to meet the target life and there is room for the extended test period, the test can continue with the remaining undamaged test bearings. The equation in Appendix 2 can also be used to set the truncated life of the remaining bearings.

### 2.2 Truncated test case study No. 1

#### Case study 2-2-1:

A request was made to conduct a test over 4 months (approx. 3,000h) for guaranteeing that 10% life of test bearings is equivalent to or better than 10% life of the volume production bearings (the Weibull slope is assumed to be  $e=1.85$ ,  $L_{10}=1,600h$ ) using three test bearings. Five testers are available for 5 months (approx. 3,600h).

The following is an explanation of how to proceed with the truncated test under the conditions of case study 2-2-1. First, use the equation (A1.6) of Appendix 1<sup>5)</sup> to calculate the truncated life  $T$  for guaranteeing that 10% life is 1,600h or more when the number of test samples is three, as follows:

$$T = (1600 - 0) \cdot \left( \frac{\ln(1 - 0.01 \cdot 90)}{3 \ln(1 - 0.01 \cdot 10)} \right)^{1/1.85} + 0 = 4680$$

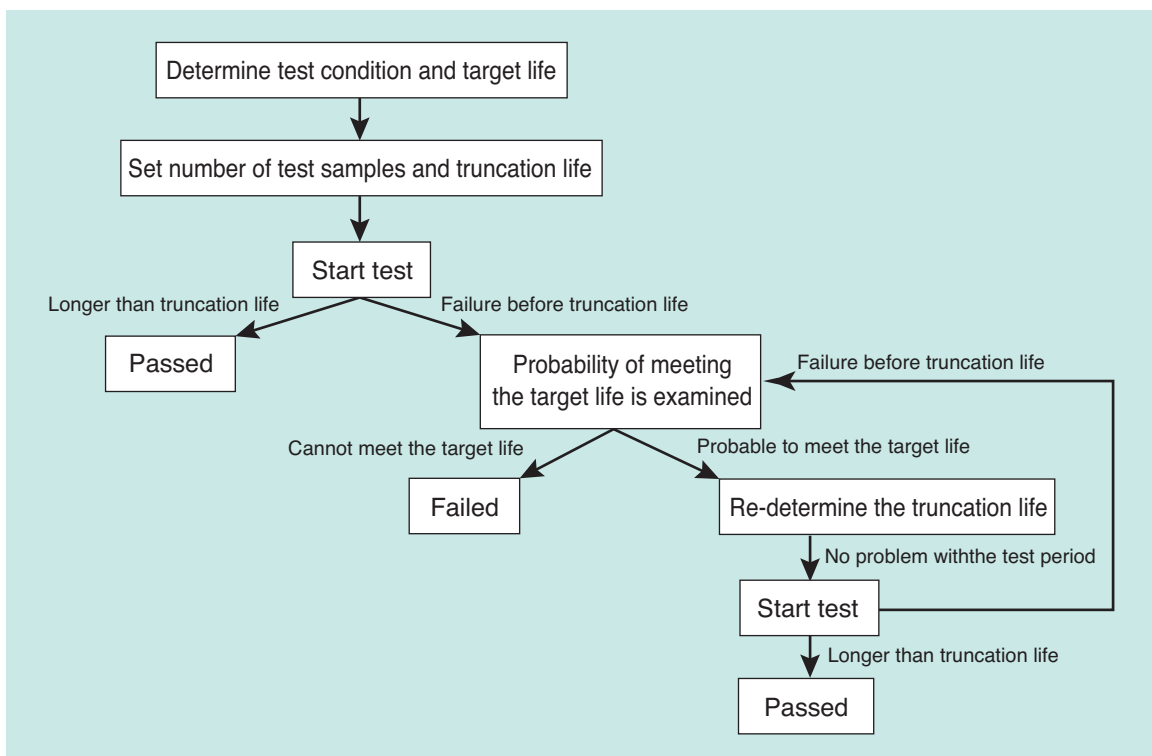


Fig. 2 Procedure in fixed time test

Where, the location parameter (hereinafter, "minimum life") is assumed to be 0; however, from the result of enormous number of past experiments<sup>6-9)</sup>, the relational expression between 10% life and location parameter<sup>10)</sup> can also be used for the assumption of the minimum life value. In addition, the Weibull slope which indicates variation of tests should also be assumed; however, the actual value from past results can be entered.

In this calculation, the truncated life to fulfill the target life of 1,600h with a confidence level of 90% was calculated to be 4,680h, when the test variation was assumed to be the same as the past result (Weibull slope of 1.85) and the number of test samples was three. Since 4,680h exceeds the required test period of 3,000h, measures to shorten the truncated life must be taken. If the number of test bearings can be increased, the truncated life can be reduced since there are additional testers available. If the test samples are increased to five, the truncated life can be reduced to 3,551h. In the following, we assume that the test period can be extended to 5 months (3,600h) and the following case study 2-2-2 is examined.

The reason why we assumed a confidence level of 90% in the above calculation is that, since general textbooks of reliability engineering<sup>11-13)</sup> do not present  $\chi$ , F, t distribution table below a confidence level of 90%, we believed that the confidence level of 90% or above was common practice. In this paper, the confidence level is set to 90% hereafter.

**Case study 2-2-2:**

The test started with the plan of five test samples and a truncated life of 3,551h. When the test time reached 2,000h, two testers failed. The test continued with the remaining three testers as there were no other alternatives.

In the following, the truncated life for guaranteeing the target life with the remaining three testers is calculated under the conditions of case study 2-2-2. Using the equation in **Appendix 1**, the truncated life  $T_R$  was obtained as shown in the following:

$$1 - 0.01 \times 10 = \exp \left[ \frac{\ln(1 - 0.01 \times 90)}{2 \left( \frac{2000 - 0}{1600 - 0} \right)^{1.85} + 3 \left( \frac{T_R - 0}{1600 - 0} \right)^{1.85}} \right]$$

$$T_R = 4319$$

$T_R$  can be solved by using a non-linear equation with a convergence calculation function of ordinary

spread sheet programs (solver function in the case of Microsoft Excel®).

In this calculation, the truncated life with the remaining three test bearings is 4,319h. Negotiations with the relevant parties is required to determine if this extended test period is allowed.

**2. 3 Truncated test case study No. 2**

**Case study 2-3-1:**

The test started with the conditions of case study 2-2-1 and a sample failed at 800h, which is shorter than the truncated life of 3,551h.

The following discusses how to examine the possibility of guaranteeing the target life by continuing the test under case study 2-3-1. In addition, a method for setting the truncated life of the remaining test bearings required for guaranteeing the target life is also discussed in case the test is to continue.

**Table 1** is the calculation result of probability that cannot guarantee the target life from the life data of the first broken test bearing using the equation (A.2.14) in **Appendix 2**. From the table, it is revealed that, if a test sample fails at 800h, the lot cannot meet the target life with an 80 to 90% probability.

If, even under this situation, a decision is made to continue the test, the truncated life of the remaining test bearings can be calculated as follows (5,030h) using the equation (A.2.14) in **Appendix 2** therefore, the test will continue for that duration, if it can be accommodated.

· Calculation of  $\alpha$

$$0.01 \cdot 10 = 1 - \exp \left\{ - \left( \frac{1600 - 0}{\alpha} \right)^{1.85} \right\}$$

$$\alpha = 5400$$

· Calculation of truncated life of the remaining test bearings

$$T_{i+1} = 0 + 5400 \cdot \sqrt[1.85]{\ln \left[ \frac{1}{1 - B^{-1}(0.01 \cdot 90, 2, 5 - 2 + 1)} \right]} = 5030$$

The above re-calculation of truncated life does not consider the life data of the failure at 800h. If that data should also be considered for the calculation of truncated life, Nelson's calculation can be used<sup>14)</sup>.

**Table 1** Confidence levels to determine if the required  $L_{10}$  (1,600h) cannot be achieved. These are calculated from life data for the bearing which is firstly failed before designated suspension time without failure.

Life of first failed bearing (h)	Confidence level (%)
1,579	60
1,301	70
1,011	80
675	90
459	95
193	99

### 3. Accelerated test

#### 3.1 Accelerated test procedure

Fig. 3 shows the accelerated test procedure. Also in accelerated tests, the test conditions and number of test samples must be determined first. In order to determine the number of test samples, it is necessary to identify a sufficient level of test samples and clarify the criteria used. For example, if a specific criteria for reliability is clarified, such as, "I want to set the number of test samples to secure reliability level that can determine a significant difference with a 90% confidence level, when there is a difference of about double in the estimated 50% life", the number of test samples can be calculated by assuming test variation (Weibull slope)<sup>5</sup>.

The relation between the number of test samples and the life ratio to determine the significant difference in estimated life at an arbitrary percent point (hereinafter, "significant life ratio") can be obtained by using the random number simulation in Appendix 3. In the actual situation, since there are restrictions in the number of available test samples, usable testers,

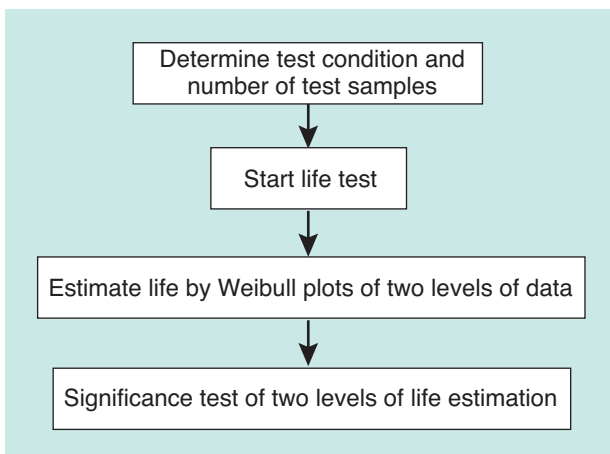


**Fig. 3** Procedure in accelerated test

test period, etc., the number of test samples is determined by considering all of the above. When the life test is started and life data at multiple levels are obtained, the respective lives can be estimated by the Weibull plot. The decision for significant difference between the estimated lives of two levels (significance test) can be made by the calculation result from the method in Appendix 3, or in a simplified manner, by using approximation equations (A4.1) to (A4.3) shown in Appendix 4. In addition, it is recommended that the interpretation of the significance test be made based on the rule shown in Appendix 5.

#### 3.2 Accelerated test case study

##### Case study 3-2-1:

The following data was obtained from the life test with seven test bearings made of material A and seven test bearings made of material B (Table 2).

**Table 2** Life data for material A and B

Life data (h)	
Material A	Material B
20	15
24	45
31	80
42	100
52	140
65	180
79	220

The following describes the significance test procedure and interpretation of the significance test results of the life data. Fig. 4 shows the Weibull plots of material A and material B. The Weibull slope of material A is larger than material B, indicating that the variation of life data is small. In addition, there are no significant differences between the lives of material A and B for 10% life; however, the life of material A is shorter than material B for 50% life. The significance test by random number simulation in Appendix 3 is made for the life data of these two levels. In this calculation, the Weibull slope of 2.07 and 1.15 were assumed, which are the estimated values of material A and B, respectively, and a confidence level of 90% was used. Significant life ratios at the percent points 10 and 50 are 5.39 times and 2.12 times, respectively. The ratio of 10% life and 50% life of material A and material B are 1.07 and 2.21, respectively, which are smaller than the significant life ratio of 5.39 for 10% life and larger than the significant life ratio of 2.12 for 50% life. Therefore, the decision of significant difference is "not significantly different" for 10% life

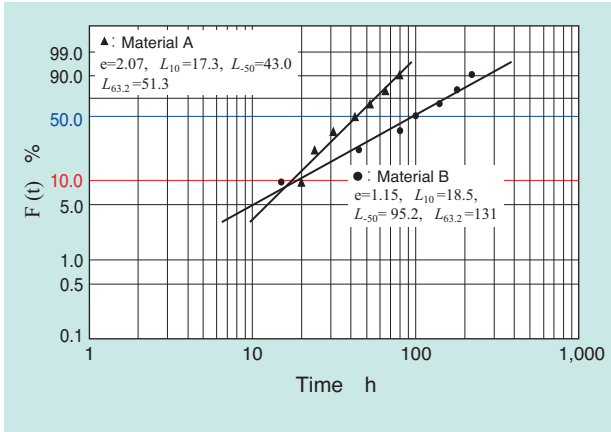


Fig. 4 Weibull plots for material A and B

and "significantly different" for 50% life. However, this result is not contradictory. This result can be said, "comparing the lives of material A and material B, there is no difference in frequency of short life data rarely observed at 10%; however, the average life of material A is shorter than material B." Since this significance test result is as shown in Fig A5.1 (b) of **Appendix 5**, the decision "the life of material A is shorter than material B" is considered to be reasonable.

When the approximate expressions (A4.1) and (A4.2) in **Appendix 4** are used for the significance test, the Weibull slope of 1.61, which is an average of two levels of Weibull slope, should be assumed.

The following shows the significant life ratio calculated by using the equation in **Appendix 4**.

· Significant life ratio for 10% life

$$L_{10R} = 1 + \left[ \frac{1}{0.007474 \{ \ln 9.106 (1.051 - 0.01 \cdot 90) \}^{3.151}} \right]^{1/1.61}$$

$$= 4.48$$

· Significant life ratio for 50% life

$$L_{50R} = 1 + \left[ \frac{1}{0.009349 \{ \ln 36.74 (1.051 - 0.01 \cdot 90) \}^{3.108}} \right]^{1/1.61}$$

$$= 1.94$$

The significant life ratio obtained from these approximation expressions are 4.48 times for 10% life and 1.94 times for 50% life, which is interpreted as "not significantly different" for 10% life and "significantly different" for 50% life, which is the same as the result obtained from the calculation in **Appendix 3**.

#### 4. Conclusion

In this paper, the procedures of the truncated test and accelerated test in rolling contact fatigue life tests were discussed. In the rolling contact fatigue life test, it is important to plan the test and process the life data based on the statistical evidence because variation of life data is significant. However, it is not easy for beginners who are not familiar with the data that follows the Weibull distribution. In this paper, planning of the rolling contact fatigue life test and interpretation of the results are described with the specific case studies so that even beginners can conduct the tests. I hope that this paper serves as a good reference for engineers and researchers who are engaged in rolling contact fatigue life tests.

## Reference

- 1) G. Lundberg, & A. Palmgren: Dynamic capacity of rolling bearing, *Acta Polytechnica* 7, Mechanical Engineering Series, 1, 3 (1947).
- 2) G. Lundberg, & A. Palmgren: Dynamic capacity of roller bearing, *Acta Polytechnica* 96, Mechanical Engineering Series, 2, 4 (1952).
- 3) Shigeo Shimizu: Introduction to Reliability Design for Machinery, Suurikogakusha, Tokyo, (2006) 36.
- 4) Takumi Fujita: Design method for life test to achieve both speed and reliability and statistical test method for test results (2nd Report) - Consideration for points to remember in analysis of life data that follow the Weibull distribution - ,Rolling Elements Technical Committee of the Japan Society for Precision Engineering, Proceedings of Academic Frontier Symposium of Meiji University, (2010).
- 5) T. Fujita: Rolling Contact Fatigue Life Test Design and Result Interpretation Methods Maintaining Compatibility of Efficiency and Reliability, *J. ASTM international*, ASTM STP 1524, 7 (2010) 179-198, Paper ID JAI102492.
- 6) T. Tallian: Weibull distribution of rolling contact fatigue life and deviations therefrom, *ASLE Trans.*, 5, 1(1962) 183.
- 7) B. Snare: How reliable are bearings, *The ball bearing journal*, 162(1970) 3.
- 8) Masao Kuroda: Load rating and life of rolling bearings, *Lubrication*, 17 (1972) 569.
- 9) Junzo Okamoto, Takeo Yoshioka, Takashi Fujiwara, Kiyoshi Fujita, Tokio Kitahara and Shizuo Koizumi: Experimental study regarding the minimum life of rolling bearings, *Lubrication*, 22 (1977) 307.
- 10) ISO/TS16281, (2006).
- 11) For example, Jiro Yamauchi: Statistical Tables, Japanese Standards Association, (1986) 241.
- 12) For example, Shigeichi Moriguchi: Quality Control Course: New Edition Statistical Method Rev, Suurikogakusha, (1999), 262.
- 13) For example, Shigeichi Moriguchi: New Edition JUSE Numerical Tables, JUSE Press Ltd., (2000), 5.
- 14) W. Nelson: Weibull analysis of reliability data with few or no failure, *Journal of Quality Technology*, 17 (1985) 140.
- 15) W. Nelson: Analysis of Life Data, JUSE Press Ltd., (1988) 272.
- 16) R. B. Abernethy, *The New Weibull Handbook* 5th edition, (2006) chapter 6-15.
- 17) R. B. Abernethy, *The New Weibull Handbook* 5th edition, (2006) chapter 6-19.
- 18) Takumi Fujita and Toshihiko Sasaki: Significance Test of Rolling Contact Fatigue Life Estimated by Weibull Plots, *Tribologist*, 59, 10 (2014) 667-673.
- 19) L. Johnson: *The Statistical Treatment of Fatigue Experiments*, Elsevier (1964) 37.
- 20) M. Matsumoto & T. Nishimura: Mersenne twister: A623-dimensionally equidistributed uniform pseudorandom number generator, *ACM Transaction on modeling and computer simulations special issue on uniform random number generation*, 8 (1998) 3.
- 21) For example, Tetsuaki Yotsuji: *Probability Distribution Random Number Generating Method for Calculator Simulation*, Pleiades Publishing House, (2010) 53.

## Photo of author



Takumi FUJITA  
Advanced Technology  
R&D Center

**Appendix 1**

**Equation to calculate the relation between truncated life and number of test samples when there are no failures**

If, from the population of the cumulative failure probability  $F(x)$ ,  $N$  test bearings are extracted, the probability  $P_k$  that the life of  $k$  bearings among them fall below the time  $T$  (or loading cycles) follow binomial distribution of (A1.1)<sup>15)</sup>.

$$P_k = \frac{N!}{k!(N-k)!} F^k(T) (1-F(T))^{N-k}$$

$$= \frac{N!}{k!(N-k)!} R(T)^{N-k} (1-R(T))^k \dots \text{(A1.1)}$$

Where,

$F(T)$  : cumulative failure probability of the Weibull distribution  
 $R(T)$  : cumulative probability of survival,  $F(T)=1-R(T)$

Therefore, the probability that the number of test samples with life that falls below time  $T$  becomes 0 among  $N$  samples (none in  $N$  samples) can be expressed with  $k=0$ , by equation (A1.3) using cumulative distribution function  $F(x)$  of the Weibull distribution of equation (A1.2).

$$R(x) = 1 - F(x) = 1 - \left[ 1 - \exp \left\{ - \left( \frac{x - \gamma}{\alpha} \right)^e \right\} \right]$$

$$= \exp \left\{ - \left( \frac{x - \gamma}{\alpha} \right)^e \right\} \dots \text{(A1.2)}$$

Where,

$e$  : Weibull slope,  $\alpha$  : scale parameter,  
 $\gamma$  : location parameter

$$P_0 = \frac{N!}{0!(N-0)!} R(T)^{N-0} (1-R(T))^0 = R(T)^N$$

$$= \exp \left\{ -N \left( \frac{T - \gamma}{\alpha} \right)^e \right\} \dots \text{(A1.3)}$$

When  $\alpha = \alpha_u$ , if the probability of equation (A1.3) is 0.1, among  $N$  extracted bearings from the population  $\alpha = \alpha_u$ , the event that bearings with a life less than time  $T$  is zero has a probability of 0.1, which is rare; therefore, the assumption of  $\alpha = \alpha_u$  discarded with a probability of 0.9 (confidence level of 90%) (null hypothesis). That is, this event should be interpreted as the probability that  $\alpha$  of the population becomes over  $\alpha_u$  is 90%. From the above, the relation between number of test samples  $N$  that  $\alpha = \alpha_u$  with confidence level  $C\%$  and a truncation life  $T_1$  of the undamaged bearings can be expressed with equation (A1.4).

$$1 - 0.01C = \exp \left\{ -N \left( \frac{T_1 - \gamma}{\alpha_u} \right)^e \right\} \dots \text{(A1.4)}$$

Arranging equation (A1.4) with relational expression (A1.5), equation (A1.6) can be obtained.

$$F(x) = 0.01n = 1 - \exp \left\{ - \left( \frac{L_n - \gamma}{\alpha_u} \right)^e \right\} \dots \text{(A1.5)}$$

$$T_1 = (L_n - \gamma) \cdot \left( \frac{\ln(1 - 0.01C)}{N \ln(1 - 0.01n)} \right)^{1/e} + \gamma \dots \text{(A1.6)}$$

Where,

$n$  :  $n\%$  of life

Equation (A1.6) is an expression showing the relation between the number of test samples  $N$  that can guarantee the target life of  $L_n$  with a confidence level of  $C\%$ , and truncated life  $T_1$  of the undamaged bearings.

Next, the situation that  $N$  bearings stay undamaged until the end of their life data  $t_1, t_2, \dots, t_n$  is examined.

From the population with a cumulative probability of survival  $R(x)$ ,  $N$  test bearings are extracted. Since the life data  $t_1, t_2, \dots, t_n$  are simultaneously obtained, the joint probability can be expressed as follows:

$$\prod_{i=1}^N R(T_i) = \exp \left\{ - \left( \frac{t_1 - \gamma}{\alpha} \right)^e \right\} \times \exp \left\{ - \left( \frac{t_2 - \gamma}{\alpha} \right)^e \right\} \times$$

$$\dots \times \exp \left\{ - \left( \frac{t_N - \gamma}{\alpha} \right)^e \right\} \dots \text{(A1.7)}$$

Applying the same concept mentioned earlier, when  $\alpha = \alpha_u$ , if the probability of equation (A1.7) is 0.1, the situation that the above mentioned data is obtained can only occur with a probability of 0.1 when  $N$  test samples are extracted from the population of  $\alpha = \alpha_u$ , which is rare, the assumption of  $\alpha = \alpha_u$  is discarded with a probability of 0.9. That is, this event should be interpreted as the probability that  $\alpha$  of the population becomes over  $\alpha_u$  is 90%. From the above, the relation between the number of test samples  $N$  that  $\alpha \geq \alpha_u$  with confidence level of  $C\%$  and the truncated life of the undamaged bearings can be expressed by the equation (A1.8).

$$1 - 0.01C = \exp \left\{ - \left( \frac{t_1 - \gamma}{\alpha} \right)^e \right\} \times \exp \left\{ - \left( \frac{t_2 - \gamma}{\alpha} \right)^e \right\} \times$$

$$\dots \times \exp \left\{ - \left( \frac{t_N - \gamma}{\alpha} \right)^e \right\} \dots \text{(A1.8)}$$

Arranging equation (A1.8) with relational expression (A1.5), equation (A1.9) is obtained<sup>16)</sup>.

$$1 - 0.01n = \exp \left[ \frac{\ln(1 - 0.01C)}{\sum_{i=1}^N \left( \frac{t_i - \gamma}{L_n - \gamma} \right)^e} \right] \dots \text{(A1.9)}$$

**Appendix 2**

**Equation used in the case study in Section 2.3**

If, from the population of the cumulative failure probability  $F(x)$ ,  $N$  test bearings are extracted, the probability  $P_k$  that the life of  $k$  bearings among them fall below the time  $T$  (or loading cycles) follow binomial distribution of (A2.1).

$$P_k = \frac{N!}{k!(N-k)!} F^k(T) (1-F(T))^{N-k}$$

$$= \frac{N!}{k!(N-k)!} R(T)^{N-k} (1-R(T))^k \dots \text{(A2.1)}$$

Where,

$F(T)$  : cumulative failure probability of the Weibull distribution  
 $R(T)$  : cumulative probability of survival,  $F(T)=1-R(T)$

On the other hand, when the second shortest life data of  $N$  test samples extracted from the cumulative failure probability  $F(x)$  exceeds the time  $T_2$  is when there are 0 and 1 test bearing which lives fall shorter than the time  $T_2$  among  $N$  test bearings. Therefore, the probability that the second shortest life data among  $N$  test bearings exceeds the time  $t_2$  can be obtained by equation (A2.2) using the law of the sum of probability<sup>17)</sup>.

$$P_0 + P_1 = R(T_2)^N + NR(T_2)^{N-1}(1-R(T_2)) \dots \text{(A2.2)}$$

Using the same concept as **Appendix 1**, the relation between truncated life  $T_2$  of one failed bearing that  $\alpha \geq \alpha_u$  with a confidence level of  $C\%$  and the number of test samples  $N$  can be expressed by equation (A2.3).

$$1 - 0.01C = P_0 + P_1 = \exp\left\{-\left(\frac{T_2 - \gamma}{\alpha_u}\right)^e\right\} +$$

$$\left\{N \exp\left\{-\left(\frac{T_2 - \gamma}{\alpha_u}\right)^e\right\} \times \exp\left\{-\left(\frac{T_2 - \gamma}{\alpha_u}\right)^e\right\} \dots \text{(A2.3)}\right.$$

Similarly, the relation between the truncated life  $T_{i+2}$  of  $i$  failed bearing that  $\alpha \geq \alpha_u$  with a confidence level of  $C\%$  and the number of test samples  $N$  can be expressed by equation (A2.4).

$$1 - 0.01C = \sum_{k=0}^{i-1} P_k$$

$$= \sum_{k=0}^{i-1} \frac{N!}{k!(N-k)!} F^k(T_{i+1}) (1-F(T_{i+1}))^{N-k} \dots \text{(A2.4)}$$

On the other hand, since the probability that all events occur is 1, equation (A2.5) is obtained.

$$1 = \sum_{k=0}^{i-1} P_k + \sum_{k=i}^N P_k \dots \text{(A2.5)}$$

From equations (A2.4) and (A2.5), the following relation can be obtained.

$$0.01C = \sum_{k=i}^N P_k$$

$$= \sum_{k=i}^N P_k \frac{N!}{k!(N-k)!} F^k(T_{i+1}) (1-F(T_{i+1}))^{N-k} \text{(A2.6)}$$

$\sum_{k=i}^N P_k$  is called order statistics<sup>15)</sup> and can be expressed by equation (A2.7).

$$\sum_{k=i}^N P_k = \frac{N!}{(i-1)!(N-i)!} \int_0^{F(T_{i+1})} t^{i-1} (1-t)^{N-i} dt \dots \text{(A2.7)}$$

A recursive equation can be obtained if partial integration is applied to the right side of the equation (A2.7), to derive equation (A2.6). Next, when  $\Gamma$  function is used to rewrite the factorial part of the right side of equation (A2.7), equation (A2.8) is obtained.

$$\sum_{k=i}^N P_k = \frac{\Gamma(N+1)}{\Gamma(i)\Gamma(N-i+1)} \int_0^{F(T_{i+1})} t^{i-1} (1-t)^{N-i} dt \dots \text{(A2.8)}$$

On the other hand, the relation of (A2.9) exists between the gamma function and beta function  $\beta(x, y)$  (different from beta distribution function).

$$\frac{\Gamma(x+y)}{\Gamma(x)\Gamma(y)} = \frac{1}{\beta(x, y)} \dots \text{(A2.9)}$$

When equation (A2.8) is rewritten using the relation of equation (A2.9), equation (A2.10) is obtained.

$$\sum_{k=i}^N P_k = \frac{1}{\beta(i, N-i+1)} \int_0^{F(T_{i+1})} t^{i-1} (1-t)^{N-i} dt \dots \text{(A2.10)}$$

This leads to the cumulative distribution function of the beta distribution function expressed by equation (A2.11).

$$\sum_{k=i}^N P_k = \frac{1}{\beta(i, N-i+1)} \int_0^{F(T_{i+1})} t^{i-1} (1-t)^{N-i} dt$$

$$= \beta(F(T_{i+1}), i, N-i+1) \dots \text{(A2.11)}$$

From equations (A2.6) and (A2.7), equation (A2.12) is obtained.

$$\beta(F(T_{i+1}), i, N-i+1) = 0.01C \dots \text{(A2.12)}$$

When equation (A2.12) is modified using the inverse function of the cumulative distribution function of the beta distribution function and the inverse function of cumulative failure probability  $F(x)$ , we obtain equations (A2.13) and (A2.14).

$$B^{-1}(0.01C, i, N-i + 1) = F(T_{i+1}) \dots\dots\dots (A2.13)$$

$$T_{i+1} = F^{-1}(B^{-1}(0.01C, i, N-i + 1))$$

$$= \gamma + \alpha \cdot \sqrt[e]{\ln \left[ \frac{1}{1 - B^{-1}(0.01C, i, N-i + 1)} \right]} \quad (A2.14)$$

Where,

$B^{-1}(0.01C, i, N-i + 1)$  : inverse function of cumulative distribution function of the beta distribution function,

$C$  : confidence level %,

$N$  : number of test samples

$i$  : truncation life of undamaged condition is calculated by  $i=1$ , truncation life of failure of  $1 \dots k$  samples is calculated by  $i = 2 \dots k+1$

In addition,  $\alpha$  of equation (A2.14) can be obtained by substituting the target life  $L_n$  into equation (A1.5), if the target life is available. This equation is for calculating the truncated life of the remaining test bearings. However, it can be applied for the decision of not being able to meet the target life with a probability of 90% if the first test bearing fails before the truncated life, because when  $i$  is substituted by 1 and  $C$  is substituted by 10, it indicates that the target life can only be met with a probability of 10% during the truncated life of all samples.

As shown above, truncated life can be calculated using the inverse function of the cumulative distribution function of the beta distribution function. The cumulative distribution function of the beta distribution function can be obtained, in principle, from binomial probability and if the conditions of the binomial probability (random extraction of test bearings, sufficient number in the population) are established, it gives the exact result in the truncated life calculation. In addition, regarding the inverse function of the cumulative distribution function of the beta distribution function, the calculation of equation (A2.14) can be easily performed since ordinary spreadsheet programs provide the functions (in case of Microsoft Excel®, betainv function).

### Appendix 3

#### Significance test using random simulation<sup>18)</sup> (calculation method for significant life ratio)

This appendix discusses how to conduct significance test of life at an arbitrary percent point using Weibull random number. Random simulation can identify variation of life ratio from two levels of data obtained from two sets of data extracted from the population of the same life. If the life ratio obtained from the actual test is greater than the variation of the life ratio obtained from the random simulation, it means that the lives of two levels contain a bigger difference than the variation, in other words, a significant difference. The variation of life ratio obtained from this random simulation is the significant life ratio. The following shows the calculation method of significant life ratio using Weibull random number.

- (1) With Weibull, plot two levels of data obtained from the life test of test samples  $N_1$  and  $N_2$  and find the respective Weibull slopes  $e_1$  and  $e_2$ . For life estimation with the Weibull plots, use the calculation method in Johnson's literature<sup>19)</sup>.
- (2) Determine the percent point for calculating variation of life ratio.
- (3) Assume the lives of two levels  $L_{n,1}$  and  $L_{n,2}$  at the percent point determined in (2)  $n$  are the same (value of 1), obtain the scale parameter of Weibull distribution  $\alpha_1$  and  $\alpha_2$ .
- (4) Generate Weibull random numbers that follow the Weibull distribution of two levels obtained from (1) to (3) above, for the number of test samples,  $N_1$  and  $N_2$ , respectively. Weibull random numbers can be obtained by obtaining uniform random numbers generated by the Mersenne Twister method<sup>20)</sup> and applying the inverse function method<sup>21)</sup> to them.
- (5) Plot the two sets of Weibull random numbers generated in (4), estimate the lives at percent point  $n$  determined in (2) and obtain the life ratio.
- (6) Repeat the operation of (4) and (5) for more than 10,000 times to obtain the range of life ratio with a confidence level of  $C\%$ .

The range of life ratio obtained from the above procedure indicates degree of variation with a probability of  $C\%$  when life ratios are compared by extracting  $N_1$  and  $N_2$  test bearings from two levels of populations with the Weibull slopes of  $e_1$  and  $e_2$ , and the lives at the percent point  $n$  are the same. Therefore, if the life ratio of two levels is greater than the variance, the lives of the two levels have significant difference with a confidence level of  $C\%$ .

#### Appendix 4

##### Approximation equation for significant life ratio<sup>18)</sup>

Significant life ratio varies depending on the number of test samples for each level  $N_1$  and  $N_2$ , Weibull slope  $e_1$  and  $e_2$ , percent point for comparing life difference  $n$ , and confidence level  $C$ . Appendix 3 indicated how to calculate the significant life ratio that changes by these six parameters using Weibull random numbers. This method, however, has a disadvantage of having to create calculation programs.

In the calculation using Weibull random numbers, Weibull slopes indicating the variation of test and number of test samples are assumed to be different between two levels; however, in the actual tests, the Weibull slopes are often similar if the test conditions and the steel type are the same, and number of test samples tends to be the same unless there is any special reason. Also, the percent points to compare the life difference are almost always 10, 50 and 63.2%. The percent point of 63.2% is the percent point that corresponds to the scale parameter of the Weibull distribution. Therefore, the approximation equation which can calculate the significant life ratio of two levels for the same number of test samples and Weibull slopes at the percent points of 10, 50 and 63.2 with a confidence level of  $C\%$  can cover a vast majority of the situations. The following shows approximation equations of significant life ratio obtained by a regression analysis of significant life ratio from random simulation.

- Significant life ratio for 10% life

$$L_{10R} = \left[ 1 + \frac{1}{0.007474 \{ \ln 9.106 (1.051 - 0.01C) N \}^{3.151}} \right]^{1/e} \quad (\text{A4-1})$$

- Significant life ratio for 50% life

$$L_{50R} = \left[ 1 + \frac{1}{0.009349 \{ \ln 36.74 (1.051 - 0.01C) N \}^{3.151}} \right]^{1/e} \quad (\text{A4-2})$$

- Significant life ratio for 63.2% life

$$L_{63.2R} = \left[ 1 + \frac{1}{0.01068 \{ \ln 41.48 (1.051 - 0.01C) N \}^{3.059}} \right]^{1/e} \quad (\text{A4-3})$$

Where,

$N$  : number of test samples,  $e$  : Weibull slope,

$C$  : confidence level

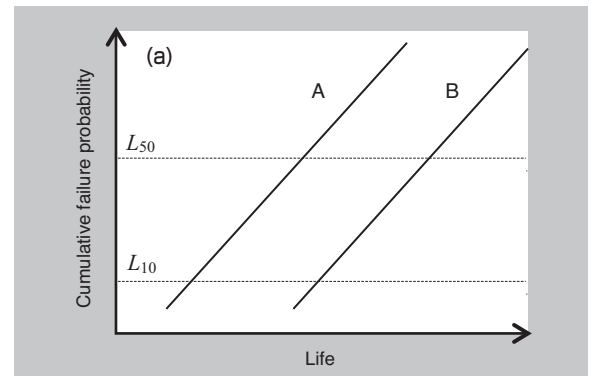
Applicable range :  $N \leq 50$ ,  $0.5 \leq e \leq 10$ ,  $80 \leq C \leq 99$

#### Appendix 5

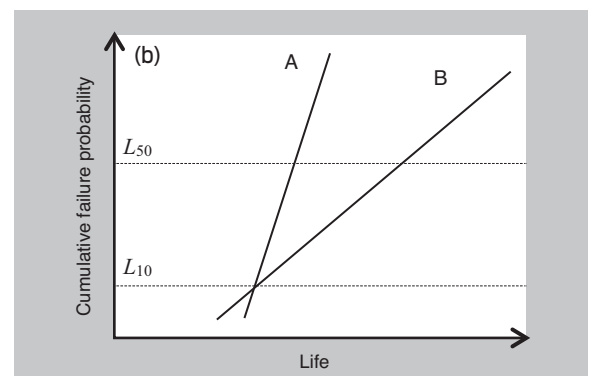
##### Interpretation of significance test result

The following describes the interpretation of significance test results under each situation of assumed 2 levels of Weibull plots.

- (a) Significance test results show that the variations of life of both levels are the same (the same Weibull slope) and A has a shorter life for both 10% life and 50% life. In this case, the interpretation is "A's life is shorter than B."



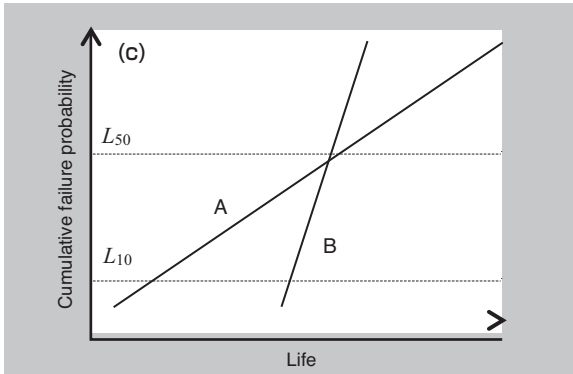
- (b) Significance test results show that the variance of life A is small (Weibull slope of A is large) and no significant differences exist for 10% life but A's life is shorter for 50% life. We can interpret that there are no differences in a short life that rarely occurs with a probability of 10%, but there is a difference for the average life. Even if A's life is equivalent to B for 10% life, it is shorter for 50% life, which is the average life; therefore, the interpretation "A has a shorter life than B" is considered appropriate.



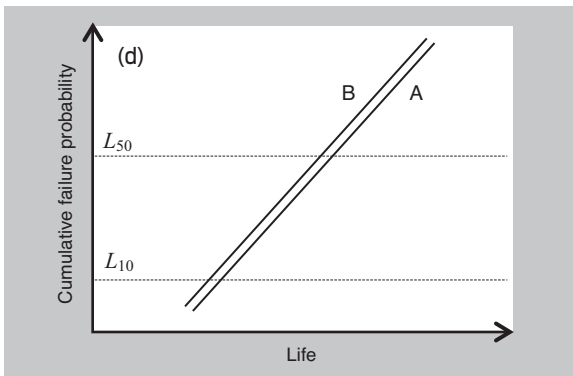
- (c) Significance test results show that the variance of life of A is large (A's Weibull slope is small) and A's life is short for 10% life and no significant difference for 50%.

Even if A's life is equivalent for 50% life, which is the average life, under the situation that it is short for 10% life, it indicates that A's life has a larger variation and unstable quality; therefore, the

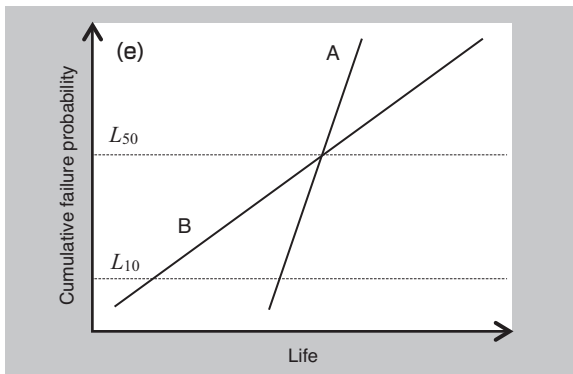
interpretation of "Although A's life is equivalent to B, its variation is large" is considered to be adequate.



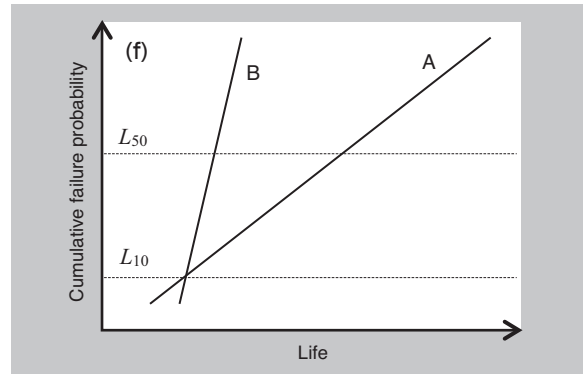
(d) Significance test results show that the variances of life for both are equivalent (the same Weibull slope) and there are no significant differences for either 10% or 50% life. In this case, the interpretation is "A's life is equivalent to B."



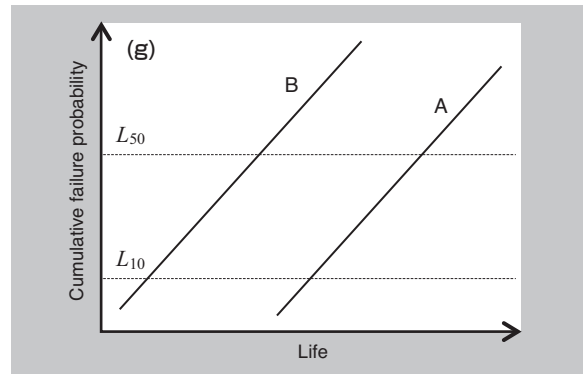
(e) Significance test results show that the variance of life of A is small (A's Weibull slope is large) and A's life is long for 10% life and no significant differences for 50%. To indicate that A's life is equivalent for 50% life, which is the average life, with small variation, the interpretation of "Although A's life is equivalent to B, its variation is small" is considered to be adequate.



(f) Significance test results show that the variance of life A is large (the Weibull slope of A is small) and no significant differences exist for 10% life but A's life is longer for 50% life. A's life is mostly long; however, it may be almost the same for a short life that may occur rarely with a probability of 10%. In this case, the interpretation "Although A's life is longer than B, its variance is large" is considered to be adequate.



(g) Significance test results show that the variances of life for both are equivalent (the same Weibull slope) and A's life is long for either 10% or 50% life. In this case, the interpretation is "A's life is longer than B."



# Rolling Contact Fatigue Life of Thrust Ball Bearing under Low Lambda Condition



Takumi FUJITA\*  
Naoya HASEGAWA\*  
Naoya KAMURA\*  
Toshihiko SASAKI\*\*

Rolling contact fatigue (RCF) testings of thrust ball bearing under boundary lubrication condition (low lambda condition) are conducted while changing test conditions of load, rotational speed and combination of surface roughnesses for bearing component parts. The RCF test results and measurements of surface

roughnesses of before and after the tests show that the raceway surface with larger roughness promotes the surface initiated failure of the other component. In addition, they demonstrate that the behavior of change in surface roughness during rolling contact depends on the test conditions and influences RCF life accordingly. These results suggest that RCF life of rolling bearing used under low lambda conditions should be estimated considering not only analytical relationship between repeated stress in subsurface and surface roughness during RCF, but also experimental database of the running-in behavior depending on RCF conditions.

## 1. Introduction

In an effort to reduce friction in automobiles and industrial machines, development of low viscosity lubricants is underway. Along with this trend, the use of rolling bearings in low lubrication condition (hereinafter, low  $\Lambda$  condition, where  $\Lambda$  is a film parameter which is the ratio of oil film thickness and sum of the square root mean square roughness of two objects) will increase; therefore, the importance of prediction technique and life improvement technology of rolling contact fatigue life (hereinafter, "life") under low  $\Lambda$  conditions is expected to increase.

The study on life under low  $\Lambda$  condition became active in the latter half of the 1960s, along with the development of theory of elastohydrodynamic lubrication (EHL theory), both domestically and internationally<sup>1-19)</sup>. The relation between film parameter  $\Lambda$  and life ratio based on the research of Tallian<sup>1)</sup> and Skurka<sup>2)</sup> is called the ASME (American Society of Mechanical Engineers) recommended diagram<sup>3)</sup> and is a very well known study in the field. Since the latter half of the 1980s, Akamatsu et al. have been studying the relation between various parameters on surface roughness and life<sup>20-24)</sup>, rolling speed and life<sup>25-27)</sup>, and pointed out that life under low

$\Lambda$  conditions does not only depend on  $\Lambda$ , but also on various parameters of surface roughness and operating conditions.

Currently, the most recent and generally well known life prediction methods for low  $\Lambda$  condition are ISO (International Organization for Standards) 281<sup>29)</sup> based on research outcome by Ioannides et al.<sup>28)</sup> and life formula by JIS (Japan Industrial standards) B1518<sup>30)</sup>. This life formula includes a coefficient called  $\kappa$ , which is used to correct predicted life depending on lubrication conditions; therefore, using this coefficient makes it possible to predict life under low  $\Lambda$  conditions. However, this coefficient does not take into account severe conditions of projection contact of surface roughness (root mean square slope  $Rdq$  of  $4^\circ$  or more). Therefore, life prediction under those conditions cannot be performed with the life formulae of ISO and JIS. In addition, as Akamatsu et al. point out, life under the low  $\Lambda$  conditions is affected by operating conditions and various parameters of surface roughness; however, the life formulae by ISO and JIS cannot make a life prediction by taking these conditions into account. ISO and JIS may posit that life formulae considering large surface roughness, special operating conditions or special surface characteristics are not generally required. However, considering that

\* Advanced Technology R&D Center

\*\* Professor, Faculty of Human Sciences, Kanazawa University

limit design technology is required at the actual production sites of rolling bearings due to a restriction in processing methods or for pursuing productivity improvement or reduction of production costs, that the operating conditions of rolling bearings are widely different by users and that bearings with special surface characteristics are actually used<sup>31)</sup>, establishment of universal life prediction methods which can take those conditions into account are desirable.

For establishment of life prediction methods under low  $\Delta$  conditions, various life tests under low  $\Delta$  conditions and observation of the findings from a tribology viewpoint are indispensable; however, there are few reports of systematic life tests under low  $\Delta$  conditions. Particularly, there are no reports regarding life tests under low  $\Delta$  conditions for thrust ball bearings. In this paper, life test results under low  $\Delta$  conditions of thrust ball bearings are reported with consideration of causes that determine life and life prediction under low  $\Delta$  conditions based on the test results.

## 2. Test method

**Table 1** shows the life test conditions. The test was conducted with thrust ball bearings of part number 51105 by changing surface roughness of the inner/outer rings and steel rolling elements, oil type, oil temperature, number of rolling elements, test load and rolling speed. The inner/outer rings and steel rolling elements of the thrust bearings are made of high carbon chromium bearing steel type 2 (hereinafter, "SUJ2") with standard hardening and tempering. The hardness of the inner/outer rings and steel rolling elements of thrust bearings were HRC62 and HRC64, respectively. Oil bath lubrication was used and  $\Delta$

obtained from the Hamrock-Dawson's film thickness calculation formula<sup>32)</sup> was 0.1 or less in all conditions. For lubricant oil, JX Nippon Oil & Energy turbine oil with no additives was used for all tests. For Test Nos. 1 - 9, steel rolling elements of root mean square roughness (hereinafter, " $R_q$ ") of 0.22  $\mu\text{m}$  were used. Among them, with Test Nos. 1 - 6, the effect of surface roughness of the inner/outer rings and load can be checked, with Test No. 1 and No. 7, the effect of the rolling speed can be checked, with Test No. 7 and No. 8, the effect of oil temperature can be checked, and with Test No. 3 and No. 9, the effect of load period can be checked. Test Nos. 10 - 12 intentionally created an aggregation of micro peeling (hereinafter, "peeling") on the inner/outer rings of the bearings by making the surface of the steel rolling elements rougher. Here, peeling is defined as the aggregation of several 10 - 100  $\mu\text{m}$  of length, and flaking is defined as an individual delamination larger than that size. The effect of load on peeling can be checked with Tests No. 10 - 12.

**Table 1** shows the calculated life  $L_{10h}$ , calculated with a method used for general life calculation of ball bearings<sup>33)</sup>, and the values of correlation factor for operating conditions read out from the ASME diagram (hereinafter, " $a_3$ ").

Since the ASME diagram does not present  $a_3$  values when  $\Delta$  is 0.6 or less, the value of 0.164 under the column  $a_3$  is the minimum value read out from the ASME diagram.

**Table 1** Test conditions

Test No.	Surface roughness $\mu\text{m}$		The number of rolling element	Load kN	Contact stress GPa	Rotaion speed $\text{min}^{-1}$	Viscosity grade, Temperature	Oil Film parameter $\Delta$	Calculated life $L_{10h}$	Correlation factor $a_3$
	Inner and outer ring	Rolling element								
1	0.25	0.22	3	5.88	3.9	1500	VG32, 110°C	0.071	14	0.164
2	0.25	0.22	3	4.26	3.5	1500	VG32, 110°C	0.073	37	0.164
3	0.25	0.22	3	2.70	3.0	1500	VG32, 110°C	0.076	145	0.164
4	0.65	0.22	3	5.88	3.9	1500	VG100, 110°C	0.058	14	0.164
5	0.65	0.22	3	4.26	3.5	1500	VG100, 110°C	0.059	37	0.164
6	0.65	0.22	3	2.70	3.0	1500	VG100, 110°C	0.061	145	0.164
7	0.25	0.22	3	5.88	3.9	500	VG150, 110°C	0.069	42	0.164
8	0.25	0.22	3	5.88	3.9	500	VG32, 70°C	0.072	42	0.164
9	0.25	0.22	6	5.39	3.0	1500	VG32, 110°C	0.076	73	0.164
10	0.25	0.54	3	5.88	3.9	1500	VG150, 110°C	0.081	14	0.164
11	0.25	0.54	3	2.70	3.0	1500	VG150, 110°C	0.086	145	0.164
12	0.25	0.54	3	0.98	2.1	1500	VG150, 110°C	0.092	3031	0.164

### 3. Test results

#### 3.1 Life test results

Fig. 1 shows an example of the Weibull plots (Test No.1) and Table 2 shows the estimated lives obtained from the Weibull plots of Test Nos.1 - 12, respectively. For life estimation with the Weibull plots, the L. G. Johnson method<sup>(34)</sup> was used for calculating median rank and analysis was made by adjusting the Weibull slope to 1.1. The reason why the Weibull slope was adjusted is to make a comparison with the calculated life (calculated using Rolling Bearing Catalog<sup>(37)</sup>), which is calculated with a Weibull slope of 1.1<sup>(35, 36)</sup> (10/9 for point contact and 9/8 for line contact, to be exact). In Test Nos. 10 - 12 where the damage mode was peeling, since each peeled piece is small, vibration that occurs at the initial stage of peeling was small, making it difficult to stop the test at the initial stage of peeling. Therefore, the life data in Table 2 shows the stage where peeling had proceeded until it was detected by vibration.

Fig. 2 shows typical delamination modes in Test Nos. 1 to 9 and Nos. 10 to 12. Most of the damage

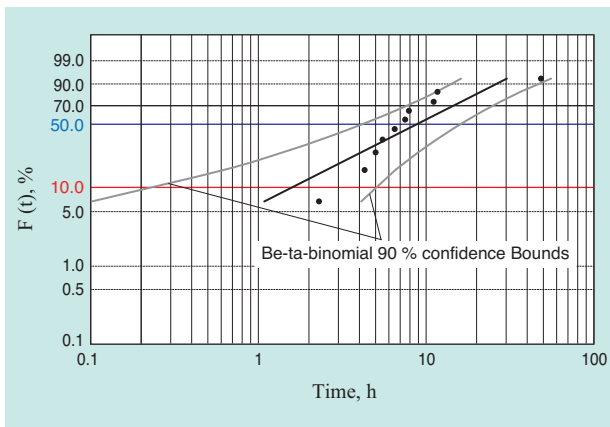


Fig. 1 Weibull plots of failure time for test No.1

occurred at the inner/outer rings; however, in Test Nos. 5 and 6, the steel rolling elements were partially damaged. The damage mode in Test Nos. 1 - 9 was flaking and in Test Nos. 10 – 12, peeling. In Test No. 10, both peeling and flaking were observed. In addition, in Test Nos. 10 - 12, the peeling location was characteristic and was found more on the inner diameter side of the rolling contact trajectory.

Fig. 3 shows the relation between the estimated life and calculated life. The number near each plot in the figure indicates the Test No.

The calculated life of the horizontal axis takes  $a_3$  into account.

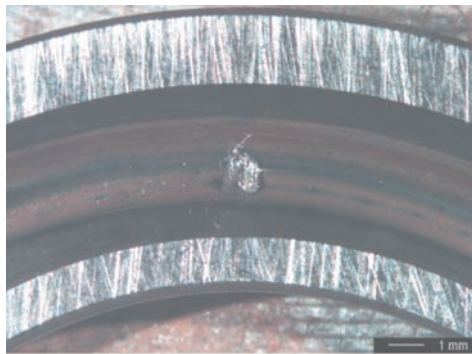
The following is an itemized summary of the findings from Test Nos. 1 to 12.

- 1) In Test Nos. 1 - 9, the ratios of the estimated life and the calculated life were in the range between 0.6 and 2.6, and no enormous difference existed between the estimated life and calculated life under any conditions.
- 2) In Test Nos.10 - 12, the ratios between the estimated life and the calculated life ( $L_{10}/a_3 L_{10h}$ ) were in the range from 0.004 to 0.4, and the difference between the estimated life and calculated life was more significant under small load conditions.
- 3) The surface roughness of the inner/outer rings before the test was different for Test Nos. 1 - 3 and Test Nos. 4 – 6, but the ratios of the estimated life and calculated life were 0.7 – 0.94 and 0.6 - 1.1, respectively, and no significant life differences were observed between the two conditions.
- 4) In Test Nos. 1 - 3 and Nos. 4 - 6, the effect of load was observed respectively, and the life was inversely proportional to the cubes of the load.
- 5) The effect of rolling speed was observed in Test No. 1 and No. 7, and the ratio of the estimated life and calculated life of Test No. 7 with slow rolling

Table 2 Results of RCF testing

Test No.	1	2	3	4	5	6	7	8	9	10	11	12	
The number of test specimen	10	10	13	10	14	11	10	11	11	10	8	8	
The number of failure parts	Flaking of Inner or Outer ring	10	9	8	9	7	7	10	11	9	10	0	0
	Peeling of Inner or Outer ring	0	0	2	1	3	1	0	0	1	10	8	8
	Failure of Rolling element	0	1	0	0	4	2	0	0	0	0	0	0
	Suspended	0	0	3	0	0	1	0	0	1	0	0	0
Estimated $L_{10}$ (h)	1.6	5.4	22.5	2.5	6.6	13.5	10.2	17.8	10.6	1.0	1.8	2.0	
Estimated $L_{50}$ (h)	8.8	29.8	124.9	14.1	36.3	74.7	56.4	98.1	58.7	5.4	10.2	11.0	
Calculated $L_{10h}$	14	37	146	14	37	146	42	42	73	14	146	3031	
$a_3 \times L_{10h}$	2.3	6.0	23.9	2.3	6.0	23.9	6.9	6.9	11.9	2.3	23.9	497.1	
$L_{10} / (a_3 \times L_{10h})$	0.69	0.89	0.94	1.10	1.09	0.56	1.47	2.57	0.89	0.43	0.077	0.004	

- speed was about 2.1 times greater than Test No. 1.
- 6) In Test Nos. 7 and No. 8, the effect of oil temperature can be seen and the ratio of the estimated life and calculated life of Test No. 8 with low oil temperature was about 1.7 times greater than Test No. 7.
- 7) In Test Nos. 3 and No. 9, the effect of loading cycle can be seen and the ratio of the estimated life and calculated life of Test No. 9 with a short loading cycle was not much different from Test No. 3.



(a) Flaking for Test No.1



(b) Peeling for Test No. 12

Fig. 2 Typical failure for test No.1 and test No.12

### 3. 2 Surface roughness of inner/outer rings and steel rolling elements before and after test

Bearings with low  $\Delta$  conditions are considered to be affected by surface roughness of the inner/outer rings and steel rolling elements of the bearings. The following shows the results of the surface roughness investigation of the inner/outer rings and steel rolling elements before and after the tests.

Table 3 shows the average (average of measurement data of test samples shown in the table) of  $Rq$  and root mean square slope (hereinafter,  $Rdq$ ) of the inner/outer rings and steel rolling elements before and after the test. Where,  $Rq$  and  $Rdq$  show the degree of surface roughness of raceway and slope of projections of surface roughness, respectively, and are the parameters used as indices to indicate severity of projection contact of surface roughness in the paper by Ioannides et al. <sup>28)</sup>. These measurement results are the values obtained by using a stylus type surface roughness measurement instrument/profilometer, in a direction perpendicular to the rolling contact trajectory for inner/outer rings and an arbitrary direction for steel rolling elements of bearings. The measurement positions are selected from undamaged areas. In addition, JIS <sup>38)</sup> was followed for conditions of measurement.

From Table 3,  $Rq$  and  $Rdq$  before and after the test for each area where the surface roughness conditions of the inner/outer rings were different before the test (Test Nos. 1 - 3 and Test Nos. 4 - 6) were extracted and compared. The results are shown in Fig. 4. After the tests,  $Rq$  and  $Rdq$  of the inner/outer rings were found to be smaller than before the tests in all conditions, indicating that the surface of the inner/outer rings was "run-in" after testing (reduction of  $Rq$  and  $Rdq$  during testing is called "run-in"). In Test Nos. 1 - 3 and Test Nos. 4 - 6 where surface roughness levels of the inner/outer rings were quite different,  $Rq$  and  $Rdq$  of the inner/outer rings exhibited differences after the tests, and  $Rq$  and  $Rdq$  of Test Nos. 4 - 6 were greater than Test Nos. 1 - 3 before the test and after delamination started. After the tests,  $Rq$  and  $Rdq$  of the inner/outer rings of Nos. 1 - 3 were  $0.07 - 0.15 \mu m$  and  $0.54 - 1.60^\circ$ , respectively and  $Rq$  and  $Rdq$  of the inner/outer rings of Nos. 4 - 6 were  $0.26 - 0.43 \mu m$  and  $1.03 - 3.48^\circ$ , respectively. On the other hand, the steel rolling elements did not run-in well as opposed to the inner/outer rings in any condition, and  $Rq$  after testing indicated little reduction in all conditions. In addition,  $Rdq$  did not show significant reduction as observed with the inner/outer rings.

$Rq$  and  $Rdq$  after Test Nos. 1 - 12 extracted from Table 3 are shown in Fig. 5. The reason why Fig. 5(a)

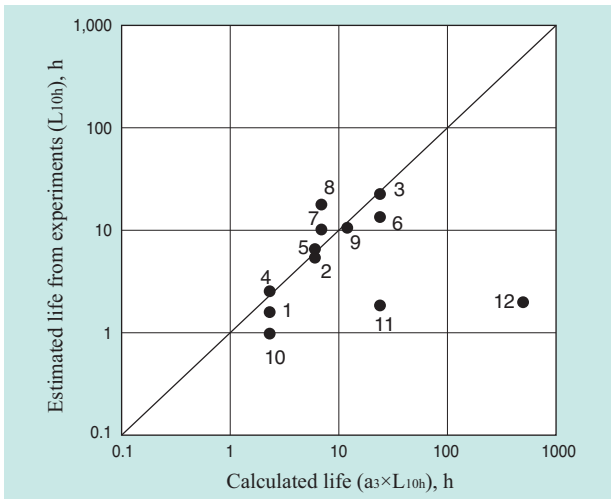
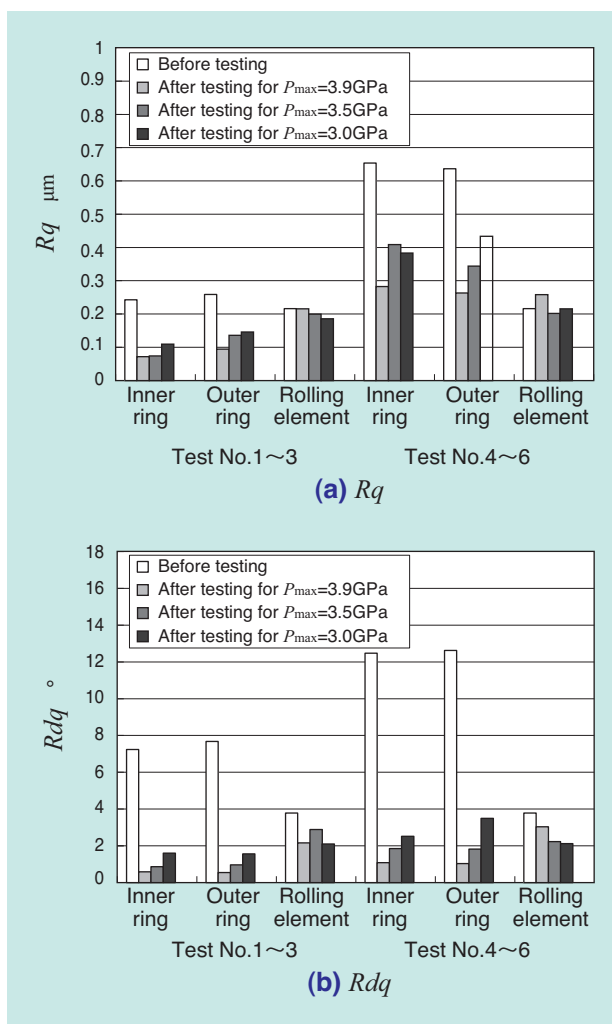


Fig. 3 Correlation diagram between calculated life ( $a_3 \times L_{10h}$ ) and estimated life from experimental results

**Table 3** Average of surface roughness before and after testing

Test No.	Parts	Before testing			After testing			Test No.	Parts	Before testing			After testing		
		N	$Rq$ $\mu\text{m}$	$Rdq$ $^\circ$	N	$Rq$ $\mu\text{m}$	$Rdq$ $^\circ$			N	$Rq$ $\mu\text{m}$	$Rdq$ $^\circ$			
1	I	10	0.24	7.24	7	0.07	0.58	7	I	10	0.24	7.24	10	0.17	0.63
	O	10	0.26	7.68	7	0.09	0.54		O	10	0.26	7.68	10	0.13	0.88
	E	5	0.22	3.78	21	0.22	2.16		E	5	0.22	3.78	30	0.17	1.86
2	I	10	0.24	7.24	7	0.07	0.86	8	I	10	0.24	7.24	11	0.11	0.67
	O	10	0.26	7.68	7	0.14	0.96		O	10	0.26	7.68	11	0.13	0.62
	E	5	0.22	3.78	21	0.20	2.89		E	5	0.22	3.78	32	0.21	1.23
3	I	10	0.24	7.24	10	0.11	1.60	9	I	10	0.24	7.24	11	0.14	1.28
	O	10	0.26	7.68	10	0.15	1.56		O	10	0.26	7.68	11	0.18	1.44
	E	5	0.22	3.78	30	0.19	2.10		E	5	0.22	3.78	66	0.23	2.94
4	I	10	0.65	12.48	10	0.28	1.08	10	I	10	0.24	7.24	Peeling		
	O	10	0.64	12.63	10	0.26	1.03		O	10	0.26	7.68	Peeling		
	E	5	0.22	3.78	10	0.26	3.04		E	6	0.54	9.52	10	0.34	3.79
5	I	10	0.65	12.48	14	0.41	1.85	11	I	10	0.24	7.24	Peeling		
	O	10	0.64	12.63	14	0.34	1.82		O	10	0.26	7.68	Peeling		
	E	5	0.22	3.78	14	0.20	2.23		E	6	0.54	9.52	7	0.36	5.30
6	I	10	0.65	12.48	11	0.38	2.52	12	I	10	0.24	7.24	Peeling		
	O	10	0.64	12.63	11	0.43	3.49		O	10	0.26	7.68	Peeling		
	E	5	0.22	3.78	11	0.22	2.11		E	6	0.54	9.52	7	0.39	5.85

O :Outer, I :Inner, E :Element, N :Number



**Fig. 4** Average of  $Rq$  and  $Rdq$  before and after testing for test No. 1 to 6

(d) do not show the results of the inner/outer rings from Test Nos.10 - 12 is because peeling was observed throughout the raceways of the inner/outer rings. Observing the inner/outer rings after the tests,  $Rq$  and  $Rdq$  tended to decrease more when contact pressure was higher. No significant difference, depending on the test conditions, was observed for  $Rq$  of steel rolling elements after the Test Nos. 1 - 9; however, the difference was smaller for  $Rdq$  in Test Nos. 7 and 8 where the rolling speed was lower. In Test Nos. 1 - 9 and Test Nos. 10 – 12, where surface roughness levels of steel rolling elements were quite different,  $Rq$  and  $Rdq$  of steel rolling elements exhibited difference after the tests, and  $Rq$  and  $Rdq$  of Test No., 10 - 12 were greater than Test Nos. 1 - 9 before the test and after delamination started. For the steel rolling elements for Test Nos. 1 - 9,  $Rq$  showed little difference before and after the tests; however,  $Rdq$  showed decrease from  $3.78^\circ$  at the initial stage of testing to  $1.23 - 3.04^\circ$ , although there were some variances between different Test Nos. For the steel rolling elements in Test Nos. 10 - 12,  $Rq$  decreased from  $0.54 \mu\text{m}$  of the initial stage to  $0.34 - 0.39 \mu\text{m}$ , and  $Rdq$  decreased from  $9.52^\circ$  of the initial stage to  $3.79 - 5.85^\circ$ . The surface of steel rolling elements did not "run-in" well compared to inner/outer rings in any Test Nos.

### 3. 3 Relation between test conditions and damage mode

In Test Nos. 1 - 12, most of the inner/outer rings of the test samples were damaged (Table 2). In Test Nos. 5 and 6, where  $Rq$  and  $Rdq$  of the inner/outer

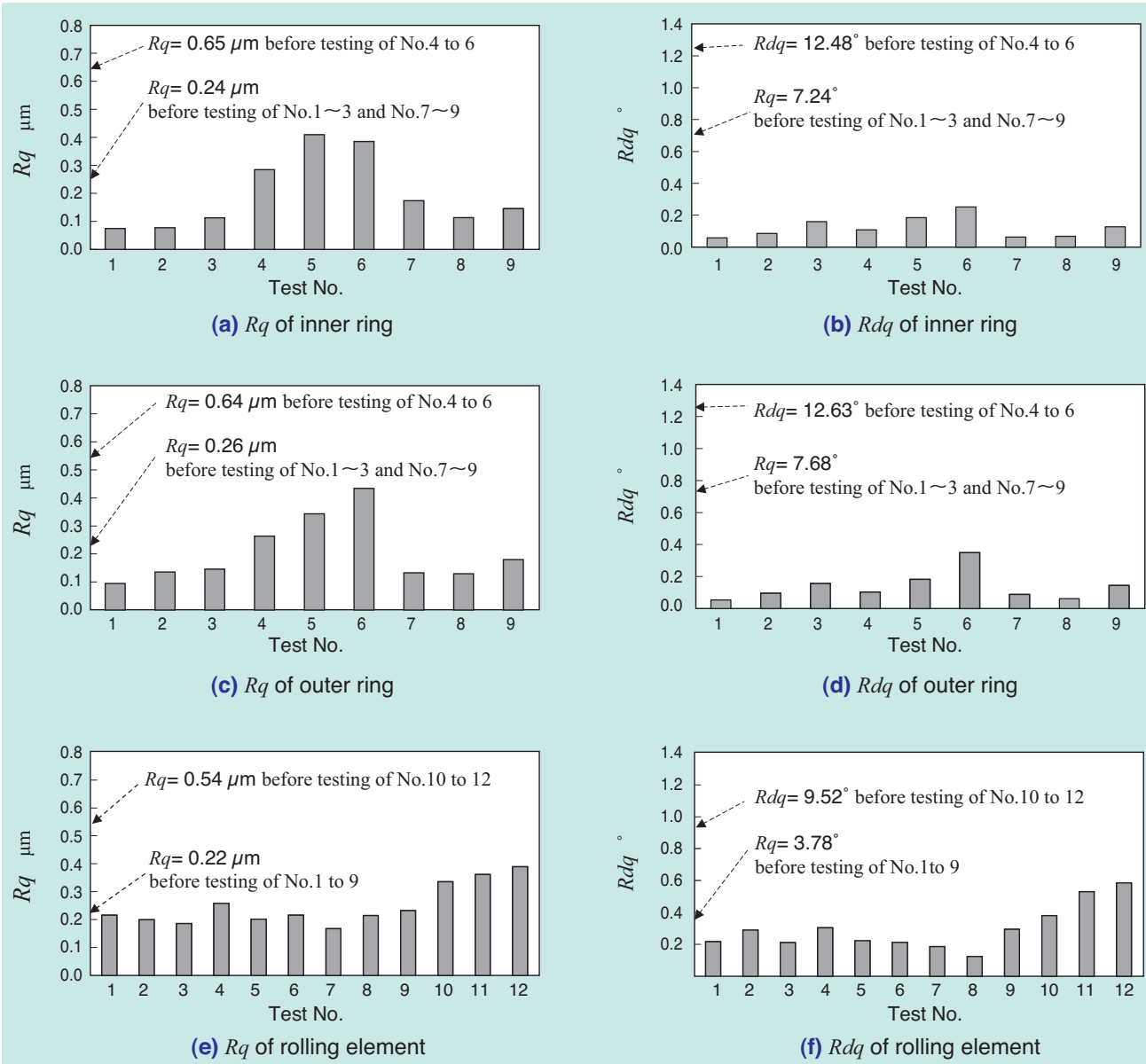


Fig. 5 Average of  $Rq$  and  $Rdq$  after testing for test No. 1 to 12

rings were large and load was relatively low, damage was observed in the steel rolling elements of some test samples (Table 2).

In Test Nos. 1 - 9, where  $Rq$  and  $Rdq$  for steel rolling elements were relatively small, the damage mode was flaking, and in Test Nos. 10 - 12, where  $Rq$  and  $Rdq$  were large, the damage mode was peeling (Table 2 and Fig. 2). In Test No. 10, both flaking and peeling were observed (Table 2).

In addition, peeling was more frequently observed on the inner diameter side of the rolling contact trajectory (Fig. 2).

### 3. 4 Relation between surface roughness and life

In Test Nos. 1 - 3 and Test Nos. 4 - 6, where  $Rq$  and  $Rdq$  of the inner/outer rings were quite different before the tests,  $Rq$  and  $Rdq$  showed differences after the

tests; however, little difference was observed in life (Table 2 and Table 3).

In Test Nos. 7 and 8, where the rolling speed was low,  $Rdq$  of the steel rolling elements was smaller than in other conditions and life tended to be longer than the calculated life (Table 2 and Table 3).

In Test Nos. 1 - 9, where  $Rq$  and  $Rdq$  of the steel rolling elements at the initial stage of tests were relatively small, no enormous difference was observed between the estimated life and calculated life (Fig. 3) and the life was inversely proportional to the cubes of the load. On the other hand, in Test Nos. 10 - 12, where  $Rq$  and  $Rdq$  of the steel rolling elements at the initial stage of the tests were relatively large, life was almost constant regardless of the load and the difference from the calculated life was more significant for smaller loads (Fig. 3).

## 4. Discussion

In this Chapter, observations are made on the test results from the previous Chapter and considerations required for life prediction under low  $\Lambda$  condition and ongoing challenges are discussed.

### 4.1 Effect of $Rq$ , $Rdq$ and run-in on progress of rolling contact fatigue

In our testing, we observed that the inner/outer rings of most of the test samples experienced damage. The reasons are assumed as follows:

Since the steel rolling elements are less "run-in" compared to the inner/outer rings, the surface roughness of the steel rolling elements became relatively larger than the inner/outer rings, so that the rolling contact surface of the rolling elements "attacked" the raceways of the inner/outer rings (hereinafter, the property that the parts with larger  $Rq$  and  $Rdq$  promote progress of fatigue of the trajectory surface of the counterpart is called "aggressiveness.") With thrust ball bearings, the inner/outer rings receive fatigue on the same raceway. In contrast, the steel rolling elements change the rolling contact surface due to friction force produced by spinning within the bearings, resulting in the progress of fatigue throughout the entire spherical surface. In addition, since the steel rolling elements are harder than the inner/outer rings, they have an advantage over the inner/outer rings from a standpoint of strength, which is another reason why the inner/outer rings receive damage before the steel rolling elements, in addition to higher aggressiveness of the rolling contact surface of the rolling elements. However, under the test conditions where  $Rq$  and  $Rdq$  were large during testing (Test Nos. 5 and 6), there were cases where the steel rolling elements were damaged before the inner/outer rings. Therefore, the aggressiveness of the rolling contact surface of the counterpart of the damaged parts is assumed to be the largest factor for determining life. In addition, under conditions where there were differences in surface roughness of the inner/outer rings before the tests (Test Nos. 1 - 3 and Nos. 4 - 6), no significant differences in life were observed. That can be also attributed to the fact that there were no differences in aggressiveness of the rolling contact surface of the rolling elements since there was little difference in  $Rq$  and  $Rdq$  of the rolling elements before and after the tests in Test Nos. 1 - 6. Furthermore, the reason why the life under low rolling speed conditions was longer than the calculated life compared with other conditions assumes that the aggressiveness of the rolling elements on the inner/outer rings was reduced due to better "run-in" under the low rolling speed conditions. It is not clear which surface roughness parameter, between  $Rq$  and

$Rdq$ , is more appropriate as an index to indicate aggressiveness to the counterpart; however, in view that in the case of tests with a small rolling speed, there was life difference while no differences were observed in  $Rq$  but there were differences in  $Rdq$ , and that there is a view that the increase of contact stress in the true contact point can be obtained by  $Rdq$  in Appendix A of the paper by Ioannides et al.<sup>28</sup>),  $Rdq$  may be more appropriate as an index to indicate aggressiveness on the raceways of the counterpart. Fig. 6 shows the contact condition of two surfaces with the same  $Rq$  and different  $Rdq$  in schematic form. Considering that the top of the projections of the large  $Rdq$  surface is likely to fall into the small  $Rdq$  surface, the area around the projections may be close to the status under hydrostatic pressure stress, which may be advantageous for fatigue. At any rate, it is considered that the life under low  $\Lambda$  conditions, such as the tests we have conducted, is determined by the aggressiveness of the trajectory surface of the counterpart to the area of delamination.

Previously, we discussed that the lower rolling speed contributed to the run-in of the rolling contact surface of the steel rolling elements. It can be also interpreted that when the rolling speed is low, life is relatively longer, so the increase of the loading cycle may have contributed to the reduction of surface roughness of the steel rolling elements. Therefore, we have reviewed the relation between the rolling speed with constant load cycle and  $Rq$  and  $Rdq$  of steel rolling elements after the tests. The test conditions are shown in Table 4 and test results in Fig. 7, respectively. As it is evident from the figure,  $Rq$  and  $Rdq$  are likely to decrease as the rolling speed becomes lower. Taking advantage of this property, a test was conducted to clarify the phenomenon of extended life when the trajectory surface is run-in with low speed rotation. The test conditions are shown in Table 5 and test results in Fig. 8, respectively. Before conducting the test under the regular condition of  $1,500 \text{ min}^{-1}$ , the lives of the bearings were compared with run-in operation and without run-in operation shown in Table 5.

All three test samples with run-in operation showed a life of 4,000h or more, and all of four test samples without run-in operation showed a life of 40h or less. This result is an example that run-in operation with slow rotation can significantly affect life.

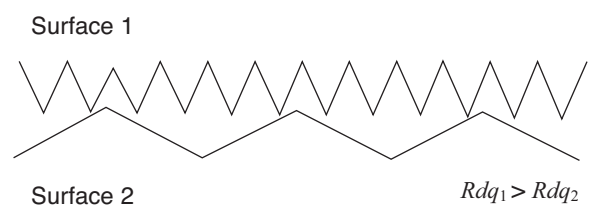
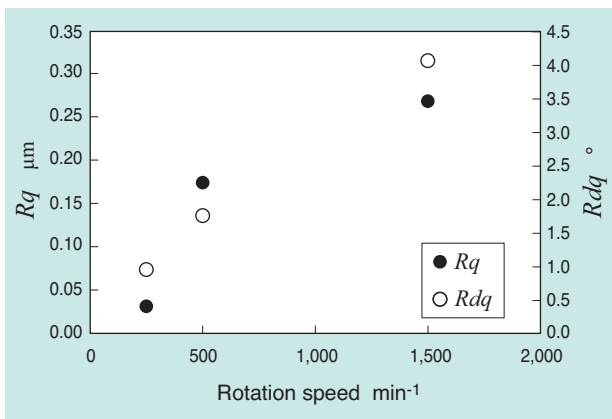


Fig. 6 Schematic of contact condition for raceway surfaces with same  $Rq$  and different  $Rdq$  ( $Rdq_1 > Rdq_2$ )

**Table 4** Test condition to investigate  $Rq$  and  $Rdqq$  after rolling contact under different rotation speed

Type number of rolling bearing	51105
Surface Roughness of inner and outer ring before rolling contact	$Rq = 0.25\mu\text{m}$ , $Rdq = 7.45^\circ$
Surface Roughness of rolling element before rolling contact	$Rq = 0.54\mu\text{m}$ , $Rdq = 9.52^\circ$
The number of rolling element	3
Load and maximum contact stress	2.7 kN, $P_{\text{max}} = 3.0 \text{ GPa}$
Lubricating oil	Turbine oil VG32
Temperature of Lubricating oil	110°C
Rotation speed	250, 500, 1,500 $\text{min}^{-1}$
Oil film parameter	0.008 ~ 0.048
The number of rotation	261,000



**Fig. 7**  $Rq$  and  $Rdq$  after rolling contact under different rotation speed  
The number of rotation is 261,000

Akamatsu and Miller et al. report that when the rolling speed is in the range of 0.05 - 16.4 msec of passing time of contact ellipse (the smaller value indicates faster rolling speed; hereinafter, "contact time"), life is proportional to the power of 0.4 of the contact time<sup>26)</sup>. In the test we conducted, the contact time under slow rolling speed and fast rolling speed was in the range of 0.25 - 0.96 msec, indicating a difference of about four times. The improvement of life due to this difference can be estimated to be around 1.7 times, which mostly matches with the life tests conducted (Test Nos. 7 and 8). The report by Akamatsu and Miller et al. does not mention the reason why life is extended with a slow rolling speed. We assume that life is extended because the raceway becomes more run-in with slow rolling speeds. Now, the reason why slow rolling speeds result in more run-in is still unclear, which is a question to be addressed in the future.

**4.2 Effect of  $Rq$ ,  $Rdq$  and tangential force on damage mode**

Appendix A of the paper by Ioannides et al., which was the basis of ISO281:2007 published in 2007<sup>28)</sup>, discusses the concept of correction coefficient  $a_{\text{ISO}}$  of life

**Table 5** Test condition to investigate effect of running operation on RCF life

Type number of rolling bearing	51105
Surface Roughness of inner and outer ring before rolling contact	$Rq = 0.25\mu\text{m}$ , $Rdq = 7.45^\circ$
Surface Roughness of rolling element before rolling contact	$Rq = 0.54\mu\text{m}$ , $Rdq = 9.52^\circ$
The number of rolling element	3
Load and maximum contact stress	2.7 kN, $P_{\text{max}} = 3.0 \text{ GPa}$
Lubricating oil	Turbine oil VG32
Temperature of Lubricating oil	110°C
Rotation speed	Running-in operation: 250 $\text{min}^{-1}$ RCF testing: 1,500 $\text{min}^{-1}$
The number of rotation in running-in operation	261,000 (8.7 hours)
Surface Roughness of inner and outer ring after running-in operation	$Rq = 0.23\mu\text{m}$ , $Rdq = 1.15^\circ$
Surface Roughness of rolling element after running-in operation	$Rq = 0.03\mu\text{m}$ , $Rdq = 0.95^\circ$

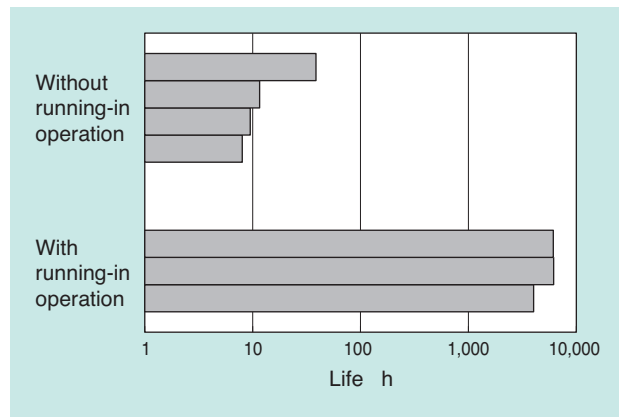


**Fig. 8** Results of RCF testing with and without running-in operation

formula. In the discussion, the probability of survival of the rolling bearings  $S$  can be expressed by equation (1).

$$\ln\left(\frac{1}{S}\right) = \ln\left(\frac{1}{S_{\text{hertzian\_scale\_stress}}}\right) + \ln\left(\frac{1}{S_{\text{surface\_stress}}}\right) + \ln\left(\frac{1}{S_{\text{subsurface\_stress}}}\right) \quad (1)$$

Equation (1) indicates that the probability of survival of rolling bearings is determined by the probability of survival for each damage mode generated by the following three types of stress.

- (1) Hertzian-scale\_stress of the first term: Stress generated under apparent contact (Hertzian contact) surface and stress that generates ordinary subsurface initiated flaking under good lubrication conditions
- (2) Surface\_stress of the second term: Stress to generate damage from the surface by frictional force induced by contact of projections on rough

surfaces with a relatively moderate slope ( $Rdq \leq 4^\circ$ ) under sparse lubrication conditions

- (3) Subsurface\_stress of the third term: Stress to generate damage from the top surface by locally large alternating shear stress that works on the area immediately below the high contact pressure from the contact of projections on rough surfaces with a relatively large slope ( $Rdq > 4^\circ$ ) under sparse lubrication conditions

In the following, we examine the test results assuming that the stress that determines the life of rolling bearings can be classified as above:

Under the condition in the initial stage, where  $Rq$  and  $Rdq$  for steel rolling elements were relatively small (Test Nos. 1 - 9), the damage mode was flaking, and under the condition, where  $Rq$  and  $Rdq$  were large (Test Nos. 10 - 12), the damage mode was peeling. Considering that in Test Nos. 1 - 9,  $\Delta$  was 0.11 or less at the end of the test (after run-in), and  $Rdq$  was less than  $4^\circ$  in all areas after the test, even if it was more than  $4^\circ$  for inner/outer rings before the test, the stress to determine the life is assumed to be (2) Surface\_stress. The damage mode by this (2) Surface\_stress was flaking in most test samples. On the other hand, in Test Nos. 10 - 12, considering that  $\Delta$  was smaller than the cases of Test Nos. 1 - 9, and  $Rdq$  of the steel rolling elements was considered to be almost always  $4^\circ$  or more during the test, the stress that determines the life is assumed to be (3) Subsurface\_stress. There is room for discussion if the stress which generated peeling in Test Nos. 10 - 12 was alternating the shear stress working on the immediately below projection contact area of surface roughness; however, it can be assumed that when  $Rdq$  is large, damage mode changes with the severity of contact of projections of surface roughness, creating peeling before flaking generated by (2) Surface\_stress. In one test (Test No. 10) both flaking and peeling were observed. That seems to be the result of racing by two damage modes, namely, flaking due to (2) Surface\_stress and peeling created by contact of raceways with a large  $Rdq$ . In Test Nos. 1 - 9, life of flaking by (2) Surface\_stress is inversely proportional to the cubes of load; however, in Test Nos. 10 - 12, life of peeling is mostly constant to the load. Therefore, in Test No. 10 where the load was large, there were no differences in the life of both damage modes, and flaking and peeling appeared at the same time (Table 2).

The reason why the life of flaking by (2) Surface\_stress is inversely proportional to the cubes of the load is unclear. However, this relation indicates that life can be predicted only by multiplying the conventional life formula by the life adjusting factor obtained from the ASME diagram for flaking by (2) Surface-stress. In contrast, as

the life of peeling is not inversely proportional to the cubes of the load, but mostly constant to the load, correction is not possible by multiplying the conventional life formula by the factor obtained from the ASME diagram. Peeling seems to occur with projections of large  $Rdq$  creating high contact stress on the raceway of the counterpart. Considering that, when peeling is about to occur, the contact stress on the projection contact area is reaching the final limit which the bearing steel can support as it goes through work hardening and residual stress generation (hereinafter, "shake down limit"<sup>39</sup>), these test results can be rather easily described. As described in the paper by Ioannides et al.<sup>28</sup>, if  $Rdq$  indicates the contact stress of the projection contact area, when its value exceeds a certain value, the contact stress of the projection contact area will have reached the shake down limit regardless of the load condition, and the change of load only affects the contact area. Therefore, since the contact stress of that projection contact area is the same in any condition, peeling occurs mostly on the same loading cycle. This seems to be the reason why the peeling life becomes insensitive to the load. Considering this mechanism, peeling should stop occurring if the maximum  $Rdq$  of each area becomes less than a certain value (in our tests,  $4^\circ$  or less) before a certain loading cycle (in our testing,  $10^5 - 10^6$ ). This means that if peeling occurs in the bearings or not can be experimentally confirmed by examining if  $\Delta$  during the test becomes 3 or more,  $Rdq$  of each area decreases to  $4^\circ$  or less before loading cycle of  $10^5 - 10^6$ , as a guideline.

The reason why peeling was observed more on the inner diameter side of the rolling trajectory seems to be that the inner diameter side of the inner/outer rings of thrust bearings is the driven side in two cylinder tests, and the outer diameter side is the driving side. Where, the driven side and driving side are also called the low speed side and high speed side, the indicating raceway where the direction of action of the tangential force is the same as the direction of rolling and the raceway where the tangential force is in the opposite direction, respectively. The fact that life decreases on the low speed side is also indicated by Way's study<sup>40</sup>, and there is a discussion that the reason for decrease of life is due to the difference of stress states and difference of crack propagation behaviors<sup>41,42</sup>. In any event, it seems that the reason why the damage due to peeling was more significant on the inner diameter side of the rolling trajectory is because the peripheral speed of the inner diameter side of the inner/outer rings was slower than the peripheral speed of the steel rolling elements and the direction of action of tangential force was aligned with the rolling direction on the inner diameter side of the inner/outer rings.

### 4.3 Life prediction under low $\Delta$ condition and further challenges

From the above life test results and subsequent observation, the following conclusions were obtained for life prediction under low  $\Delta$  conditions.

- 1) Life under low  $\Delta$  conditions is affected by surface roughness of the counterpart of the damaged part.
- 2) Surface roughness of each part of the rolling bearings changes during operation and those changes are affected by operating conditions such as load, rotation speed, etc.
- 3) Under low  $\Delta$  conditions, two damage modes, namely, flaking and peeling are observed and the types of stress that cause the damage are different.
- 4) Flaking occurs due to surface stress by friction force induced by the contact of projections of surface roughness, and the life is affected by  $Rdq$ .
- 5) Peeling occurs by contact of raceway and rolling contact surface with  $Rdq$  of more than a certain value, and the life is affected by the relation between the direction of tangential force and rolling direction.

From the above, for life prediction under low  $\Delta$  conditions, technology to estimate stress conditions on the top surface is required considering  $\Delta$  that constantly changes by run-in, surface roughness and frictional force. In addition, it is considered that a database of experiments with behavior of changes in surface roughness depending on operating conditions is required.

If the status of stress that repeatedly acts on the raceway by  $\Delta$  and surface roughness that changes during operation can be found, fatigue can be calculated in a time series using SN diagram, Goodman diagram, Miner's law, etc. enabling more universal life prediction. Another consideration to be made is the residual stress distribution distributed below the rolling contact surface and hoop stress by fitting. In this report, although residual stress and hoop stress were not discussed, these stresses affect equivalent stress of the raceway and stress ratio. For establishing a more universal life prediction method under low  $\Delta$  conditions, estimation technology of the stress status of the true contact area considering constantly changing  $\Delta$  by run-in, surface roughness, residual stress and hoop stress, and a database of run-in behavior depending on operational conditions are required.

## 5. Conclusion

In this paper, life test results under low  $\Delta$  conditions for thrust ball bearings were discussed. Also, factors determining life under low  $\Delta$  conditions and life prediction methods were examined.

- 1) Under the test conditions in this report, the inner/outer rings of the bearings experienced damage in most cases. This is because surface roughness of the steel rolling elements did not decrease as much as the inner/outer rings during the tests and the rolling contact surface of the rolling elements attacked the raceways of the inner/outer rings.
- 2) No differences in life were observed in the tests with different inner/outer surface roughness before the tests. That is because there were no differences in surface roughness of the steel rolling elements.
- 3) Under the conditions of slow rolling speed, the life tended to be longer than the calculated life. That is because decrease of surface roughness of steel rolling elements during the tests was more significant under slow rolling speeds.
- 4) Two damage modes, namely, flaking and peeling were observed under the test conditions in this report. Which damage mode occurs is determined by how much surface roughness decreases during the tests.
- 5) In the case where the damage mode was peeling, life was insensitive to the loads. That is because the surface pressure of the true contact area had exceeded the shake down limit under the condition of severe contact of surface roughness.
- 6) More peeling was observed on the inner diameter side of the rolling contact trajectory. That is because the inner diameter side of the inner/outer rings is in line with the direction of the action of tangential force and the rolling direction.
- 7) For establishment of a more universal life prediction method under low  $\Delta$  conditions, estimation technology of stress status of the true contact area considering constantly changing  $\Delta$  by run-in, surface roughness, residual stress and hoop stress, and a database of run-in behavior depending on operating conditions are required.

This paper is a transcript of the paper "Rolling Contact Fatigue of Thrust Ball Bearing under Low Lambda Condition" published in "The Journal of Japanese Society of Tribologists" Vol. 60, No. 11 (2015) 741 of the Japanese Society of Tribologists with minor revisions. We thank the Japanese Society of Tribologists, who gave us permission for publishing it here.

## References

- 1) T. E. Tallian: On competing failure modes in rolling contact, ASLE Trans., 10, 4 (1967) 418.
- 2) J. C. Skurka: Elastohydrodynamic lubrication of roller bearings, J. Lubr. Technol. Trans. ASME, 92, 2 (1970) 281.
- 3) Rolling-Element committee lubrication division of ASME, Catalog Card Number 170-179492 (1971).
- 4) C. H. Danner: Fatigue life of tapered roller bearings under minimal lubrication films, ASLE Trans., 13, 4 (1970) 241.
- 5) Y. P. Chiu, T. E. Tallian & J. I. McCool: An engineering model of spalling fatigue in rolling Contact, I.: The subsurface model, Wear, 17 (1971) 433.
- 6) T. E. Tallian & J. I. McCool: An engineering model of spalling fatigue failure in rolling Contact, II.: The surface model, Wear, 17 (1971) 447.
- 7) T. E. Tallian: An engineering model of spalling fatigue failure in rolling contact, III.: Engineering discussion and illustrative examples, Wear, 17 (1971) 463.
- 8) R. A. Hobbs: Fatigue lives of ball bearings lubricated with oils and fire-resistant fluids, EHL symp. IME C1 (1972) 1.
- 9) C. A. Moyer: Relating lubrication parameters and rolling contact fatigue life in mixed EHL regime, EHL symp. IME C1 (1972) 95.
- 10) G. H. G. Vaessen & A. W. J. de Gee: Rolling contact fatigue of maraging steels of different production history: Influence of film thickness/roughness ratio, EHL symp. IME C7 (1972) 40.
- 11) S. Anderson & T. Lund: Ball bearing endurance testing considering elastohydrodynamic lubrication, EHL symp. IME C36 (1972) 138.
- 12) I. M. Felsen, R. W. McQuard & J. A. Marzani: Effect of sea water on the fatigue life and failure distribution of flood-lubricated angular contact bearing, ASLE Trans., 15, 1 (1972) 8.
- 13) J. Y. Liu, T. E. Tallian & J. I. McCool: Dependence of bearing fatigue life on film thickness to surface roughness ratio, ASLE Trans., 18, 2 (1975) 144.
- 14) D. F. Li, J. J. Kauzlarich & W. E. Jamison: Surface roughness effects on fatigue in partial EHD Lubrication, J. Lubr. Technol. Trans. ASME, 98, 4 (1976) 530.
- 15) N. G. Popinceanu, M.D. Gafitanu, S.S. Cretu, E.N. Diaconescu & L. T. Hostiu: Rolling contact fatigue life and EHL theory, Wear, 45 1 (1977) 17.
- 16) Masatoshi Tokuda, Mitsutoshi Nagabuchi and Shigeo Ito: Peeling Damage on Rolling Contact Surface of Bearings, Bearing Engineer, 45 (1977) 8.
- 17) Kyozauro Furumura, Shinichi Shirota and Kiyoshi Hirakawa: The Subsurface-initiated and Surface-initiated Rolling Fatigue, NSK Bearing Journal 636 (1977) 1.
- 18) Hirotohi Takada, Susumu Suzuki and Etsuo Maeda: Effect of lubrication on fatigue life of rolling bearings, Lubrication, 26, 9 (1981) 645.
- 19) Hirotohi Takada: Life and surface roughness of rolling bearings, Lubrication, 27, 2 (1982) 105.
- 20) Y. Akamatsu: Peeling damage due to rolling contact fatigue, SAE technical paper series 891909 (1989).
- 21) Y. Akamatsu, N. Tsusima, T. Goto, K. Hibi & K. Ito: Improvement of roller bearing fatigue life by surface modification, SAE technical paper series 910958 (1991).
- 22) Y. Akamatsu, N. Tsusima, T. Goto & K. Hibi: Influence of surface roughness skewness on rolling contact fatigue life, Trib. Trans., 35, 4 (1992) 745.
- 23) Yoshinobu Akamatsu: Improvement of Roller Bearing Fatigue Life by Surface Roughness Modification, Lubrication, 37, 7 (1992) 533.
- 24) Fuyuki Ito and Yoshinobu Akamatsu: Effect of Roughness of Counterpart on Rolling Contact Fatigue Life, Proceedings of Tribology Conference, Spring 1995, (1995) 535.
- 25) J. R. Miller: Roller bearing life estimation at low speed and high stress, Proceeding of international tribology conference in Yokohama, (1995) 1381.
- 26) J. R. Miller & Y. Akamatsu: Effect of low speed on roller bearing fatigue life, Trib. Trans., 40, 1 (1997) 129.
- 27) Yoshinobu Akamatsu: Effects of Low Speed on Rolling Bearing Fatigue Life, NTN Technical Review, 67 (1998) 59.
- 28) E. Ioannides, G. Bergling & A. Gabelli: An Analytical formulation for the life of rolling bearings, Acta Polytechnica, Mechanical Engineering Series, 137(1999).
- 29) ISO281:2007: Rolling bearings -Dynamic load ratings and rating life, (2007).
- 30) JIS B 1518: Rolling Bearings - Dynamic Load Ratings and Rating Life (2013).
- 31) NTN Catalog: HL Bearings, CAT. No 3020/J.
- 32) For example, Masayoshi Muraki: Tribology, Science of Friction and Lubrication Technology, Nikkan Kogyo Shimbun, Ltd., (2008) 216.
- 33) For example, Junzo Okamoto: Calculation of Ball Bearings, (1991) 65.
- 34) L. Johnson: The Statistical Treatment of Fatigue Experiments, Elsevier (1964) 37.
- 35) G. Lundberg & A. Palmgren: Dynamic Capacity of Rolling Bearing, Acta Polytechnica 7, Mechanical Engineering Series, 1, 3 (1947).
- 36) G. Lundberg & A. Palmgren: Dynamic Capacity of Roller Bearing, Acta Polytechnica 96, Mechanical Engineering Series, 2, 4 (1952).
- 37) NTN Catalog: Rolling Bearings, Overview Catalog, CAT. No. 2202-X/J.
- 38) JIS B 0601: Geometrical Product Specifications (GPS)- Surface texture: Profile method-Terms, definitions and surface texture parameters, (2001).
- 39) T. A. Harris: Rolling bearing analysis 4th ed., Wiley & Sons Inc., (2001) 853.
- 40) S. Way: Pitting due to rolling contact, J. Appl. Mech., 2, 2 (1935) A49.
- 41) Norimune Soda: Bearings, Iwanami-Shinsho, (1964) 176.
- 42) Motohiro Kaneda, Yukitaka Murakami and Hirohiko Yatsuzuka: A Fracture Mechanical Study on Contact Fatigue Crack Propagation, Lubrication, 30, 10 (1984) 739

## Photo of authors



Takumi FUJITA  
Advanced Technology  
R&D Center



Naoya HASEGAWA  
Advanced Technology  
R&D Center



Naoya KAMURA  
Advanced Technology  
R&D Center



Toshihiko SASAKI  
Professor,  
Faculty of Human Sciences,  
Kanazawa University

## Speeding up of Parallel Link Angle Control Equipment



Kenzou NOSE\*  
Hiroshi ISOBE\*  
Seigo SAKATA\*

NTN has developed an improved Parallel Link Angle Control Equipment that can control the angle with two-degree-of-freedom fast and widely. Enhancing the drive mechanism, link part, and control method of the unique parallel link mechanism, this equipment can be improved repeat positioning accuracy and positioning speed more than our conventional equipment. Furthermore, we had developed the grease dispensing system and appearance inspection system there are adapted this equipment.

### 1. Introduction

The parallel link mechanism is drawing attention for its high-speed handling of industrial robots. This mechanism connects base and end effectors using multiple parallel links, and has various types of configurations, such as the Steward-Gough type, rotational type and linear fixed type<sup>1)</sup>.

The parallel link angle control unit that the authors have developed adopts a special parallel link that is different from the previously mentioned types. It is smaller and has a wider angle of movement, which allows it to achieve fast and high precision two-degree of freedom angular positioning<sup>2)</sup>.

This article discusses the configuration, performance, control technology and applications of the improved unit, which offers higher speed than the previous unit.

### 2. Basic configuration of the parallel link mechanism

Conceptual diagrams of the parallel link mechanism and spherical link of this system are shown in Fig. 1 and Fig. 2. This mechanism takes three rows of link systems, each consisting of a base-end side arm, central link and top-end side arm (the 1st - 3rd in Fig. 1), and places them parallel between the base-end side link hub and top-end side link hub. The base-end

side link hub serves as the base of the mechanism and the top-end side link hub is used to install the end effector. The joints of each member of the link systems are turning pairs.

The base-end side arm of a 3-row link system is connected to its central link on one end and the base-end side link hub on the other end. The center lines of the rotation axes of the base-end side arm, central link and base-end side link hub all intersect at one point. Having the same structure at the top-end side, this parallel link mechanism has a structure that is composed of two "spherical links". Each member moves on the two spheres S and S', with the respective intersections at their centers as shown in Fig. 2. The attitude of the parallel link mechanism is defined by angles: bend angle  $\theta$  and the angle of traverse  $\phi$ . The bend angle  $\theta$  is the inclination angle between the central axis of the base-end side link hub and central axis of the top-end side link hub. The angle of traverse  $\phi$  is the angle of rotation of the central axis of the top-end side link hub when viewed from the central axis of the base-end side link hub. Because of this structure, the base-end side and the top-end side always move symmetrically against the bisecting plane made by the intersection of two spheres S and S', which compose two spherical links<sup>2)</sup>.

This parallel link mechanism is characterized by a wide operation range and high-speed/high-precision

\* New Product Development R&D Center

motion. It is also characterized by the ability to make the moving part light and compact by separating the movable part and driving part, and by possessing no singular points within the operation range due to the adoption of the spherical link structure. In addition, it is able to run cables and tubes through the central space without being twisted, even with continuous rotation in one direction.

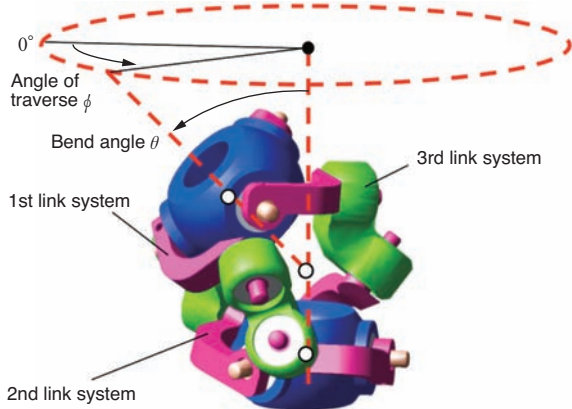


Fig. 1 Unique parallel link mechanism

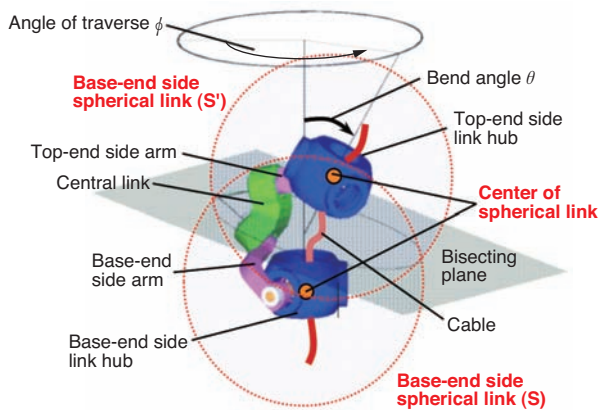


Fig. 2 Conceptual diagram of spherical link

### 3. Parallel link angle control unit

The conventional unit is shown in Fig. 3, the enhanced version is shown in Fig. 4, and conceptual diagrams are shown in Fig. 5 and 6. In both versions, the movable range of the bend angle  $\theta$  is within  $45^\circ$ ; however, it can be extended to a max. of  $90^\circ$  by using an optional design.

Since the internal space of the conventional unit is small and the end effector is installed at the top-end, there is a long distance from the base to the top-end of the end effector and a large moment of inertia, which makes it difficult to achieve faster operation. In

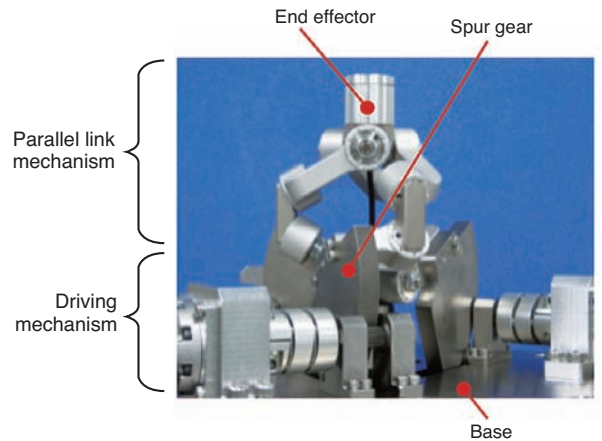
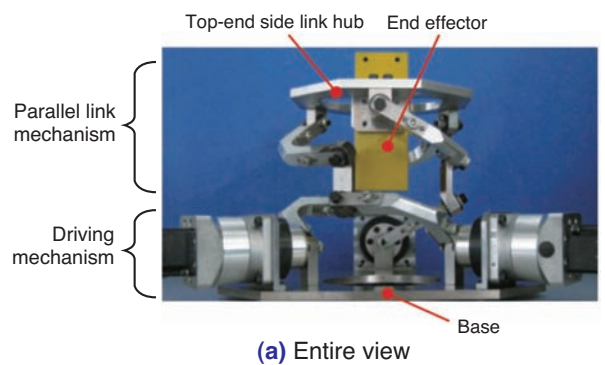
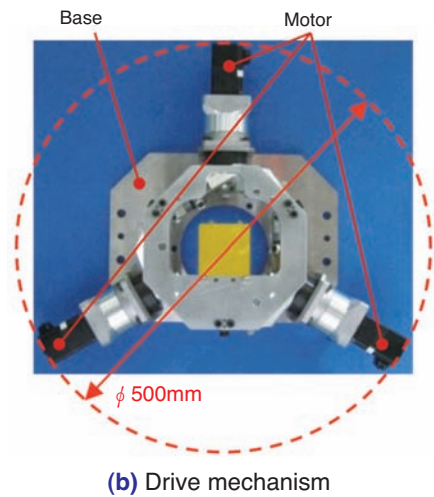


Fig. 3 The structure of Parallel Link Angle Control Equipment (conventional)



(a) Entire view



(b) Drive mechanism

Fig. 4 The structure of Parallel Link Angle Control Equipment (improvement)

addition, the cabling arrangement of the end effector is complex. Furthermore, it has safety and maintenance issues because the spur gear of the driving mechanism is exposed.

The following discusses the improved model that solves the above issues by adopting an integrated structure of a reducer and motor for the driving mechanism, and enhancing the link structure.

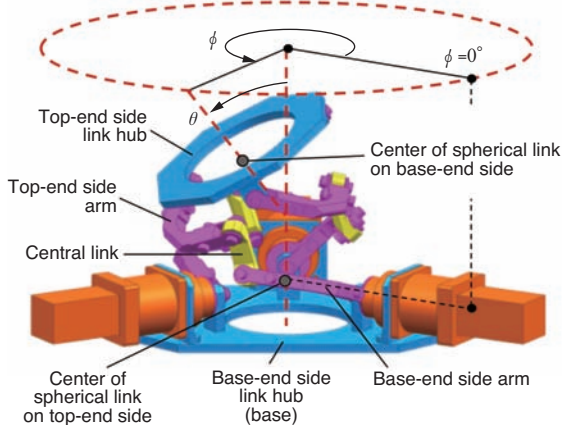


Fig. 5 Conceptual diagram of parallel link mechanism (improvement)

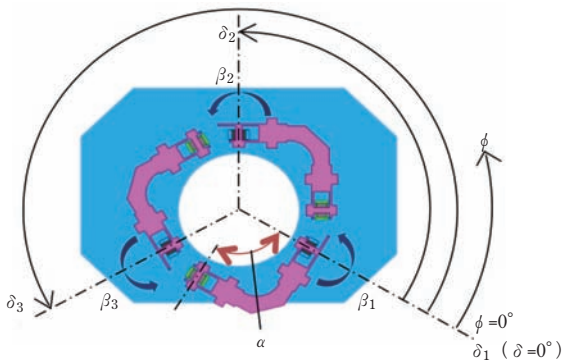


Fig. 6 The arrangement of the base end link mechanism

### 3.1 Parallel link mechanism

This unit uses pre-loaded angular contact ball bearings for the turning pair of the parallel link mechanism to reduce friction and eliminate the gap between the joints. The improved model adopts an integrated base-end side link hub and base, and places the turning pair on the outer diameter side which creates more internal space in the parallel link mechanism than the conventional unit so that the end effector and cabling for the end effector can be placed inside. These modifications reduce the moment of inertia when the end effector is installed, which enables faster operation while maintaining motion

precision. Furthermore, the increased internal space allows for easier arrangement of cables.

### 3.2 Driving mechanism

The attitude of the top-end side link hub expressed by the bend angle  $\theta$  and angle of traverse  $\phi$  can be determined when two of the three angles of rotation on the base-end side arm are identified. However, as shown in Fig. 4 (b), each arm of this unit is driven by its respective motor to cancel out the backlash of the driving mechanism by restricting the 3-row link systems in order to improve positioning accuracy.

The conventional unit uses a spur gear to transmit the driving force of the motor to each base-end side arm<sup>2)</sup>. The driving mechanism of the improved unit (Fig. 4) eliminates the exposed spur gear of the conventional unit, and replaces it with a motor with the reducer directly installed on each base-end side arm. As a result, the outer diameter of the entire system is larger, but the height is reduced and safety and reliability are improved.

### 3.3 Teaching console

A teaching console (hereinafter, "console") has been developed for introduction to production lines. Fig. 7 shows a conceptual diagram of position registration by XYZ coordinates, Fig. 8 (a) shows the JOG operation screen and Fig. 8 (b) shows the console screen for inputting the coordinates. These operation screens are used for the registration and fine tuning of the position using a cross key, and for directly entering the XYZ coordinates. In addition, registration of multiple movement patterns and setting of operational conditions can be made. These capabilities are effective for setting and resetting movement, and improving efficiency at work sites. In addition, editing software has been developed, which can be used on personal computers to easily adjust movement patterns. Furthermore, this editing software enables data to be read from the console in order to adjust and back up of the movement patterns.

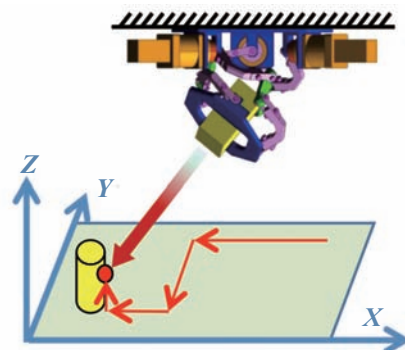
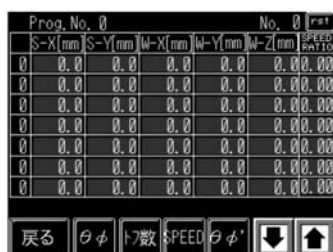


Fig. 7 Move imagine by installation alignment



(a) JOG operation screen



(b) Coordinate input screen

Fig. 8 Operation screen of teaching console

### 4. Control method

#### 4.1 Method for instructing angles to motors

Angles are instructed to motors by obtaining the angles of rotation for each base-end side arm  $\beta_n$  ( $\beta_1, \beta_2, \beta_3$ ) from the instructed angles ( $\theta$  and  $\phi$ ). The three motors are synchronously controlled to start and end operation at the same time by obtaining the difference between the current angles at each base-end side arm  $\beta'_n$  ( $\beta'_1, \beta'_2, \beta'_3$ ) and the target angles of rotation from the instructed angles  $\beta_n$  ( $\beta_1, \beta_2, \beta_3$ ). The instructed speed is given as the synthesis of rotational speed of the three base-end side arms  $V$  and the instructed speed for each motor  $V_n$  is calculated by equation (1). In addition, the motors are driven by "ramp-up/down" control in the shape of a trapezoid as shown in Fig. 9.

$$V_n = \frac{V (\beta'_n - \beta_n)}{\sqrt{(\beta'_1 - \beta_1)^2 + (\beta'_2 - \beta_2)^2 + (\beta'_3 - \beta_3)^2}} \quad (n=1, 2, 3) \dots \dots \dots (1)$$

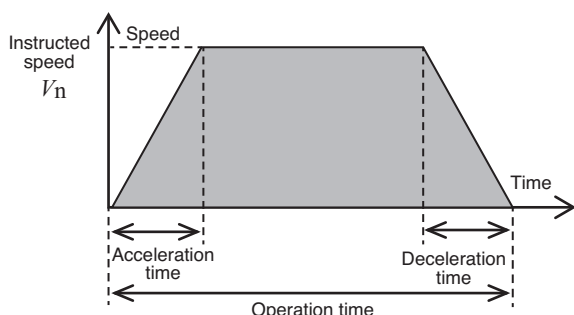


Fig. 9 Drive pattern of motor

#### 4.2 Operating accuracy and vibration reducing control algorithm

An algorithm to improve operating accuracy was introduced by the Preshaping Command Input method<sup>3)</sup>. The operating accuracy was determined by evaluating grease application accuracy when it was applied in the greasing operation, as described later.

The grease application was evaluated by a visual inspection after applying grease on evaluation sheets under a predetermined condition. Evaluation sheets, shown in Fig. 10, were used to test how grease was applied to several points on the sheets by changing acceleration and deceleration. The grease application diameter is approx.  $\phi$  3.5mm and the application point diameter is  $\phi$  1mm. The evaluation was scored by giving plus 1 point if the application point was completely covered by grease, 0 points if the point was marginally covered, minus 1 point if partially covered, and minus 2 points if not covered at all, as shown in Table 1.

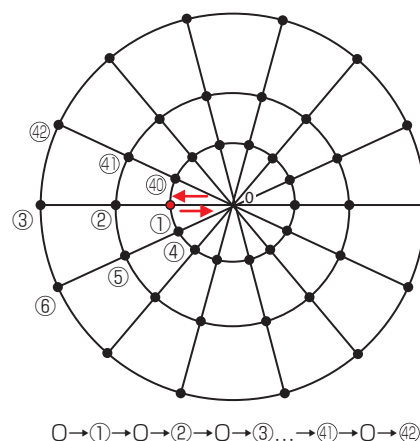


Fig. 10 Grease dispensing sequence

Table 1 Evaluation method of grease dispensing accuracy

Application accuracy	◎	○	▲	×
Application position				
Evaluation score	1	0	-1	-2

Evaluation results are shown in Fig. 11. The natural frequency of the unit used in the test was 53 ms/period. The vibration of the tip after positioning could be reduced by setting the acceleration and deceleration time to one period of the unit's natural frequency. This reduction in tip vibration enables high application accuracy.

In a similar test, application accuracy deteriorated after a short traveling distance. It is assumed that when the traveling distance is short, the actual acceleration/deceleration time is shorter than the period of the natural frequency, which prevents the suppression of vibration when the tip stops. Therefore, when the traveling distance is small, the control algorithm is changed to automatically calculate the instructed speed to make the acceleration and deceleration times equivalent to one period of the natural frequency. This is accomplished by eliminating the constant speed time in the trapezoid previously mentioned, making it a triangle shape. As a result, the vibration of the tip after positioning was reduced.

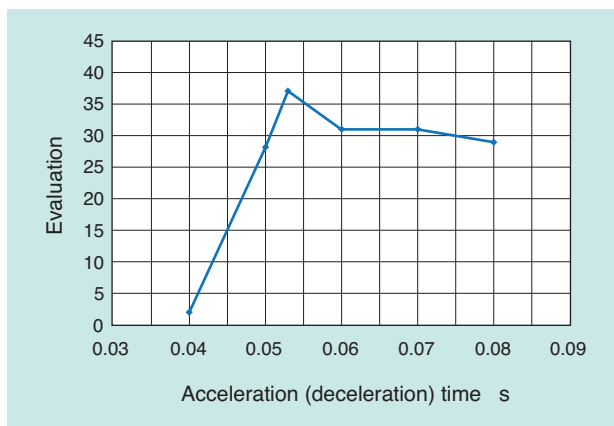


Fig. 11 Grease dispensing accuracy

## 5. Application examples

### 5.1 Grease applicator

The specifications and performance comparison of the conventional unit and improved unit when they were applied to grease applicators are shown in Table 2. An example configuration of the grease applicator using the improved unit is shown in Fig. 12 (a).

In this configuration, the work is moved by the XY stage and the attitude of the dispenser is controlled by this unit. This configuration uses a non-contact type dispenser which injects grease by compressed air.

The improved unit encloses the end effector in the internal space of the parallel link mechanism. Therefore, the distance between the nozzle position of the dispenser installed on the top-end side link hub and the base is shorter. As a result, the positioning accuracy of the nozzle during repetitive operation could be improved (Table 2). Also, since the moment of inertia for the positioning system is smaller, the natural frequency becomes larger, allowing higher application speed.

The grease applicator achieved a high speed application of 10 points/sec on the matrix sheet (\*1). It also enables an automated greasing process for works with complex shapes by application from slanted directions. Fig. 12 (b) shows an example of application on the side of the gear which is not possible by application from the top<sup>4)</sup>.

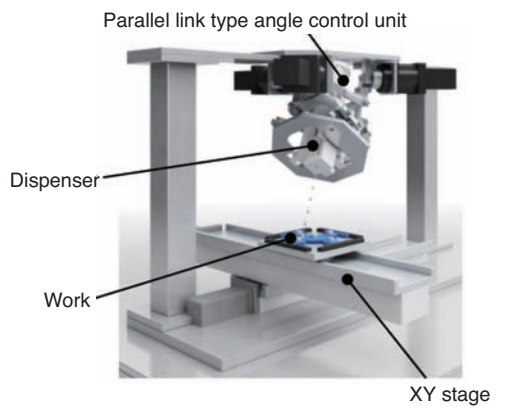
### 5.2 Visual inspection system

The configuration of the visual inspection system using the improved unit is shown in Fig. 13. In this configuration, the work is moved by the XYZ stage at the bottom, and the attitude of the camera is controlled by the unit. Inspection of the sides and edges of the work, as well as detection of missing bolts in recessed areas, can be automated in a compact configuration without using multiple cameras.

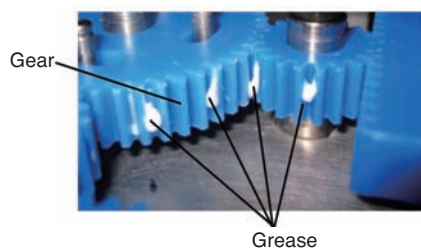
Table 2 Performance comparison

		Conventional unit	Improved unit
Size mm (Outer diameter x height)	Without dispenser	φ 400×107.5	φ 500×190
	With dispenser	φ 400×262.5	φ 500×230
Mass (kg)		10	
Max. carrying capacity (kg)		1.0	
Movable range °		Bend angle θ : 0-45 Angle of traverse φ : 0-360 (unlimited)	
Positioning accuracy for repetitive operation	Angle °	±0.065	
	Nozzle position mm	±0.22	±0.15
Natural frequency (Hz) (When dispenser is installed)		25.6	27
Application speed s/point *1		0.095	0.089

\*1 Application time per point when applying grease on 49 points of matrix sheet (7 x 7 point, 10mm of interval) (grease amount: 5mg/point)



(a) System configuration of grease dispensing



(b) Grease dispensing sample

Fig. 12 System configuration example of grease dispensing

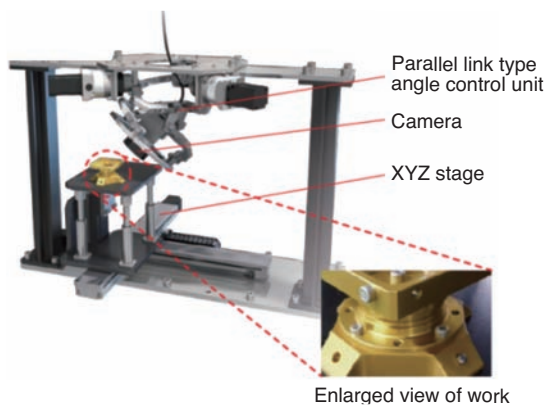


Fig. 13 System configuration example of visual inspection

## 6. Summary

We have developed a parallel link angle control unit using a special parallel link mechanism with two rotational degrees of freedom and the end effector placed inside the internal space. By reviewing the driving mechanism and controlling methods, we have improved the life, safety, positioning accuracy and operation speed from conventional units. We are working on deploying units in production facilities to be used for grease application and visual inspection. In the future, we will work on expanding deployment into many other fields such as medical/welfare and living environments, which will further contribute to the evolution of automation and robotization.

## References

- 1) The Robotics Society of Japan, Robotics Hand Book, New Edition, Corona Publishing, 2005, 297
- 2) Hiroshi Isobe, Yukihiro Nishio: Parallel Link High Speed Angle Control Equipment (PHACE), NTN TECHNICAL REVIEW, No. 80, (2012), 42-47.
- 3) Neil C. Singer, Warren P. Seering, Preshaping Command Inputs to Reduce System Vibration, J. Dyn. Syst. Meas. Control, Vol.112, No. 1, (1990) 76-82
- 4) Hiroshi Isobe, Yukihiro Nishio, Keisuke Sone, Hiroyuki Yamada, Yoshio Fujikawa: Parallel Link High Speed Angle Control Equipment, Proceedings of the Japan Society for Precision Engineering Spring Meeting, 2013, (2013), 809-810.

## Photo of authors



Kenzou NOSE  
New Product Development  
R&D Cente



Hiroshi ISOBE  
New Product Development  
R&D Cente



Seigo SAKATA  
New Product Development  
R&D Cente

## Propeller Blade Bearings for Aircraft Open Rotor Engine



Guillaume LEFORT\*

The Propeller Blade Bearings for Open Rotor Engine SAGE2 were developed by NTN-SNR in the frame of the Clean Sky aerospace programme. The goal of this project is to design, manufacture and test the propeller blade bearings for the upstream and downstream propellers of SAGE 2 Open Rotor.

The propeller blades of the two rotors are attached to engine cases and are orientated at various angles by the two independent Pitch Control Mechanisms.

The propeller blade bearings ensure the transfer of aerodynamic and centrifugal loads to the respective engine cases while allowing the pitch change of the blades.

Based on its know-how, its scientific knowledge and Research studies, NTN-SNR developed a new bearing architecture, completed a general mitigation test plan, successfully passed the validation tests and delivered the bearings for the Open Rotor Sage2 demonstrator.

### 1. Introduction

The SAGE2 counter-rotating open rotor is an aircraft engine concept developed in the frame of the European Union Programme "Clean Sky". It is the most attractive aircraft engine concept to reduce the fuel consumption and the gas emission (CO<sub>2</sub>, NO<sub>x</sub>, ...). In fact, this concept allows improving the propulsive efficiency and the thermal efficiency while growing up the by-pass ratio (higher the by-pass ratio is, lower the fuel consumption is with the same weight).

However, before introducing this concept in production, several technical issues had to be solved. A lot of innovative works had to be studied for the integration of the open rotor to the aircraft and for the propulsive part (gearbox, propeller blade design, propeller blade integration: pitch change mechanism, propellers blade bearings).

NTN-SNR was selected by the EU to design, develop and manufacture the propeller blade bearing prototypes for this demonstrator, which are one of the critical parts for Open Rotor Engine.

In this paper, we briefly discuss about the context of the project and present the propeller blade bearings developed by NTN-SNR for this engine.

### 2. Context of the project

#### 2.1 Clean Sky programme

Clean Sky is the most ambitious aeronautical research programme ever launched in Europe. Its mission is to develop breakthrough technologies to significantly increase the environmental performances of airplanes and air transport, resulting in less noisy and more fuel efficient aircraft, hence bringing a key contribution in achieving the Single European Sky environmental objectives. 6 technologies are studied in Clean Sky (see Fig. 1).



Fig. 1 Technologies studied by Clean Sky programme

\*NTN-SNR Roulements, R&D Aerospace Design Office

In the frame of this R&D programme, NTN-SNR answers to a call for proposal about propeller blade bearing activity in the frame of Sustainable And Green Engine technologies (SAGE).

The NTN-SNR proposal has been classified as the top ranked one, against others proposals and NTN-SNR has been officially selected on the project on October 19<sup>th</sup> 2012.

### 2.2 Open Rotor Architectures

The Open Rotor architecture is an aircraft engine composed of a gas generator and 2 propellers. The gas generator provides the mechanical energy to rotate the 2 propellers, as shown on the Fig. 2.

This concept combines the qualities of the turbopropulsor (propulsive efficiency, thermal efficiency) and the benefits of the turbojet engine (higher flight speed, lightness,...).

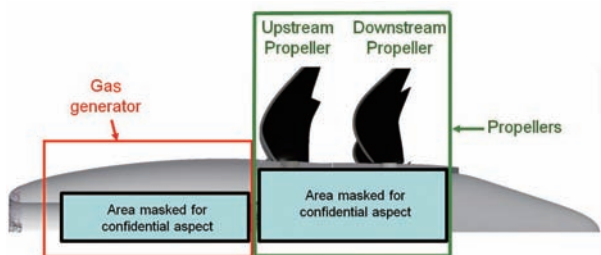


Fig. 2 Open Rotor architecture

### 2.3 Schedule

The 34 months duration project has cost €1.5 million with 50% of EU contribution.

The schedule is described on the Fig. 3.



Fig. 3 Project schedule (civil year)

### 2.4 Customer specification and technical challenges

Regarding the propeller blade bearings, NTN-SNR has a very good experience in the concepts for commercial turboprop aircraft already in production. However, due to the SAGE2 technical specification and the location of the propellers, none of the current blade bearing designs can be used on the open rotor concept. The Fig. 4 and Fig. 5 show the differences between current blade bearing specification and SAGE2 open rotor blade bearing specification.

The 4 main bearings specific challenges for this innovative application were:

- Criteria 1: High level of loads (especially centrifugal force) with +15% compared to the current application
- Criteria 2: Large temperature range and high level of maximum temperature (-55°C to 180°C): twice higher than current application
- Criteria 3: Smaller allocated room to design the solution than existing one
- Criteria 4: The sealing device has to be inserted in the new propeller blade bearing. The current design doesn't include the sealing device inside the bearing.

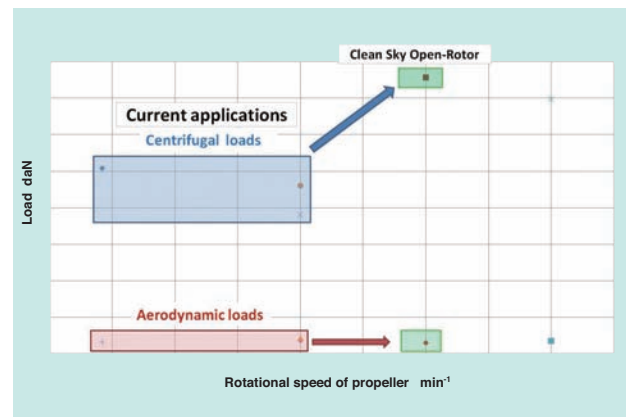


Fig. 4 Loads comparison between current applications and SAGE2 Open rotor specification

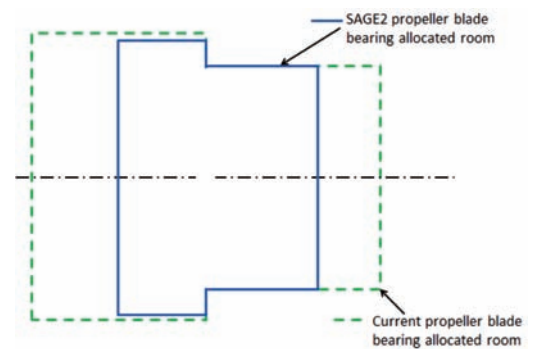


Fig. 5 Propeller blade Bearing allocated room differences between current applications and SAGE2 Open rotor specification

### 3. Technical solution

#### 3.1 Objectives

The goal of this project was to design, manufacture and test the propeller blade bearings for 2 propellers of SAGE 2 Open Rotor (See Fig. 6).

The propeller blades of the two rotors are linked to engine cases (bearing housing) and are orientated at various angles. The propeller blade bearings ensure the transfer of aerodynamic and centrifugal loads to the respective engine cases while allowing the pitch change of the blades.



Fig. 6 Location of Propeller Blade bearings on the engine

These propeller blade bearings are one of the critical Open Rotor Architecture parts. Without efficient, reliable and safety propeller blade bearings, no Open Rotor Engine could be introduced in mass production on the commercial civil aircraft.

The main functions of these bearings are:

- Allow oscillatory rotation between the engine case and the propeller blade shaft
- Transmit the centrifugal and aerodynamic loads from the propeller blade to the engine case
- Resist to the environment (thermal, fluids,...)
- Ensure the stiffness between the propeller blade root and the engine case
- Resist to a load caused by the loss of propeller blade

#### 3.2 Description of the technical studies

To meet the specification requirements, 3 innovative works were conducted:

- A) design a new bearing architecture addressing criteria 1, 2, 3 and partially 4

- B) develop a new complex tribological system in order to minimise the friction torque and avoid any raceway wear (criteria 1 and 2)

- C) develop an innovative sealing system answering to criteria 4.

Regarding all the risks existing on this project a mitigation plan was established and completed.

#### A) Bearing architecture

Based on criteria 1 and 3, several architectures of bearings have been defined and calculated using specific new adapted Finite Element methodology.

This new methodology has been developed during the project because the constraints of integration, especially the complex thermal gradient and the stiffness of parts. Eventually, only two architectures meet the specifications and based on these calculations (See Fig. 7), the best bearing architecture was selected. The selected architecture is a double row angular contact ball bearing.

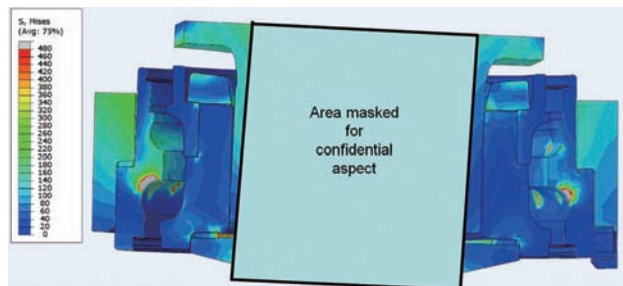


Fig. 7 Stress distribution of finite element calculation

#### B) Tribological system selection

It is important to highlight that the contact lubrication is a key parameter for the success of this project because both the life duration of the bearing and the bearing starting torque depend on the contact lubrication. Due to the extreme specification, the lubrication cannot be done by one type of lubricant. Therefore, NTN-SNR has developed a complex tribological system to allow for good bearing lubrication (See Fig. 8). This selection was divided into three steps:

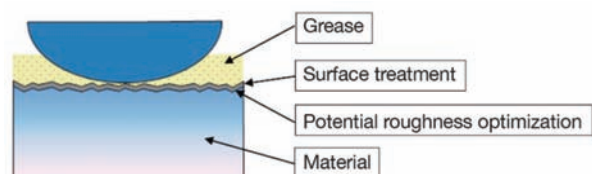


Fig. 8 Complex tribological system developed

### B-1) Exploration of existing solutions

The aim of this task was the exploration of all existing lubricant solutions. This task was based on NTN-SNR experiences, literature and supplier experiences. It is important to highlight that the major criterion for the lubricant is the capacity to sustain very high contact pressure (up to 4 GPa). It is also a challenge for the surface treatment.

12 potential greases and several surface treatments were studied.

Only the four best greases and the best surface treatment were further studied in the following step.

### B-2) Tribological solution definition

The target of this step was to select three best solutions regarding the global tribological behaviour. NTN-SNR explored the different types of lubricants (greases and surface treatment defined previously) and the combination of the different types. The impact of the bearing ring materials and their heat treatment was also evaluated. The ring and ball materials are established by the bearing sizing. Several solutions were studied for three other components.

**The three best tribological systems were selected regarding laboratory test results.**

### B-3) Validation of the selected solutions

The aim of this task was to test three best selected solutions in representative conditions, studying the "False Brinelling Effect" on three test benches: at room temperature, at high temperature and at low temperature. The first two test rigs already existed at NTN-SNR and the last one had to be built (See Fig. 9).

These 3 solutions were compared with the solution of reference used on the current application for the test at room and low temperature. However, the high



Fig. 9 False Brinelling test bench

temperature tests were performed to validate the good behaviour of the solutions at 180°C, where the reference is not valid. These tests performed the equivalent in service time on the three best solutions.

**Conclusion: Based on all these tests, NTN-SNR defined and developed a customised complex tribological system which has the same performance as the propeller blade root "in service" solution in an environment respecting the requirements criteria.**

### C) Sealing device

Intensive work has also been done to design complex sealing devices to avoid the leakage of lubricant outside of the bearing and the penetration of pollution inside the bearing. In fact the bearing sealing system is composed of two seals: the upper seal and the lower seal as shown on the Fig. 10. The maximal equivalent pressure applied on the upper seal by the centrifugation of the grease is about 16 bars with safety factor. In addition, at low temperature, the grease has to have a low viscosity to ensure a good lubrication of bearing.

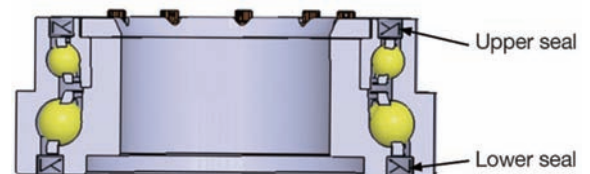


Fig. 10 Sealing system

The detailed study of sealing, including functional analysis, risk analysis and product Failure Mode and Effect Analysis dedicated to the sealing, was done with the supplier. Due to the specificity of the requirement and to optimise the integration aspect (torque, weight, cost ...), the architecture of the lower and upper seals used on the bearing assembly is not the same. The Finite Element calculations showed larger displacements of the seal seatings than existing applications. Therefore, the seal design has to be reinforced to take into account these displacements.

Due to the high level of risk, a sealing validation plan was performed. It consists of six tests:

- **Material compatibility tests:**

These are laboratory tests to validate the good behaviour of the seal material with the materials (fluids or chemical components) that could be in contact with the seal during its life.

• **“Raffer test”:** ( shown on Fig. 11)

This is a fatigue pressure test to study the behaviour of the seal regarding complex cycles and endurance.

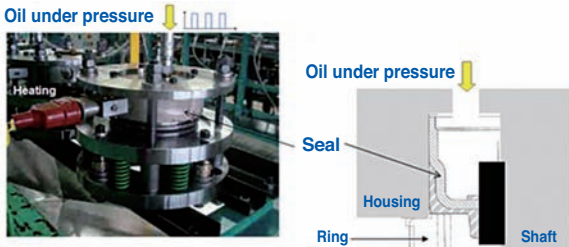


Fig. 11 “Raffer test”



Fig. 12 Starting test measurement test bench

• **Adhesive test:**

This test aims to validate the good adherence between the elastomer part of the seal and the frame.

It is important to highlight that an adhesive issue could result also in a non-optimised seal design which puts a high level of strain on the link between the elastomer and the frame.

• **Dismounting test:**

This test measures the load necessary to disassemble the seal of the bearing in order to demonstrate that there is no displacement of the seal and deflector during the engine test.

• **Starting torque measurement on seal:**

This test aims to measure the starting torque of the seal alone. The torque value measured by this test is used to compare the starting torque of the three solutions.

• **Starting torque measurement on standard representative bearing in terms of diameter, ball size and number of balls:**

This test mitigates the risk of having a starting torque higher than the specification. In fact, if the bearing torque is too high, the actuator which controls and changes the blade pitch angle cannot modify the angular position of the blade. Thus the engine does not work. A specific test methodology was developed for this project. The Fig. 12 shows the test bench.

The results are shown in the Fig. 13.

The best seal design regarding performance and life duration was assembled on the bearing prototypes.

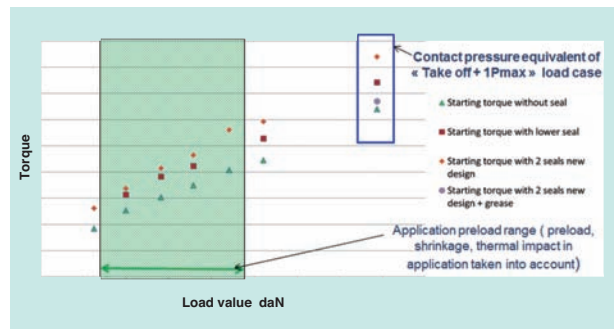


Fig. 13 Example of torque measurement results obtained

**3. 3 Results**

After the completion of the three innovative works, the bearings were manufactured. After that, the prototype bearings were validated:

- For criteria 1, 2 (partially) and 3, the good behaviour of the bearing under load was validated with tests on ball bearing on a compression/torsion test machine (see Fig. 14). The results are shown on the Fig. 15. The two bearings successfully passed the limit and ultimate load tests. And the torque under load is two times lower than the starting torque requirements included in the course of the project. The two bearings will allow:
- Good behaviour of the engine, allowing oscillatory rotation between the engine case and the propeller blade, transmitting centrifugal and aerodynamic loads from the propeller blade to the engine case, ensuring the stiffness between the propeller blade root and the engine case
- Safe working of the engine, avoiding the loss of propeller blade.
- The criteria 4, is only validated by the “Raffer” tests performed on the seals.

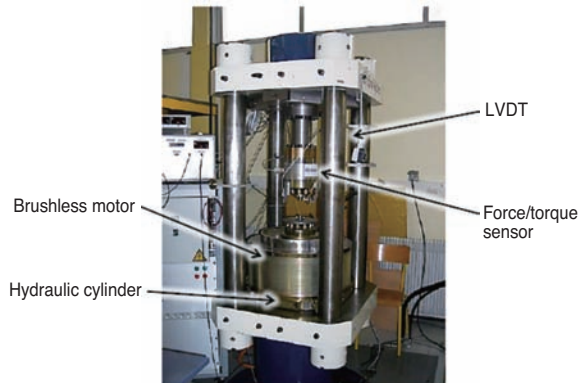


Fig. 14 Compression/torsion test machine

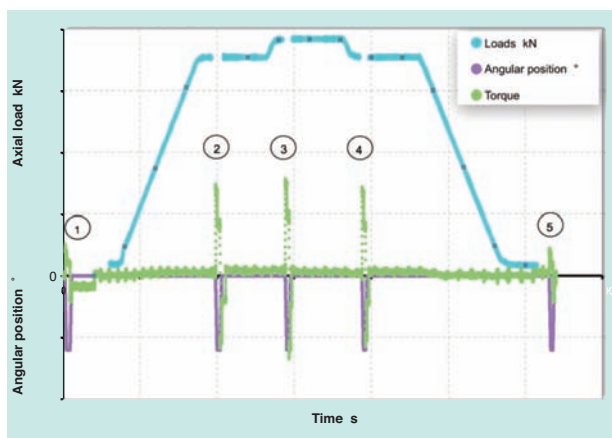


Fig. 15 Results of the validation tests

The project developed and thoroughly tested the bearing prototypes up to TRL5. As a result, the bearings for the two SAGE 2 demonstrator propellers with the substantiation documents have been delivered to the customer.

The bearing and its 13 different components were manufactured following all the aerospace quality standards.

## 4. Conclusion

In conclusion, during this project, NTN-SNR has developed:

- a new compact self-lubricated architecture of bearing
- a new complex tribological system to allow a good lubrication of bearing under extreme conditions (centrifugation loads and high temperatures)
- a new sealing device compliant with high pressure fatigue safety margin.

All these innovations will be definitely validated on SAGE2 Open Rotor demonstrator during a ground test campaign. The Open rotor demonstrator will be tested in the South of France at the end of CY2016.

The bearing solution developed in the frame of this project by NTN-SNR will now become one of the technical standard for all the blade root application (unducted or ducted propeller) which works in high speed conditions, high temperature environment, in a small allocated room where sealing and self-lubricant are requested. (See Fig. 4)

These bearings contribute to the positive environmental impact of the Open Rotor engine:

- CO<sub>2</sub> emission reduction: -15% to -17%
- Noise reduction: -6 to -9 dB

The impact of the innovative technologies developed for these bearings could be applied on several aerospace applications (propeller blade bearings, fan blade bearings, main rotor blade bearings, swash plates, ...). Moreover the tribological system could be applied on other bearings for industry market or automotive market.

4 patents were applied based on the results of these studies.

Out of 482 projects, NTN-SNR was ranked within the 10 best projects.

Photo of author



Guillaume LEFORT  
NTN-SNR Roulements  
R&D Aerospace  
Design Office

# Products Introduction of Composite Material for Industrial Machinery



**Shinji KOMATSUBARA\***  
**Toshihiko MOURI\*\***  
**Takuji HARANO\*\***  
**Tamaki MIZUTANI\*\*\***

NTN Composite Material Product Division has developed the mechanical parts and bearings, and the unit module products by a wide range of materials and technology such as resin material, magnetic material and fluid dynamic pressure technology. This paper introduces our products that meet

various required characteristics of industrial machinery such as medical instrument, food machinery, hydraulic equipment and information device etc.

## 1. Introduction

NTN's composite material business is working on the development of products leveraging technologies related to resin material, sintered metal, magnetic material and fluid dynamic, and combining these technologies with unit module products. Our composite material products meet the various demands of the industrial machine industry and automobile industry as products that: achieve both high functionality and productivity by combining a blend of additives to give several functions to the materials, and have unique designs that are only possible to make by using a metallic mold. These products are produced by the associated companies indicated in Fig. 1. In this article, we will introduce you to a choke coil used in MRI medical devices, as an example of magnetic material products. We will also introduce high strength machine parts with mechanical properties equivalent to ingot materials as an example of

sintered metal products, hydrodynamic bearings for thin-type fan motors used for information devices, and resin sliding components, specifically resin-based sliding bearing units and resin rolling bearings with excellent handling properties. for

## 2. Choke coil for high current MRI

The MRI (magnetic resonance imaging) device, shown in Fig. 2, is required to take clear pictures in a short time. Therefore, it uses high currents to produce strong magnetic fields and high frequency drives to realize high-speed image processing. For power supply circuits, choke coils for high currents are used to remove noise generated in circuits. Choke coils are required to maintain low-loss and stable properties up to high current/high frequency bandwidths.

NTN developed magnetic materials using low-loss amorphous alloy powder, which can be used for injection molding, and applied it to choke coils for MRI <sup>1)</sup>.



Fig. 1 Composite material products of NTN Group



Fig. 2 Medical Magnetic Resonance Imaging

\*Fluid Hydrodynamic Bearing Dept. Composite Material Product Division

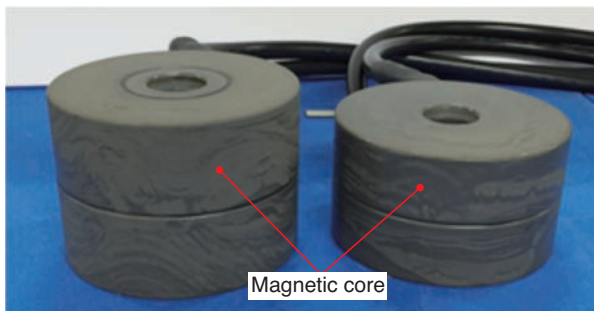
\*\*Engineering Dept. NTN Advanced Materials Corporation

\*\*\*Engineering Dept. NTN Engineering Plastics Corporation

### 2.1 Features

Fig. 3 shows NTN's choke coils for MRI power supply. The magnetic, core covering exterior is generally made by compression molding of amorphous alloy powder. However, amorphous alloy powder has poor moldability and is limited in size and shape. It is also fragile, so it is not easy to handle. NTN has succeeded in expanding the range of shapes for magnetic cores by making the material injection moldable.

Presently, 125A - 300A types are in volume production.



Type 300A                      Type 260A  
**Fig. 3** Choke coil for MRI power supply

### 2.2 Performance

The material used for magnetic cores is the composite material "AS10", made of iron-based amorphous powder that does not have a crystalline structure, and resin material.

AS10 was compared to the conventional ferrite/iron-silicon (Fe-6.5Si) magnetic material with an inductance deviation rate (DC bias characteristic), which serves as a measure of the magnetic field generation capability when a high current is applied. The result is shown in Fig. 4.

In addition, the inductance change rate (frequency response) when frequency is changed to a high frequency bandwidth is shown in Fig. 5.

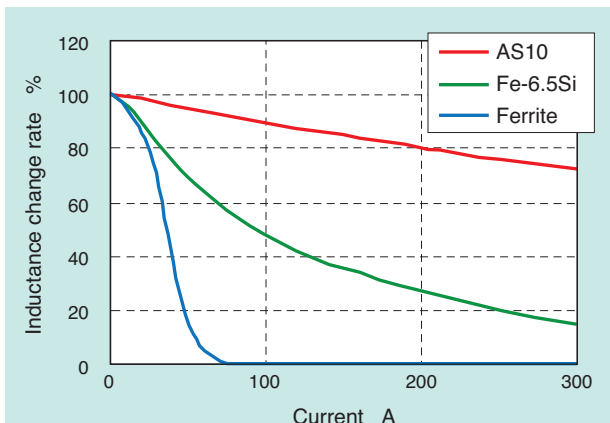


**Fig. 4** DC bias characteristics

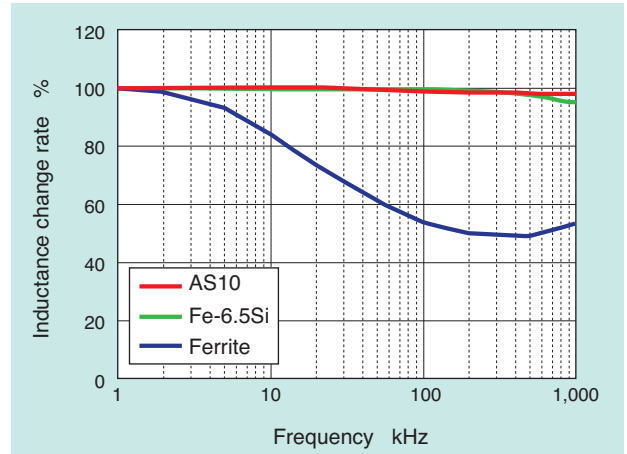


**Fig. 5** Frequency characteristics

Since AS10 is stable with small inductance change in a high current/high frequency, it is a material suitable for operating conditions of choke coils for high currents.

Moving forward, we will expand the use of this material for various applications in industrial machines and automobile industries which require high currents and stable high frequency responses.

### 3. High-density/high strength sintered machine parts

One of the manufacturing methods of machine parts is powder metallurgy. Powder metallurgy is superior in productivity and material yield compared with machining from ingot steel, and reduces the cost of machining by applying a near net shape process. However, sintered machine parts usually have poorer mechanical properties than ingot steel due to pores in the part that are inherent to the process.

NTN developed sintered machine parts with higher density and strength than the conventional products by optimizing the material, mold and heat treatment<sup>2,3)</sup>. This expanded the range of application of sintered parts in areas where ingot steel was used for its mechanical properties. In this article, a sintered machine part with high density and high strength is introduced, taking oil pumps for industrial machines as an example.

Oil pumps for industrial machines are widely used for construction machines, machine tools and printing machines which use hydraulic power as the power source. Fig. 6 shows the structure of a vane pump, which is a type of oil pump. Its components have complex shapes, and therefore, powder metallurgy is suitable for production of these components.

However, along with the recent increase of compact and lightweight oil pumps, the components are

becoming smaller and thinner. Therefore, in applications under high pressure, with an increased risk of fluctuation of hydraulic pressure/flow rate that leads to component fracture, conventional sintered machine parts cannot be used. NTN is proposing the use of the developed high density/high strength sintered machine parts for rotors and cam rings shown in Fig. 6.

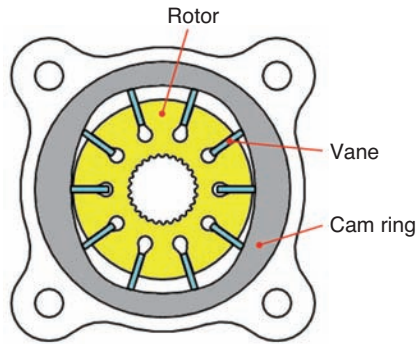


Fig. 6 Vane pump

### 3. 1 Methods for manufacturing high-density/high strength sintered materials

Increasing density and reducing pores are the most effective measures for increasing strength of sintered machine parts. The following describes methods for manufacturing high-density/high strength sintered materials

#### 3. 1. 1 Material

We have developed a material with high compression properties for high density when used for powder molding. Graphite with treatment for anti-segregation was mixed with a partially alloyed powder of Ni and Mo diffusively joined to Fe. Additionally, lubricant was added at a certain proportion for ensuring release from the mold and preventing seizure.

#### 3. 1. 2 Molding pressure and density

Fig. 7 shows the relationship between the molding pressure for powder molding and the resulting density for the developed product as well as a conventional

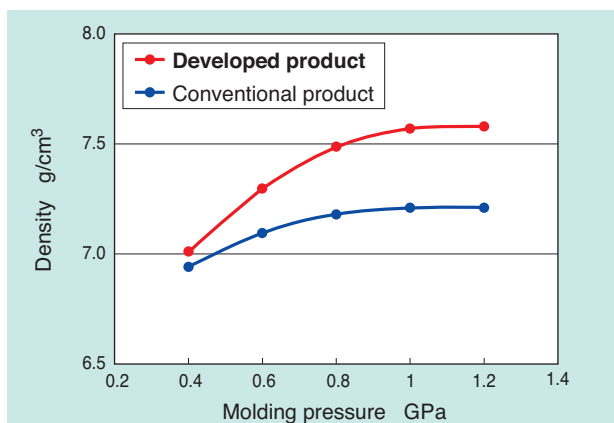


Fig. 7 Relations of compacting pressure and the density

material for sintered machine parts. Density increases as the molding pressure increases for both materials; however, the conventional product plateaus at 7.2 g/cm³, while the developed product reached 7.6 g/cm³.

#### 3. 1. 3 Heat treatment

Heat treatment is applied for increasing the mechanical properties. Carburizing, quenching, tempering, and carbonitriding, etc. can be used as the heat treatment process.

### 3. 2 Mechanical properties

The mechanical properties of the developed product, which uses the material described in the previous section and molded with higher pressure (0.8GPa) and treated with carburizing, quenching and tempering, were compared with the mechanical properties of a conventional material for sintered machine parts and also the properties of ingot steel (high carbon chromium bearing steel). Fig. 8 shows the comparison of ring compression fatigue strength. In addition, Fig. 9 shows the comparison of the measurement result of Young's modulus.

While the density of the conventional product was 7.1 g/cm³, the density of the developed product was 7.5 g/cm³, and the true density ratio against steel of the developed product was 96%. As a result, the fatigue strength of the developed product was 340 MPa, approximately 2.3 times that of the conventional product.

The Young's modulus of the developed product was 180 - 200 GPa, equivalent to the ingot steel, SUJ2.

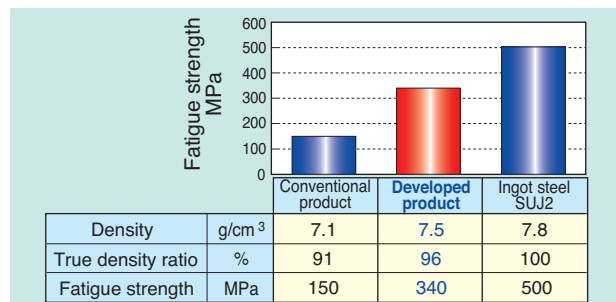


Fig. 8 Ring compressive fatigue strength

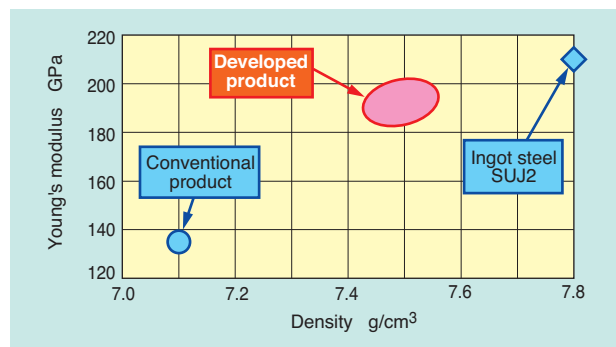


Fig. 9 Relations of density and the Young's modulus

Presently, we are proceeding with ongoing development for higher density/strength of this material for even broader deployment of this technology.

#### 4. Thin type hydrodynamic BEARPHITE for fan motor applications

Quietness is highly required for fan motors for cooling mobile terminals such laptops, and NTN's fluid hydrodynamic bearings "Hydrodynamic BEARPHITE" are used to achieve this requirement. Hydrodynamic BEARPHITE offers high levels of quietness by non-contact support of shafts and bearings through an oil film. In recent trends of thin enclosures, installed cooling fan motors are also becoming thin. As the length of the supporting bearings also becomes short, the load carrying capacity of the bearings decreases. They produce noise when the shaft and bearings come into contact due to a lack of load carrying capacity. Therefore, high load carrying capacity is required for thin-type hydrodynamic BEARPHITE.

NTN has developed thin-type hydrodynamic BEARPHITE to solve the above issue by applying a new material. The product is shown in Fig. 10.

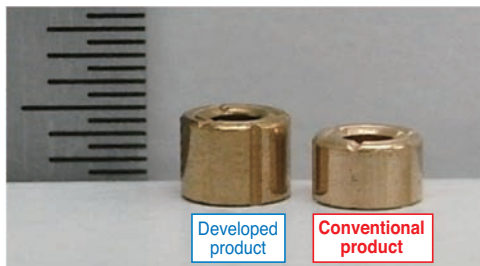


Fig. 10 Appearance of Hydrodynamic BEARPHITE

##### 4.1 New material

Hydrodynamic BEARPHITE is a type of sintered, oil-impregnated bearing manufactured by a powder metallurgy process and therefore contains pores in the outer and inner surfaces of the bearings. While these pores have an important function of retaining and delivering lubricating oil, the pressure generated by the hydrodynamic effect escapes through these pores into the bearings, and it is necessary to control the pores in order to ensure high load carrying capacity.

In general, pores on the outer and inner surfaces of the bearings can be refined by using powder of minute particles to suppress the generated pressure. On the other hand, this is likely to produce more burrs since the minute particles of the powder penetrate the small gaps of the mold and deteriorate fluidity and moldability.

NTN has succeeded in both retaining productivity and improving load carrying capacity by developing a new material, optimizing the size and shape of the particles. Fig. 11 shows the comparison of the inner diameter surface of the developed and conventional bearings. It reveals that the pores of the developed product are refined compared with the conventional product.

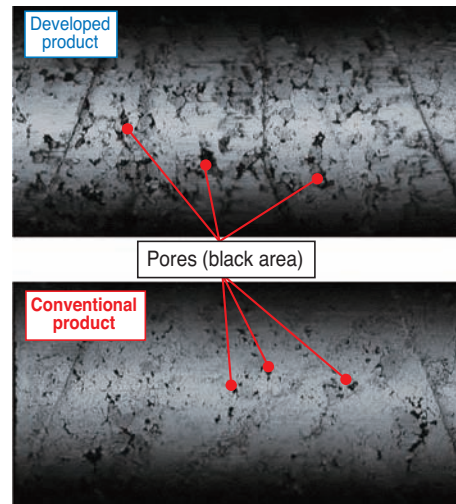


Fig. 11 State of inner surface

##### 4.2 Formation of oil film

The formation of an oil film was compared between the developed product and conventional product used in actual fan motors. Results are shown in Fig. 12. Assuming the actual operating conditions, the fan motor experienced cycles of being repeatedly shaken and then left undisturbed while it was in operation, and measurements were taken as to whether the shaft and hydrodynamic BEARPHITE were in contact using the electric resistance method. Based on the detected voltage, the contact status was set as 0% of the oil film formation ratio and non-contact status as 100% of

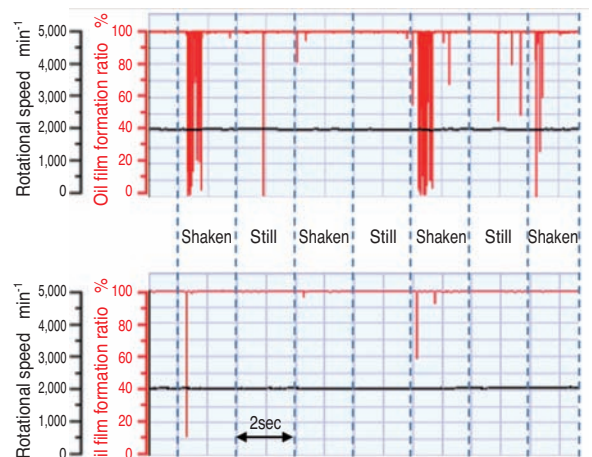


Fig. 12 Test result of contact of shaft and BEARPHITE

the oil film formation ratio. Even in severe conditions when the conventional product indicated contact status, the oil film formation was good in the developed product, indicating that load carrying capacity had improved.

From these results, it was determined that the developed product is able to maintain a high level of quietness for fan motor applications, even in more severe operating conditions.

Hydrodynamic BEARPHITE using newly developed material will be applied not only for thin fan motors for mobile devices, but also for larger cooling fan motors such as for general industrial machines and automobiles. In addition, we would like to actively expand application of this product to other areas, not only fan motors. And we will continue our development for further improvement of functionality and productivity.

## 5. Resin products for food machines

Food machines used in food production lines and facilities are under strict control in order to provide the safety and security of food. From selection of materials that comply with the "Standard for Instruments, Containers and Packages Made of Synthetic Resin" based on the Food Sanitation Act, to the requirement of high temperature/high pressure cleaning for every production process, the operating conditions are strict for sanitation control. Therefore, stainless steel and resin materials are used for food machine components.

NTN distributes resin products for food machines leveraging the material and design benefits of resin.

### 5. 1 Sliding material BEAREE FL3642 for food machines

Sliding materials for food machines are required to have good friction/wear resistance, heat resistance, chemical resistance and water resistance properties, as well as a clean appearance. For example, carbon is undesirable because of its dark, black color.

Fig. 13 shows BEAREE FL3642, broadly used as the sliding material for food machines.



Fig. 13 Products of BEAREE FL3642

### 5. 1. 1 Features

- (1) Light yellow with a clean appearance
- (2) Excellent friction/wear resistance, chemical resistance and water resistance properties
- (3) Extremely low friction coefficient at start-up and ultra low speed operation
- (4) Good compatibility with stainless steel
- (5) Usable in high temperatures (260°C)

### 5. 1. 2 Specific wear rate

Since food machines are exposed to high pressure cleaning methods, performance in dry and wet conditions is emphasized. Therefore, the specific wear rate of FL3642 and other materials were compared in dry conditions and in water. The test conditions are shown in Table 1 and results in Fig. 14.

Compared with PTFE material containing glass fiber, which is a sliding material, the specific wear rate of FL3642 is higher in dry conditions, but 1/60 the wear rate value of the PTFE material in water. Also, compared with the sliding material for water use, FL3700, it has equivalent performance in both dry and wet conditions<sup>4</sup>).

Table 1 Test conditions for wear test

Tester	Thrust tester
Surface pressure	0.98MPa
Peripheral speed	32m/min
Mating material	SUS304
Lubrication	Dry, water
Time	50h

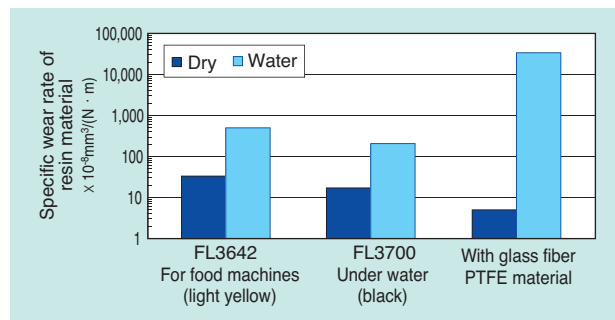


Fig. 14 Comparison of comparative abrasion quantity of FL3642 with other NTN resin materials

### 5. 2 Resin sliding bearing unit for special environments

The bearing units shown in Fig. 15 are used for chain conveyor bearings for cleaning machines and disinfection systems. The fluorocarbon resin sliding bearings are enclosed between the stainless steel inner ring and outer ring, and incorporated in the housing. They are grease-less and maintenance-free bearing units, which are easy to install in the machines. Table 2 shows the constituting materials. The design and manufacture of this product is tailored to the specifications of our customers.

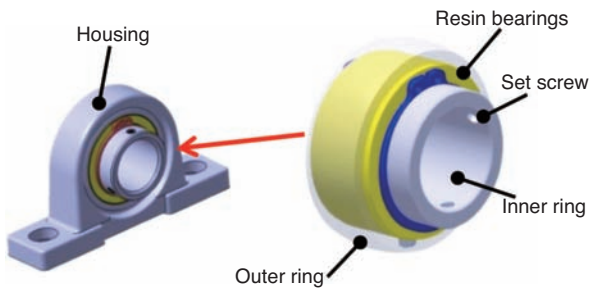


Fig. 15 Sliding bearing unit for special environment

Table 2 Constituting material

Component parts	Material
Inner ring	SUS304
Outer ring	SUS304
Set screw	SUS304
Resin bearings	BEAREE FL3642/FL3700
Housing	SCS13 (Stainless cast steel)

### 5.3 Resin based thrust rolling bearings

These bearings are light and stainless thrust rolling bearings that combine NTN's proprietary resin cages and ceramic balls. The constituting materials are shown in Table 3 and an image of the product is shown in Fig. 16. The material of the cage is fluorocarbon resin blended with special additives. The cage has excellent heat resistance and a low coefficient of friction to prevent adhesion of food.

In addition, excellent handling properties were achieved by creating a unique shape for the cage pocket so that the balls are retained when installing bearings to the equipment, yet easy to remove for disassembling and cleaning. Currently, these bearings are used by food machine manufacturers and used in food contact areas.

#### 5.3.1 Features

- (1) Lightweight and rust-free material
- (2) Usable in high temperatures (200°C)
- (3) Excellent handling properties
- (4) Easy to detect foreign objects after cleaning due to light color

Table 3 Constituting material

Component parts	Material
Cage	BEAREE FE5002
Ball	Ceramic



Fig. 16 Plastic thrust rolling bearing

## 6. Conclusion

This article introduced various composite material products made of resin, sintered, and magnetic materials, with new designs and technology for meeting diverse requirements of industrial machines.

NTN will create modules and units based on these products. We are poised to propose value-added products that meet the market trend of being easy to handle for customers, and contribute to the development of industrial machines.

## References

- 1) Takuji Harano, Shinji Miyazaki and Hajime Katsuura: Introduction of Magnetic Material Products, NTN TECHNICAL REVIEW No. 80 (2012) 87-91.
- 2) Tomonori Yamashita and Tomokazu Sonozaki: Introduction of Sintered New Products for Automobile, NTN TECHNICAL REVIEW No. 81 (2013) 74-76.
- 3) Takahiro Okuno and Naoki Yashiro: Improvement in Strength of Sintered Machine Parts, NTN TECHNICAL REVIEW No. 82 (2014) 21-25.
- 4) Yoshio Oki and Takuya Ishii: Sliding property of PTFE composite material under water, THE TRIBOLOGY No. 148 (1999) 48-49.

Photo of authors



Shinji KOMATSUBARA  
Fluid Hydrodynamic Bearing Dept.  
Composite Material Product  
Division



Toshihiko MOURI  
Engineering Dept.  
NTN Advanced Materials  
Corporation



Takuji HARANO  
Engineering Dept.  
NTN Advanced Materials  
Corporation



Tamaki MIZUTANI  
Engineering Dept.  
NTN Engineering Plastics  
Corporation

The Japan Society for Precision Engineering, Spring Meeting, 2015, Best Presentation Award  
 2015 The Japan Society for Precision Engineering, Young Engineer Award

# Parallel Link High Speed Angle Control Equipment

Naoya KONAGAI

## 1. Overview

We have developed Parallel Link High Speed Angle Control Equipment (hereinafter, "equipment") by applying the special parallel link mechanism of two rotational degrees of freedom, and deployed this equipment to grease dispensing, automatic welding, and appearance inspection. This equipment, which allows high-speed/high precision positioning and granular motion in a wide operating range that accommodates a 90° working angle and 360° traverse angle, was recognized at The Japan Society for Precision Engineering Spring Meeting, 2015, and received Best Presentation Award and Young Engineer Award.

## 2. About Parallel Link High Speed Angle Control Equipment

The equipment achieved smooth operation with two rotational degrees of freedom and high-speed/high precision operation by controlling all three links of the 4-joint, 3-link parallel link mechanism, canceling backlash with a balance of driving forces from the three motors, and reducing settling time by controlling acceleration/deceleration<sup>1 to 4)</sup> Fig. 1 shows the standard offering of this equipment. Speed and positioning repeatability are improved by enclosing the end effector in the internal space of the link and reducing the moment of inertia. Due to its high speed and superior maneuverability, the equipment has been adopted in grease applications where short takt time and high reliability are required, such as in production lines of automotive components. Furthermore, it is also deployed in automatic welders, leveraging its capability of drawing fine trajectory<sup>5)</sup>.

## 3. Deployment to automatic welders

Fig. 2 shows the configuration of an automatic welder using this equipment with a welding torch. The parallel link mechanism for automatic welders is a mirror symmetric type<sup>6)</sup> and each component is redesigned from the standard products to secure space for installing the welding torch. In order to install heavy and long welding torches, the equipment is fixed on the XY stage with the tip of the parallel link

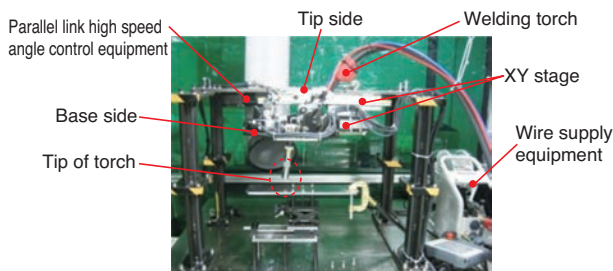


Fig. 2 System configuration of automatic welding machine

mechanism facing upward to reduce the moment of inertia, and the welding torch is positioned so that it penetrates the internal space of the link mechanism in order to achieve fast and refined operation. By controlling the position of the welding torch in this configuration, it can weld around the entire circumference of columns with the welding torch in an inclined position.

## References

- 1) Hiroshi Isobe, Yukihiro Nishio: Parallel Link High Speed Angle Control Equipment (PHACE), NTN TECHNICAL REVIEW, No. 80, (2012), 42-47.
- 2) Hiroshi Isobe: Parallel Link High Speed Angle Control Equipment – Basic Configuration and Application for Grease Dispensing, Machine and Tool, February Issue, (2013) 83-87.
- 3) Hiroshi Isobe, Yukihiro Nishio, Keisuke Sone, Hiroyuki Yamada, Yoshio Fujikawa: Parallel Link High Speed Angle Control Equipment, Proceedings of the Japan Society for Precision Engineering Spring Meeting in 2013, (2013), 809-810.
- 4) Hiroshi Isobe, Yukihiro Nishio, Seigo Sakata, Naoya Konagai, Hiroyuki Yamada and Yoshio Fujikawa: Parallel Link High Speed Angle Control Equipment - Implementation on Grease Application Equipment -, Proceedings of the Japan Society for Precision Engineering Spring Meeting in 2014, (2014), 1087-1088.
- 5) Naoya Konagai, Hiroshi Isobe, Seigo Sakata, Kenzou Nose, Hiroyuki Yamada and Yoshio Fujikawa: Parallel Link High Speed Angle Control Equipment, Proceedings of the Japan Society for Precision Engineering Spring Meeting in 2015, (2015), 605.
- 6) Keisuke Sone, Hiroshi Isobe and Koji Yamada, Actuator Unit with Two Degrees of Freedom for Bending Angle of 9 Degrees - High Angle Active Link -, Machine Design, Vol 47, No. 11, (2003) 60.

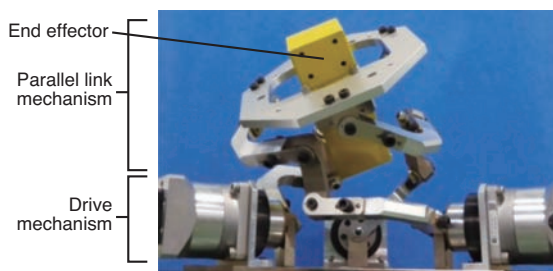


Fig. 1 Parallel link high speed angle control equipment

## Photo of author



Naoya KONAGAI  
 New Product Development  
 R&D Center

## 2014 "The Japan Society of Mechanical Engineers, Materials & Processing Division, Division General Award (New Technology Development)"

# Materials Development about the Sintered Bearing Prepared by Unification Forming of Different Metals Powder

Toshihiko MOURI Yoshinori ITOU Yosuke SUGAI Eiji YUASA

### 1. Introduction

"Material Development on Sintered Bearings Prepared by Unification Forming of Different Metal Powder," presented in the 2014 Annual Meeting sponsored by The Japan Society of Mechanical Engineers, received the division general award in the Materials & Mechanics/Materials & Processing Division.

This article describes the development of materials for "multi-layer oil-impregnated sintered bearings" for joints of hydraulic shovels (Fig. 1), etc. These multi-layer oil-impregnated sintered bearings have been developed by NTN, and achieve low friction and wear resistance, and high strength while being low cost<sup>1)</sup>.



Fig. 1 Application example

### 2. Structure

The structure of multi-layer oil-impregnated sintered bearings is shown in Fig. 2. Multi-layer oil-impregnated sintered bearings are comprised of two layers, with different materials in the inner and outer layers. They are characterized by integrated forming of this two-layer structure via powder molding, instead of press fitting or adhesion. The inner layer is made of hard ferrous material, with copper added to achieve both low friction and wear resistance.

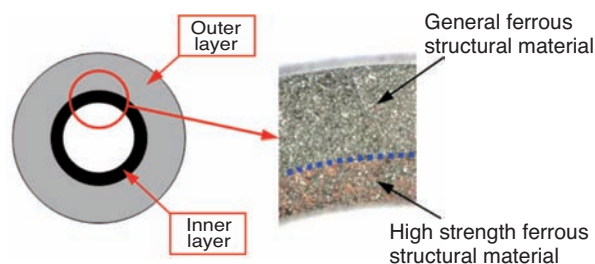


Fig. 2 Structure of the Multi Layer BEARPHITE®

The outer layer uses strong and less costly ferrous material blended with a metal with a low melting point to improve strength.

### 3. Features

Multi-layer oil-impregnated sintered bearings exhibit high strength and superior wear resistance with a two-layered structure using two different materials.

- 1) Radial crushing strength: 500 MPa or more without heat treatment
- 2) Possible to correct distortion after heat treatment with a sizing operation; no machining is required

### 4. Summary

This product achieves both low friction and wear resistance and high strength by the integrated forming of different materials. We will continue contributing to the market through development of new products.

### References

- 11) Yosuke Sugai and Toshihiko Mouri: Multi-Layer BEARPHITE, NTN TECHNICAL REVIEW 80, (2012) 83-86.

Photo of authors



Toshihiko MOURI  
Engineering Dept.  
NTN Advanced Materials  
Corporation



Yoshinori ITOU  
Engineering Dept.  
NTN Advanced Materials  
Corporation



Yosuke SUGAI  
Sales Technology Dept.  
Composite Material  
Product Division



Eiji YUASA  
Emeritus Professor,  
Tokyo City University

2015 Annual Innovation Product Award

# Machine Tool Main Spindle Bearings with Air Cooling Spacer

Wenwei WU

Michihiko KOSAKA

## 1. Introduction

NTN's "Machine Tool Main Spindle Bearings with Air Cooling Spacer" (hereinafter, "Bearings with Air Cooling Spacer") was recommended in the technical magazine "MM Modern Manufacturing", which has the largest circulation in China (25,000 copies/issue, 52 issues/year), as a candidate for "Annual Innovation Product Award" for 2015 and received the award based on votes from the internet and expert judges.

"Bearings with Air Cooling Spacer" are products using new technology which can allow for both high speed and high rigidity at a high level for the main spindles of machine tools by applying air cooling technology to the bearings.

## 2. Structure of bearings with air cooling spacer

Structure of "Bearings with Air Cooling Spacer" is shown in Fig. 1. NTN's proprietary eco-friendly air-oil lubrication nozzle is applied to the outer ring spacers between the angular contact ball bearings in a back-to-back arrangement (DB arrangement) for reductions in air-oil and noise. Additionally, a separate air cooling nozzle is included.

Three air cooling nozzles are placed along the circumference of the bearing oriented in the rotational

direction of the spindle at positions offset about the axial center. The compressed room-temperature air injected from the nozzles goes through the space between the inner and outer spacers as well as inside the bearings. It then revolves in the rotational direction of the spindle and cools down the bearings.

This product has been introduced in separate articles in detail <sup>1, 2)</sup>.

## 3. Summary

NTN has achieved both high speed and high rigidity at a high level by using air cooling technology to the bearings used in the main spindles of machine tools. "Bearings with Air Cooling Spacer" developed with this new technology are expected to allow for higher speed, higher rigidity, and improved reliability, as well as contribute to overall manufacturing.

## References

- 1) Onda, Fukada, Yamamoto and Yoshino: Machine Tool Main Spindle Bearings with Air Cooling Spacer, NTN TECHNICAL REVIEW, No. 82, (2014) 38-43
- 2) Nasu, Okamoto, Yamamoto and Yoshino: Machine Tool Main Spindle Bearings with Air Cooling Spacer, NTN TECHNICAL REVIEW, No. 84, (2016) 52-57

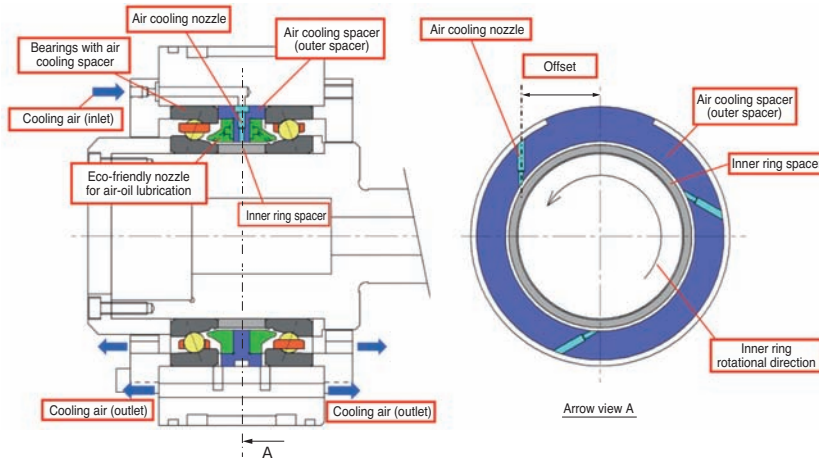


Fig. 1 Structure of the bearing with air cooling spacer

Photo of authors



Wenwei WU

Industrial Machinery  
Technology Department,  
NTN (China) Investment Corporation



Michihiko KOSAKA

Industrial Machinery  
Technology Department,  
NTN (China) Investment Corporation

EQUIP AUTO 2015 INNOVATION AWARD



Press Connected Spline Hub Joint

Sebastien GUILLAUME

Claire BIANCHIN

1. Introduction

Equip'Auto is the largest Automotive Aftermarket Show in France. It takes place every two year in Paris.

The promotion of innovations useful for aftermarket is one of the priorities of Equip'Auto, with the "Grand prix internationaux de l'innovation". This challenge awards gold, silver & bronze trophy, in 5 categories.

NTN-SNR attended the show, with a stand to exhibit the range of NTN-SNR automotive products dedicated to aftermarket.



NTN-SNR applied for the "Grand prix internationaux de l'innovation" with the presentation of a light weight wheel hub, in the category of 'OEM & new technologies'.

2. Structure of Press Connected Spline (PCS) hub joint with aluminum centering

The innovation presented by NTN-SNR is a Press Connected Spline Hub joint, developed by NTN, with an aluminum wheel & break disc centering developed by NTN-SNR.



Compare to a standard solution, the mass of the wheel hub & CVJ assembly is reduced by 21.2%, with 18.2% by PCS & 3% by aluminum centering.

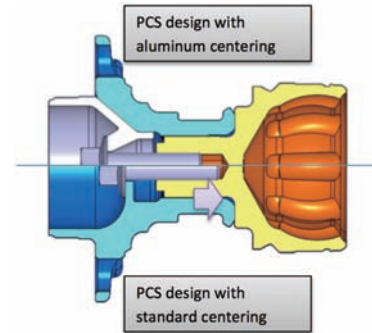
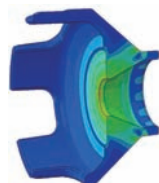
This solution has been applied on a Renault demonstration vehicle called 'Eolab' that achieve a mileage of 2L / 100km.

3. Detail explanation of aluminum centering

The target of aluminum centering development is to save mass, but also to simplify the manufacturing of the hub. The hub is easier to forge, and the small splines of PCS are possible to manufacture with a standard process (the tool can pass through).

The geometry of the aluminum centering has been optimizing by FEM with two criteria:

- 1) Stay below 170 MPa of stress in the aluminum under the axial load of the nut due to tightening, to be able to use low cost aluminum for mass production.
- 2) Keep the displacement in the centering area below 5 microns.



4. NTN-SNR award

With an attendance of more than 95,000 visitors, and the presence of 1,400 exhibitors (who 60 % of international), EQUIP automobile 2015, who is kept from 13 till 17 October, confirmed its position of international, essential meeting in France.

The "Grand prix internationaux de l'innovation" exists since 1985. The jury consists of more than 60 journalists, from more than 20 countries.

The NTN-SNR presentation to the jury explained the advantage of this innovation: CO<sub>2</sub> emission reduction, mileage increase, noise reduction, and also the possibility of easy maintenance by the short length of the CVJ spline.

The jury awarded NTN-SNR for this innovation, with the silver trophy.

5. Summary

Press connected Spline Hub Joint & aluminum centering is a solution to answer automotive market demand. This product also demonstrates the strength of NTN group, with, on one hand, the possibility to propose improvements on both the wheel hub & CVJ, and on the other hand, the common input of both Japan & France R&D center.

NTN-SNR will continue to promote Press connected Spline Hub Joint & aluminum centering to European car makers.



Photo of authors



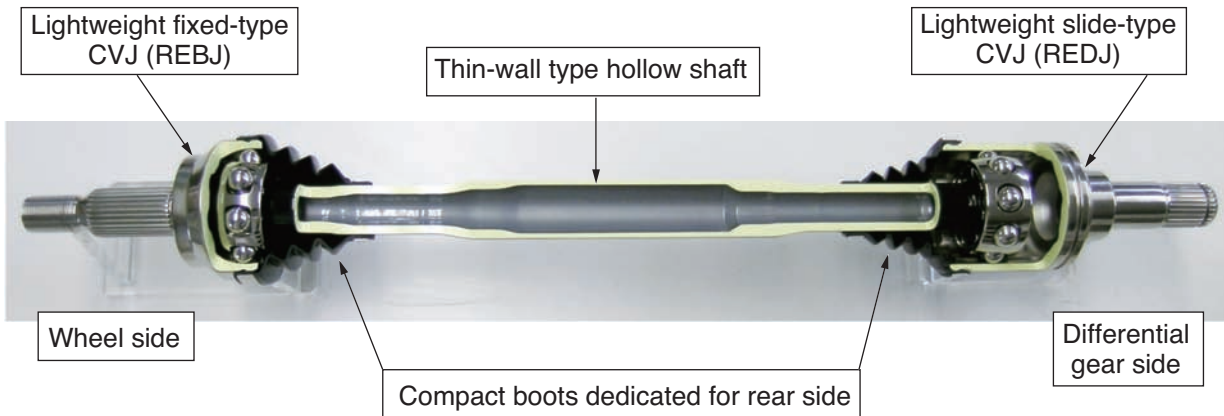
Sebastien Guillaume  
NTN-SNR ROULEMENTS  
Automotive business unit  
R&D - Wheel bearing



Claire Bianchin  
NTN-SNR ROULEMENTS  
Automotive aftermarket  
communication

## Lightweight Rear Drive Shaft

30% lighter than the conventional product • Significant weight reduction achieved by new joints (REBJ and REDJ) with dedicated design for compact rear drive shafts!



### Features

#### Lightweight/compact

- (1) 2.2 kg lighter (30% less than conventional products) per drive shaft
- (2) 3-5% reduction of CVJ outer ring outer diameter

- Fixed type/slide type CVJ with dedicated design for the rear side
- Thin-walled type hollow shaft
- Compact boots dedicated for the rear side

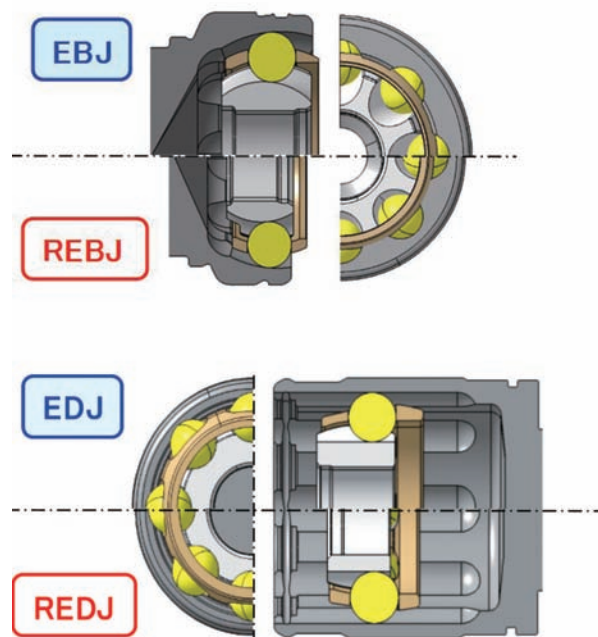
### Applications

- Rear drive shaft for rear wheel drive and four wheel drive vehicles



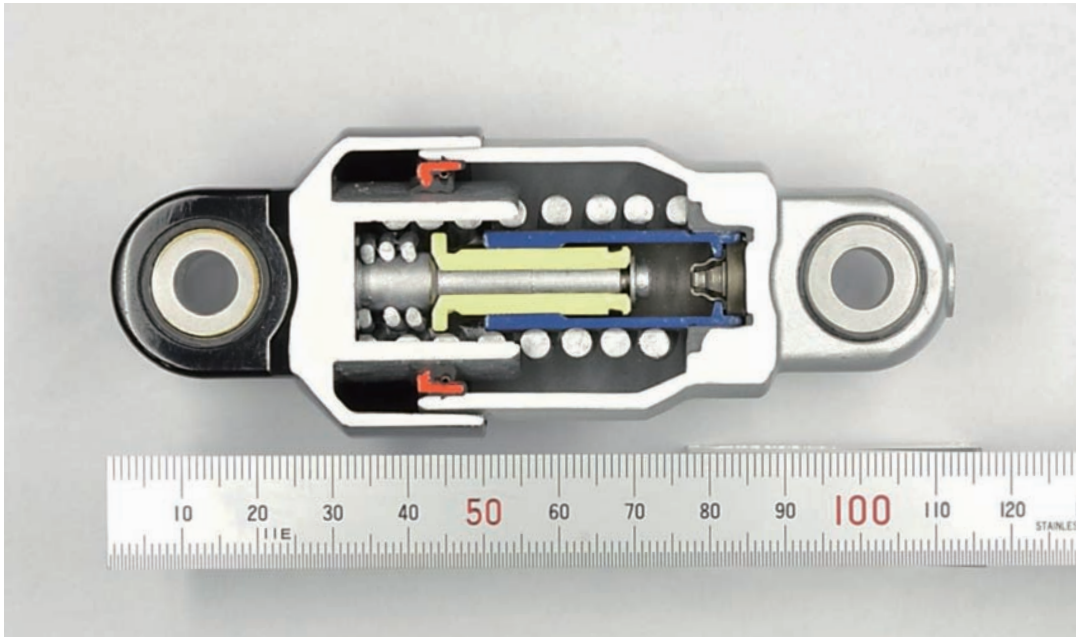
### Structure

Comparison with conventional products (EBJ+EDJ)



## Auto Tensioner with Variable Damper Mechanism for ISG\* Equipped Engines

Achieve both belt slip prevention when starting the engine and low fuel consumption, which was difficult with conventional products, with the variable damper mechanism



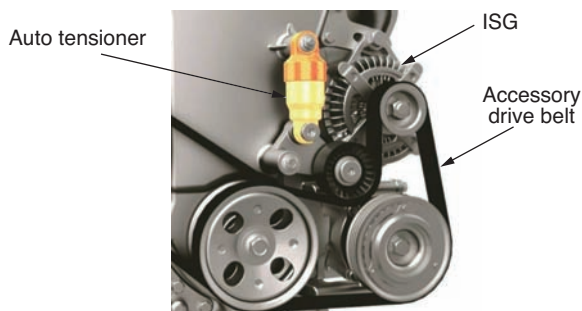
### Features

#### Achievement of both improved fuel economy and high stability

- (1) Maintain low belt tension for regular driving to improve fuel economy
- (2) Prevent belt slip by instantaneously generating high belt tension when the ISG functions as a starter
- (3) Equivalent size and durability as the conventional product

### Applications

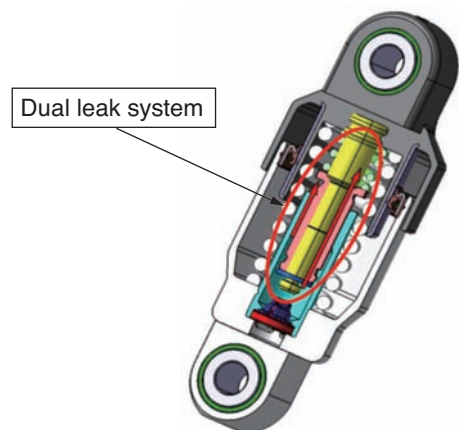
#### ● Tension adjustment for automobile engine accessory drive belts



### Structure

#### Adoption of dual leak system

- (1) Mechanism to automatically switch the oil flow path depending on the operating condition of the engine
- (2) Check valve structure that opens/closes with the balance of spring force and hydraulic power



\* Abbreviation of Integrated Starter Generator. Motor with integrated generator and starter.